TRIBHUVAN UNIVERSITY
INSTITUTE OF ENGINEERING
PULCHOWK CAMPUS
DEPARTMENT OF CIVIL ENGINEERING

FINAL YEAR PROJECT REPORT
ON
ASSESSING CLIMATE CHANGE IMPACTS ON CROP YIELD: A CASE OF TULSIPUR, DANG

Submitted By:

Bhakti Lekhak (075 BCE 033)
Bishal Bastola (075 BCE 046)
Chandra Jyoti Karna (075 BCE 048)
Dipesh Banjade (075 BCE 053)
Md. Zuber (075 BCE 080)
Nabin Kalauni (075 BCE 083)

Supervisor:

Prof. Dr. Vishnu Prasad Pandey

APRIL 2023

TRIBHUVAN UNIVERSITY
INSTITUTE OF ENGINEERING
PULCHOWK CAMPUS
DEPARTMENT OF CIVIL ENGINEERING

FINAL YEAR PROJECT REPORT
ON
ASSESSING CLIMATE CHANGE IMPACTS ON CROP YIELD: A CASE OF TULSIPUR, DANG

IN PARTIAL FULFILMENT OF THE REQUIREMENT FOR THE AWARD OF BACHELOR'S DEGREE IN CIVIL ENGINEERING
(Course Code: CE755)

Submitted By:

Bhakti Lekhak (075bce033)
Bishal Bastola (075bce046)
Chandra Jyoti Karna (075bce048)
Dipesh Banjade (075bce053)
Md. Zuber (075bce080)
Nabin Kalauni (075bce083)

Supervisor:

Prof. Dr. Vishnu Prasad Pandey

APRIL 2023

COPYRIGHT

TRIBHUVAN UNIVERSITY
INSTITUTE OF ENGINEERING
PULCHOWK CAMPUS
DEPARTMENT OF CIVIL ENGINEERING

CERTIFICATE

This is to certify that this final year project work entitled **"Assessing Climate Change Impacts on Crop Yield: A Case Study of Tulsipur, Dang"** has been examined and declared successful for the fulfilment of academic requirement towards the completion of bachelor's degree in civil engineering.

……..
Project Supervisor
Prof. Dr. Vishnu Prasad Pandey

……
HOD, Department of Civil Engineering
Prof. Dr. Gokarna Bahadur Motra

…….
External Examiner
Dr. Pawan Bhattarai

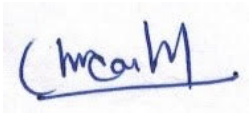

……...
Internal Examiner
Dr. Ram K. Regmi

ACKNOWLEDGEMENT

The success of any project work requires a lot of guidance and assistance from many people, and we are extremely fortunate to have had it in abundance throughout our final year. First, we are very thankful to **the Department of Civil Engineering**, Pulchowk Campus, for organizing this project work and assigning brilliant supervisors to us. We respect and thank **Prof. Dr. Vishnu Prasad Pandey** for giving us an opportunity to do this project work and providing us all the support, patience, motivation, and immense knowledge, which not only helped us complete the project on time but also widen our horizon of knowledge from a broader perspective. Acknowledgement would be incomplete without a word of appreciation for **Dr. Nirman Shrestha**, regional researcher at International Water Management Institute, without whose expert guidance and unwavering support, this report would never have come into fruition.

In addition, we would like to extend our appreciation to **IOE, TU** for their support to the students of higher education, the inclusion of project in the syllabus; their generosity to the student body is incomparable. Finally, yet importantly, we would like to express our gratitude to respondent farmers of Tulsipur for their candor and willingness to spend time with us.

B.E. Project Group 2075

Bhakti Lekhak (075bce033)

Bishal Bastola (075bce046)

Chandra Jyoti Karna (075bce048)

Dipesh Banjade (075bce053)

Md. Zuber (075bce080)

Nabin Kalauni (075bce083)

PREFACE

Institute of Engineering (IOE), an institute under Tribhuvan University (TU) offers a four-year undergraduate course in Bachelor of Civil Engineering. In this course, the final year project needs to be undertaken by the students to expand their theoretical knowledge into a broader application in the vast world of Civil Engineering. Under the supervision of a professor, students are required to form groups of six to carry out a specific study or analysis, which can be either design type, dissertation type or experimental type.

This final year project report, titled **'Assessing Climate Change Impacts on Crop Yield: A Case Study of Tulsipur, Dang'** is part of the final year project carried out by six students of IOE, Pulchowk Campus and supervised by professors in the field of water resources: Prof. Dr. Vishnu Prasad Pandey. The purpose of this report is to evaluate the impact of climate change on crop yield in our study area and understand the use and working of different tools to carry out such analyses. It also aims to project the future climate in those regions not only to envision the possible events in the future but also to assist the concerned strategists and stakeholders to develop better mitigation measures in the future.

We believe this report fulfills all the necessary criteria of the institution as a final year project and hope it assists in carrying out similar studies in the future. Any feedback and suggestions are welcome.

ABSTRACT

Climate change has created a serious concern for food security, extreme hydrological conditions, environment, ecology, health, and even entire human civilization. A developing country like Nepal is even more vulnerable to climate change impacts due to our weak infrastructure. Climate change is projected to have devastating impacts on crop yield. This study aims to assess the impacts of climate change on crop water requirements and crop yield in Tulsipur, Dang. It also aims to aid climate research in Nepal by the development of climate information system and projection of future climate in the region using Global Climate Models (GCMs).

Temperature and precipitation data from stations all over Nepal were acquired in a gridded format by Kriging with External Drift (KED) interpolation. For the projection of future data, five CMIP6 based GCM models were used, and bias corrected to form an ensemble. Future climatic data was obtained under two Shared Socioeconomic Pathways Scenarios (SSPs): SSP245 and SSP585. The multi-model ensemble (MME) approach was used to minimize uncertainty associated with model predictions, and GCMs proposed were selected. The quantile mapping (QM) method was used for correcting the biases in the GCMs, and the RQUANT method was chosen for rainfall data, while the 'PTF: linear method' was used for temperature data. A crop simulation model (AquaCrop) was calibrated and validated using cultivar-specific and less conservative parameters obtained from farmer surveys, input climatic daily data, and soil properties. The calibrated model was then used to predict future crop yield scenarios for rice and wheat under different irrigation strategies and fertility stress levels.

The data acquired from the climate information system has shown a good fit ($R^2 = 0.913$) with nearby station data in Tulsipur and hence shows promising utility in replacing station data as starting point for future climate studies. Additionally, climate projection studies show that Dang is expected to experience progressive warming and increased rainfall in future (2021-2100). Wet seasons are projected to continue receiving more rainfall and rising temperatures which is likely to induce extreme events such as flooding. Conversely, dry winter seasons are likely to be drier and hotter in the future, which is detrimental to winter crops. The results of our study show a positive response of crop yield to climate change. Rice yield is projected to increase by as much as 112% by 2100 under extreme carbon emission scenarios. Similarly, wheat yield is projected to increase as much as 165% under similar ideal conditions. On the other hand, crop water requirements are projected to increase for both rice and wheat. The study also provides useful information for climate change adaptation and mitigation strategies in Nepal and recommends further research to improve the accuracy and reliability of crop simulation.

TABLE OF CONTENTS

LIST OF FIGURES

LIST OF TABLES

ABBREVIATIONS AND ACRONYMS

APSIM	Agricultural Production Systems sIMulator
AR4	Fourth Assessment Report
AR6	Sixth Assessment Report
BODC	British Oceanographic Data Centre
CC	Canopy Cover
CDC	canopy decline coefficient
CIS	Climate information systems
CMIP	Common Model Intercomparison Project 6
CRMSD	centralized root mean square deviation
DAP	Di-Ammonium Phosphate
DHM	Department of Hydrology and Meteorology
DJF	December January February
DoA	Department of Agriculture
DSSAT	Decision-Support System for Agro
EPIC	Environmental policy integrated climate
ETo	Evapotranspiration
FACE	Free Air Carbon dioxide Enrichment
FAO	Food and Agriculture Organization of the United Nations
FF	Far Future
GCMs	Global Climate Models
GDD	growing degree days
GDI	Gross Development Index
GDP	Gross Development Product
GIS	Geographic Information System
GLOFs	glacial lake outburst floods
GoN	Government of Nepal
GUI	Graphical User Interface
GWT	Ground Water Table
HIo	Harvest index
ICIMOD	The International Centre for Integrated Mountain Development
IOOS	Integrated Ocean Observing System
IPCC	Intergovernmental Panel on Climate Change
IWM	independence weighted mean
KGE	Kling-Gupta Efficiency
LAI	leaf area index
MAE	Mean Absolute Error
MBE	mean bias deviation

MF	Mid future
MME	Multi Model Ensemble
MoALD	Ministry of Agriculture and Livestock Development
NARC	National Agricultural Research Council
NetCDF	Network Common Data Form
NF	Near Future
NIR	Net Irrigation Requirement
NRFD	National Recommended Fertilizer Dose
OGC	Open Geospatial Consortium
OLR	outgoing longwave radiation
PTF	Pedotransfer function
QM	Quantile Mapping
RAW	Readily Available water
RBG	Red, Green, and Blue
RCM	Regional climate model
RCPs	Representative Concentration Pathways
RMSE	Root Mean Square error
RQUANT	Robust Quantile
Scorr	Spatial correction
SPAW	Soil-plant-air-water
SRES	Special Report on Emissions Scenarios
SSPs	Shared Socioeconomic Pathways
TT	technology Transfer
TWR	Total water requirement
UNFCCC	United Nations Framework Convention on Climate Change
WOFOST	World Food Studies

1 INTRODUCTION

1.1 Background

Climate change refers to the long-term variation in observable climate statistics such as precipitation, temperature, CO_2 concentrations, etc., as shown in **Figure 1.1** and **Figure 1.2**. The scientific community is still divided on whether a distinction should be made between climate change attributable to human drivers and natural causes. For instance, the Intergovernmental Panel on Climate Change (IPCC) defines climate change as "any change in climate over time, whether due to natural variability or as a result of human activity" whereas the United Nations Framework Convention on Climate Change (UNFCCC) defines it as a "change of climate that is attributed directly or indirectly to human activity that alters the composition of the global atmosphere and that is in addition to natural climate variability observed over comparable time periods" (IPCC, 2018). But regardless of these differences, there is unanimous support, backed by heaps of evidence, that human actions are the major cause behind climate change (Anderegg et al., 2010; Doran & Zimmerman, 2009; Oreskes, 2004). The Fourth Assessment Report (AR4)published by IPCC concluded that anthropogenic warming, mostly in the form of greenhouse gases, is a major driver behind climate change (Solomon S, et. al., 2007).

Although predicting climate change and the adaptation in response to climate change is a complex task with heaps of uncertainties (Raäisaänen, 2007), advances in science and technology have allowed us to model these changes to a remarkable degree of accuracy with some projections extending far into the future up to 2100 (Hulme et al., 2001). However, there is no need to see so far into the future to realize the impacts of climate change. They have been seen worldwide in the form of frequent and intense extreme climatic events such as floods, droughts (Liu et al., 2021); reduced crop yields (Wing et al., 2021); vulnerability of terrestrial (Field et al., 2007), freshwater (Woodward et al., 2010), and marine ecosystems (Doney et al., 2012); high risk to food and water security (Wheeler & von Braun, 2013); rise in sea level (Bindoff et al., 2007); melting of polar ice (Turner & Marshall, 2011); and many more; with these events expected to grow in intensity as well as frequency in the coming years.

Climate change is projected to adversely affect global agriculture and food security all over the world (Calzadilla et al., 2013). Water pollution and soil erosion caused by extreme precipitation in wet seasons and droughts in dry seasons are expected to detriment agricultural productivity (Boxall et al., 2009). Moreover, changes in precipitation patterns could impact groundwater recharge (Bates et al., 2008). On top of that, increasing temperatures will shorten the crop cycle, increase irrigation water requirements and consequently reduce crop yield (Fischer et al., 2007).

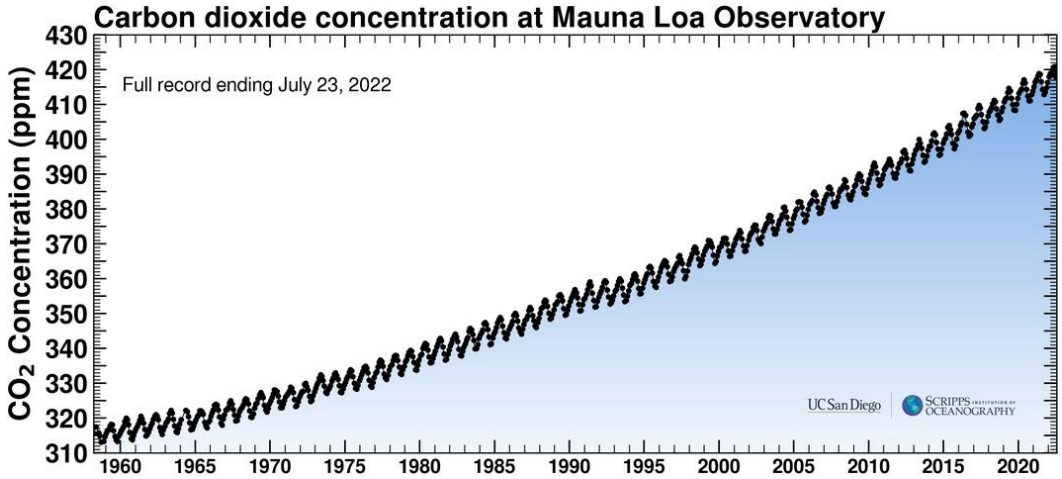

Figure 1.1: The infamous "Keeling Curve" that shows increasing amounts of CO_2 concentration in the Earth's atmosphere based on measurements taken at the Mauna Loa Observatory, Hawaii. (Ralph F. Keeling & Charles D. Keeling, 2017)

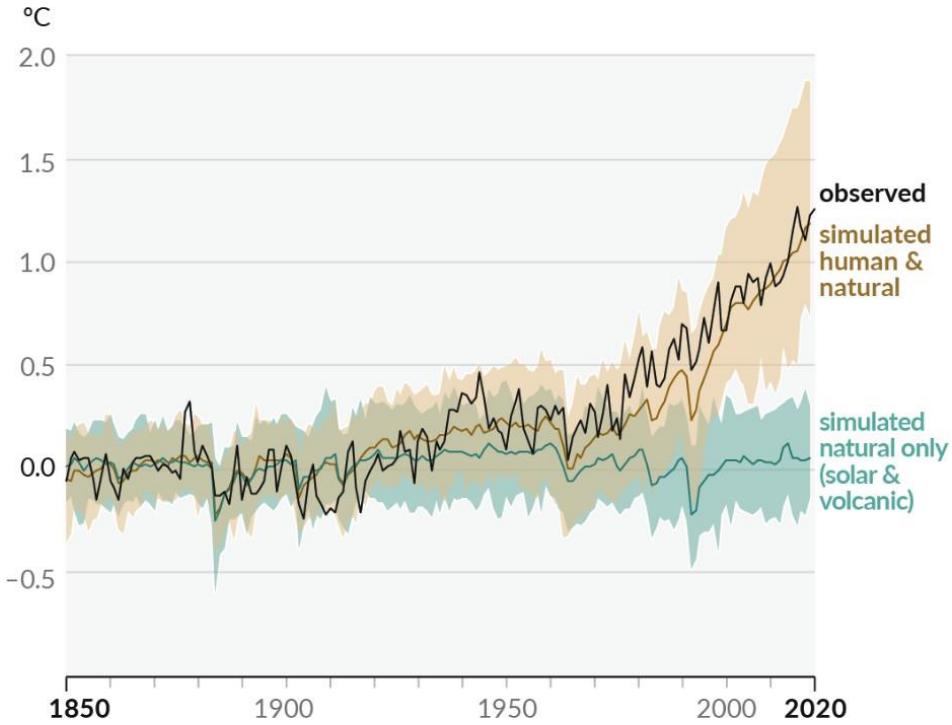

Figure 1.2: Rising global surface temperature and the contribution of human activities behind this dramatic rise. (IPCC, 2021a)

Climate variability poses a considerable risk to rainfed farming systems and irrigated systems could also be negatively affected by changes in river flow due to climate change (Falloon & Betts, 2010). (Knox et al., 2012) estimated that crop yield may decline in South Asia by nearly 8% by the 2050s and various other studies have found robust evidence of reduced crop yield productivity due to climate change (Mendelsohn, 2008; Parry et al., 2004).

Developing countries like Nepal are at a high risk of climate change because of their weak adaptability and increased pressure on natural resources due to rapid urbanization (Adger, 2006; Yohe & Tol, 2002). On top of that, Nepal is at a higher risk due to its location in the high terrain of the central Himalayas, which is susceptible to extreme weather conditions leading to consequent flash floods, landslides, and glacial lake outburst floods (GLOFs) (ICIMOD, 2011). A World Bank

(WB) report states that climate change could have an unprecedented impact on food security in South Asia (WorldBank, 2010).

1.2 Problem Statement

Nepal could face serious consequences in terms of agriculture and food security because of climate change. Agriculture is the major sector of the Nepalese economy. It provides employment opportunities to 66% of the total population and contributes about 36% in the Gross Development Product (GDP) (FAO, 2022). Hence, it is paramount that studies investigating the impacts of climate change are carried out in Nepal. While many studies have been carried out to assess the impact of climate change on crop yield in Nepal (Shrestha et al., 2013, 2014), there is room to improve because of advances in climate modeling (Eyring et al., 2016). Researchers investigating the impact of climate change on agriculture in Nepal have yet to use the new Coupled Model Intercomparison Project Phase 6 (CMIP6) introduced in the Sixth Assessment Report (AR6) by IPCC that has introduced new ways of analyzing, evaluating, and improving our climate models (IPCC, 2021b). A detailed deep-dive study in Dang district is yet to be carried out.

Increasing CO_2 and temperature coupled with precipitation variability due to climate change can have conflicting results on crop yield that are hard to predict. On one hand, higher atmospheric CO_2 promotes faster photosynthesis (Morison, 1987) and better regulation of crop transpiration (Drake et al., 1997). On the other hand, increased temperature leads to higher rates of crop transpiration and water demand (Peng et al., 2004). Which one of these phenomena outshines the other in a complex eco-biological dance of competing variables is a tough task to predict and literature suggests that the response can vary greatly depending on the crop and local climatic conditions (Bouras et al., 2019). Hence, given the significance of agriculture in our country, characterization of climate change impacts on crop yield is of prime importance.

Most climatic studies undertaken in Nepal use station measurements of precipitation and temperature provided by the Department of Hydrology and Meteorology (DHM). The network of meteorological stations used by DHM is sparse and available data are insufficient to characterize the highly variable precipitation spatial distribution (Dangol et al., 2022). This is especially true for mountain areas, where the complexity of the precipitation distribution is combined with the measurement difficulties. Therefore, it is necessary to develop interpolation models to estimate precipitation in areas where precipitation has not been measured, using data from the surrounding weather stations, and generate a continuous dataset. Moreover, the data from DHM, although spanning a long-time range, have substantial gaps in some stations. There are also some anomalies in data that most likely arise because of human error in recording and storing data (Chand et al., 2021). So, most research studies in Nepal involving this data usually begins by assessing the data quality and correcting anomalies and missing measurements (Adhikari et al., 2022). So, there is a need for a consistent, continuous and reproducible data product in the context of Nepal. Since climate information services are indispensable in carrying out research on climate change adaptation and mitigation in vulnerable countries (Goddard, 2016), an information system will be built on top of the data product to improve researchers' access to high quality climate data in Nepal.

To meet the aforementioned research gaps, this study will first build a climate information system of climate data all over Nepal and assess its suitability. Then the climate data will be used to investigate the effects of climate change on agriculture in Dang District. Hence this study will

serve to meet the twofold needs of developing a climate information system as well as researching the impact of climate change on crop yield in Nepal.

1.3 Objectives

The broad goal of this study is to evaluate the impact of climate change on crop yield in Dang district. The specific objectives include:

- To develop a user-friendly climate information system of precipitation and temperature data
- To project the future climate under Shared Socioeconomic Pathways (SSP) scenarios
- To evaluate impact of climatic and non-climatic changes on crop yield

The scope of the study covers the following:

- Acquisition of time series data of precipitation and temperature from DHM
- Development of Graphical User Interface (GUI) application
- Selection of suitable Global Climatic Model (GCM)
- Bias correction and downscaling
- Modeling of climate variables under different Shared Socioeconomic Pathways (SSPs)
- Farmer survey and soil textural analysis
- Evaluation of crop yield using soil data from the study area under projected climatic conditions using AquaCrop.

1.4 Limitations

The following are the limitations of our study:

- Due to sparse distribution of climate stations in the mountainous regions of Nepal, interpolated climate data in these regions have a high degree of error and uncertainty.
- Downscaling of GCM output to higher resolution introduces boundary interactions that may lead to error propagation. Only five GCMs have been selected and they might not be adequate to fully characterize climate of Dang.
- AquaCrop does not account for the effect of extreme weather events such as heatwaves, floods and droughts, and plant diseases, which are projected to increase in frequency and severity due to climate change.

2 LITERATURE REVIEW

2.1 Climate Information System

Climate change is one of the most significant challenges facing the world today, and it is expected to have far-reaching impacts on the global economy, the environment, and human society. As shown in **Figure 2.1**, the key approaches to combating climate change can be classified as "mitigation," which aims to minimize or halt the release of greenhouse gases to limit future changes, and "adaptation," which involves evaluating the impacts, creating resilience to them, and making appropriate arrangements for anticipated changes. However, in recent years, there has been an increasing recognition of the role of "information" that can help countries and communities adapt to the changing climate (Goddard, 2016).

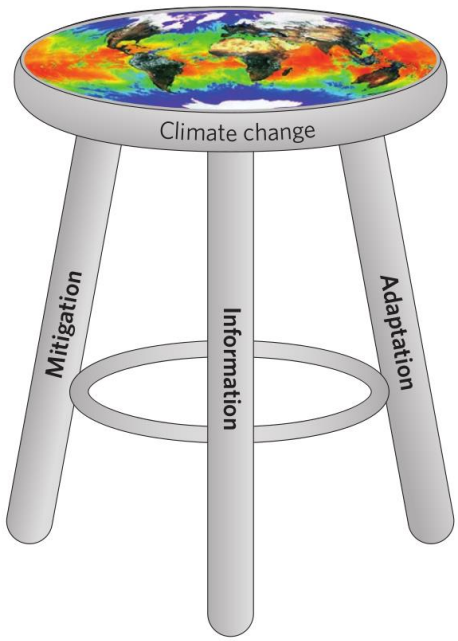

Figure 2.1: The three-pronged response to climate change: mitigation, adaptation, and information (Trenberth et al., 2016)

Climate information systems (CIS) are essential tools for monitoring, predicting, and managing the impacts of climate change. They provide users with the data and information they need to make informed decisions about climate-related risks and opportunities. CIS can help to identify areas that are particularly vulnerable to climate change, as well as areas where climate-related opportunities may exist. They can also help to inform policies and strategies for climate change adaptation and mitigation (Vincent et al., 2017). Climate information systems are particularly relevant in countries that are vulnerable to climate change. These countries often lack the resources and infrastructure to effectively manage climate risks and adapt to the changing climate(Dulal et al., 2010). CIS can provide these countries with the data and information they need to make informed decisions about climate-related risks and opportunities. They can also help to inform

policies and strategies for climate change adaptation and mitigation (Dinku et al., 2018; Smit & Wandel, 2006).

2.2 Future Climate Projection

According to IPCC, Global Climate Models are numerical models representing the physical processes in the atmosphere, ocean, land surface, and cryosphere. The fundamental building block of these models is fundamental physics and various equations governing the universe. These equations include Newton's law of motion, mass conservation, thermodynamic energy equation, hydrodynamic state equation, etc. (Edwards, 2011). These Global Climate Models (GCMs) are models used to project climate in the future. GCM models are developed by a group of people working together in assistance of Common Model Intercomparison Project (CMIP) and the latest models available are CMIP 6 models.

2.2.1 Selection of GCM

Selection of GCM model depends on various factors such as spatiality of observed data, topographical nature of area, etc. There are certain uncertainties associated with GCM models and using all GCMs is not practical. So, it is a must to select GCM for robust climate projection. Basically, there are 3 ways for selecting a GCM model they are:

- Validation approach
- Image formation approach
- Extremes approach

A. Validation approach (Nyunt et al., 2016)

- We start by assessing the model's capacity to represent the most important mesoscale and local climatic characteristics that affect seasonal evolution and the amount of precipitation in large basin area.
- Rainfall, outgoing longwave radiation (OLR) in the local domain, SST, zonal wind, etc. in the regional domain are considered using climatological monthly long-term mean spatial correlation (Scorr) and root mean square error (RMSE) in past years.
- Scoring is done.

$$S_{corr} = \frac{\sum_{i=1}^{N}(x_i - \overline{x})(y_i - \overline{y})}{\sqrt{\frac{1}{N}\sum_{i=1}^{N}(x_i - \overline{x})^2(y_i - \overline{y})^2}} \quad 2.1$$

$$E_{RMS} = \sqrt{\frac{1}{N}\sum_{i=1}^{N}(x_i - y_i)^2} \quad 2.2$$

The GCM that has a greater Scorr and a lower RMSE than the GCM mean receives a score of 1. If any of the two requirements is met, a score of 0 is given; if neither is met, a score of -1 is given. Every key variable is subjected to this scoring system, and the aggregate of the scores for each GCM is computed. This method is used to select a handful of GCMs not the best GCM.

B. Image formation approach (Hamed et al., 2022)

- The three basic color bands of Red, Green, and Blue (RBG) for Precipitation, Tmax, and Tmin are used respectively in the process to construct a full image that serves as a reference for observed historical climate.
- The same is done for an image depicting a GCM-simulated climate.
- As a consequence, it is possible to compare the reference image with the simulated image as a pair.
- To evaluate the similarities between characteristics of observed and GCM climatology pictures, the robust Kling-Gupta Efficiency (KGE) measure is applied.

Each band produces a separate grayscale picture. The brightness of each pixel is represented by the picture. The most popular pixel format is called a "byte image," and it stores each pixel's brightness as an 8-bit integer with a value between 0 and 225. Using Equation 2.3, climate variables were rescaled to an 8-bit integer.

$$Y_n = \frac{[x_n - \min(x)] \times 255}{\max(x) - \min(x)} \qquad 2.3$$

Where $x_n$stands for the climatic variable, Y_n for the transformed value, and max(x) and min(x) for the variable's maximum and minimum readings. To form a picture, this procedure is repeated for each band and combined. Image similarity is measured by KGE given by Equation 2.4.:

$$KGE = 1 - \sqrt{\left((r-1)^2 + \left(\frac{\mu_s}{\mu_{ref}} - 1\right)^2 + \left(\frac{\sigma_s/\mu_s}{\sigma_{ref}/\mu_{ref}} - 1\right)^2\right)} \qquad 2.4$$

The reference image's mean and the simulated image's mean are represented by μ_s and μ_{ref} respectively. And the reference image's standard deviation and the simulated image's standard deviation are represented by σ_s and σ_{ref}, respectively. KGE has a value between 1 and -infinity, where 1 denotes a perfect match.

C. Extremes approach (Fenech et al., 2002)

According to the extremes (max/min) method, it is better to prepare taking into account all possibilities that any GCM offers. This method employs both the projections for the largest change and the least change as the range of factors to take into account while planning.

2.2.2 Different scenarios for climate projection

We are unable to forecast the course that the climate may follow in light of the uncertainties in socioeconomic growth, technological advancement, and emissions for the future. Therefore, we experiment with various climate-related scenarios and assess the outcomes.

Worldwide, there are several teams who work on climate modeling. It would be exceedingly challenging to compare one research to another if they all utilized various measurements and had different baselines and beginning points. The same manner, communication between climate modeling organizations would become more difficult and time-consuming. Models could not be tested against other distinct, independent models. The expense of maintaining models is an

additional issue. The demand for and shortage of the necessary powerful computers are both acute. It would be unfeasible to have simulation programming that required starting from scratch for each experiment. Scenarios offers a framework for streamlining the experiment construction process. (Wayne, 2013).

The first set of climate change scenarios, known as IS92, were released by the Intergovernmental Panel on Climate Change (IPCC) in 1992. The Special Report on Emissions Scenarios (SRES), a collection of the IPCC's second wave of forecasts, was published in 2000. In response to requests for SRES enhancements, the IPCC sped up the creation of the Representative Concentration Pathways (RCPs) in 2007. After that SSPs were subsequently introduced.

A. RCPs

When attempting to forecast how future global warming will affect climate change, a variety of elements must be considered. Future greenhouse gas emissions are a crucial factor. Technology advancements, alterations in energy production and land usage, regional and global economic conditions, and population expansion must all be considered. Based on assumptions on economic activity, energy sources, population growth, and other socioeconomic aspects, an RCP provides a set of beginning values and the expected emissions up to 2100, listed in **Table 2.1**.

Table 2.1: Different RCP Scenarios, along with radiative forcing (Wayne, 2013)

Name	**Radiative forcing**	**CO_2 equi (p.p.m)**	**Temp Anomaly (°C)**	**Pathways**
RCP8.5	8.5 Wm^2 in 2100	1370	4.9	Rising
RCP6.0	6 Wm^2 post 2100	850	3.0	Stabilization without overshoot
RCP4.5	4.5 Wm^2 post 2100	650	2.4	Stabilization without overshoot
RCP 2.6 (RCP3PD)	3 Wm^2 before 2100, Declining to 2.6 Wm^2 by 2100	490	1.5	Peak and decline

B. SSPs

In order to conduct research on the effects, adaptation, and mitigation of climate change, a novel scenario framework for climate change research visualizes merging paths of future radiative forcing and its related climatic changes with alternative routes of socioeconomic growth. The four different RCPs on the first dimension of the matrix depict climatic outcomes, while the Shared Socioeconomic Pathways (SSPs) on the other dimension define potential reference expectations about anticipated socioeconomic development in the absence of climate policy or climate change (O'Neill et al., 2014). These pathways are listed in **Table 2.2.**

As mentioned earlier combining future radiative forcing in the year 2100 with socio- economic scenarios, we get updated scenarios. For example, SSP585 is an extreme case scenario with radiative forcing of 8.5 watt per square meter at the end of 2100 (Bai et al., 2021).

2.2.3 Downscaling and bias correction

According to climate change forecasts, there will be changes in availability of water, and the frequency and severity of major hydrological events will alter. General Circulation Models (GCMs) are frequently used for climate simulations of the present and the future. For research on the impacts of climate change, high-resolution projections are crucial since the output of GCMs is linked with significant errors and biases. Researchers use downscaling approaches to calibrate the GCMs' raw forecasts in order to solve this problem.

There are two main downscaling strategies: statistical downscaling and dynamic downscaling. These strategies are based on the ideas and mathematics employed in these methods. A statistical correlation between historical observed data and GCM model data for the same time period is created for statistical downscaling. Future climate data projections are made using the defined connection.

Table 2.2: Different SSP Scenarios, along with the challenges associated (O'Neill et al., 2014)

SSP	Challenges	Illustrative starting points for narratives
SSP1	Low for mitigation and adaptation	Sustainable development proceeds at a reasonably high pace, inequalities are lessened, technological change is rapid and directed toward environmentally friendly processes, including lower carbon energy sources and high productivity of land
SSP2	moderate	An intermediate case between SSP1 and SSP3.
SSP3	High for mitigation and adaptation	Unmitigated emissions are high due to moderate economic growth, a rapidly growing population, and slow technological change in the energy sector, making mitigation difficult. Investments in human capital are low, inequality is high, a regionalized world leads to reduced trade flows, and institutional development is unfavorable, leaving large numbers of people vulnerable to climate change and many parts of the world with low adaptive
SSP4	High for adaptation low for mitigation	A mixed world, with relatively rapid technological development in low carbon energy sources in key emitting regions, leading to relatively large mitigating capacity in places where it mattered most to global emissions. However, in other regions development proceeds slowly, inequality remains high, and economies are relatively isolated, leaving these regions highly vulnerable to climate change with limited adaptive capacity.

SSP	Challenges	Illustrative starting points for narratives
SSP5	High for mitigation and low for adaptation	In the absence of climate policies, energy demand is high and most of this demand is met with. carbon-based fuels. Investments in alternative energy technologies are low, and there are few readily available options for mitigation. Nonetheless, economic development is relatively rapid and itself is driven by high investments in human capital. Improved human capital also produces a more equitable distribution of resources, stronger institutions, and slower population growth, leading to a less vulnerable world better able to adapt to climate impacts.

We favor statistical downscaling strategies for our investigation. Based on the statistical correlation between the historical GCM raw data and observed precipitation data, the bias in the past and future GCM raw precipitation data was adjusted. On the data, bias fixes were made. Numerous possible bias correction methods have been put forth, according to a literature analysis, and they each function differently depending on the situation. This idea emphasizes the significance of examining the possible functions of different bias correction strategies and then choose the best ones to post-process the GCMs projection. The subject has already been addressed in a number of research. For instance, (Jakob Themeßl et al., 2011) assessed the effectiveness of numerous bias correction approaches and came to the conclusion that the QM methods were maybe the best available choice to correct the raw GCMs' results.

Quantile mapping has been the most effective approach of bias reduction (Berg et al., 2012). In general, statistical transformations are implemented using QM approaches for post-processing the results of climate models. The statistical transformations involve employing mathematical functions to convert the distribution functions of the modeled variables into the observed ones (Enayati et al., 2021).

(Enayati et al., 2021) mentioned that the robust empirical quantiles (RQUANT) methods were excellent options for correcting the bias of rainfall data, whereas all bias correction methods for the temperature variable performed fairly well, with the robust empirical quantiles (RQUANT) method performing the best. There are two significant PTF: scale exceptions: SSPLIN. The GCM/RCM combinations' clearly improved temperature modeling skills are mostly to blame for this.

A. Temperature

The robust empirical quantiles (RQUANT) technique outperformed the others when it came to bias correction for the temperature variable. SSPLIN are two notable PTF: scale exceptions. This is mostly due to the GCM/RCM combinations' clearly greater modeling ability for temperature as compared to rainfall.

B. Precipitation

(Enayati et al., 2021) revealed that robust empirical quantiles (RQUANT) approaches were among the best options for reducing the bias of rainfall data among the various bias correction methods. The best solutions to correct the bias of the rainfall variable appeared to be QUANT and RQUANT since they not only improved the R and CRMSD criterion but also produced a value of σ that was close to 1 (the desired value).

2.2.4 Performance evaluation criteria

The QMs results should be cross validated with reference to historical observed data, just like any other modeling procedure linear correlation coefficient, normalized standard deviation, centralized root mean squared deviation (CRMSD) are three performance evaluation criteria that can be used with the Taylor diagram to assess a variety of outputs (Jolliff et al., 2009; Liang et al., 2017; K. E. Taylor, 2001).

$$R = \frac{\frac{1}{N}\sum_{i=1}^{N}\left(x_i^o - \overline{x}^o\right)\left(x_i^m - \overline{x}_i^m\right)}{\sigma^o \sigma^m} \quad 2.5$$

$$\sigma_* = \frac{\sigma_m}{\sigma_o} \quad 2.6$$

$$\text{CRMSD} = \left(\frac{1}{N}\sum_{i=1}^{N}\left[\left(x_i^o - \overline{x}_i^o\right) - \left(x_i^m - \overline{x}_i^m\right)\right]^2\right)^{0.5} \quad 2.7$$

Where, σ^o and σ are standard deviations of the observed and modeled datasets, respectively; and N = number of the available historical data. R is a dimensionless coefficient that varies from –1 to +1. The estimated R approaches its boundary values of -1 or +1 when correlation between x^o and x^m increases (R. Taylor, 1990). σ_* is also dimensionless whose value is +1 ideally, which corresponds to observed and simulated outputs being identical. The performance of model depends on R value, if the value is closer to +1 the performance of model is good. The CRMSD value would also fall as the model's performance increased (Jolliff et al., 2009). The model performs better when CRMSD is closer to 0, which in a perfect world would be equal to 0. In the end, the Taylor diagrams' principal goal is to create a visual foundation that makes it easier to compare three quantitative values. (i.e. CRMSD, R, and σ_*).

The mean bias error (MBE), which measures the bias's size and direction, is another performance evaluation criterion in addition to the Taylor diagram. Positive and negative MBE values, on the other hand, signify under- and over-estimation, respectively, while a zero value denotes the lack of bias in the data provided. Mathematical representations of MBE include (Willmott & Matsuura, 2005):

$$\text{MBE} = \frac{\sum_{i=0}^{n}(x_i^o - x_i^m)}{n} \quad 2.8$$

2.2.5 Multi model ensemble

Using a single independent GCM is insufficient to estimate climate change (Bai et al., 2021; Semenov & Stratonovitch, 2010). In IPCC reports, four categories of uncertainty were highlighted.

First, internal variability uncertainty stems from the chaotic and spontaneously varying nature of the climate system. Second, model uncertainty results from omissions, idealizations, and incomplete knowledge of the climate system represented by the model. Third, uncertainty in future natural radiative forcing stems from unpredictable solar and volcanic activities. Fourth, uncertainty in future natural radiative forcing stems from reliance on socioeconomic factors.

Due to these uncertainties, a multi-model ensemble is created for a robust climate prediction under the assumption that errors cancel out if the models are independent (Tebaldi & Knutti, 2007). A brand-new independence weighted mean (IWM) technique was created by (Bishop & Abramowitz, 2012) to solve inter-model interdependence. It seeks to identify the linear combination of a set of model simulations that reduces the mean square difference (MSD) in relation to the data.

2.3 Climate Change Impacts on Crop Yield

It is evident that climate change has major effects on air temperature, CO_2 concentration, evaporation power of the atmosphere (ET_0), and rainfall pattern. The atmospheric CO_2 concentration is likely to increase by 2 ppm per year in the next 10 years(IPCC, 2018). Due to the increase in this CO_2 concentration air temperature is increasing and as consequences also reference evapotranspiration increases. Also due to climate change rainfall pattern is likely to alter and less predictable, more extreme events (Liu et al., 2021). The effect of CO_2 concentration on crop yield has been studied with the help of Free Air Carbon dioxide Enrichment (FACE) experiments and show that high concentration of CO_2 improves water productivity (Ainsworth & Long, 2005). Increased temperature cause heat stress in plant, which is limiting factor for most crop plants, it leads to altered metabolic functions affecting its leaves, flower buds and roots (Tsukaguchi et al., 2003). Increase in temperature causes rapid loss of water from plants and soil surface causing reduced water availability and lead to water stresses in plants. Increased temperature and altered rainfall can create more favorable conditions to the pests and disease leading to increased pressure on crops, this can result in lower yield and promote the use of more pesticides which have a negative impact on the environment. Extreme events such as intense rainfall cause flooding and soil erosion which can negatively impact soil fertility and crop yields(Moriondo et al., 2011). Droughts and other stress (affecting the canopy development, closing of stomata and altering) are undesirable. The soil water content is directly influenced by changing rainfall patterns and rising temperature that augment evapotranspiration. The combined effect of an increase of the crop production by increase in CO_2 concentration and decrease of the production as a result of weather conditions have to be understood well.

Crop yield studies can be carried out by running field experiments to assess yield response to environmental factors. But it will take many years for valid recommendations because we require lots of field weather conditions, different crop species, soil conditions, different management and irrigation treatment. So instead of conducting field experiment over many years we run small number of field experiments, capture few sets of conditions and use crop simulation models, calibrate and validate it for specific crops, soil type, atmospheric conditions and use that model to

run lots of simulations for different climates, soil conditions, management practices and irrigation water supply conditions with the help of crop modelling software.

2.3.1 Crop modeling

Crop models are able to quantitatively simulate crop physiological processes on a daily basis. Many mathematical models were developed for crop simulation during the 1960s by several research groups. Depending upon the purpose and objective of the crop model, we can distinguish two modeling approaches: scientific and engineering. Scientific approach mainly aims at improving our understanding of crop behavior, its phenology, and its response to environmental changes. It is also meant to be more mechanistic, based on laws and theory on how the system functions. It is useful to formulate innovative technologies for agricultural crop production. Scientific models need relatively complicated input parameters which are not easily available and also are restricted to specific crops, hence are not used widely for different crops and locations. DSSAT, APSIM, WOFOST, CropSyst, EPIC Model, etc. are examples of scientific models (Shrestha, 2014). On the other hand, the engineering modeling approach attempts to provide robust management advice to farmers or predictions to policy makers (Passioura, 1996). It is meant to be functional, based on the mixture of well-established theory and robust empirical relationship. CROPWAT (Smith, 1992), BUDGET (Raes et al., 2006), AquaCrop (Raes et al., 2009; Steduto et al., 2009), etc. are examples of some engineering models widely used for different crops and locations. Unlike other crop models (i.e., radiation-driven or carbon-driven growth engine), AquaCrop model is water driven growth engine model, which is simple, robust and accurate (Steduto et al., 2009). This model has been widely applied in precision agriculture practices such as crop monitoring, intelligent irrigation management and yield prediction before harvest (Foster et al., 2017). For our research AquaCrop will be used for crop simulation.

2.3.2 AquaCrop

AquaCrop model is a water driven growth engine model developed by the Land and Water Division of FAO which describes the interaction between the plant and soil. AquaCrop simulates yield response to water of herbaceous crops under different biophysical and management conditions and is particularly suited to address conditions where water is a key limiting factor in crop production. It is a point-based model, i.e., we are interested in fields in which plants are cultivated. Due to its simplicity, accuracy and robustness, this model has been widely applied with acceptable accuracy in agriculture practices such as crop monitoring, intelligent irrigation management and yield prediction before harvest. AquaCrop uses only a relatively small number of explicit parameters and mostly intuitive input-variables which are commonly available input requiring simple methods for their determination. On the other hand, the calculation procedures are grounded in basic and often complex biophysical processes to guarantee an accurate simulation of the response of the crop in the plant-soil system (Book, 2016). The interaction between plant and soil is strongly dependable on the conditions in the soil. Also, the system has to be link to the outside world. At an upper boundary, AquaCrop looks at the weather conditions, rainfall, evaporating power of atmosphere (ET_0), and CO_2 concentration. At the lower boundary AquaCrop considers groundwater table (GWT) to which water from system will drain or if GWT is at shallow depth, water can move upward by capillary rise action from water table to the subsoil. Soil-plant interaction is also affected by field management such as soil surface practices, level of fertility and irrigation management. This process described by the AquaCrop is shown in **Figure 2.2**.

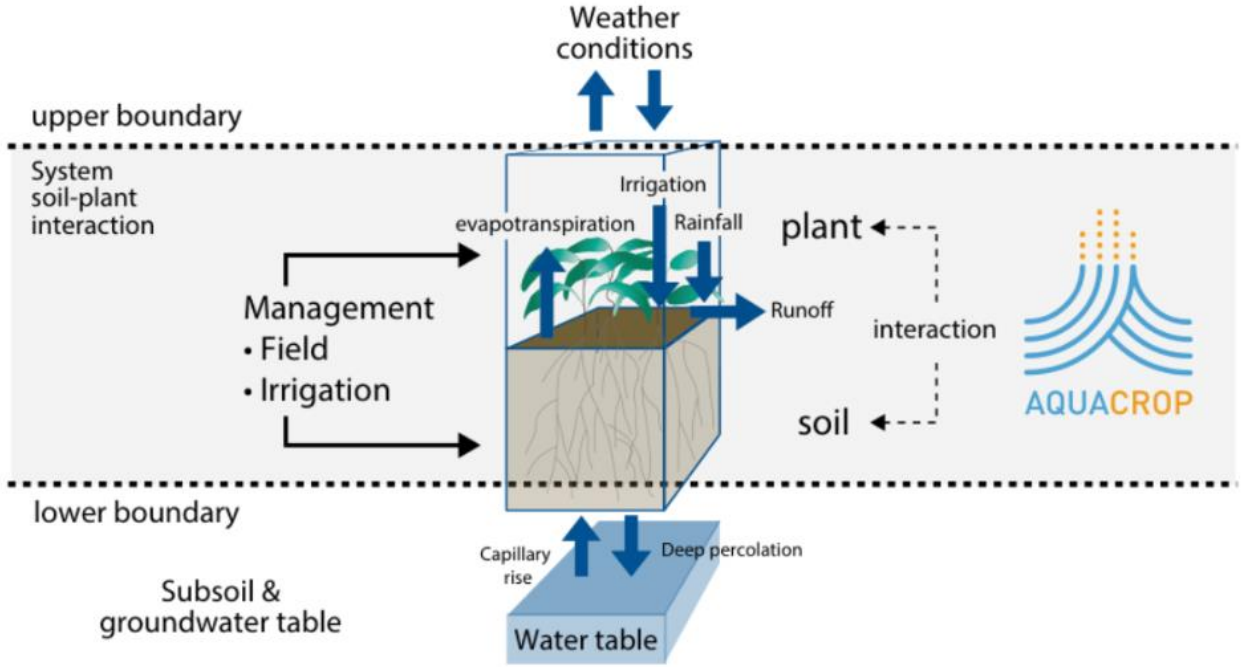

Figure 2.2: Soil-Plant Interaction System described by AquaCrop (Salman et al., 2021)

Inputs consist of weather data, crop and soil characteristics, and management practices that define the environment in which the crop will develop. Outputs consist of simulations of crop canopy development response to water, biomass production, yield response water, soil water and salt balances (FAO) (**Figure 2.3**).

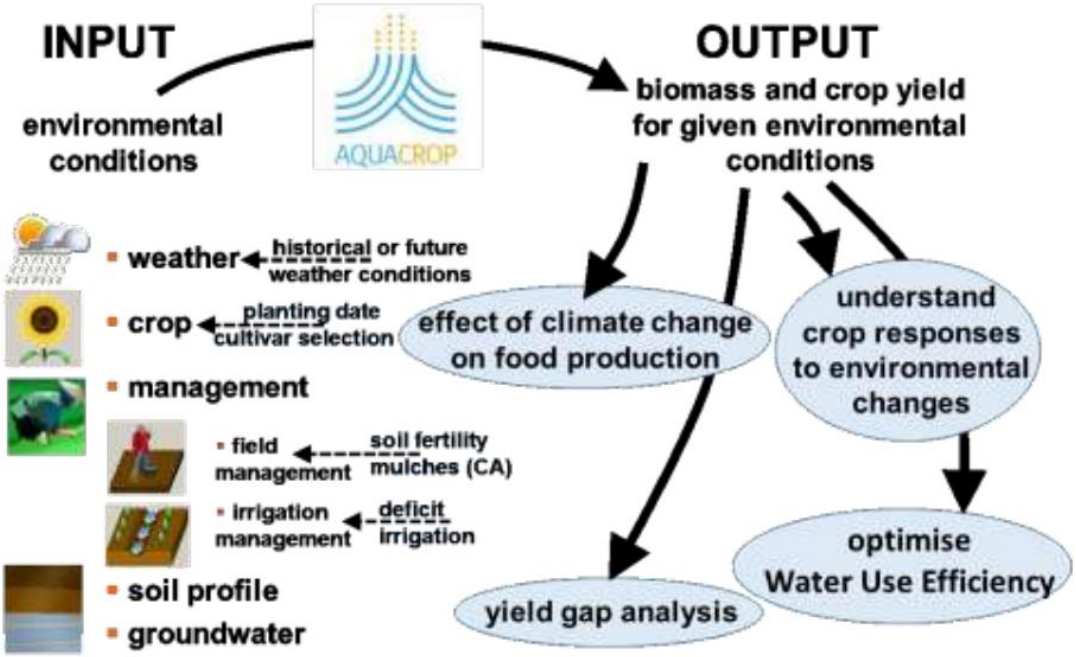

Figure 2.3: Input and output parameters of AquaCrop(FAO, 2017)

A. Benefits of AquaCrop

Most of the crop simulation models require highly detailed input data and information about crop growth that are not available in most locations worldwide. This limitation is addressed by the AquaCrop model, it requires a relatively small number of explicit and mostly intuitive parameters

that can be determined by simple methods. AquaCrop has its distinct feature than other crop models, some of its unique features are green canopy cover is used to simulate canopy expansion whereas many crop models use leaf area index. This feature of AquaCrop is advantageous as simulated output can be used to relate directly to the easily accessible data obtained from field observation and satellite image (remote sensing). For example, NDVI (Normalized Difference Vegetation Index) for data obtained from satellite observation on earth correlates strongly with fractional green canopy cover and can be used to calibrate and validate simulated output of AquaCrop (Raes et al., 2009). AquaCrop considers an inclusive range of water stress impacts on transpiration than most other water-driven crop models. In addition to stomata closure, leaf expansion reduction and early canopy senescence are also considered for water stress impacts on transpiration. Finally, AquaCrop considers an often-changing effects of a range of environmental stressors, concisely water and temperature, on crop nourishment, and encapsulate the impact of elevated atmospheric carbon dioxide concentrations on crop water productivity (Foster et al., 2017). Moreover, AquaCrop also considers the effect of soil fertility and soil salinity by indirect approach based on relative biomass obtained in field observation under different fertility levels and soil and water salinity condition (Foster et al., 2017).

B. Practical applications of AquaCrop

AquaCrop is a crop-water productivity model that can be used in both rain-fed and irrigated agriculture under different environmental conditions. The practical applications of AquaCrop are listed below:

- Understand the crop response to environmental changes (Book, 2016).
- Analyze the yield gap in which we compare the actual yield cultivated in a field, farm or a region with potential yield that can be obtained in that environment.
- Optimize ET water productivity by adjusting the planting date, cultivar selection, field management practices (e.g., Soil fertility, mulches) or irrigation strategies e.g., deficit irrigation.
- Calculate the irrigation water requirements for designing irrigation scales and generating irrigation schedules.
- Helps farmers to select crops for available water supply.
- Study the effect of climate change on agriculture by calibrating and validating AquaCrop for past historical climatic data and running it for future climate projection data.
- Make scenarios for policy makers (water administrators and managers, economists, policy analysts and scientists)(Book, 2016).

2.3.3 Input data requirement of AquaCrop

AquaCrop requires a relatively small number of explicit parameters and mostly intuitive variables. Those parameters are either commonly available or require a very simple method for their determination. Simulation of AquaCrop model requires input data consisting of weather data, specific crop type, soil profile and field and irrigation management data (**Figure 2.4**). However, AquaCrop contains a complete set of input parameters in the database of the model that can be selected for a particular crop and adjusted for different soil or crop types, fine-tuned to the local condition.

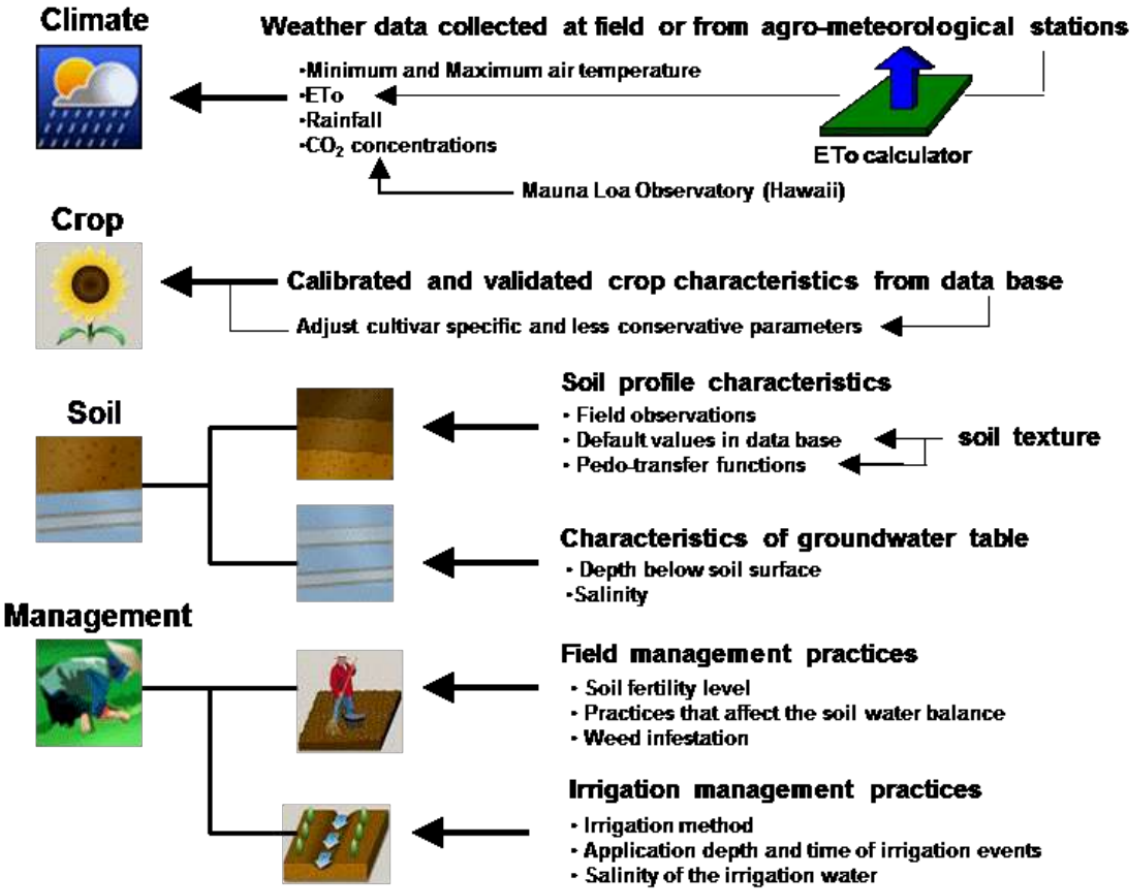

Figure 2.4: Input parameters required for AquaCrop.(FAO, 2017)

A. Climatic data:

The weather data required by the AquaCrop are reference evapotranspiration (ET_0), minimum and maximum air temperature, rainfall and mean annual CO_2 concentration. Air Temperature is used to calculate growing degree days which determines the crop development and phenology. Rainfall and ET_0 are determinants of water balance of the soil root zone, air CO_2 concentration affects crop transpiration and biomass production. ET_0, Tmax, Tmin and rainfall are derived from typical records of agrometeorological stations, and the air CO_2 concentration is the annual mean measured by the Mauna Loa Observatory in Hawaii. The past, since 1902 and current CO_2 concentration values are stored in the AquaCrop database while those for future years need to be entered by the users. By using other CO_2 files with projected atmospheric composition for the future, crop response for climate change scenarios can be tested. Climatic data can be entered daily, ten-daily or monthly. However, AquaCrop will need daily data since AquaCrop simulates daily time steps. In AquaCrop there are procedures which convert ten days or monthly data to daily data. The larger the aggregation of the imported data, the less reliable the outcome is (Book, 2016).

Reference evapotranspiration (ET_0) expresses the evaporating power of the atmosphere at a specific location and time of the year, and it determines the rate of crop transpiration and soil evaporation. ET_0 considers evapotranspiration (crop transpiration + soil evaporation) from a reference hypothetical grass surface with an assumed height of 0.12m, albedo (the part of solar radiation gets reflected) 23%, surface resistance (rs) 70s/m which is resistance for well-watered crop, and aerodynamic resistance (ra) $208/U_2$ where U_2 is wind speed at 2m height (**Figure 2.5**).

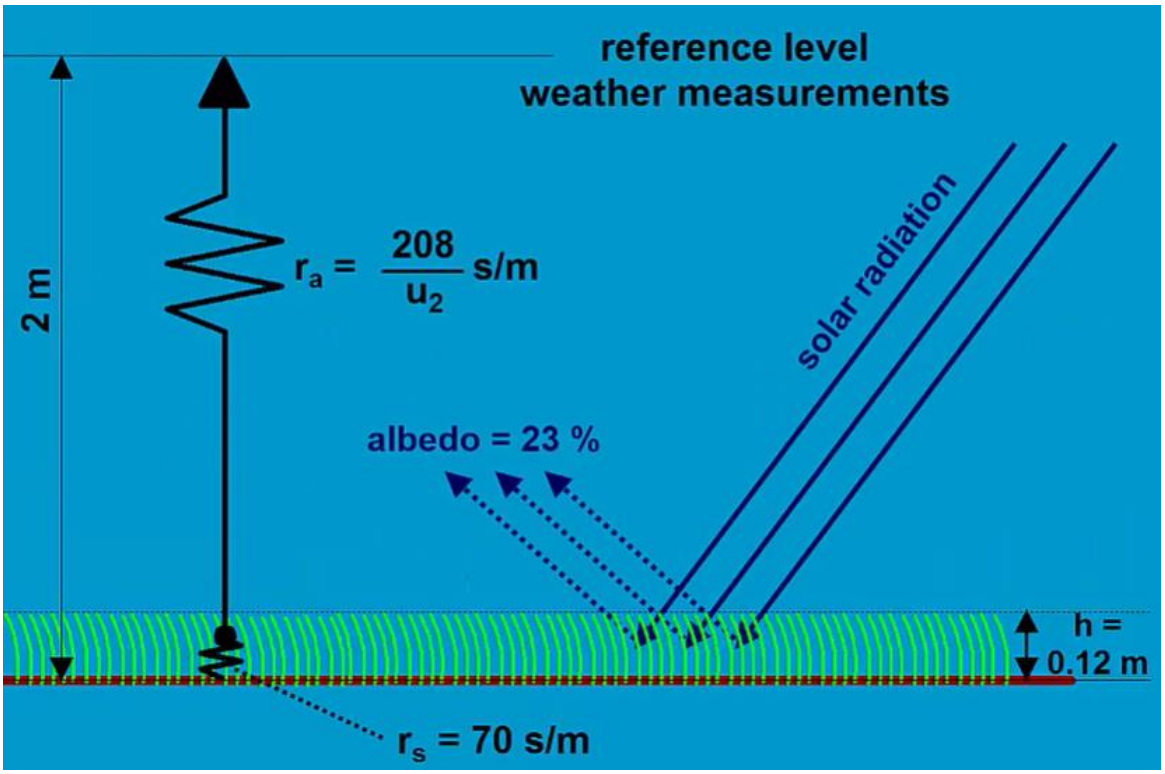

Figure 2.5: Reference level weather measurements (Food and Agriculture Organization of the United Nations, 2016c)

AquaCrop consists of an ET_0 calculator based on FAO Penman-Monteith equation which requires meteorological data to compute reference evapotranspiration ET_0. ET_0 calculator can handle daily, ten-day and monthly climatic data. The data can be given in a wide variety of units and climatic parameters.

$$ET_0 = \frac{0.408 s_c \frac{-R_n - Q_G}{86400s} + \frac{\gamma 900 u_2 (e_s - e_a)}{T + 273}}{s_c + \gamma(1 + 0.34u_2)} \qquad 2.9$$

Where,

ET_0 = reference evapotranspiration [mm/day],
R_n = net radiation at the crop surface [MJ/m^2/day],
Q_G = soil heat flux density [MJ/m^2/day] which can be neglected (Q_G=0),
T = mean air temperature [°C],
u_2 = wind speed measured at 2 m height [m/s],
e_s = saturation vapor pressure [kPa],
e_a = actual vapor pressure [kPa],
e_s-e_a = saturation vapor pressure deficit [kPa],
s_c = slope vapor pressure curve [kPa/°C],
γ = psychrometric constant [kPa/°C].

This Equation 2.9 requires information about energy sources like radiation and air temperature. Energy sources will quantify vaporization of liquid water, and it requires aerodynamic terms like air humidity and wind speed that will quantify vapor removal. Additionally, station characteristics like latitude for the computation of the extra-terrestrial radiation (ra) and the maximum hours of

bright sunshine (day length) and altitude in meters above sea level to compute the psychrometric constant (γ) are required.

B. Crop parameters:

There are two types of crop parameters in AquaCrop: conservative and non-conservative. Conservative crop parameters are crop specific which do not change with time, management practices, geographic location, climate, or cultivars while non-conservative crop parameters which are cultivar specific are affected by field management, planting mode, condition in the soil profile, climate etc. In the database of AquaCrop FAO has calibrated and validate the series of crops, when loading specific crop, we do not need to calibrate the conservative parameters as they are valid for all cultivars and in all environments also they have been calibrated with crop data grown under favorable and non-limiting conditions, but remain applicable for stress condition through their modulation by stress response function. However, the user has to specify the non-conservative parameter for the local condition in which crop is grown. For the field experiments canopy development are measured in terms of growth stages, green canopy cover, effective root length, and aboveground biomass on biweekly basis by plucking two plants per plot (Abedinpour et al., 2012). For this research crop parameters will be collected from farmer field experiments conducted in the study area. Data require to tune the crop parameters are:

- Types of planting method.
- Transplanting date.
- Number of Plants transplanted per m^2.
- Size of canopy cover per seedling.
- Time to reach 90% emergence.
- Maximum canopy cover
- Time to reach maximum canopy cover.
- Date of flowering after DAP.
- Duration of flowering.
- Date of Senescence
- Date of Maturity

C. Soil parameters:

Data pertaining to the soil of experiment site required as input parameters for AquaCrop are number of soil horizons, soil texture, field capacity (θ_{FC}), permanent wilting point (θ_{PWP}), saturated hydraulic conductivity (K_{sat}) and volumetric water content at saturation (θ_{sat}). AquaCrop provides indicative values for different soil textural classes. Users can either use its indicative values or derive the data from soil texture content (sand, silt, clay) with the help of pedo-transfer function using SPAW model (Shrestha et al., 2014). Also, after specifying the soil data, AquaCrop estimates the Curve Number (CN) and readily evaporable water (REW) automatically.

D. Irrigation and Field Management:

Irrigation and field management during the experiment are two important components considered in the AquaCrop model. Irrigation management comprised data pertaining to both the situations of rain-fed and irrigation. Irrigation management specifies the irrigation method (determines what fraction of soil surface is wetted) amount (How much?) and events (When to apply?) along with the water quality. In AquaCrop we can specify events applied in the field and we can generate the

schedule based on time criteria and depth criteria. Time criteria can be of several types: (a) when the root zone depletion reaches a specific threshold expressed in mm or as %RAW (Readily Available Water); (b) at a fixed interval (useful in case of rotational method of irrigation among irrigation groups) which can change during the season and might become shorter when the weather becomes hotter, and the crop is more developed; (c) when the layer between bunds drops below a minimum level in case of paddy rice irrigation. Water layers vary during the growing cycle. It may be small at transplanting and then gradually increase throughout the season. While depth criteria are of two types. In the back to field capacity criteria, we can even specify an extra amount of water that has to be added above or below field capacity. In the fixed application dose, only the net application has to be specified. These criteria are selected in function of local practices, soil and crop parameters and irrigation method. We can also use indicative values for irrigation interval and application depth as shown in **Figure 2.6**.

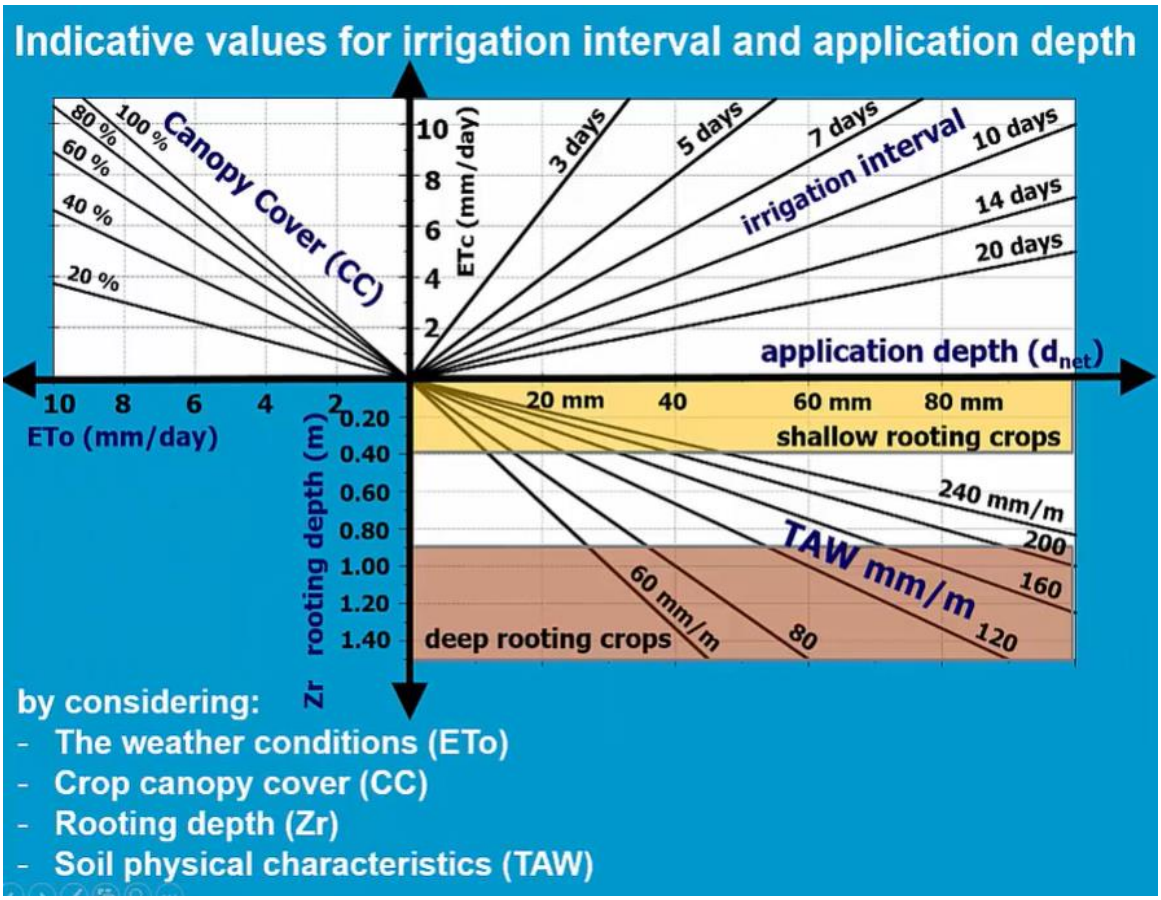

Figure 2.6: Indicative values for irrigation interval and application depth(Food and Agriculture Organization of the United Nations, 2016b)

Field management specifies field surface practices, mulches, soil fertility and weed management. Field surface practice is the estimate of surface runoff and practices affecting surface runoff. Surface runoff is simulated in AquaCrop by the curve number method. AquaCrop considers infiltration rate to determine curve number; curve number and infiltration rate vary inversely. Mulches reduce soil evaporation. The user has to specify soil cover and type of mulch. Depending upon the type of mulch, the reduction in evaporation will be different. Soil fertility level is specified in the field management in terms of relative biomass but how the crop reacts to fertility stress is however a crop parameter and thus it is calibrated in the crop file. Crop development and its production also gets affected by the weeds through competition for the available resources such as

light, water, and nutrients. In AquaCrop, the effect of weed competition is simulated in a simple way by considering the effect on green canopy cover and crop transpiration (Salman et al., 2021).

2.3.4 Calculation scheme of AquaCrop

AquaCrop considers four steps to simulate the final crop yield that are easy to understand and elucidate modeling approaches. The four steps (which run in series at each daily time step) consist in the simulation of:

A. Development of Canopy Cover

Crop development considers how crops grow above ground, canopy of the crop expands, production of biomass and root system below ground in the soil. In terms of canopy development this is where a crop diverges a little bit from the number of other models, lots of model use Leaf Area Index (LAI) for the modeling of canopy development, but AquaCrop models canopy development in terms of green canopy cover. The green canopy cover (CC) is the soil surface covered by the green canopy per unit ground surface area. It provides quick and accessible source of data for calibrating the model and it ranges from zero (bare soil) or at sowing (0 % of the soil surface covered by the canopy) to a maximum value at mid-season which can be 1 when a full canopy cover is reached (100 % of the soil surface covered by the canopy).

Canopy development for non-limiting conditions is described in AquaCrop with only a few crop parameters: maximum canopy cover, logistic type equation and senescence (**Figure 2.7**).

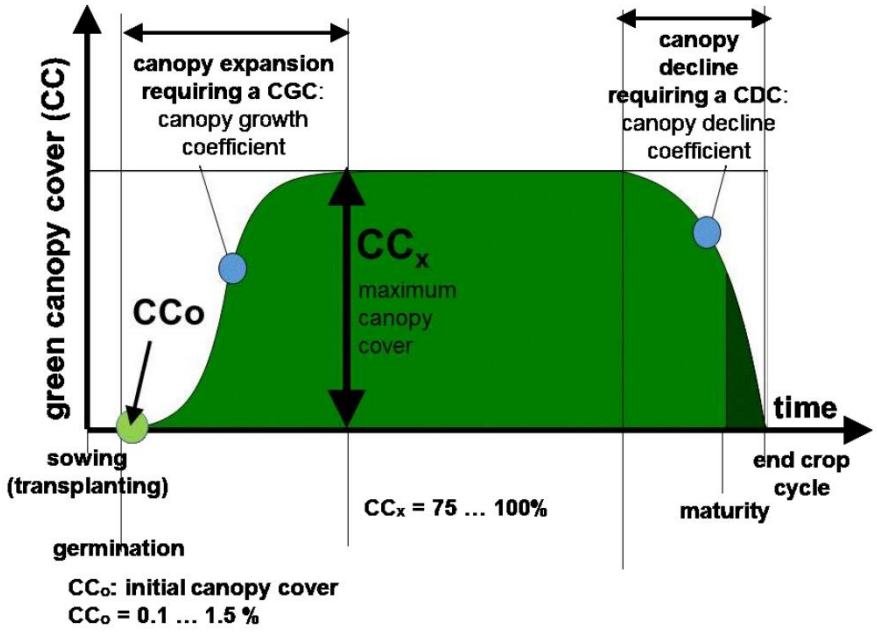

Figure 2.7: Canopy Development for non-limiting condition(FAO, 2017)

The initial canopy cover at the germination (CCo) i.e., canopy cover at 90% emergence which is plant density times size of the canopy cover per seedling is very small (are generally around 1%). After the germination period canopy cover (CC) increases logistically till it reaches maximum canopy cover. Logistical increment of the canopy cover is described by the canopy growth coefficient. In the mid-season canopy cover reaches its maximum value. Once the CCmax is reached, CC remains constant. Maximum Canopy cover (CCx) varies with crop type and planting

density (generally around 75% up to 100%). When plant density is dense CCx is likely to be 100% and if plant density is thin or rare, CCx will be much smaller. In the late season natural senescence of the crop occurs and green canopy cover declines exponentially which is described by a Canopy Decline Coefficient (CDC). By adjusting daily, the soil water content in the soil profile, AquaCrop keeps track of the stresses which might develop in the root zone. To keep track of the soil water content in the root zone (Wr) and the soil water stress, AquaCrop updates the soil water balance at each daily time step (Salman et al., 2021). In a schematic way root zone is depicted as a reservoir in which water content varies depending on the input (rainfall, irrigation, capillary rise)and output(deep percolation, surface runoff, crop transpiration, soil evaporation) of water. If there is lots of rainfall or irrigation, water content in the root zone will increase and will come above Field Capacity (FC). This will result in deep percolation. While in the absence of rainfall, irrigation water content (WC) in the root zone drops and crops become under stress. AquaCrop considers three thresholds in the reservoir. When water level drops below a threshold, crop water stress starts to develop. Soil water stress might affect the leaf and hence canopy expansion and if severe might trigger early canopy senescence; The effect of soil water stress on canopy cover is described by two water stress coefficients KSexp,w and KSsen. When the water content drops below leaf expansion threshold, the value of KSexp,w becomes smaller than 1 and canopy expansion becomes slow. Moreover, when the water content in the root zone drops below threshold for canopy senescence, KSsen becomes smaller than 1 and canopy decline is triggered. Similarly, when water level drops below threshold of stomata closure, it causes reduction in crop transpiration by reducing Ks value to less than 1 which is the description of scheme 2. i.e., the lower the soil water content below the threshold, the stronger is the water stress (Salman et al., 2021).

So, considering the stresses at any day of the season, AquaCrop will simulate the actual canopy development which is of course quite different from the development under non-limiting conditions (see **Figure 2.8**). The same thing is true for the root development where other stress levels determine the root zone expansion.

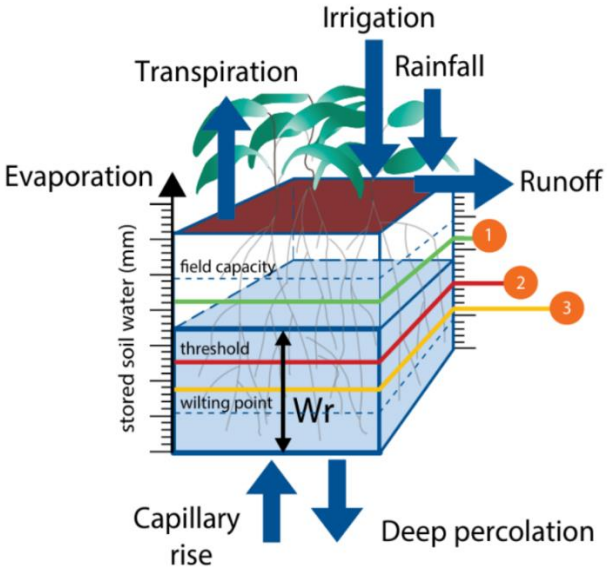

Figure 2.8: Root zone depicted as a reservoir with the indication of thresholds, where the green, red and yellow line represents canopy expansion threshold, stomatal closure and canopy senescence threshold respectively.(Salman et al., 2021)

When simulating crop development, AquaCrop describes the development, expansion of canopy cover which is above ground level as well as development of the root below the ground level. Root development starts during the half of the time period of 90% emergence; however, its effectiveness in the soil water balance calculation occurs only after the period of 90% emergence and corresponding rooting depth is called minimum effective rooting depth (Zn) (Raes et al., 2009). The expansion rate is affected by soil physical (temperature, mechanical impedance, aeration) and chemical characteristics (pH, salinity, high levels of aluminum or manganese). Water stress also affects the root zone expansion when water level drops below stomata closure, as such less CO_2 can be taken up and less root mass can be developed which ultimately causes the slower rate of root zone expansion. Root deepening is slow in soil layer with low penetrability but below the restrictive layer expansion rate is normal again (**Figure 2.9**).

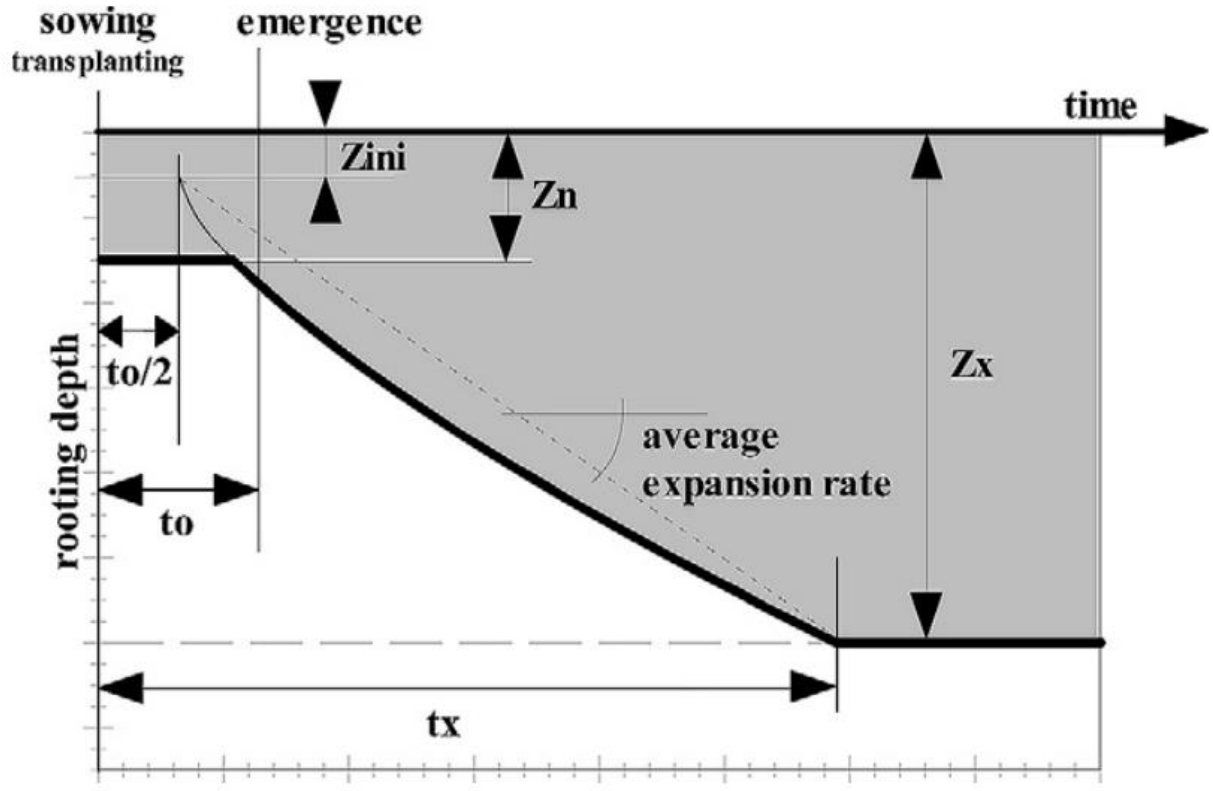

Figure 2.9: Schematic representation of a generalized rooting depth development with time.(Steduto et al., 2009)

Crop development can be specified in calendar days or growing degree days (GDD). The development of green canopy cover and deepening of the root system are simulated as the function of time. When running AquaCrop in growing degree days (GDD), the heat units accumulated during a day which is calculated by subtracting the base temperature (Tbase) from the average air temperature (Tavg) are used to adjust the expansion of green canopy cover and deepening of the root system. Where Tbase is temperature below which crop development does not progress (Hsiao et al., 2009). It is a conservative parameter. If the average temperature (Tavg) is below the base temperature (Tbase), no heat units can be accumulated during that day and GDD is zero. In AquaCrop an upper threshold temperature (Tupper) is considered as well above which there is no additional benefit for the growth of the crop. The idea of switching from calendar mode to thermal

mode is to adjust the length and duration of development stages to the temperature regimes of the distinctive years.so if we plant in another year or we plant at another day the temperature regimes during the crop cycle will be different in a such the length and duration of the development stages will be different as well. By running AquaCrop into thermal time, AquaCrop will automatically adjust calendar mode to temperature regime of the year.

B. Crop Transpiration

For well-watered soil, Trx (Transpiration for well water condition) is calculated by multiplying the reference evapotranspiration (ET_0) with a crop coefficient (KcTr). The crop coefficient is proportional to CC and hence varies throughout the life cycle of the crop in correspondence with the simulated canopy cover. In mid-season the canopy ages slowly and undergoes reduction in crop transpiration and photosynthesis capacity. Once senescence is triggered the reduction in transpiration becomes stronger. And crop transpiration coefficient (KCTr) is crop coefficient for maximum crop transpiration (KCTr-x) times the canopy cover adjusted for micro advective effects (CC*). Advective effects cause Tr (transpiration) to be more just proportional to CC and soil evaporation less as it is proportional to the (1-CC) i.e. uncovered soil. Actual crop transpiration (Tr) is Transpiration for well water condition (Trx) times stress coefficient (Ks). Here the stress coefficient considers water stress and soil salinity stress. In AquaCrop water stress can develop due to shortage of water; this results in stomata closure and it is described by the water stress coefficient for stomata closure (KSsto) (shown in **Figure 2.10**). AquaCrop also describes the effects of excess water i.e. when there is too much water in the root zone, water logging problem arises and there will be deficient aeration condition and this effect is described by the water stress coefficient for water logging (KSaer) (shown in **Figure 2.11**).

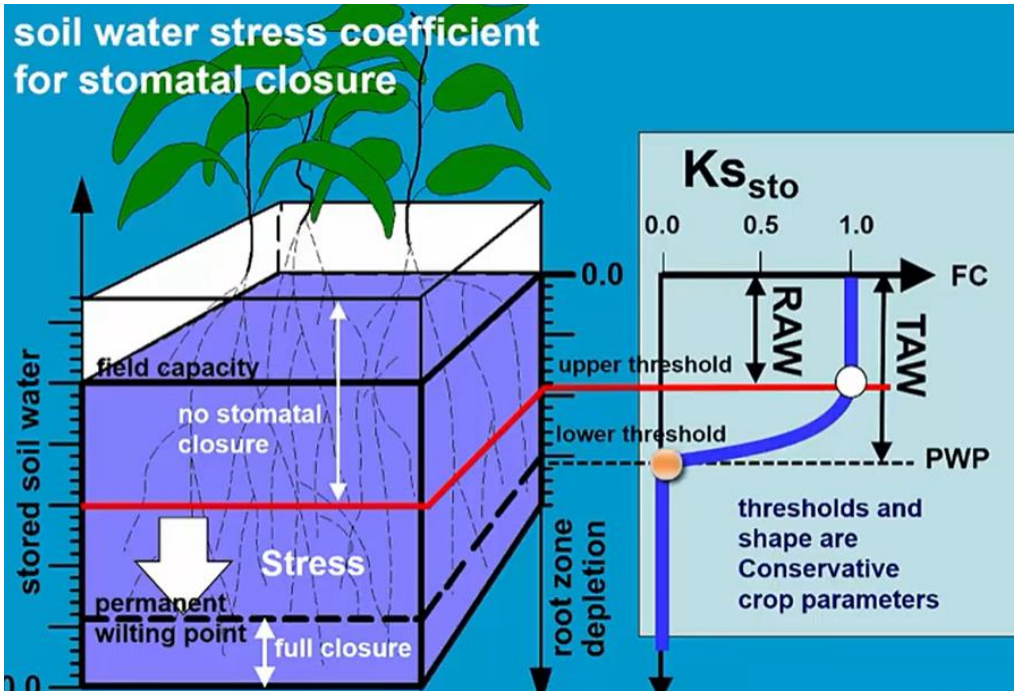

Figure 2.10: Soil water stress coefficient for stomatal closure(Food and Agriculture Organization of the United Nations, 2016a)

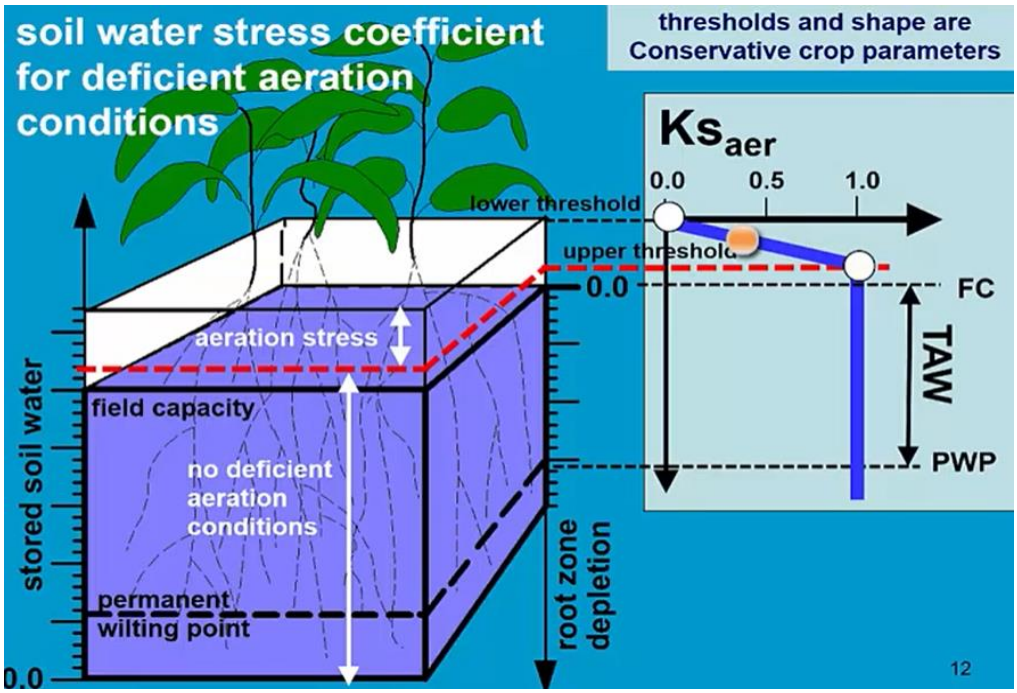

Figure 2.11: Soil water stress coefficient for deficient aeration conditions(Food and Agriculture Organization of the United Nations, 2016a)

An overview of all factors affecting simulation of crop transpiration are shown in **Figure 2.12**.

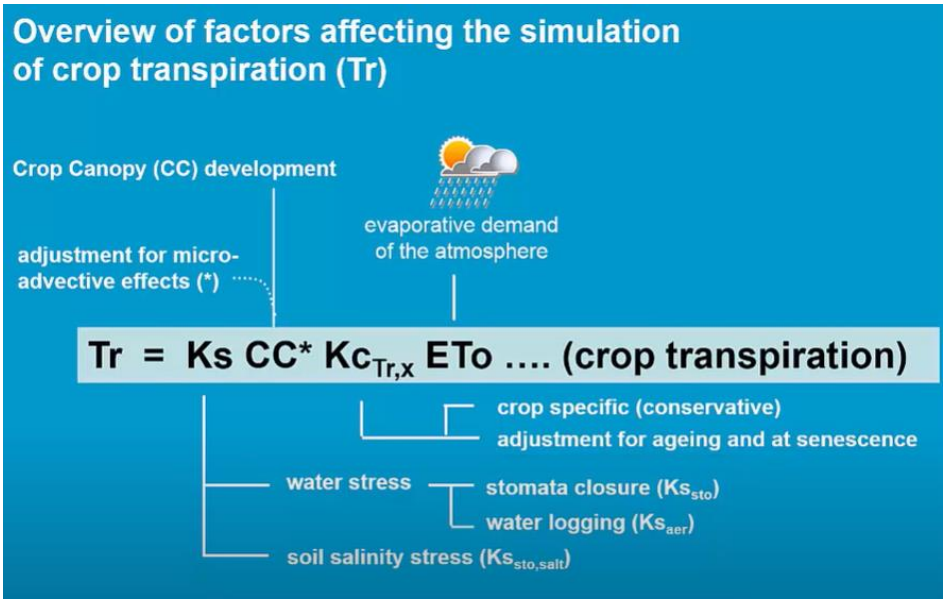

Figure 2.12: Factors affecting crop transpiration.(Food and Agriculture Organization of the United Nations, 2016a)

C. Above-Ground Biomass

In AquaCrop, distinction made between crop transpiration and soil evaporation. Crop takes up water by the roots and that water is transported to the leaves where it escapes as water vapor through the stomata. The same pathway is used to take CO_2 and by photosynthesis in the presence of sunlight, CO_2 will be converted to carbohydrates which is the building block of biomass (**Figure 2.13**). So, there is a direct link between crop transpiration and biomass production.

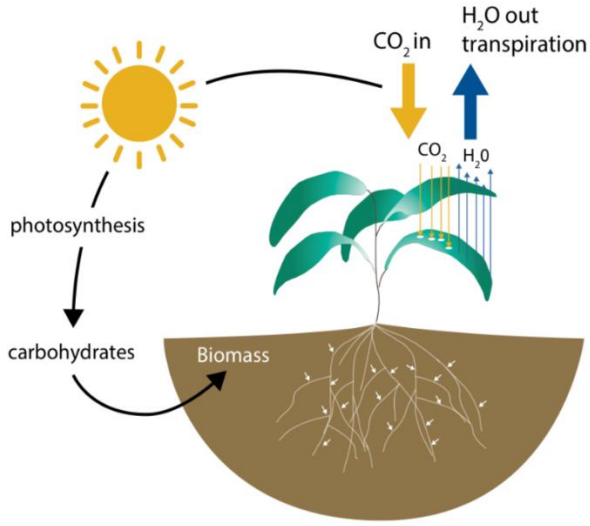

Figure 2.13: Photosynthesis process where CO_2 and available water get converted to carbohydrates (Salman et al., 2021)

The above ground biomass produced is proportional to the cumulative amount of crop transpiration (ΣTr). The direct relationship between crop transpiration and biomass production is given by biomass water productivity (which gives the slope of the line in the transpiration biomass curve). There exists a stable and conservative nature between biomass and cumulative transpiration for given climatic conditions and location. In diverse climatic conditions the slope of the line differs so AquaCrop normalizes the water productivity (WP*) for the climate, that normalization is done by dividing the daily amount of water transpired by the daily amount of ET_0 which is valid for diverse locations and seasons. Normalization is valid for specific CO_2 concentration i.e., reference CO_2 concentration of atmosphere (369.41 ppm which is CO_2 concentration in the year 2000). An adjustment of WP* CO_2 concentration in other years is done by multiplying with a correction factor (fCO_2). The correction factor depends on the ratio of and difference between [CO_2] in the arbitrary reference year (year 2000) and in the year when the crop is grown (Vanuytrecht et al., 2014). The correction factor is larger than 1 for the higher CO_2 concentration compared to 2000, and smaller than 1 for lower CO_2. Another adjustment of WP* considers the difference between production in vegetative and yield formation stages for particular crops. This adjustment of WP* accounts for differences in chemical composition of vegetative biomass and harvestable organs. Typically for the crops which make oil or products that are rich in lipids or proteins, lots of carbohydrates is needed to make that product as such the relationship between transpiration (the uptake of CO_2) and biomass production will become smaller during the yield formation. This effect is simulated in AquaCrop by multiplying WP*, in the yield formation stage, with a reduction coefficient (fyield). The WP* and the adjustment in the yield formation stages are conservative crop factors which the user has not to tune to the environment (**Figure 2.14**).

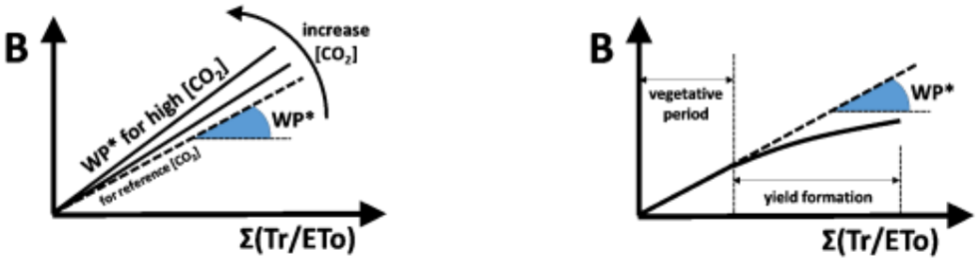

(a) **(b)**

Figure 2.14: The effect of (a) [CO_2] on biomass production and (b) Synthesized production on WP*(FAO, 2017)

Along with this normalization Biomass production is reduced due to fertility stress (KSwp) and cold stress (Ksb). When air temperature or GDD fall below upper threshold Ksb becomes less than 1 which cause WP*adj <WP*(WP*adj=Ksb times WP*) and ultimately less biomass production. Stress coefficient for lower temperature integrates the effect of low temperature, reduced light intensities and shorter days. And Biomass production response to soil fertility will be discussed later in the calibration of soil fertility.

An overview of factor affecting the simulation of the ground biomass production (B) is shown in **Figure 2.15**.

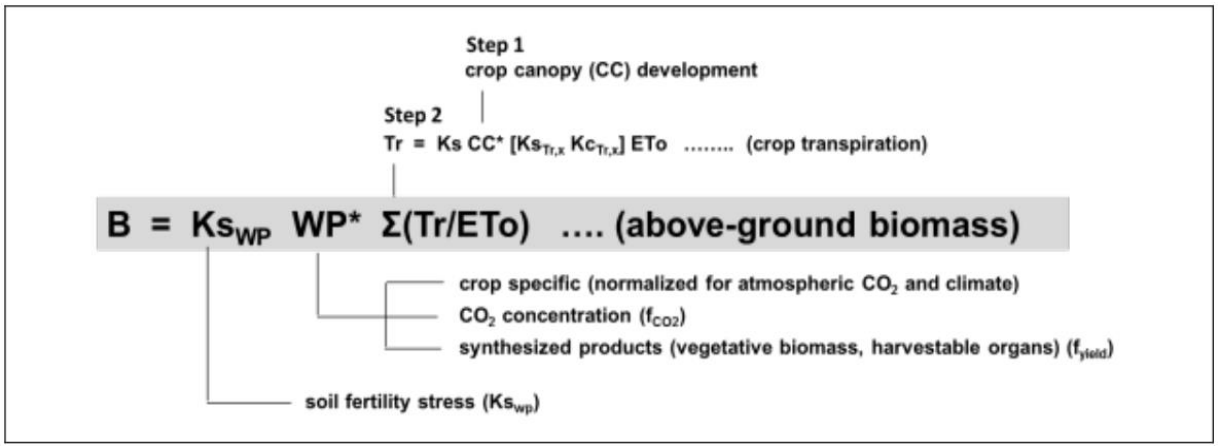

Figure 2.15: Ground Biomass Production (B)(FAO, 2017)

D. Crop Yield

The simulated above ground biomass (B) integrates all photosynthetic products (stem, leaves, flowers, grains) assimilated by the crop during the season. By using a Harvest Index (HI), which is the fraction of B that is the harvestable product, crop yield (Y) is obtained from B. During the season the harvest index might vary from reference value. The variation depends upon the timing and extent of water and heat stresses. The actual HI is obtained by adjusting, during simulation, the reference Harvest Index (HIo) with an adjustment factor for stress effects. Adjustment factor could be greater than one or less than one, it depends on the timing of stress and its severity. Positive effect on the Harvest index occurs when water stress affects the leaf growth (i.e., KSexp<1) and it is only possible when vegetative grow is still possible, for this we must distinguish between the determined crop and undetermined crop. When water stress affects leaf growth and

stomata closure (KSsto<1) are not closed yet, then carbohydrate is used to fill the grains instead of making new leaves. This results in positive adjustment of the harvest index. The adjustment depends on the magnitude of the stress, crop type (conservative crop parameters) and the length of the period of potential vegetative growth which is limited for the determined crops but can extend till senescence for the undetermined crops. However, when during the yield formation water stress effect stomata closure, less CO_2 can be taken up, less carbohydrates can be produced and as such there is less material to fill the grains, and this results in a decline of HI. During flowering water stress and temperature stress might result in a failure of pollination (KSpol) as such there will be less flowers thus HI might go down. Actually, the crop makes too many flowers, there is always an excess of flowers which are not necessary to make potential fruits. When there is stressed period, it can be water stress; it can be cold or heat stress, the impact on the harvest index depends on the number of flowers which were not pollinated, if at the end of the flowering, sufficient flowering was still pollinated to have potential fruits then HI is not affected. However, when the stress period is long and severe the total amount of flowers which were pollinated might not be sufficient to have potential fruits, at that moment the HI will decline. AquaCrop keeps track of daily values of KSexp, KSsto and KSpol and integrates their effect on HI in a single adjustment for HIo.

During Yield formation HI gradually increases, it is zero at flowering and then after a small lag phase it linearly increases till physiological maturity. The building up of the HI is simulated differently depending on the type of crop. For fruits and grain producing crops it starts from flowering and then linearly increases till physiological maturity. For roots and tuber crops, it starts from the tuber formation and the shape of increased HI is different from linear, and for leafy vegetables crops, it starts from the germination and very quickly the reference HI is reached (**Figure 2.16**).

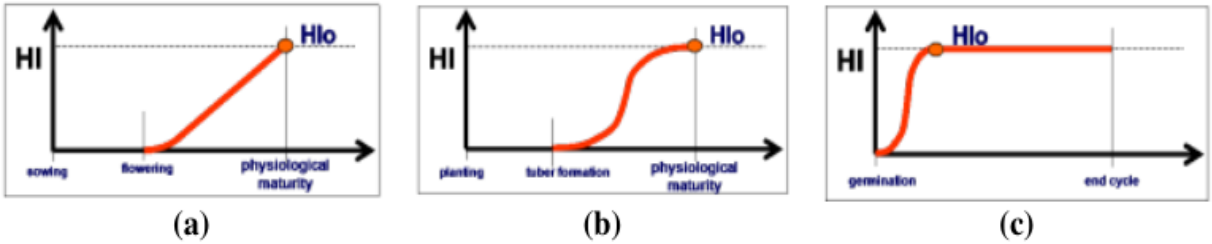

Figure 2.16: Building up of the harvest index for (a) fruits and grain producing crops, (b) root and tuber crops, and (c) leafy vegetables.(FAO, 2017)

Although HIo is conservative crop parameters, when water stress triggers the senescence, it needs to be adjusted because there will be insufficient green canopy cover to reach HI and there will be no sufficient energy to fill the grains. Therefore, HI which is reached at the end of the crop cycle might be smaller than HIo as shown in **Figure 2.17**.

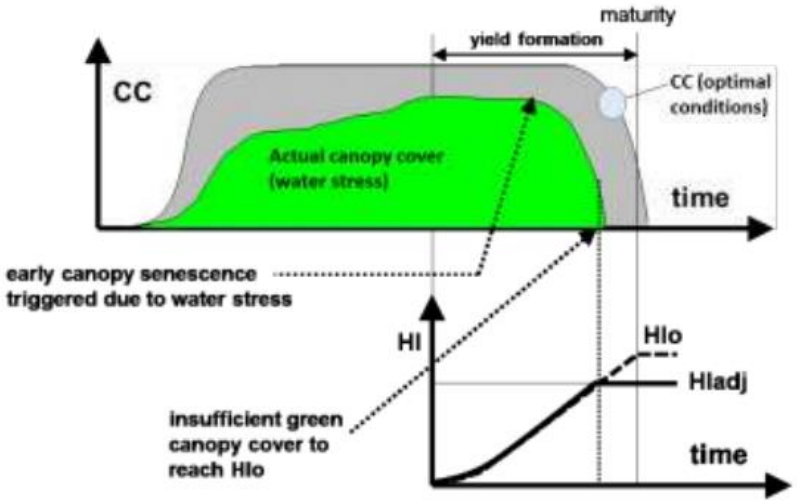

Figure 2.17: Adjustment of HIo for insufficient green canopy cover(FAO, 2017)

An overview of final crop yield is shown in **Figure 2.18**.

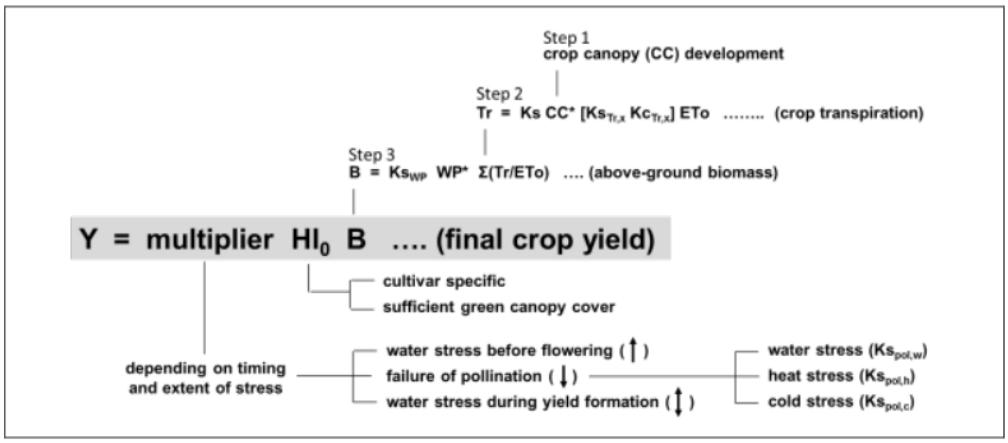

Figure 2.18: Factors affecting the simulation of the final crop yield.(FAO, 2017)

The overall process considered by the AquaCrop for the simulation process is depicted in **Figure 2.19**.

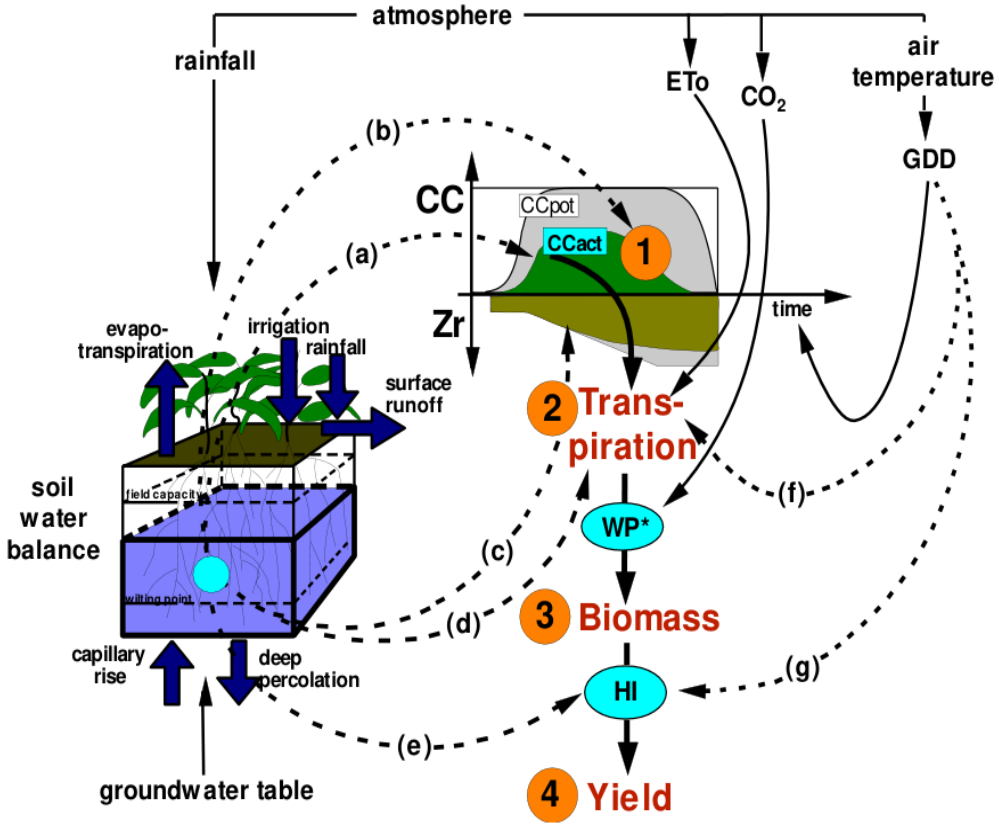

Figure 2.19: Calculation Scheme of AquaCrop with indication of the four steps, and the process (dotted arrows) affected by water stress (a to e) and temperature stress (f to g). (FAO, 2017)

CC is green canopy cover; Zr, rooting depth; ET_0, reference evapotranspiration; WP*, normalized biomass water productivity; HI, harvest index; and GDD, growing degree day. Water stress: (a) slows canopy expansion, (b) accelerates canopy senescence, (c) decreases root deepening but only if severe, (d) reduces stomatal opening and transpiration, and (e) affects harvest index. Cold temperature stress (f) reduces crop transpiration. Hot or cold temperature stress (g) inhibits pollination and reduces HI.

2.3.5 Crop Response to Fertility stress

Deficiency in fertility level on the soil causes smaller canopy cover and decrease of the biomass water productivity (WP*) during the growing cycle (Book, 2016) as shown in **Figure 2.20**. To encounter this effect, Aquacrop crops consider an indirect approach considering various stress coefficients instead of considering nutrient balances and fixing those stress coefficients; it provides categories of fertility levels ranging from non-limiting to severe stress (Raes et al., 2009). In Aquacrop, the effect of soil fertility on canopy development and biomass production are described by four stress coefficients (Shrestha et al., 2014).

i. Stress coefficient for Canopy expansion (Ksexp,f) which target canopy growth coefficient.(CGC);
ii. Stress Coefficient for maximum canopy cover (Ksccx) targeting maximum canopy cover.
iii. Stress Decline canopy coefficient (fcDecline) targeting canopy cover (CC) once maximum CC has been reached; and,
iv. Stress coefficient for biomass water productivity (Kswp) targeting on Biomass water

productivity (WP*).

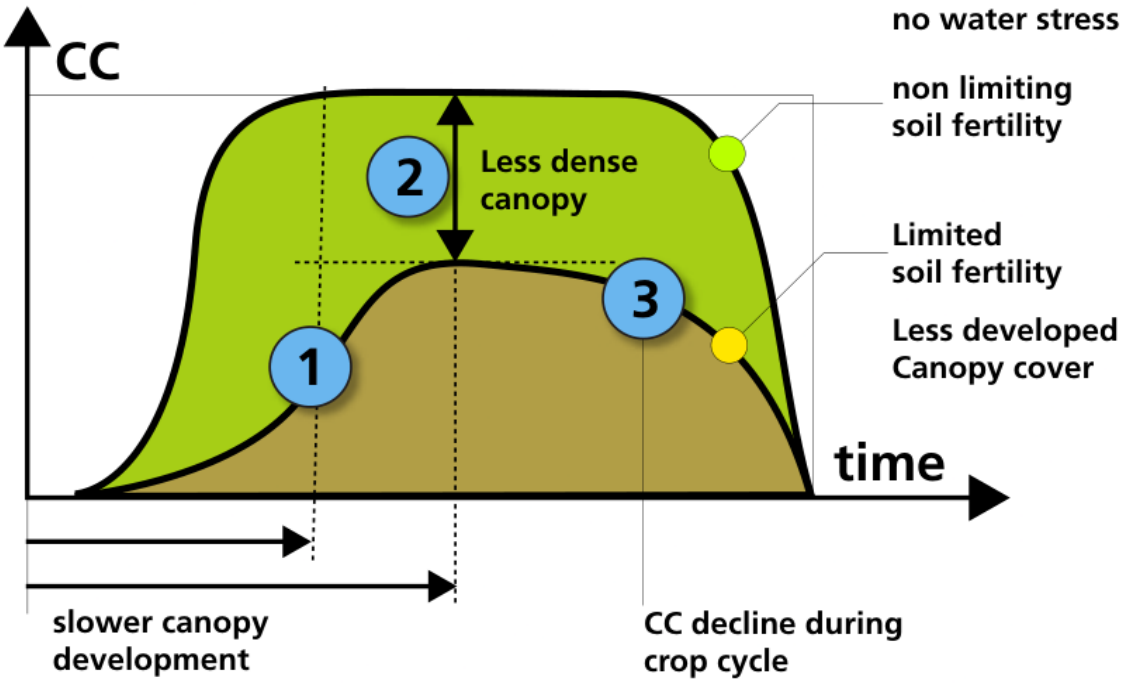

Figure 2.20: Effect of Soil fertility on Canopy Cover (CC)

Also, the effect on soil fertility on water productivity (WP*) is not linear throughout the season (**Figure 2.21**).

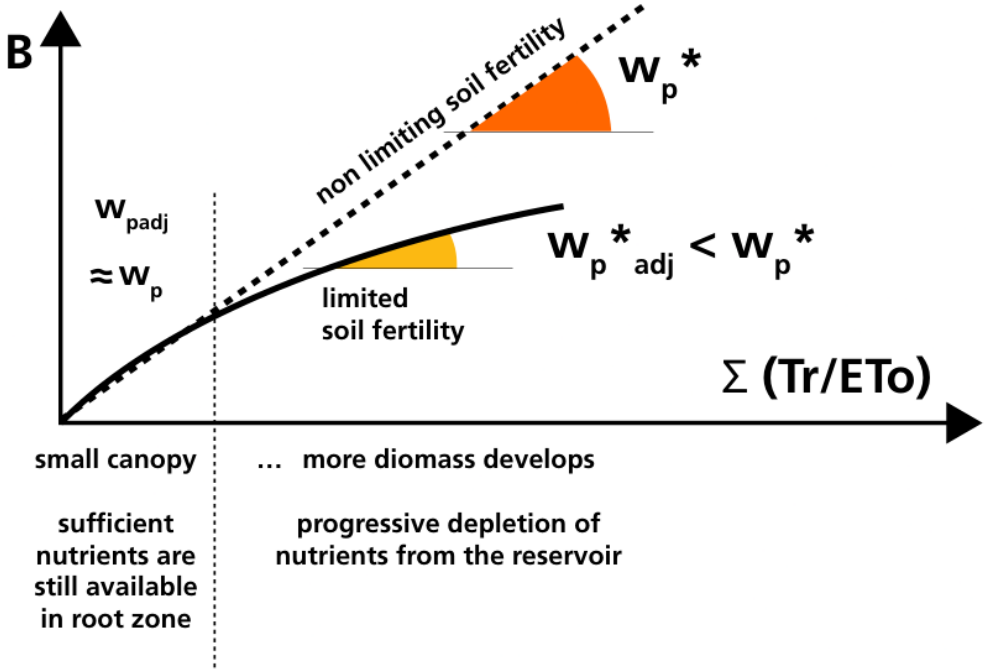

Figure 2.21: Effect of Soil Fertility on Biomass water productivity (WP*)

In addition to this Soil fertility, however, has positive effects on crop yield in the Arid environment. Because due to poor soil fertility the crop will not be able to grow vigorously as a consequence consume less water and can survive longer in the field before early canopy senescence kicks and this results in a higher yield and higher water productivity (WP*).

2.3.6 Crop morphology and phenology

A. Rice

- Introduction

Rice (Oryza sativa) is an edible, starchy cereal grain that is grown on a grass plant. Rice belongs to family Poaceae. It is widely grown and consumed throughout the world, particularly in Asia. It is an important staple food for over half of the world's population, providing a significant source of carbohydrates, proteins, and essential vitamins and minerals. The cultivation of rice involves preparing the land by plowing, leveling, and flooding the fields with water. The seeds are then sown in the flooded fields and allowed to grow. As the plants grow, they require consistent flooding and proper fertilization to ensure healthy growth and high yields. Harvesting rice involves cutting the mature rice plants and threshing the grains from the straw. The grains are then dried, milled, and polished to produce the familiar white rice that is commonly consumed.

In Nepal, rice is the main crop grown for food, followed by maize and wheat. With an average productivity of 3.2 t/ha and a total area of roughly 1.5 million ha, Nepal produces 4.8 million tons of paddy rice annually. Rice is cultivated in three distinct agro-ecological regions viz., Terai (the Gangetic plains), mid hill and high hill with a share of 68%, 28%, and 4%, respectively (Gauchan et al., 2014). The per capita consumption of rice in Nepal is 138kg, and it contributes 16% to the agriculture GDP and 52% to the total cereal consumption in the country. Nepal ranks 17th in rice production and 64th in rice productivity in the world. Till date, the Nepal Agriculture Research Council (NARC) has developed 82 rice varieties and an additional 48 hybrid rice varieties have been registered with the Government of Nepal.

- Morphology

A number of nodes and internodes make up the rice plant's jointed stem. The rice stem, often referred to as the haulm or culm, is typically cylindrical, upright, hollow at the internodes, and solid at the nodes. The different types have different internode counts and lengths. Ten to twenty internodes could be present. Seminal, nodal, and lateral roots make up the fibrous root system that rice plants develop. The radical develops the seminal root as the rice grain germinates by breaking through the coleorhizae and glume that surrounds it. The seminal root produces lateral roots. Adventitious roots form from the basal nodes as the seedlings grow. The majority of the roots are broken off when seedlings are hauled out, but new roots quickly grow again.

A leaf will grow at the culm's node or nodal area. On the culm, leaves are produced alternately in opposing directions. At each node, a leaf develops. The amount of leaves that each variety produces varies. The flag leaf is the highest leaf beneath the panicle. Because it provides photosynthetic materials, primarily to the panicle, the flag leaf significantly contributes to the filling of grains. The leaf blade and sheath are one piece. The leaf blade and the leaf sheath are connected by a ring-shaped collar. The culm above the node is encircled by the leaf sheath. An inflorescence known as

a panicle is the final part of the rice tiller. The topmost internode of the culm is where the inflorescence or panicle is carried. The panicle produces spikelets of rice that grow into grains.

- Phenology

The study of the timing and length of the many growth stages of rice plants, from sowing to harvesting, is known as rice phenology. Rice phenological stages refer to the different growth and development stages of rice plants.

The main stages of rice phenology include:

a. Vegetative Stage: The vegetative stage starts from the time of sowing or transplanting of the seedlings and lasts until the beginning of the reproductive stage. During this stage, the rice plant grows rapidly and develops its leaves, stems, and roots. The vegetative stage can be further divided into three sub-stages: germination, seedling, and tillering. Germination is the initial stage of rice growth when the seed begins to sprout, and the radicle (root) and coleoptile (shoot) emerge from the seed coat. The seedling stage begins once the coleoptile has emerged from the soil surface, and the first true leaves appear. The seedling will continue to grow and develop new leaves, stems, and roots during this phase. The tilling stage begins once the rice plant has developed several leaves and stems. During tillering, the plant will produce multiple tillers or new shoots from the base of the plant, which will grow into new stems and leaves.

Reproductive Stage: The reproductive stage starts with the emergence of the panicle and lasts until the beginning of the ripening stage. This is the critical stage for rice production, as it determines the yield potential of the crop. The reproductive stage can be further divided into two sub-stages: booting and heading.

b. Booting is the stage when the panicle emerges from the flag leaf sheath, and the stem begins to elongate. At this stage, the rice plant stops producing tillers, and all the energy is diverted towards the development of the panicle. Heading is the stage when the panicle becomes visible and starts to develop its flowers. During this stage, the rice plant produces its flowers, which eventually develop into grains.

c. Ripening Stage: The ripening stage starts from the stage when the grains are fully formed and lasts until the time of harvest. During this stage, the grains begin to mature and change color from green to yellow or brown. The ripening stage can be further divided into two sub-stages: milking and maturing. Milking is the stage when the grains are still soft and milky, and the moisture content is high. At this stage, the grains are not yet fully matured and cannot be harvested. Maturing is the stage when the grains become fully mature and dry, and the moisture content is low. At this stage, the grains can be harvested and stored for further use.

The duration of each of these stages can vary depending on factors such as the variety of rice, the temperature and moisture conditions, and the availability of nutrients. Understanding rice phenology is important for predicting the timing of planting and harvesting, and for developing strategies to optimize rice production.

- Ecology and drought resistance

Rice is a C3 crop, which means that it uses the C3 photosynthetic pathway to fix carbon dioxide during photosynthesis. C3 plants, including rice, are adapted to cooler and moister environments, and are usually grown in temperate regions or at high altitudes.

In the C3 photosynthetic pathway, the plant takes in carbon dioxide from the air through tiny openings in its leaves called stomata. The carbon dioxide is then used to produce a three-carbon compound called 3-phosphoglyceric acid (3PGA), which is then used to produce sugars and other organic compounds. Rice is a very important C3 crop, especially in Asia, where it is a staple food for billions of people. It is a highly adaptable crop that can be grown in a variety of conditions, from wetlands to dry upland areas. However, rice is also a high water-use crop, and its cultivation has significant environmental impacts, particularly in terms of water use and greenhouse gas emissions.

The ecology of rice involves the interactions between the crop and its environment, including soil, water, climate, and biotic factors such as pests and diseases. Rice can be grown in irrigated or rainfed ecosystems, with different varieties adapted to different conditions. The crop requires large amounts of water, and the management of water resources is critical to its productivity and sustainability. In terms of soil, rice can grow in a wide range of soil types, but performs best in soils that are fertile, well-drained, and have good water-holding capacity. Soil fertility is important for maximizing yields, and the use of organic matter and fertilizers can help maintain soil productivity.

Rice is also affected by climate factors such as temperature, rainfall, and sunlight. Different rice varieties have varying tolerances to these factors, and the timing of planting and harvesting is critical to avoid adverse weather conditions. In terms of pests and diseases, rice is vulnerable to a wide range of pathogens and insect pests. Integrated pest management strategies are necessary to control these pests, including the use of resistant varieties, cultural practices, and chemical controls when necessary. Overall, the ecology of rice is complex and requires careful management to ensure sustainable and productive crop production.

Drought resistance is a critical trait for rice because it is grown in many regions where water resources are limited. Rice plants are susceptible to water stress at various growth stages, and prolonged drought can significantly reduce crop yields. However, rice has evolved different mechanisms to tolerate drought stress and maintain its productivity.

One of the most important mechanisms of drought resistance in rice is the ability to adjust its growth and development in response to water availability. When water is scarce, rice plants reduce their transpiration rates by closing their stomata, which reduces water loss through transpiration. This leads to a reduction in growth and development, allowing the plant to conserve water and survive drought periods.

Another mechanism of drought resistance in rice is the ability to maintain its photosynthetic capacity under water-limited conditions. Rice plants can adjust their photosynthetic machinery to optimize carbon fixation and reduce water loss during drought. This allows the plant to maintain its energy production and prevent a decline in yield during periods of water stress.

Additionally, rice has developed several adaptive traits that contribute to its drought resistance, such as deep root systems that can access deeper soil layers for water, and the ability to store

carbohydrates and water in its stems and leaves. These traits help rice plants to withstand drought periods and maintain their productivity.

Through breeding and genetic engineering, researchers have also developed rice varieties that are more tolerant to drought stress. These varieties have improved traits such as deeper root systems, higher water-use efficiency, and enhanced osmotic adjustment capacity. These advances in rice breeding and genetics hold promise for improving drought resistance and ensuring the sustainability of rice production in water-limited regions.

B. Wheat

- Introduction

Wheat (Triticum aestivum L.) is an important cash crop that is grown on 762,373 hectares of land in Nepal. It is grown in about 36% of total arable land. Nepal was first introduced to wheat by nearby nations like India and China. Most of Nepal's Terai region is where wheat is farmed. The Lichchhavi period (300-879 AD), according to historical documents, is when wheat production in Nepal was first attested. Wheat agriculture grew and took off during the Malla era (1200–1769 AD), becoming a significant crop in the area.

In Nepal nowadays, wheat is one of the most significant crops and is widely grown throughout the nation. The Terai region, the Mid-hills, and a few of the high hills are the main growing areas for wheat in Nepal. Wheat is a staple food for many Nepalese people and is important to the nation's food security. In Nepal, rice and wheat together account for 525g of daily calories per person. The rice-wheat cropping system, in which wheat is planted in the same field following rice, has been commonly used in Nepal for a very long period. In the Terai region of Nepal, where single-crop rice farming is still taking place in substantial portions, the growth of rice-wheat systems is viable (Timsina & Connor, 2001).

- Morphology

Wheat is an annual grass up to 1.2 m tall with simple erect and hollow culms. The root system of wheat is a fibrous and shallow system consisting of primary, secondary, and tertiary roots. The primary root emerges from the seed and grows downwards, developing secondary roots as it elongates. These secondary roots also produce tertiary roots that spread horizontally and interconnect with neighboring roots. Wheat roots can extend up to 1.5 meters in depth but are mainly concentrated in the topsoil layer, between 0-30 cm. The fibrous nature of the wheat root system allows it to absorb water and nutrients efficiently, making it well-suited to a wide range of soil types.

The stem is the main shoot of the wheat plant, and it supports the leaves, flowers, and grains. The stem is made up of nodes and internodes. Tillers are additional stems that grow from the base of the plant. They arise from axillary buds on the lower nodes of the main stem and can contribute significantly to the final yield of wheat.

The nodes of the stem of wheat plants sprout long, narrow leaves. The leaf's flat surface is called a blade. Sheath is the portion of the blade that encircles the stem at the base. Ligule is a small, thin structure that protrudes from the top of the sheath. Auricle: the small, ear-like structure that protrudes from the base of the blade and attaches to the sheath.

The wheat flower system is known as a spike and consists of many small flowers arranged in a unique pattern. The ear of wheat consists of a central shaft or stem called the axis. The axis is divided into parts called spikelets, each containing multiple flowers or flowers. The flowers are arranged in two rows on each side of the spikelet. Each flower has three stamens (male reproductive structures) and one pistil (female reproductive structures). The pistil consists of the stigma, style and ovary. The ovaries develop into wheat grains or wheat grains after fertilization.

Wheat seeds are small, dry, oval structures used to propagate and grow wheat. Wheat seeds contain all the nutrients and genetic material needed to germinate and grow into a mature wheat plant capable of producing grain. Wheat seeds vary in size and shape depending on the wheat variety but are typically around 3-4 mm long and 2-3 mm wide. Wheat seeds also vary in color from light brown to dark brown depending on the variety.

- Phenology

The stages of wheat growth can be divided into different stages based on the appearance and development of the plant. The well-known stages of wheat development are Tillering, stem elongation, heading and maturation, depicted in **Figure 2.22**.

a. Tillering stage: The tillering stage is an important stage in the development of wheat plants. It occurs during the vegetative period and is characterized by the emergence of new shoots, called shoots, from the base of the main trunk or crown. Tilling usually begins about two to three weeks after planting, depending on environmental conditions such as temperature, humidity, and nutrient availability. At this stage, the plant is actively growing and building a biomass that ultimately determines the yield potential of the crop. The number of shoots that emerge at the Tillering stage depends on the wheat variety, planting density, and management method. In general, the more shoots a wheat plant produces, the greater its potential yield, but there are limits to how many shoots a plant can support.
b. Stem elongation stage: It is the next stage of wheat development after the Tillering stage. At this stage, the wheat grows rapidly, stalks are elongated, heads and ears are formed, and finally the grains are set. The stem elongation stage usually occurs about 4-5 weeks after planting, depending on environmental conditions such as temperature and humidity. At this stage, wheat is highly dependent on nutrients and moisture, and stress and deficiencies lead to reduced yield and quality. The stem elongation stage is critical to the ultimate yield potential of the crop. This is because the number of potential grain-bearing shoots is determined, and this is the time when plants allocate resources to head formation and shoot development. Proper management at this stage includes timely fertilization, weed control, and disease and pest control. The stem elongation phase usually lasts about 3-4 weeks. Wheat then enters the booting stage, where the head begins to emerge from the upper leaf sheaths.
c. Heading stage: The heading stage of wheat development is a critical stage in plant growth and development. This stage is also known as the "booting" stage because the growing wheat head (or inflorescence) is surrounded by an envelope called a boot. The propulsive stage is characterized by the emergence of wheat heads from the boot followed by the development of head spikelets and flowers. At this stage, wheat is most vulnerable to stressors such as heat, drought, disease, and pests, which can have a significant impact on crop yield and quality. Harvest time varies by wheat variety and growing conditions but is

usually about 80 to 120 days after planting, depending on temperature and length of day.

d. Maturation stage: The maturation stage of wheat development, also called maturity stage, is the final stage of growth and development of wheat plants. This stage is characterized by physiological and biochemical changes that occur as the wheat grain reaches maximum size and weight and the plant prepares for harvest. During the ripening stage, the wheat plant undergoes several changes, including the drying and hardening of the kernels, the breakdown of chlorophyll in the leaves, and the accumulation of starch and other nutrients in the kernels. The wheat kernels also change color, from green to golden brown, as they ripen. The timing of the ripening stage varies depending on the variety of wheat, the growing conditions, and the planting date, but generally occurs between 120 and 160 days after planting. Farmers often monitor the ripening stage closely to determine the optimal time for harvest, which can affect the yield and quality of the crop.

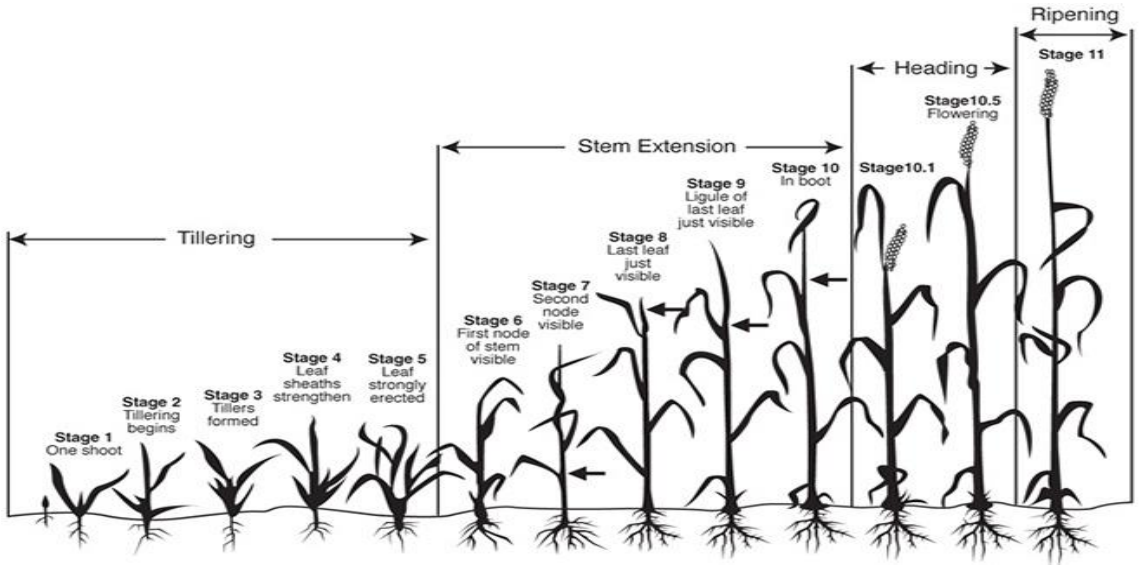

Figure 2.22: Phenological development of wheat

- Ecology and Drought Resistance

Wheat is the world's common grain. It is a hardy plant that can adapt to a variety of environments. His C3 photosynthetic plant is native to Tibet up to 4570 m altitude. can be cultivated. Wheat prefers a temperate climate with temperatures between 15 and 20°C during the growing season. The plant tolerates both hot and cold temperatures, but extreme weather conditions such as frost, heat waves, and heavy rain can adversely affect yields. Wheat needs well-drained soil rich in organic matter and nutrients. It can grow in different types of soil such as loamy, sandy and loamy soils.

Drought is a major environmental stress that can affect wheat production. It is estimated that around 33% of wheat fields in the world and about 55% in developing countries suffer from drought stress (Khayatnezhad et al., 2011). Water stress in wheat occurs when there is a shortage of water supply to the plant during critical growth stages. Wheat plants require an adequate supply of water for proper growth and development. Water stress during certain growth stages can lead to reduced plant growth, lower yield, and poor grain quality.

In order to survive drought conditions, wheat has evolved several mechanisms that allow it to conserve water and maintain growth even in low moisture environments. These mechanisms include:

- Deep root system: Wheat has a deep root system that allows it to access water stored in deeper layers of the soil.
- Reduced transpiration: During drought conditions, wheat reduces the amount of water lost through transpiration by closing its stomata (pores on the leaves). This helps to conserve water.
- Osmotic adjustment: Wheat can adjust the concentration of solutes in its cells in response to drought stress. This helps to maintain cellular turgor pressure and prevent water loss.
- Early maturation: Wheat can mature earlier in response to drought stress. This reduces the water demand of the plant and allows it to complete its life cycle before the soil moisture is depleted.
- Heat and drought tolerance breeding: Through conventional breeding or biotechnology, wheat can be more resistant to both heat and drought stress.

3 STUDY AREA

Nepal is a landlocked country located in south Asia at the latitude of 28.3949° N, and longitudes of 84.1240° E. Nepal has a border with China in the north and with India towards the east, west, and south. Nepal has an astonishing topographical variation with an altitude ranging from 60 MASL (meters above sea level) at Kechana Kalan to 8,848 MASL at Mount Everest. Nepal has a total land of 147,516 km^2 (56,956 sq mi) with a population of 29,674,920. The population growth rate per annum in Nepal is estimated at 2.3%. The national GDP contributed by agriculture is 23.95%. The estimated agricultural land area cultivated is 2.6 million hectares. The main crops are paddy, maize, and wheat along with cash crops Agro-ecologically, Nepal is divided into three regions with similar (topographic and climate)

A. Mountains
B. Hills
C. Terai

The study was implemented in Tulsipur, Dang district, located in the mid-western Terai region of Nepal. Geographically, it extends in the range 27°37 to 28°29′N latitude to 82°02′ N to 82°54′ N longitude with a total area of 2995 Km². Altitude-wise, the district's topography ranges from a low of 213 meters (Bhanpur of Sishaniya VDC) from the sea level to 2058 meters (Arkhale of Hansipur VDC) comprising hill slopes, forest lands of different types, large and small valleys, doons, ravines, streams and rivers (ref. Wikipedia). The average temperature of this district is in the range of 22-34 °C in summer and 10-25°C in winter. The average annual rainfall is 162 mm. About 37,800 ha of land is under paddy cultivation.

3.1 Demography

Tulsipur has a population of about 180,734, with a population density of 470 per km^2 (CBS 2021). There are a total of 31243 households in Tulsipur.

3.2 Location and Geography

Tulsipur lies between latitudes 28.1545° N, and longitudes of 82.3235° E. at the altitude 725MASL. Its neighboring places are Ghorahi, Manpur, and Dhanauri. It has a total land area of 384.63 km^2. The major river basin of Tulsipur is Patu, Hapur, Guwar, Sangram, and Babbai. There are 4 meteorological stations established by the Department of Hydrology and Meteorology (DHM) in the Babai River basin area in the Dang district, namely stations 507, 508, 511, and 512. Projection of precipitation data was done for all four stations whereas projection of temperature was done for stations 508 and 511. Station 508 (28.13°E, 82.30°N) was treated as a representative station for Tulsipur and chosen for crop yield simulations (**Figure 3.1**).

3.3 Agriculture

The agriculture of Tulsipur is mainly paddy along with other crops like wheat, maize, mustard, chickpea, pea, and lentil. Paddy is sown in about 55% of the total arable land. If irrigation is all year, then sown twice. Maize is sown in the upper area of Tulsipur where good facilities for

irrigation are not available. Wheat is grown in about 20% of arable land in Tulsipur. Apart from these major crops mustard is grown on about 30% of land along with potatoes, lintels, chickpeas, etc. Due to dependency on rainfall for agriculture, the change in rainfall pattern heavily affects agricultural production.

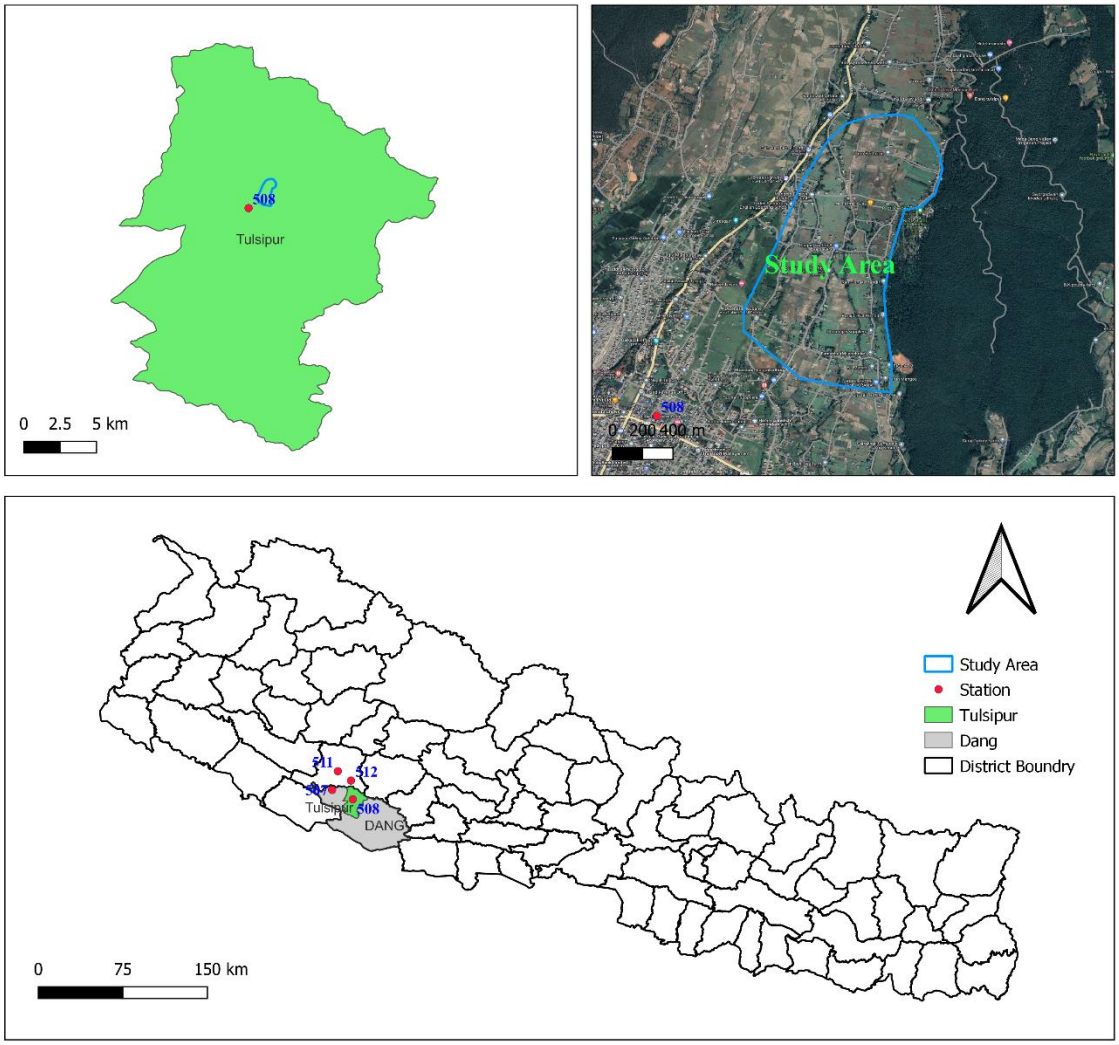

Figure 3.1: Location of study area

4 METHODOLOGY

The methodology starts with development of climate information system of historical temperature and precipitation data all over Nepal. The potential of using data from CIS as baseline for climate projection is assessed. Meteorological stations around the study area are identified and precipitation and temperature for these stations are projected under climate change scenarios using CMIP6 GCMs. Data necessary for calibration and validation of AquaCrop model is obtained via farmer survey and soil texture experiments. Validated AquaCrop model is then run under projected climatic conditions to assess climate change impacts on crop yield and water requirements. The timeline of our project is presented in ANNEX A. Schematic representation of overall methodology is shown in **Figure 4.1**.

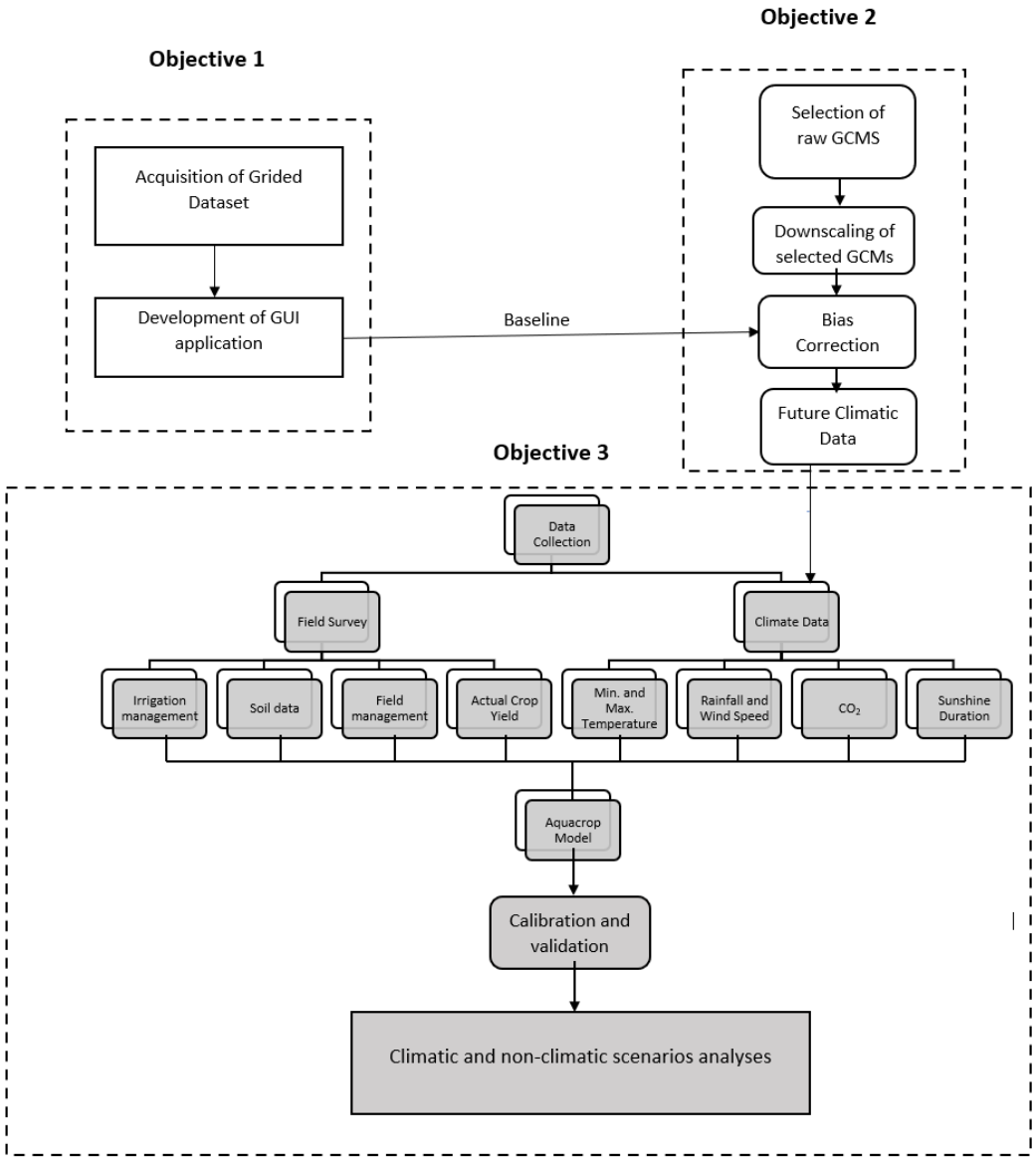

Figure 4.1: Methodological flowchart of the study

4.1 Climate Information System

4.1.1 Grid interpolation

Grid interpolation was done by means of Kriging with External Drift (KED). Kriging is the generic term for the approach used to estimate the values of variables at unmeasured places by utilizing measured locations. Utilizing the weighted average of the known data, the overall estimation procedure is carried out. The fundamental equation is represented by the following formula:

$$\hat{Z}(X_0) = \sum_{i=1}^{N} W_i \, Z(X_i) \qquad 4.1$$

In this equation $Z(X_0)$ represents the Kriging value of X_0 point; $Z(X_i)$represents the observed values of variables in eachX_i point; W_i represents the corresponding values of each $Z(X_{i}); N represents the number of points of $Z(X_0)$ to be used in Kriging estimation. The Kriging method based on the smallest mean square error method is known as the best linear unbiased estimator. The weights determined by the Kriging method depend on the semivariogram and spatial position of the data. The Kriging error average is calculated as zero and variance is calculated as the smallest.

The number of points utilized to achieve a predicted value at any X_0 point affects the calculation of weights. For each point, a weight is determined. This circumstance indicates that there is a weight account repetition for each new Kriging point (Isaaks & Srivastava, 1989). The error variance acquired through estimate is known as the Kriging variance, and the Kriging variance consists of the following:

$$\sigma_K^2 = 2\sum_{i=1}^{N} W_i \, \gamma(X_0 - X_i) - \sum_{i=1}^{N}\sum_{j=1}^{N} W_i \, W_j \gamma(X_i - X_j)$$

$$= \sum_{i=1}^{N} W_i \, \gamma(X_0 - X_i) + \lambda \qquad 4.2$$

The Kriging variance is unrelated to the data's real value. It depends on the distance between the places of the data quantity and the data. Therefore, the Kriging variance can be utilized to test prospective spots prior to gathering the actual data value and to select the optimal sites among these candidates. Kriging methods employed in line with the application domain and data structure are accessible in several forms, OK, SK, UK, Indicator Kriging (IK), CK, and KED. The KED approach was utilized in this investigation because it permits the integration of numerous factors. It also requires a simpler semivariogram analysis than collocated Kriging, which requires a semivariogram for each covariate.

KED enables the use of supplementary information that has an impact on the local spatial trend of the dependent variable and is accessible at all locations. Under the premise of a linear relationship between the dependent variable and the auxiliary variable, the KED technique creates the model. KED's use of a non-stationary random function model, which limits stationarity to a given range,

is one of its advantages. This results in a model with more local details than the OK model (Deutsch & Gailly, 1996). The KED estimator is:

$$Z^{*}_{KED}(u) = \sum_{\alpha=1}^{n(u)} \lambda_{\alpha}^{KED}(u) Z(u_{\alpha}) \qquad 4.3$$

Where $Z^{*}_{KED}(u)$ is the KED estimator at location u, λ_{α}^{KED} are the KED weights corresponding to the n samples at location u, $Z(u_{\alpha})$ are the sample values within the search neighborhood.

4.1.2 Application development

A. Frontend

Graphical User Interface (GUI) was developed in Python because of the flexibility and universality of Python as a programming language. Tkinter is one of the most popular libraries for developing GUIs in Python and will be used because of its user-friendly interface that can run on all operating systems and platforms (Python Docs, 2023). This user interface will allow users to obtain climate data for any location within Nepal in standard time series format for time interval of their interest.

B. Database

Gridded multidimensional datasets obtained from spatial interpolation are mostly stored in the Network Common Data Form (NetCDF) file format. NetCDF is an open-source set of libraries developed by University Corporation for Atmospheric Research (UCAR)'s Unidata program to enable creation, access and sharing of scientific data and metadata in an array-oriented format (Unidata, 2022). It is a self-describing data format which means it contains metadata about the stored data that can be accessed programmatically to build reusable workflows. Moreover, it is machine-independent, thus can be accessed from different computer architectures simultaneously (Rew & Davis, 1990). On top of its simplicity, flexibility and efficiency, many Application Programming Interfaces (APIs) have been developed in several popular programming languages, such as C, C++, Java, Python, etc., allowing for easy access, processing and visualization.

The Climate and Forecast (CF) Conventions are a set of community-driven guidelines on metadata of NetCDF files that aim to promote interoperability and intercomparability of data stored in different files. They provide a definitive description of each variable and an unambiguous standard to describe the spatial and temporal properties of data allowing for development of powerful software applications that can analyse, process and visualize the data without user interference (Eaton et al., 2021). The major principles behind CF conventions are to make metadata minimally redundant, readable without need for external reference and interpretable by both humans and machines (Hassell et al., 2017).

Due to the myriad benefits offered by CF-compliant data files, NetCDF-CF has been gaining rapid acceptance in the world of climate data (Hankin et al., 2010). Global leaders in gridded data products such as NASA Earth Data, British Oceanographic Data Centre (BODC), Integrated Ocean Observing System (IOOS), Open Geospatial Consortium (OGC) and many more have all suggested CF-compliant NetCDF as a recommended standard for gridded data (BODC, 2012; IOOS, 2016; NASA, 2021; OGC, 2022). Hence, NetCDF was chosen as the database for the application.

4.2 Future Climate Projection

In this study, baseline (1992-2014 for precipitation and 1980-2010 for temperature) and future (2025-2100) simulations of CMIP6 GCMs for precipitation, maximum and minimum temperature were used because CMIP6 is a substantial improvement over the preceding CMIP5 as the former includes socio-economic as well (Gidden et al., 2019). According to Jain et al. (2018) and Sood & Smakhtin (2015), uncertainties resulting from incomplete knowledge of atmospheric phenomena, approximations made during numerical modeling, spatio-temporal scales, resolutions, etc. will cause overestimation or underestimation of the values of considered climatic variables in comparison to observed variables, leading to different results for different GCMs for the same inputs. Since the multi-model ensemble (MME) provided a better match than individual GCMs in these situations, it has been widely used (Ahmed et al., 2020; Hughes et al., 2014; Tebaldi & Knutti, 2007; Yan et al., 2015).

There is no logic for selecting the number of GCMs for multi-model ensemble (Raju & Kumar, 2020). But total uncertainty associated with model predictions can be minimized by using multi-model ensembles (Scinocca et al., 2015). Hussain et al. (2017) advised against using a single GCM to measure climate change. Herger et al. (2018) reported three approaches for multi-model ensembles as; random selection of models, selection of models from performance ranking and consideration of optimal ensemble from number of ensembles but this is computationally heavy.

For our study we have selected GCMs proposed by Mishra et al. (2020) and Almazroui et al. (2020) for South Asia, daily precipitation, daily maximum and minimum temperature data from 5 CMIP6 GCMs listed in **Table 4.1**. Web address https://esgf-node.llnl.gov/search/cmip6/ was used for downloading projections of these GCMs for two scenarios SSP245 & SSP585.

Table 4.1: List of CMIP6 GCMs used in this study.

S.N.	Model Name	Country	Latitude resolution (Deg)	Longitude resolution (Deg)	Research Center
1	ACCESS-Cm^2	Australia	1.2500	1.875000	Australian Community Climate and Earth System Simulator (ACCESS)
2	EC-EARTH3	Europe	0.7018	0.703125	European Community Earth (EC Earth)
3	MIROC6	Japan	1.4000	1.400000	Japan Agency for Marine-Earth Science and Technology, Atmosphere and Ocean Research Institute, National Institute for Environmental Studies (MIROC), Japan
4	MPI-ESM1-2-HR	Germany	0.9351	0.937500	Max Planck Institute for Meteorology (MPI)
5	MRI-ESm^2-0	Japan	1.1215	1.125000	Meteorological Research Institute (MRI)

The GCMs or RCMs contain significant biases in temperature and precipitation, such as the tendency for temperatures to be consistently too hot, rainfall to be excessively high or low, rain to begin prematurely or too late, and so on. Climate models also tend to overestimate the number of days with rain and underestimate precipitation extremes. GCMs and RCMs are biased because of their poor spatial resolution (large grid boxes), oversimplified physics, and lack of understanding of the earth's climate system. As a result, before employing climate models for hydrological applications, these biases in climate models must be addressed, especially at finer spatial scales (Teutschbein & Seibert, 2012). (Jakob Themeßl et al., 2011) examined the effectiveness of a variety of bias correction techniques and concluded that QM methods could be the most effective choice for correcting biases. According to Lafon et al. (2013), QM's modified results were remarkably accurate.

It should be underlined that the QM refers to a family of procedures even if it appears that the QM methods are potentially effective ways to reduce bias in general. It is important to research which QM is most appropriate for a given situation. Thus, it is crucial to compare the effectiveness of the QM techniques in the bias correction procedure, especially for the climatic variables (such as rainfall and temperature) that are most crucial in the evaluation of the impact of water resources (Enayati et al., 2021).

(Enayati et al., 2021) reported that out of various QM techniques, robust empirical quantiles (RQUANT) methods were excellent choices for correcting the bias of rainfall data, whereas all bias correction techniques for the temperature variable performed rather well, with the notable exceptions of executed PTF: scale and SSPLIN. This is mostly because temperature is different from other climatic variables and the GCM/RCM combinations are better at modeling temperature than rainfall.

In this study, robust empirical quantiles (RQUANT) method was used to bias correct rainfall data while PTF: linear method was used to bias correct temperature data.

4.3 Climate Change Impacts on Crop Yield

AquaCrop is an engineering approach-based crop growth model developed by the Land and Water Division of FAO to estimate crop yields and water use under different climate and environmental conditions. Model simulates yield response to water of herbaceous crops (Cereals, vegetables) under different biophysical and management conditions, and is particularly suited to addresses conditions where water is a key limiting factor in crop production. AquaCrop Considers several factors such as weather condition, crop types and crop characteristics, soil properties and field management practices to predict the crop growth, water use and crop yield. AquaCrop simulates the growth of the crop and estimates the water requirement on a daily basis, allowing for the optimization of irrigation schedule and prediction of potential yield under different climate and management conditions. The calculation scheme of AquaCrop is explained in detail in Section 2.3.4.

4.3.1 AquaCrop model setup

AquaCrop Model set up requires input basic information such as climate data of the location where crops grow. Climate data includes daily rainfall data, Air maximum temperature and Air minimum temperature, sunshine duration, wind speed and relative humidity. The last five climate parameters

are used to evaluate evapotranspiration (ET_0) using ET_0 Calculator in AquaCrop. Other input parameters include crop Types and crop characteristics (see 2.3.3) and the model requires information about soil properties such as soil types, soil layer and layer depth, soil water retaining capacities. In addition to this field management practices such as irrigation schedule and fertility level are also required (see 2.3.3). Once these input parameters are fed to the AquaCrop, the model simulates the crop growth and water use, providing estimates of yield, water productivity and water use efficiency.

4.3.2 Field survey and data collection

As part of this project, a field survey was conducted in the study area of Tulsipur (see **ANNEX B**). The survey included a field visit to a selected area of Tulsipur to collect data on various aspects related to agriculture and soil samples collection. Semi-structured interviews and key informant interviews were conducted with practitioners/farmers. A questionnaire was designed to collect information on crop phenology, crop yield, and irrigation and fertilizer application (see **ANNEX C**). Face to face interviews were conducted for the data collection process. Soil samples were collected and brought back to Pulchowk Campus for soil textural analysis. In addition, secondary information was collected from the Central Bureau of Statistics, District Agriculture Development Office, Department of Hydrology and Meteorology, previously published data for similar climates, and CMIP6.

A. Soil analysis

The classification of soil texture depends on how soil particles are distributed across various particle sizes. For instance, soils with a higher proportion of fine particles are referred to as clay soils, while those with a higher proportion of coarse particles are known as sandy soils. **Table 4.2** outlines the four main particle size classes used in this classification.

Table 4.2: Soil particle size classes (Brouwer, 1985)

Size class name	**Lower diameter limit (µm)**	**Upper diameter limit (µm)**
Gravel	> 100 µm	
Sand	50 µm	100 µm
Silt	2 µm	50 µm
Clay	< 2 µm	

There are various techniques available for identifying the proportion of different particle sizes present in soil, including sieve analysis, pipette method, gravitational sedimentation, hydrometer method, and laser diffraction method. In the case of the 16 soil samples collected in the field, hydrometer method was used for textural analysis because other means of analysis were not available in the Pulchowk Soil laboratory facilities.

The hydrometer method was used to find out the soil texture of 16 samples. In this method, 100 g of air-dried grinded soil is mixed with 20 ml of 10% sodium hexametaphosphate solution. The solution breaks up the soil aggregates into separate particles. The suspension is left overnight and then mixed for 10 minutes with a standard mixer. Water is added to make 1 l in a sedimentation

cylinder. The hydrometer method uses Stoke's law to link the settling velocity of a spherical particle with its diameter in Equation 4.4 (Gee & Or, 2002):

$$v = \frac{[g * (\rho_p - \rho_l) * d^2]}{18\mu} \qquad 4.4$$

Where:

g	=	Gravitational acceleration (m·s-2)
ρ_p	=	Particle density (g·cm-3)
ρ_l	=	Density of water(g·cm-3)
d	=	Particle diameter (cm)
μ	=	Dynamic viscosity of water (Pa·s)

To measure the density of the suspension, a hydrometer, which is a glass device calibrated to float based on the Archimedes force, is used. The suspension is stirred, and the first reading is taken at 40 seconds. Any particles larger than 50 μm in diameter are assumed to have settled by this time. A second reading is taken after 3 hours, which reveals the amount of clay particles that remain in suspension. It is assumed that particles larger than 2 μm have settled at this point. When determining the relative proportions of sand, silt, and clay in the soil sample, it is important to correct temperature by subtracting 0.3 g/l for every degree above 20°C.

By measuring the relative proportions of the particle size classes, the soil textural class of the sample can be determined by using the soil textural triangle of USDA (Soil Survey Manual, n.d.).

From the analysis of soil textures obtained from lab test of soil collected during field visit as well as randomly sampled data from soil map, a uniform soil profile was considered for simulations with AquaCrop. The soil physical characteristics are presented in section 7.1.2.

B. Soil hydraulic properties

Soil data collected from the field visit were analyzed in the soil lab of Pulchowk Campus in Kathmandu to determine silt, clay, sand content for textural classification of soil. Soil Water Properties are estimated by using Pedotransfer Functions (PTF) of Saxton and Rawls (Saxton & Rawls, 2006) from textural properties of soil as it uses was verified for Chitwan (Shrestha, 2014) which is similar to our study area. The Sexton and Rawls PTF is described in **Table 4.3**.

Table 4.3: Saxton & Rawls Pedotransfer function

Parameters	Equation
θWP	$\theta WP = \theta WPt + 0.14*\theta WPt - 0.02$
θFC	$\theta FC = \theta FCt + 1.283*\theta FCt^2 - 0.374*\theta FCt - 0.015$
θsat	$\theta S = \theta FC + \theta (sat-FC) - 0.097*S + 0.043$

Parameters	Equation
θ_{WPt}	θ_{WPt} = -0.024*S + 0.487*C + 0.006*SOM + 0.005(S*SOM) - 0.013(C*SOM) + 0.068(S*C) + 0.031
θ_{FCt}	θ_{FCt} = -0.251*S + 0.195*C + 0.011*SOM + 0.006(S*SOM) - 0.027(C*SOM) + 0.452(S*C) + 0.299
$\theta_{(sat-FC)}$	$\theta_{(sat-FC)} = \theta_{(sat-FC)t} + 0.636*\theta_{(sat-FC)t} - 0.107$
$\theta_{(sat-FC)t}$	$\theta_{(sat-FC)t}$ = 0.278*S + 0.034*C + 0.022*SOM - 0.018(S*SOM) - 0.027(C*SOM) - 0.584(S*C) + 0.078

Where,

θ_{WP} = Volumetric soil water content at Permanent Wilting Point ($m^3 \cdot m^{-3}$),

θ_{FC} = Volumetric soil water content at Field Capacity ($m^3 \cdot m^{-3}$),

θ_{sat} = Volumetric soil water content at Saturation ($m^3 \cdot m^{-3}$),

θ_{WPt} = Volumetric soil water content at Permanent Wilting Point, first solution ($m^3 \cdot m^{-3}$),

θ_{FCt} = Volumetric soil water content at Field Capacity, first solution ($m^3 \cdot m^{-3}$),

$\theta_{(sat-FC)}$ = θ_{sat}-θ_{FC} ($m^3 \cdot m^{-3}$),

$\theta_{(sat-FC)t}$ = Θ_{sat}-θ_{FC}, first solution ($m^3 \cdot m^{-3}$)

C. Climatic Data

Daily historical climatic data for 1980 to 2014 was collected from a representative climatic station for the Dang district (Tulsipur: 82.30°E, 28.13°N, 683 MASL). The data set included daily rainfall, minimum and maximum air temperature for the whole period, and observed hours of bright sunshine for part of the period. The atmospheric power of the atmosphere, or reference evapotranspiration (ET_0), was calculated with the FAO Penman-Montheith method using the ET_0 calculator. Solar radiation data were estimated with the temperature difference method when it was missing, and dew point temperature was assumed to be similar to minimum temperature (Allan et al., 1998).

D. Crop data

The data related to crop yield, crop data, irrigation and fertilizer application were collected during the field visit through the questionnaire and face-to-face interviews. Detailed analysis and findings of the crop data are presented in section 7.1.1.

4.3.3 Model calibration and validation

Calibration involves adjusting the model parameters to make the model output closely match with the observed data. The process involves comparing the simulated and observed data and adjusting the model inputs until the model output is consistent with observed data. So, it is based on a trial-and-error approach in which one specific input variable has to be chosen as the reference variable at a time and adjusting only those parameters that were known to influence the reference variable the most. On the other hand, validation is the process of evaluating the model's ability to simulate the crop yield under different conditions that were not used in the calibration process. The model performance is evaluated by comparing the simulated and observed data and assessing the accuracy

of the model predictions. Based on the validation results, the model performance can be further refined to improve the model performance.

In the AquaCrop database there are a number of crop files which have been calibrated and validated for different locations under various conditions. For each crop file it provides a set of crop parameters; Conservative crop parameters are crop-specific and do not change with time, management practices, geographic location, climate or cultivars, listed in **Table 4.4**. These parameters are not needed to calibrate to the local conditions. These are calibrated in other studies with the crop data grown under favorable and non-limiting conditions but remain applicable for stress conditions through their modulation by stress response function (Hsiao et al., 2009; Shrestha et al., 2014).

Table 4.4: Conservative crop parameters (Shrestha et al., 2014; Vanuytrecht et al., 2014)

Conservative Crop Parameters	**Rice**	**Wheat**
Base Temperature(°C)	8.0	0.0
Upper temperature(°C)	30.0	26
Crop Coefficient when Canopy is complete but prior to senescence	1.1	1.1
Water productivity normalized for ET_0 and CO_2 (gram/m^2)	19	15
Possible increase (%) of HI due to water stress before flowering	None	Small
Coefficient describing positive impact of restricted vegetative growth Yield Formation on HI	Small	Small
Coefficient describing negative impact of stomatal closure during yield formation on HI	Moderate	Moderate
Allowable maximum increase (%) of specified HI	15	15
Soil water depletion threshold for canopy expansion-Upper threshold	0	0.2
Soil water depletion threshold for canopy expansion- lower threshold	0.4	0.65
Soil water depletion threshold for stomatal closure -Upper threshold	0.5	0.65
Soil water depletion threshold for canopy senescence -Upper Threshold	0.55	0.7
Minimum growing degrees required for full biomass production(°C-day)	10	14

Table 4.5: Fine- tuning of non-conservative crop parameters

Fine- Tuning of non-conservative crop parameters	**Rice**	**Wheat**
Initial Plant density (no. of plants per m^2)	45	160
Recovery/ emergence (DAP)	6	6
Maximum Canopy cover (%) (DAP)	56	50
Senescence (DAP)	99	90
Maturity (DAP)	113	122
Flowering Day (DAP)	68	77
Duration of flowering	14	18
Maximum rooting depth(m)	0.5	0.6
Time to reach maximum rooting depth (DAP)	99	76
Reference harvest index (%)	41	33

Other crop parameters, which need to be tuned are cultivar specific and less conservative parameters; parameters affected by planting/management (i.e. Types of planting method, plant density and time to 90% seedling emergence).,Cultivar specific parameters (timing of development stages i.e. time to reach maximum canopy cover (CCx), time to beginning of canopy senescence, time to physiological maturity, time to start to flowering, Duration of flowering),affected by condition in the soil profile(i.e. maximum effective rooting depth (Zx), time to reach maximum effective rooting depth or root zone expansion rate),'Cultivar class' conservative crop parameters ,and soil and management dependent parameters(response to soil fertility stress and/or Soil Salinity stress).

Table 4.6: Stages of plant growth the life cycle

Stages of plant growth the life cycle	**Duration**	**(days)**
	Rice	**Wheat**
Stage-1(Emergence or transplant recovery)	7	7
Stage-2(Vegetative stage)	61	64
Stage-3(Flowering)	31	21
Stages-4(Yield formation and ripening	14	30

Calibration of crop response to soil fertility:

Crop yield also depends on field management parameters, one of them is soil fertility management. The soil fertility level in the soil profile is a non-conservative parameter, it should be calibrated to the local environment in which the plant grows. The main objective of calibrating soil fertility is to find a setting for the four stress coefficients in such a way that the simulated biomass corresponds with the observed biomass in a field with a fertility stress (FAO, 2017). Calibration is based on the field observation of reduction in biomass production (B) and reduction in maximum canopy cover (CC) during the crop cycle in stressed fields. Calibration for crop response requires access to observed data from two well-watered field conditions, one with and other without soil fertility stress. To specify the level of fertility stress, relative biomass production (Brel) (it is a Bstress with reference to the potential biomass (Bref) that can be obtained in non-limiting conditions), maximum canopy cover (CC*) obtained in the stress field and decline of the canopy cover is

needed (FAO, 2017). Calibration of crop response to soil fertility stress is done in the crop file whereas selection of soil fertility stress level in field management.

In our project work we follow an indirect approach to calibrate soil fertility level due to lack of field observation data. Calibration is done based on farmer survey data; amount of fertilizer they applied to the field with reference to Nation Recommended Fertilizer Dose recommended by Department of Agriculture (DoA). Two fertility stress levels of 40% and 15% (scenario) for rice are used in this project to make the simulated yield correspond to yield from farmer surveys and the yield data published by MoALD. Also, to predict the yield in non-limiting condition in future scenario, no fertility stress is considered i.e., fertility stress level 0%. On the other hand, fertility stress level is considered 50% in calibration of yield of wheat and for future yield prediction, non-limiting condition has also been used i.e., 0% fertility stress.

Other parameters needed to input; includes, climate data, soil type and irrigation management practices. The soil type used in the simulation run is sandy loam observed through soil tests in labs and soil maps published by NARC. A single layer of 1m was considered for calculation.

Irrigation strategies considered in this project is according to the farmer Survey data in which they adopt full irrigation treatment; application of water 50 mm above the field capacity for every four days interval from the first five days after transplanting to last 7 days before harvesting during the crop season for rice. While in case of wheat they apply three times irrigation to the field at (22 days, 70 days, and 85 days after sowing). Weed infection management is taken as very good.

4.3.4 Model performance evaluation

AquaCrop model simulation results of crop yield, biomass and WP were compared with the observed values form the experiment during both calibration and validation processes. The goodness of fit between the simulated and observed values was corroborated by using the prediction error statistics. The root mean square error (RMSE) and model efficiency (E) were used as the error statistics to evaluate both the calibration and validation results of the model. E was used to access the predictive power of the model while RMSE indicated the error in model prediction. In this study, the model output in terms of prediction for yield was considered for evaluation of the model. The following statistical indicators were used to compare the measured and simulated values. The model performance will be evaluated using the following statistical parameters such as model efficiency (E) (Nash–Sutcliffe efficiency) given by

$$E = 1 - \frac{\sum_{i=1}^{N}(O_i - S_i)^2}{\sum_{i=1}^{N}\left(O_i - \widehat{O_i}\right)^2} \qquad 4.5$$

Where Si and Oi are predicted and actual (observed) data, $\widehat{O_i}$ is mean value of Oi and N is number of observations.

$$RMSE = \sqrt{\frac{1}{(N)\sum_{i=1}^{N}(O_i - S_i)^2}} \qquad 4.6$$

4.3.5 Scenario analysis

In our project, we conducted scenario analysis under three different headings. A hierarchical overview of scenario analysis for rice is shown in **Figure 4.2**.

A. Fertilizer Scenario

Three fertilizer scenarios are considered: low fertilizer input (40% FS), optimal fertilizer input (15% FS) and full dose fertilizer input (0% FS). 40% FS scenario indicates fertilizer application around 40% less than NRFD. 15% FS scenario represents fertilizer application slightly lower than NRFD. 0% FS indicated non-limiting scenario where crop growth is not limited by fertilizer application.

B. Irrigation Scenario

In rice, irrigation strategies have been considered based on decrease of soil water content from Field Capacity (FC). The percentage change of soil water content below FC is also termed Readily Available Water (RAW). 50% RAW scenario refers to the case when irrigation is only applied when soil moisture content drops to 50% below FC and other scenarios are also defined similarly.

C. Climate change scenarios

Climate input to AquaCrop model are obtained from two climate change scenarios: SSP245 and SSP585, which are explained in detail in 2.2.2. Ensemble mean of climatic projections given by five GCMs are taken as input in AquaCrop model for both SSP245 and SSP585 scenarios.

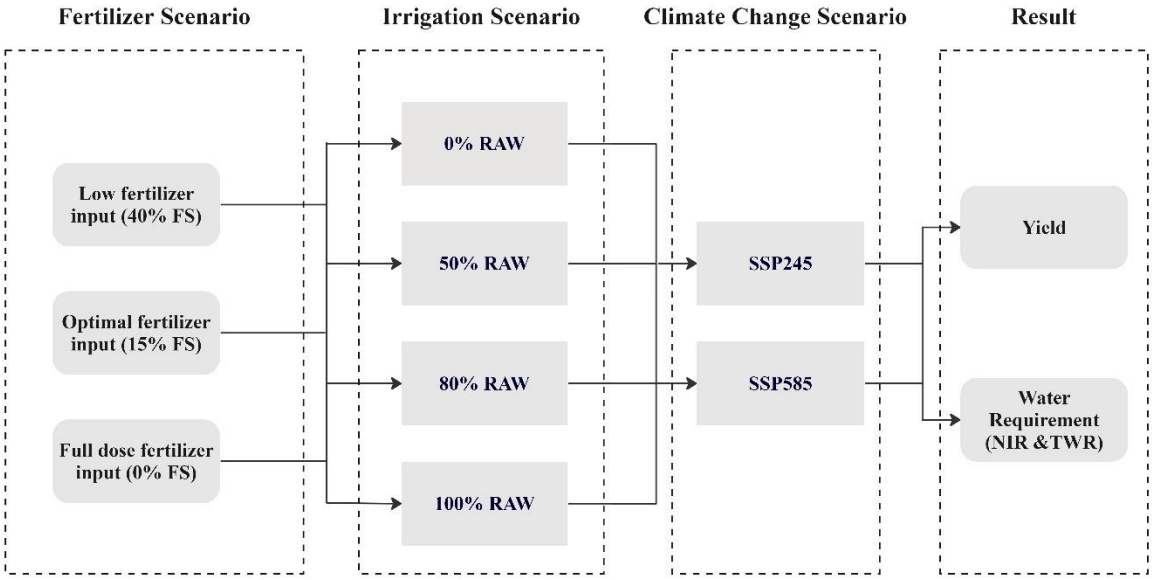

Figure 4.2: Hierarchical overview of scenario analysis for rice.

A hierarchical overview of scenario analysis for wheat is shown in **Figure 4.3**.

A. Fertilizer Scenario

Two fertilizer scenarios, defined similarly as above, are considered: low fertilizer input (50% FS) and high fertilizer input (0% FS).

B. Irrigation Scenario

Irrigation scenarios for wheat are based on number of application of water throughout the life cycle of wheat. Two scenarios are considered based on two and three times application in its lifecycle.

C. Climate change scenario

Climate change scenarios are same as that for rice.

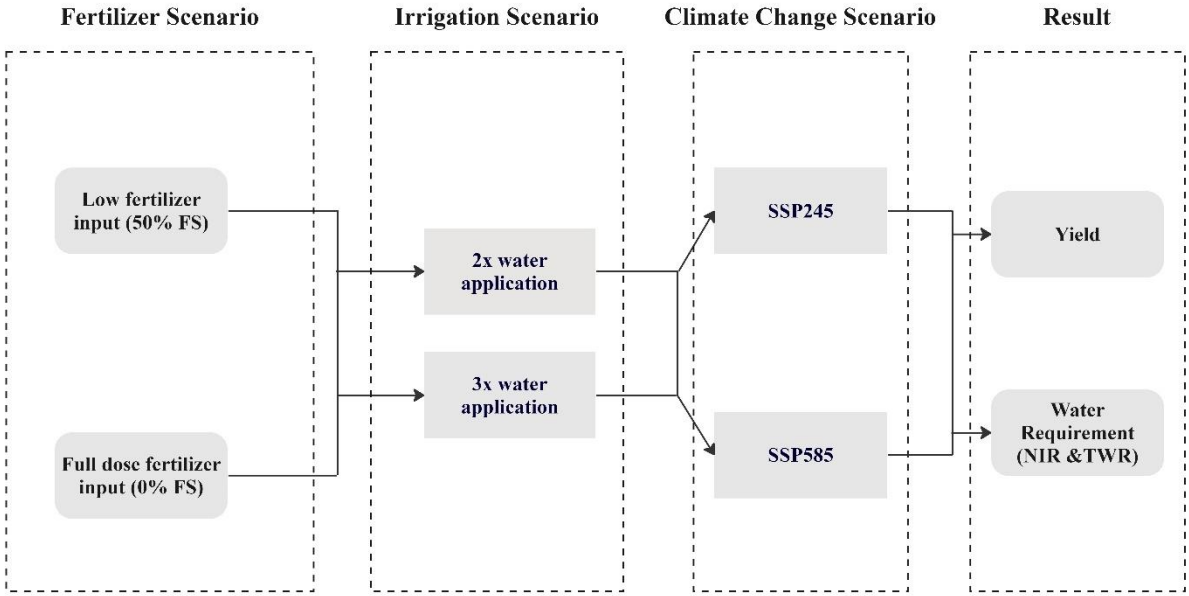

Figure 4.3: Hierarchical overview of scenario analysis for wheat.

4.4 Data and Sources

Different types of data with corresponding sources are summarized in **Table 4.7**.

Table 4.7: Data and sources

S.N.	Data	Description	Source
1.	Observed Climate	Maximum and minimum air temperature, Daily rainfall, Mean relative Humidity and Average sunshine duration.	Department of Hydrology and Meteorology (DHM)
2.	Soil physical properties	Soil water content at saturation, wilting point, field capacity, hydraulic conductivity.	Soil Lab Test and soil Sampling through Soil map published by NARC
3.	Field management practices.	Soil fertility, Practices affecting soil evaporation and/or surface runoff,	Farmer Survey
4.	Irrigation Management practices.	Irrigation method, Application depth and time of irrigation events, salinity of the irrigation water	Farmer Survey
5.	Ground Water Table (GWT)	Depth of GWT below GL.	1 m

S.N.	Data	Description	Source
6.	Initial Condition	Initial soil water content and soil salinity at various depths in the soil profile.	Farmer Survey

5 CLIMATE INFORMATION SYSTEM

5.1 Background

As the debate around climate change evolves from raising awareness to carrying out research activities to enhance adaptation and mitigation policies, access to climate data is more important than ever before (Carneiro et al., 2022). Nepal is one of the world's most vulnerable countries not only from a topographic viewpoint (ICIMOD, 2011), but also because of its weak technical and financial infrastructure (Dulal et al., 2010). Hence access to quality climate data is indispensable in Nepal to facilitate climate research that, in turn, shapes the adaptation and mitigation response to climate change.

Station data obtained from DHM are mostly in a time series format for specific station points. However, the spatial and temporal distribution of climatic variables (such as precipitation and temperature), provided by a gridded format, is crucial for a host of climate and hydrological studies (Beck et al., 2019; Isotta et al., 2014). Uniform gridded data are required in climate model calculations and evaluation of satellite observations (Xavier et al., 2016). They help in avoiding biases due to irregular distribution of station points and validating global and regional climate models (Beguería et al., 2016; Haylock et al., 2008). Due to all these reasons, gridded data products are gaining worldwide popularity. National or regional gridded data is needed to carry out local level studies because global gridded products are not good at characterizing local climatic variations (Herrera et al., 2012). So, there is a great need for gridded data products in Nepal. Hence a climate information system built on top of national gridded dataset could be vital cog in ensuring the smooth cycle of climate research and policy in Nepal.

Recognizing the need for a gridded data product in the context of Nepal, Water and Energy Commission Secretariat Nepal (WECS-Nepal) developed a 1km x 1km gridded precipitation and temperature dataset by the means of Kriging with External Drift (KED) interpolation. It covers the time period from January 1st, 1981, to December 31st, 2015. It includes 928 grid boxes in the east-west direction and 485 in the north-south direction. The climate information system was developed on top of this gridded dataset (**Figure 5.1**).

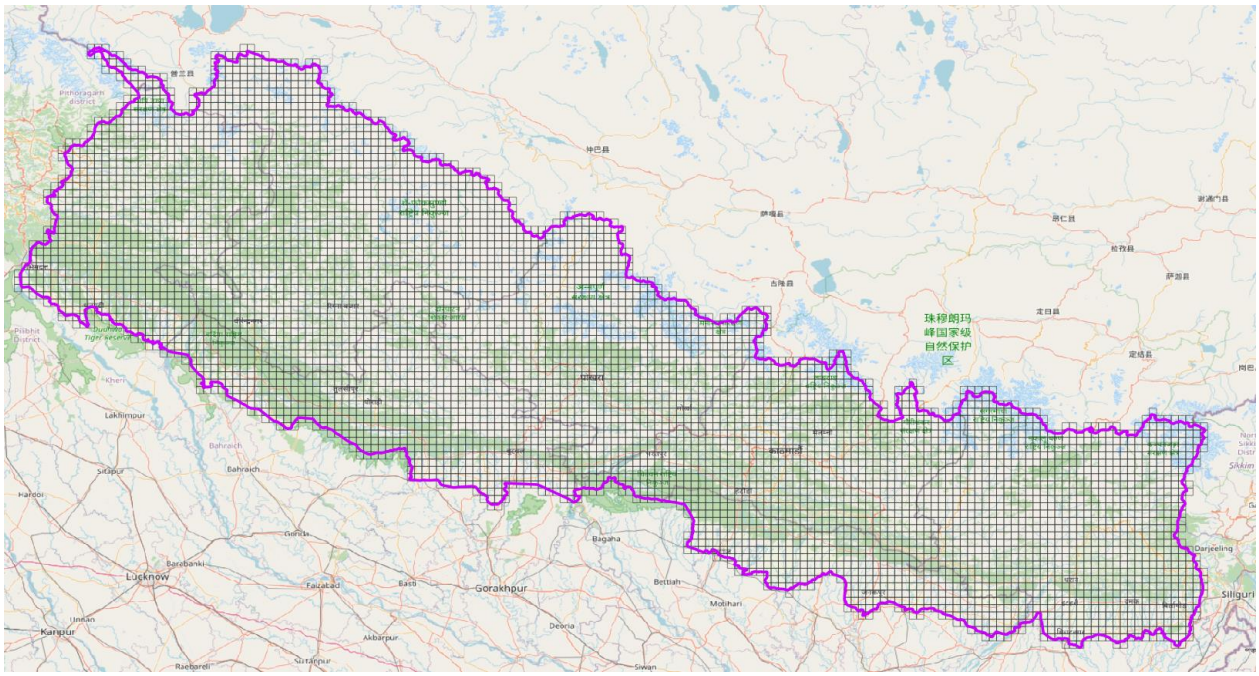

Figure 5.1: Gridded data product 1km × 1km, resolution increased in figure for clarity.

5.2 User Interface

The user interface of the climate information system is shown below. The windows in the graphical interface are explained below as numbered in **Figure 5.2**.

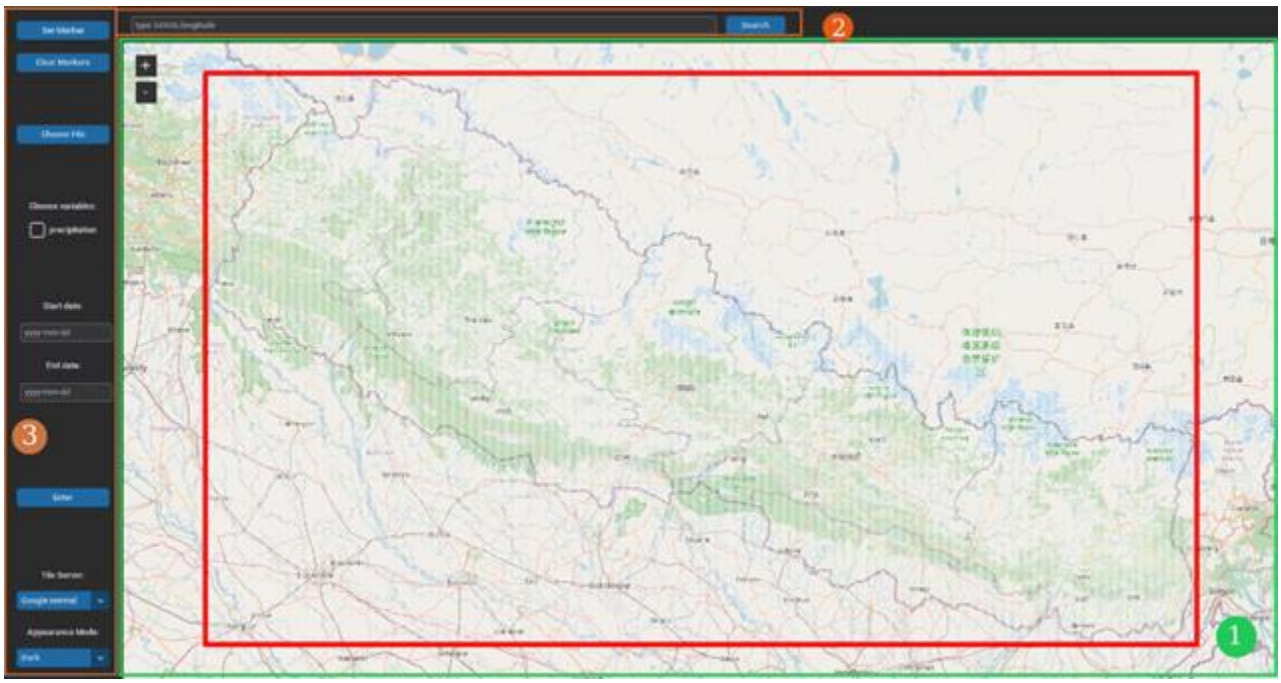

Figure 5.2: User interface of the CIS

1. Map Canvas: The map canvas shows the interactive map of Nepal and spatial bounds of the climate data available for download. The user has the option to change the appearance of the map to either OpenStreetMap or Google Maps. Users can select any point on the map canvas and right click to set markers on the map. The climate data for marked points can be downloaded from the Toolbar.
2. Search Bar: The search at the top of the interface allows users to search for specific

location inside Nepal and find their area of interest easily. Users have the option of entering the latitude and longitude of the study area (e.g.: 80.542, 23.125) or search by the address (e.g.: 'Tulsipur, Dang').

3. Toolbar: Toolbar at the leftmost side of the application gives users a variety of options on the type of climate data they wish to obtain. It allows them the option to select variable of interest such as precipitation or temperature and enter the time interval of their interest. On top of that, they can set the appearance mode of the application and select the map server that they prefer. Further instructions on using the toolbar will be explained in the Application section.

5.3 Application

This application has an intuitive interface and can be used without detailed instructions. But a detailed documentation of instructions on using the application is provided below:

- Load the database: Although the application comes pre-loaded with a database of gridded climate data for Nepal, users can manually load a different NetCDF file with the 'Choose File' button on the Toolbar. Once the file is selected, the map canvas will be updated to reflect the spatial extents of the database as shown in **Figure 5.3**.

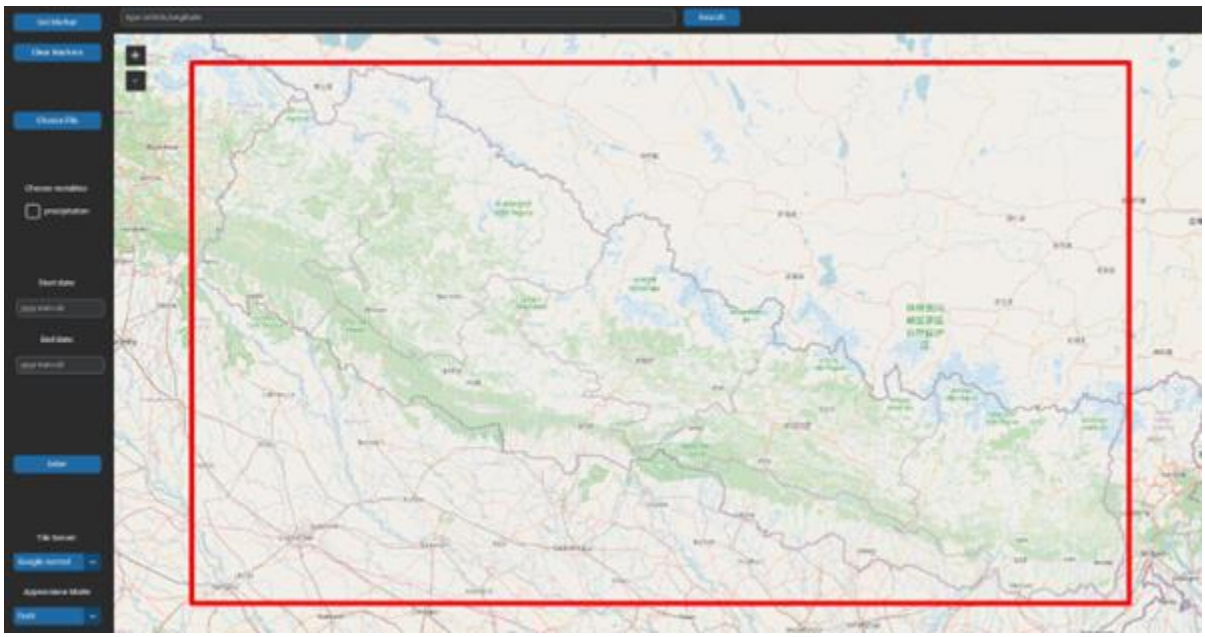

Figure 5.3: CIS: Loading the database.

- Set markers: Once the map is loaded, users can set markers on the map for the points where they would like to obtain climate data. For this, users can either right click on the canvas and select "Add Marker" or use the "Set Marker" button on the toolbar which places a marker at the center of the map canvas (**Figure 5.4**). Markers can be easily cleared via the toolbar.

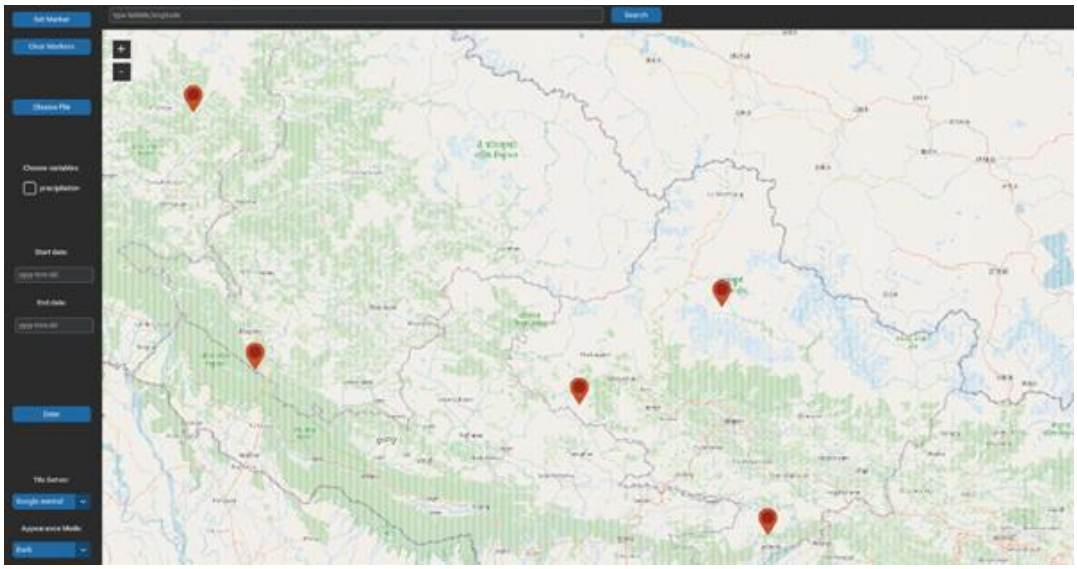

Figure 5.4: CIS: Setting markers.

- Select variables and enter time: Once all the points of interest have been marked, users should select the climate variables they would like to obtain (e.g.: precipitation, Tmax, etc.) (**Figure 5.5**). They are then prompted to enter the start and end date of their climatic time series data. Users are alerted if the dates they entered outside the bounds of the database. Once everything is filled, users can press the "Enter" button.

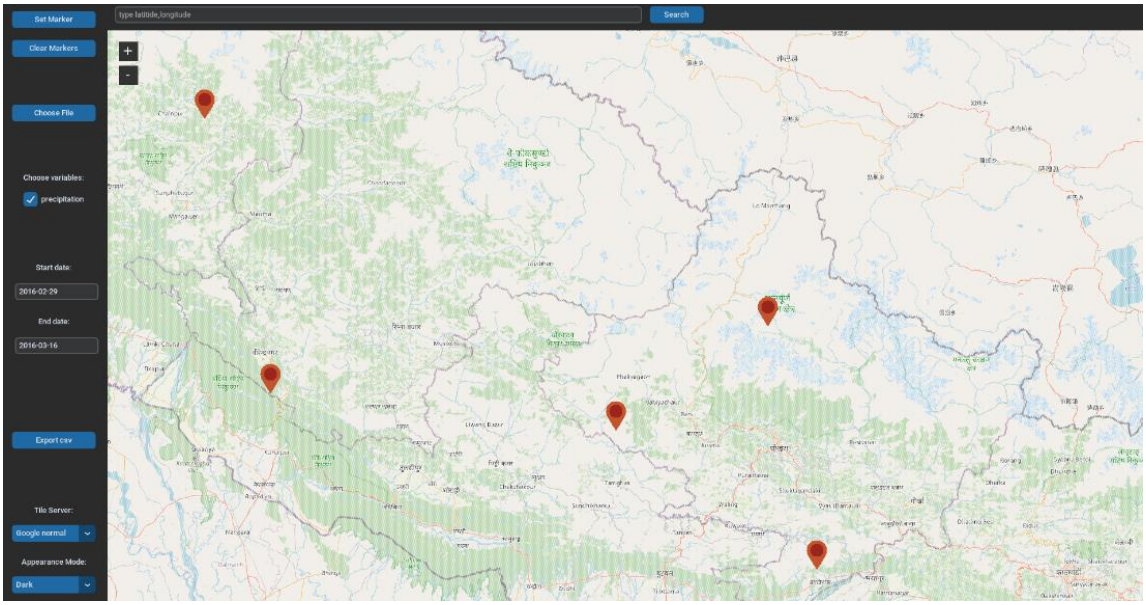

Figure 5.5: CIS: Selecting variables and entering time.

- Export csv: On pressing the "Enter" button, the application processes the user request. Depending on the length of time interval and number of markers, this can take anything from a second to three minutes. Upon completion of processing, users are prompted to select the "Export csv" button to generate the csv of their time series data. A sample csv generated by the application is shown in **Figure 5.6**.

	A	B	C	D	E	F	G	H	I	J
1	time	(29.53179, 81.35096)	(27.43165, 85.78394)	(28.28155, 83.2406)	(28.70157, 83.93824)	(27.71893, 84.16346)	(28.4314, 81.65308)	(27.29017, 87.31653)	(26.89405, 86.76172)	
2	2016-02-29 12:00:00	0	0	0	0	0	0	0	0	
3	2016-03-01 12:00:00	0	0	0	0	0	0	0	0	
4	2016-03-02 12:00:00	0	0	0	2.825638	0	0	0	0	
5	2016-03-03 12:00:00	0	0	0	0	0	0	0	0	
6	2016-03-04 12:00:00	0	0	0	0	0	0	4.093072	0	
7	2016-03-05 12:00:00	0	0	0	0	0	4.7001343	0	0	
8	2016-03-06 12:00:00	0	4.0409493	5.481525	5.619238	0	3.4917407	3.1748526	0	
9	2016-03-07 12:00:00	0	0	0	0	0	0	0	0	
10	2016-03-08 12:00:00	0	0	0	0	0	0	0	0	
11	2016-03-09 12:00:00	0	0	0	0	0	0	0	0	
12	2016-03-10 12:00:00	0	0	0	0	0	0	0	0	
13	2016-03-11 12:00:00	0	0	0	0	0	0	0	0	
14	2016-03-12 12:00:00	0	0	0	0	0	0	0	0	
15	2016-03-13 12:00:00	41.369053	2.8405812	0	5.696182	0	0	0	0	
16	2016-03-14 12:00:00	0	3.246379	11.546329	3.254961	6.5483336	0	0	0	
17	2016-03-15 12:00:00	0	0	0	2.848091	0	0	0	0	
18	2016-03-16 12:00:00	0	0	0	0	0	0	0	0	
19										
20										
21										
22										

Figure 5.6: Exported csv.

As a demonstration of the utility of such a climate information system in assisting "basic research" (Trenberth et al., 2016), this application was used to obtain precipitation data of our study area in Dang District. A plot comparing the data obtained from the interpolated product and nearest station (station 508) data in **Figure 5.7** shows good similarity with an R^2 score of 0.913 and hence could be used as a substitute for station data. The application promises to address a gaping hole in climate information accessibility in Nepal and strengthen climate research in Nepal.

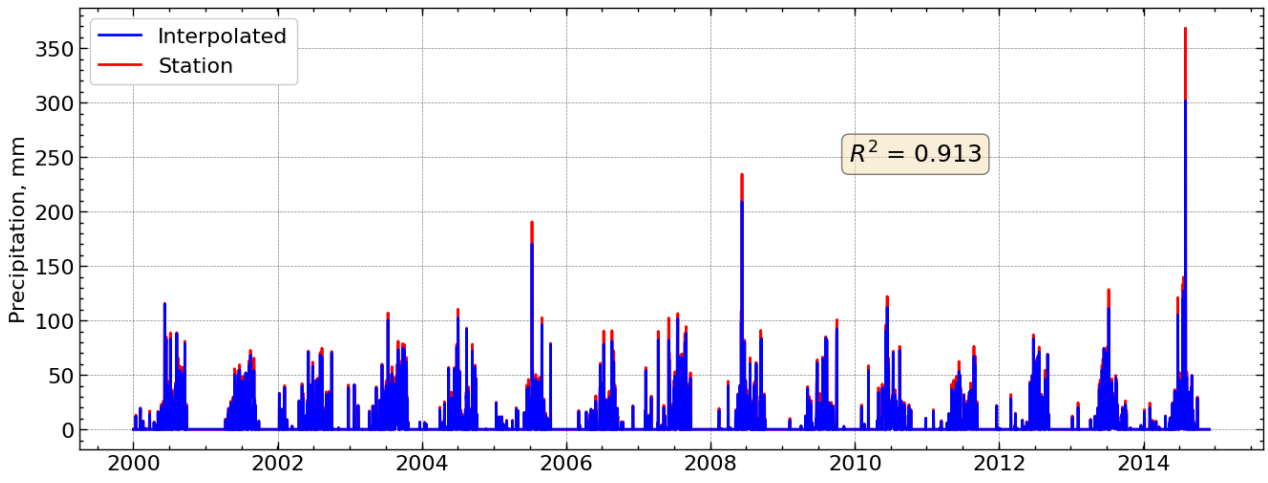

Figure 5.7: Comparison of station data with interpolated data

6 FUTURE CLIMATE PROJECTION

6.1 Performance Evaluation of Bias Correction

CMIP6 model outputs (precipitation, maximum and minimum temperatures) downloaded from https://esgf-node.llnl.gov/search/cmip6/ were used. Because of the discrepancies between observed values and GCM output during historical time periods, as illustrated in **Figure 6.1**, **Figure 6.2**, and **Figure 6.3**, raw GCM data cannot be utilized to predict the future directly. Therefore, bias correction of the GCM output is required. The bias correction of raw GCM findings for hydrological applications is strongly advised, especially for usage at smaller geographical scales (Teutschbein & Seibert, 2012). Quantile mapping (QM) has become a more effective method of bias correction for enhancing the performance of GCMs (Berg et al., 2012). The quantiles of the raw GCM data are correlated with those of the observed data using a transfer function using QM (Pandey et al., 2019).

For analyzing the performance evaluation of bias correction, the parameters (precipitation, Tmax and Tmin) for historical model data obtained from GCMs and historical observed data from 1992 to 2014 were compared before and after bias correction. Normal Standard Error (NSE), Percentage Bias (PBIAS), and R^2 are calculated for both before and after bias correction. It was observed that the models ACCESS-Cm^2 and MRI-ESm^2-0 are under predicting the precipitation and EC-EARTH3, MIROC6, and MPI-ESM1-2-HR are over predicting the precipitation variable which after bias correction are closing towards 0 which is ideal PBIAS. Also, the minimum value of NSE (0.15) and R^2(0.51) are transformed to NSE of 0.98 and R^2 of 0.98 after bias correction which is nearly close to ideal case i.e., 1 which is tabulated in **Table 6.1**

Also, all the models are under predicting the maximum and minimum temperature before bias correction with the only exception of ACCESS-Cm^2 model for maximum temperature. The PBIAS of maximum and minimum temperature ranging from 16 to -56.9 before bias correction are transformed to perfect ideal condition of 0 PBIAS for all GCMs. Also, the NSE ranging from 0.98 to -5.91 and R^2 ranging from 0.99 to 0.84 are transformed to 1 i.e., ideal condition which are tabulated **Table 6.2** and **Table 6.3**. This shows the effectiveness of bias correction. It was observed that temperature parameters performed better than precipitation parameter.

Table 6.1: NSE, PBIAS and R^2 values of precipitation before applying Bias Correction and after applying Bias Correction.

Station	Parameter	ACCESS-Cm^2		EC-EARTH3		MIROC6		MPI-ESM1-2-HR		MRI-ESm^2-0	
		Before Bias	After Bias	Before Bias	After Bias	Before Bias	After Bias	Before Bias	After Bias	Before Bias	After Bias
507	NSE	0.15	0.98	0.77	1	0.93	1	0.95	1	0.51	0.99
	PBIAS	-63.1	8	19.3	0.2	8.1	0.1	4.5	0.2	-43.6	4.6
	R^2	0.51	0.98	0.92	1	0.94	1	0.96	1	0.84	0.99
508	NSE	0.17	0.98	0.64	1	0.93	1	0.91	1	0.53	0.98
	PBIAS	-60.9	7.3	26.3	0.2	8.1	0.1	10.6	0	-40.3	6.5
	R^2	0.51	0.98	0.9	1	0.94	1	0.94	1	0.8	0.99
511	NSE	0.17	0.98	0.64	1	0.88	1	0.91	1	0.53	0.98
	PBIAS	-60.9	7.3	26.3	0.2	14.5	0.1	10.6	0	-40.3	6.5

Station	Parameter	ACCESS-CM2		EC-EARTH3		MIROC6		MPI-ESM1-2-HR		MRI-ESM2-0	
		Before Bias	After Bias	Before Bias	After Bias	Before Bias	After Bias	Before Bias	After Bias	Before Bias	After Bias
	R^2	0.51	0.98	0.9	1	0.93	1	0.94	1	0.8	0.99
512	NSE	0.55	0.99	-2.47	1	-0.82	1	-0.7	1	0.93	0.99
	PBIAS	-33.8	4.8	113.7	0.2	93.7	0.2	87.2	0	1	4.5
	R^2	0.65	0.99	0.97	1	0.97	1	0.99	1	0.93	0.99

Table 6.2: NSE, PBIAS and R^2 values of Maximum Temperature before applying Bias Correction and after applying Bias Correction

Station	Parameter	ACCESS-CM2		EC-EARTH3		MIROC6		MPI-ESM1-2-HR		MRI-ESM2-0	
		Before Bias	After Bias	Before Bias	After Bias	Before Bias	After Bias	Before Bias	After Bias	Before Bias	After Bias
508	NSE	0.6	1	-4.93	1	-5.91	1	-3.88	1	-4.3	1
	PBIAS	0.5	0	-34.6	0	-36.7	0	-31.5	0	-31	0
	R^2	0.91	1	0.93	1	0.94	1	0.92	1	0.84	1
511	NSE	-1.43	1	-3.13	1	-0.49	1	-2	1	-3.02	1
	PBIAS	15.3	0	-25	0	-5.6	0	-21.4	0	-20.9	0
	R^2	0.88	1	0.93	1	0.87	1	0.9	1	0.84	1

Table 6.3: NSE, PBIAS and R^2 values of Maximum Temperature before applying Bias Correction and after applying Bias Correction

Station	Parameter	ACCESS-CM2		EC-EARTH3		MIROC6		MPI-ESM1-2-HR		MRI-ESM2-0	
		Before Bias	After Bias	Before Bias	After Bias	Before Bias	After Bias	Before Bias	After Bias	Before Bias	After Bias
508	NSE	0.98	1	-0.75	1	-1.18	1	0.16	1	0.54	1
	PBIAS	-0.7	0	-50.2	0	-56.9	0	-34.8	0	-24.8	0
	R^2	0.98	1	0.97	1	0.99	1	0.98	1	0.95	1
511	NSE	0.7	1	-0.77	1	0.83	1	0.49	1	0.75	1
	PBIAS	16	0	-41.8	0	-11.6	0	-23.8	0	-12.2	0
	R^2	0.98	1	0.97	1	0.99	1	0.99	1	0.96	1

A. Bias Correction for precipitation

Enayati et al. (2021) analyzed a family of QM methods and concluded RQUANT (robust empirical quantiles) methods as best for correction of rainfall. So, in this study empirical robust quantile mapping was used and the result obtained as shown in **Figure 6.1** was acceptable to use the relation developed to bias correct the future GCMs output obtained under SSP245 and SSP585 scenarios. From **Table 6.1** the effectiveness of RQUANT can be seen. The PBIAS ranging from -63.1 to 93.7 before bias correction transformed to PBIAS ranging from 0 to 8.1. The NSE ranging from -2.47 to 0.93 before bias correction transformed to NSE ranging from 0.98 to 1. Also R^2 ranging from 0.51 to 0.96 transformed to R^2 ranging from 0.98 to 1.

B. Bias Correction for temperature

Enayati et al. (2021) found that all bias correction techniques, with the notable exceptions of conducted PTF: scale and SSPLIN, worked rather well for the temperature variable. This is mostly because temperature is different from other climatic variables and the GCM/RCM combinations are better at modeling temperature than rainfall is. So, in this study, PTF: linear transfer function

was used, and the result obtained as shown in **Figure 6.2** and **Figure 6.3** was acceptable to use the relation developed to bias correct the future GCM output obtained under SSP245 and SSP585 scenarios. The effectiveness of bias correction for temperature can be seen from **Table 6.2** and **Table 6.3**. The PBIAS ranging from -54.9 to 16 transformed to PBIAS of zero after bias correction. Similarly, NSE ranging from -4.93 to 0.98 is transformed to NSE of 1 and R^2 ranging from 0.84 to 0.98 transformed to 1 which shows the effectiveness of linear transform function in bias correction.

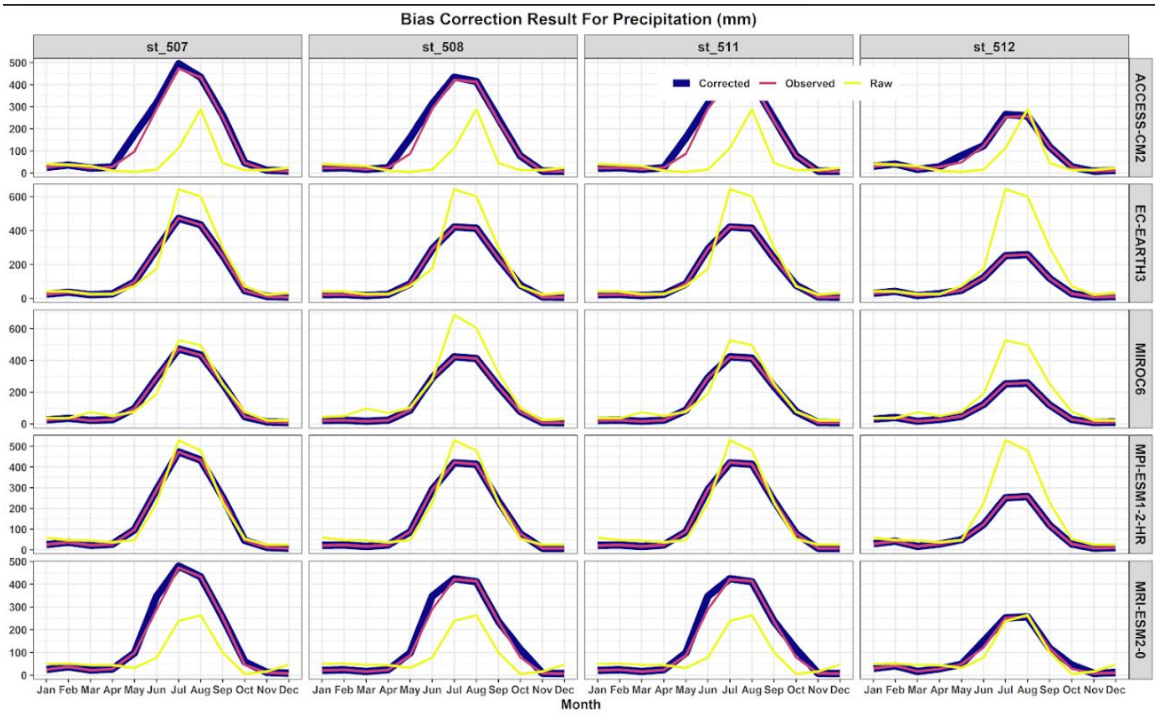

Figure 6.1: Comparison of raw and bias corrected data with observed data for precipitation of baseline period and for five GCMs used in this study.

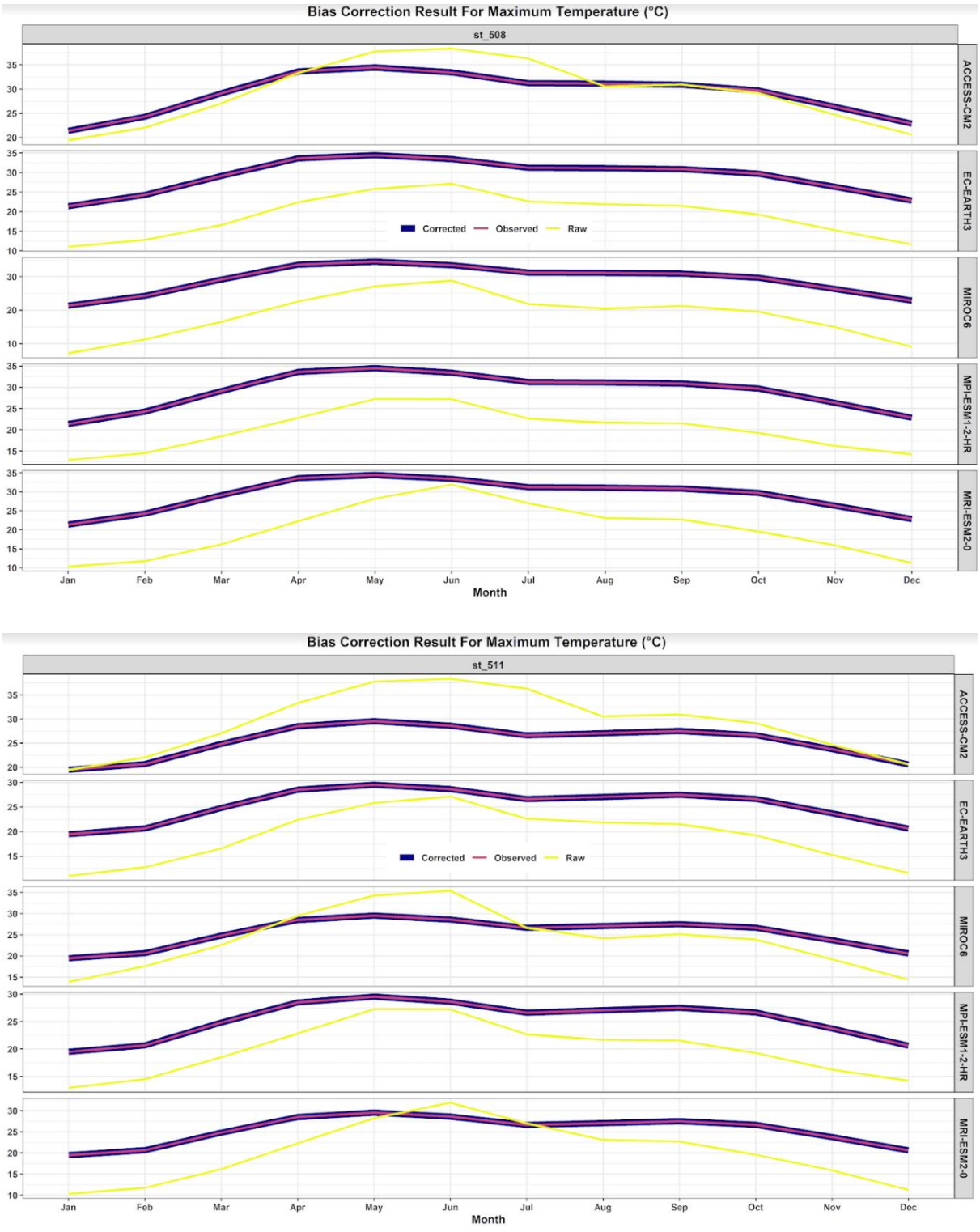

Figure 6.2: Comparison of raw and bias corrected data with observed data for maximum temperature of baseline period and for five GCMs used in study.

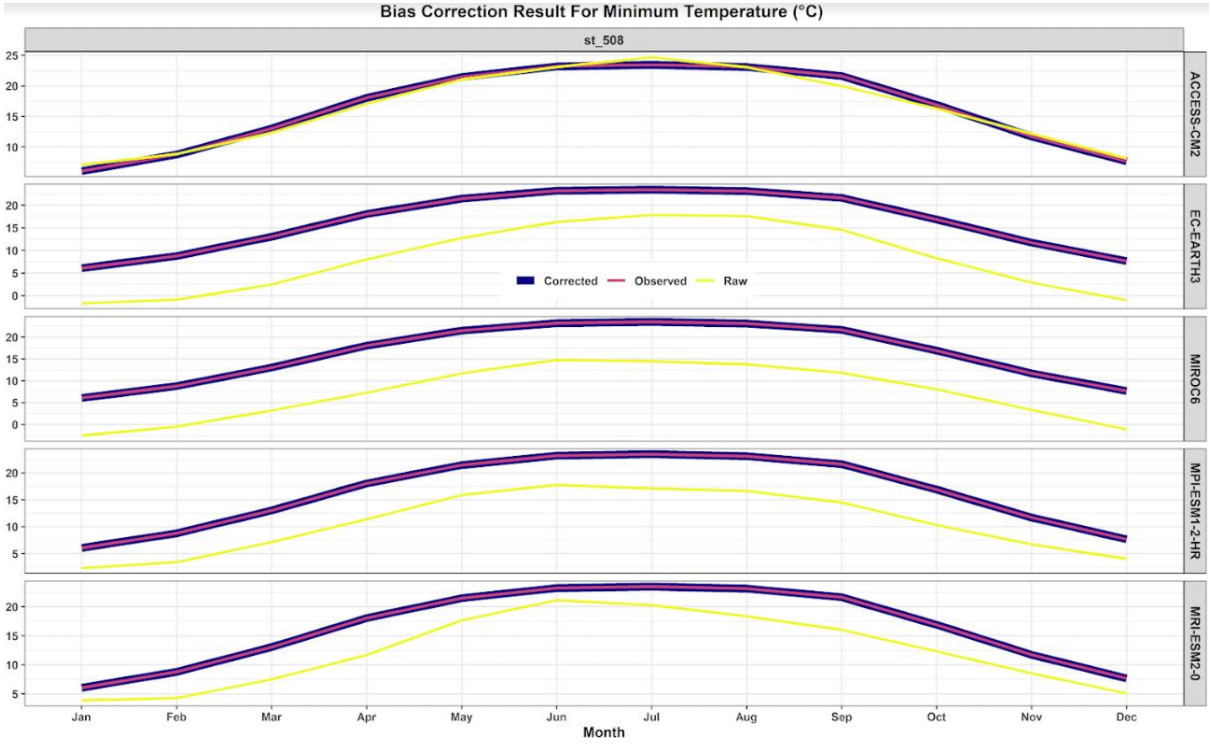

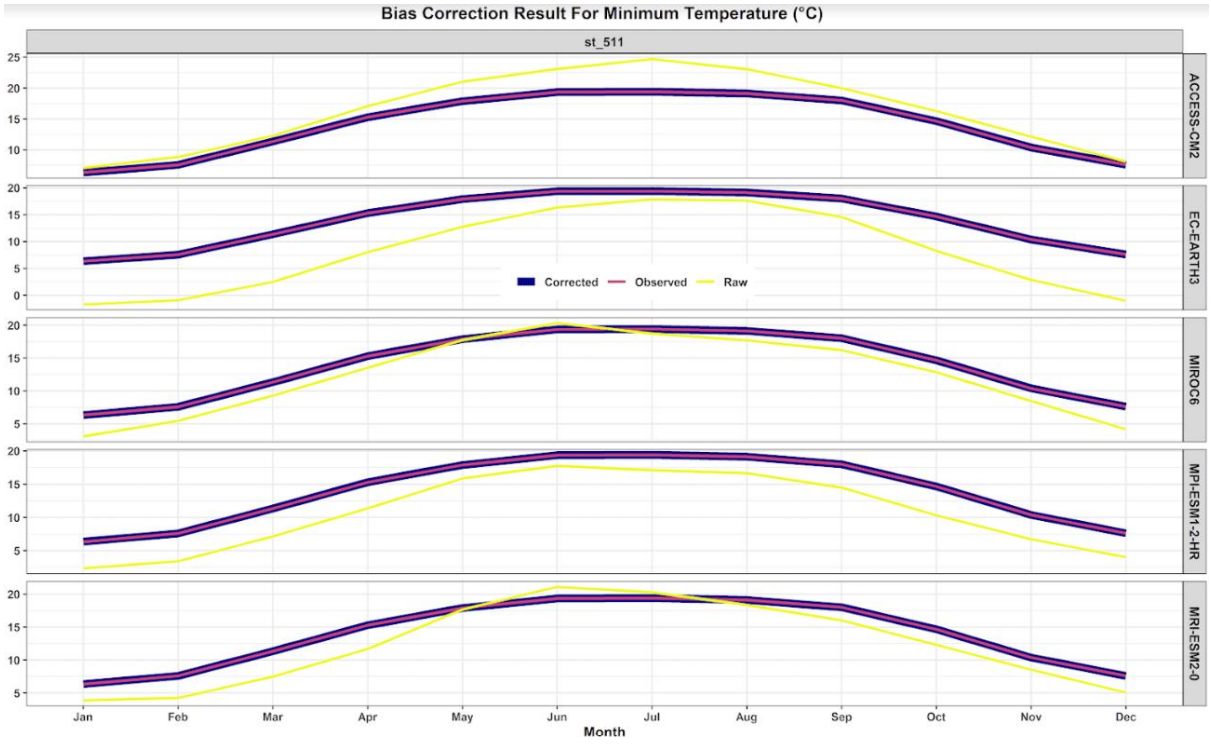

Figure 6.3: Comparison of raw and bias corrected data with observed data for minimum temperature of baseline period and for five GCMs used in study.

6.2 Projected Changes in Precipitation

Projected precipitation at an annual scale in future period shows no trend as shown in **Figure 6.4**. Annual total precipitation ranges are 1463–2530 (1583-2564) mm (NF), 1601-2495 (1446-2702) mm (MF), and 1428-2805 (1446-2702) mm (FF), respectively, for the three future periods under SSP245 (SSP585) scenarios against the baseline annual precipitation of 1721 mm. When we progress further in the future, it signifies a rise in the uncertainty range.

The five GCMs' range of predicted changes in total precipitation is depicted in **Figure 6.5**. The yearly ranges are obviously not reflective of seasonal fluctuations since the positive and negative changes over the seasons are averaged out in the annual data (Pandey et al., 2019). When using the predictions' range as a measure of uncertainty, the annual and monsoon (JJAS) precipitation have the lowest levels of uncertainty. Post-monsoon (ON) precipitation shows a substantial amount of uncertainty for all of the scenarios and futures examined. While different GCM estimates for the yearly and monsoon seasons are comparable, they diverge greatly for other seasons. The predicted changes in average annual and seasonal precipitation values for the SSP245 and SSP585 scenarios are shown in **Table 6.4** (Nayabasti, Dang), **Table 6.5** (Tulsipur), **Table 6.6** (Salyan Bazar), and **Table 6.7** (Luwamjung Bazar) based on the ensemble of five GCMs. Average yearly values are predicted to rise over the course of three future periods under the SSP245 and SSP585 scenarios, while the rate of change changes over time. From **Table 6.4** it is seen that average annual precipitation is predicted to increase by 13% in NF, 22% in MF, and 22% in FF in the SSP245 scenario compared to baseline annual precipitation. However, the range ranges over time from -15 to 47% in NF, -7to 45% in MF, and -17to 63% in FF on the annual scale. The average annual rainfall is predicted to increase by 12% in NF, 28% in MF, and 53% in FF under the SSP585 scenario. However, the range ranges over time from -8 to 49% in NF, -16 to 57% in MF, and 21 to 106% in FF on the annual scale. Similarly, rate of changes in precipitation at other stations are tabulated in **Table 6.4**, **Table 6.5**, **Table 6.6** and **Table 6.7**.

Table 6.4 shows that from NF to FF, JJAS and ON seasons had consistent rising tendencies. The DJF season has a constant progressive dropping tendency for the SSP245 scenario from NF to FF, whereas all other seasons exhibit a rising trend. The range of projection brackets increases as we travel from NF to FF, indicating a larger level of uncertainty in projection as we approach closer to the far future **Figure 6.4**. The results discussed above clearly show that climate change will result in a drier winter/dry season and wetter other seasons, which is concerning because it will cause energy and water scarcity during the dry season and may exacerbate water-related calamities like landslides and floods during monsoon season (Bajracharya et al., 2018)

Table 6.4: Change (%) in precipitation at Nayabasti station (index: 507) for SSP245 and SSP585 scenarios

Season	Parameter	SSP245			SSP585			Baseline (mm)
		NF	MF	FF	NF	MF	FF	
Annual	mean	13	22	22	12	28	53	1,721
	range	-15-47	-7-45	-17-63	-8-49	-16-57	21-106	
DJF	mean	-4	-19	-15	-11	-7	-18	69
	range	-66-61	-69-88	-75-92	-64-78	-61-72	-71-70	
JJAS	mean	11	21	23	10	28	53	1,449
	range	-20-51	-10-54	-16-65	-12-52	-10-66	9-109	
MAM	mean	21	40	16	30	30	53	146
	range	-41-108	-14-177	-53-82	-24-79	-53-103	-30-153	
ON	mean	44	53	42	39	58	131	57
	range	-73-226	-91-221	-67-204	-66-228	-82-199	-38-395	

Table 6.5: Change (%) in precipitation at Tulsipur station (index: 508) for SSP245 and SSP585 scenarios

Season	Parameter	SSP245			SSP585			Baseline(mm)
		NF	MF	FF	NF	MF	FF	
Annual	mean	13	24	24	13	28	55	1,626
	range	-10-52	-1-49	-11-63	-8-45	-12-56	20-102	
DJF	mean	-4	-22	-16	-16	-10	-20	52
	range	-63-79	-64-76	-77-91	-69-57	-68-114	-76-77	
JJAS	mean	11	21	25	10	28	52	1,361
	range	-19-53	-5-57	-9-65	-12-45	-6-62	7-103	
MAM	mean	26	43	19	34	36	60	127
	range	-32-98	-14-172	-50-82	-20-68	-43-116	-24-155	
ON	mean	50	67	44	39	54	133	86
	range	-39-181	-82-240	-62-195	-61-165	-74-175	-28-353	

Table 6.6: Change in precipitation at Salyan Bazar station (index: 511) for SSP245 and SSP585 scenarios

Season	Parameter	SSP245			SSP585			Baseline (mm)
		NF	MF	FF	NF	MF	FF	
Annual	mean	13	22	22	12	27	52	1,626
	range	-10 - 47	-6 - 44	-17 - 62	-9 - 47	-16 - 56	19 - 100	
DJF	mean	-2	-19	-13	-10	-5	-18	52
	range	-62 - 78	-71 - 92	-78 - 96	-69 - 79	-67 - 94	-74 - 85	
JJAS	mean	10	20	22	9	26	50	1,361
	range	-20 - 49	-11 - 52	-17 - 63	-12 - 47	-11 - 62	9 - 103	
MAM	mean	22	38	17	30	31	51	127
	range	-37 - 94	-13 - 158	-51 - 81	-22 - 73	-49 - 104	-29 - 142	
ON	mean	45	57	44	33	51	124	86
	range	-59 - 175	-85 - 208	-66 - 195	-56 - 154	-73 - 170	-49 - 313	
Change is reported in %								

Table 6.7: Change in precipitation at Luwamjula Bazar station (index: 512) for SSP245 and SSP585 scenarios

Season	Parameter	SSP245			SSP585			Baseline (mm)
		NF	MF	FF	NF	MF	FF	
Annual	mean	14	23	25	12	32	59	961
	range	-18 - 48	-10 - 45	-17 - 62	-9 - 52	-13 - 65	29 - 130	
DJF	mean	-6	-19	-18	-13	-9	-21	82
	range	-65 - 59	-68 - 77	-72 - 76	-61 - 70	-64 - 52	-71 - 50	
JJAS	mean	14	25	30	12	36	66	751
	range	-21 - 59	-12 - 63	-15 - 74	-12 - 56	-6 - 84	10 - 145	
MAM	mean	16	36	12	24	25	49	92
	range	-50 - 114	-21 - 171	-57 - 71	-22 - 88	-62 - 94	-36 - 163	
ON	mean	44	56	45	40	57	132	36
	range	-64 - 205	-83 - 201	-58 - 214	-59 - 187	-75 - 187	-33 - 403	
Change is reported in %								

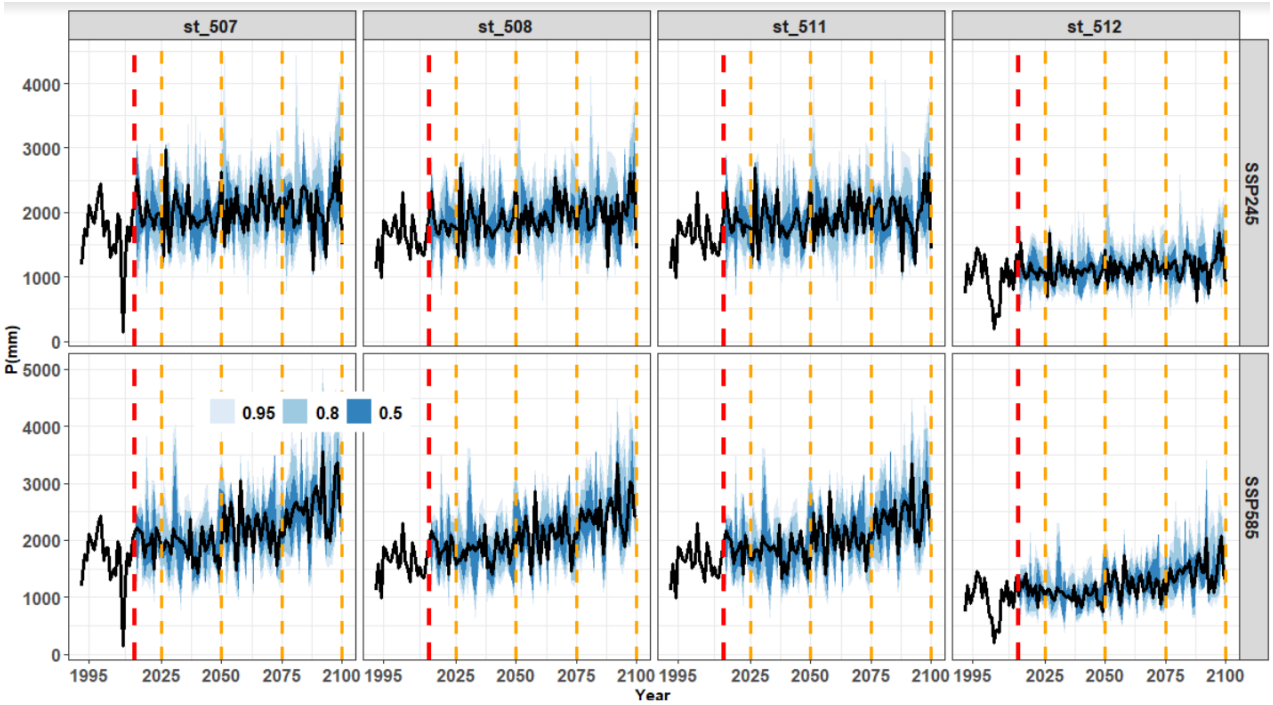

Figure 6.4: Trends in long-term annual precipitation.

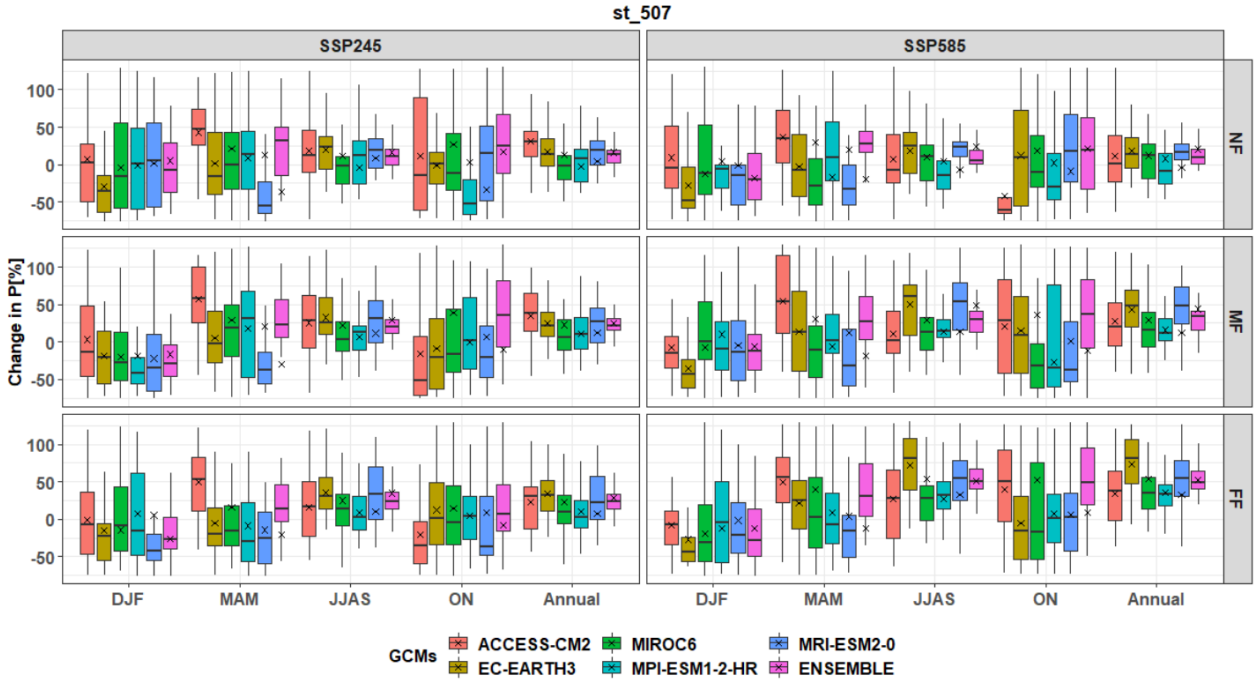
st_507
SSP245
SSP585
NF
MF
FF
Change in P[%]
100
50
0
-50
DJF
MAM
JJAS
ON
Annual
GCMs
ACCESS-CM2
EC-EARTH3
MIROC6
MPI-ESM1-2-HR
MRI-ESM2-0
ENSEMBLE

(a)

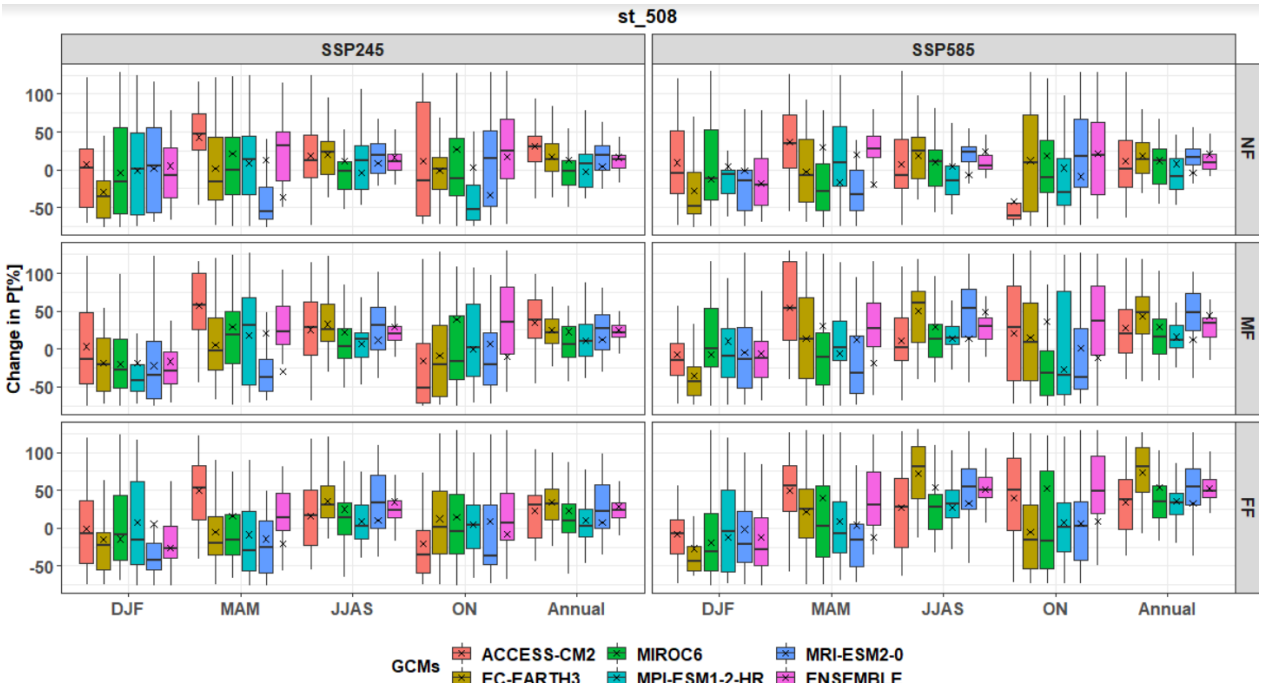
st_508
SSP245
SSP585
NF
MF
FF
Change in P[%]
100
50
0
-50
DJF
MAM
JJAS
ON
Annual
GCMs
ACCESS-CM2
MIROC6
MRI-ESM2-0

(b)

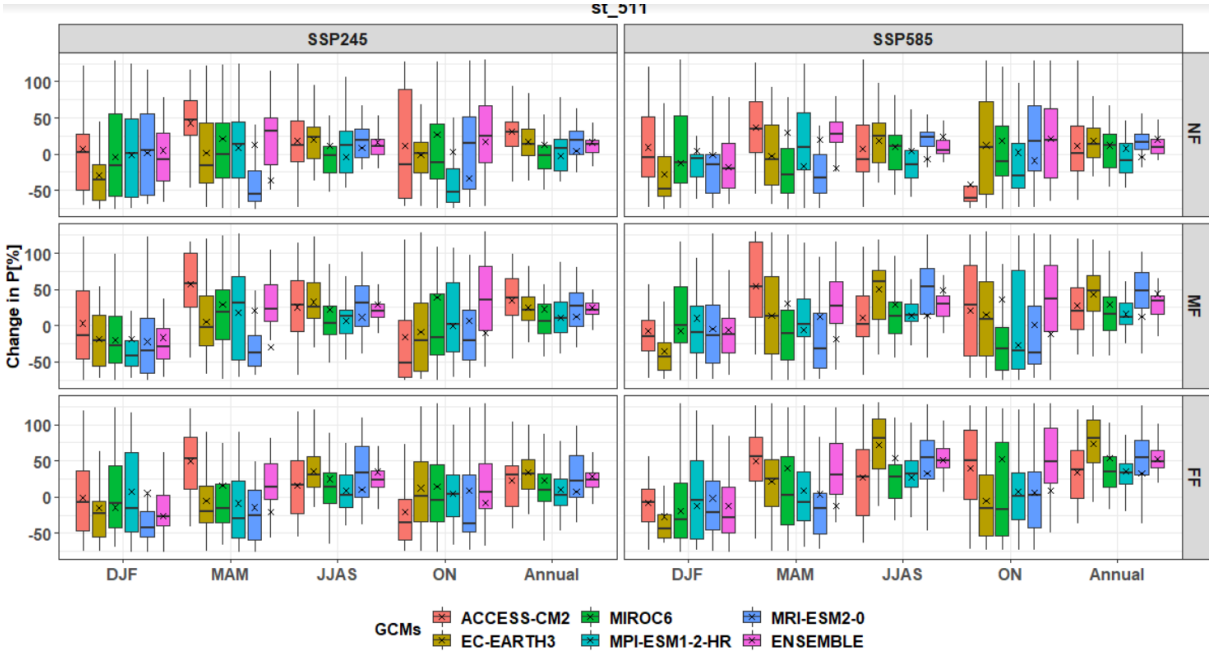

(c)

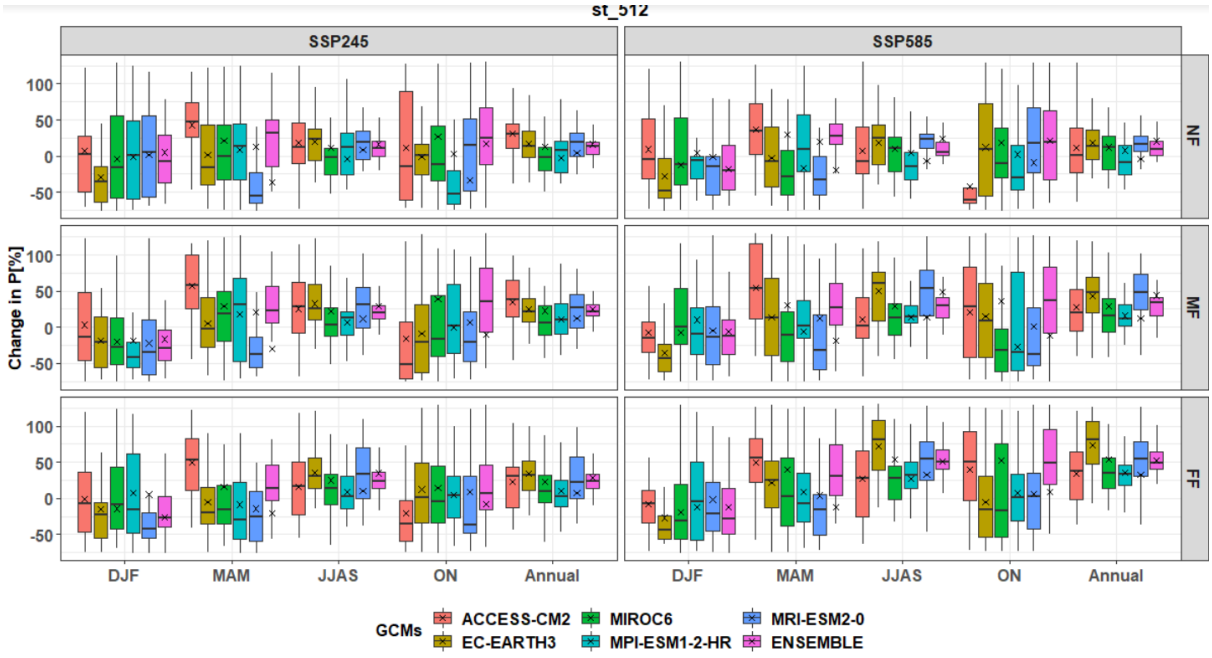

(d)

Figure 6.5: Range of projected change in annual total future precipitation across future period for five GCMs under both scenarios (SSP245 and SSP585) at (a) Nayabasti station (index: 507), (b) Tulsipur stations (index: 508), (c) Salyan Bazar station (index: 511), (d) Luwamjula Bazar station (index: 512).

6.3 Projected Changes in Temperature

The anticipated temperature shows a clear upward trend until the end of the century for both maximum and lowest temperatures, as seen in **Figure 6.6** and **Figure 6.7**. In comparison to the baseline annual average minimum temperature (29 °C), for station 508 **Table 6.8** displays the anticipated range of average annual maximum temperatures for each future period as 0.6-1.6 (0.6-2.1) % for NF, 1.4-2.6 (2-3.6) % for MF, and 2-3 (3.3-4.9) % for FF. According to **Table 6.10**, the average annual minimum temperature under SSP245 (SSP585) scenarios varies from 0.6 to 1.5

(0.4 to 2.0) % for NF, 1.4 to 2.5 (2.2 to 3.9) % for MF, and 2.1 to 2.9 (3.7 to 5.5) % for FF compared to the baseline annual average minimum temperature (16.3 °C). Similarly changes in minimum and maximum temperature at station 511 are tabulated in **Table 6.9** and **Table 6.11** respectively. As the future draws nearer, the range in both scenarios grows, indicating more uncertainty in the far future **Figure 6.6** and **Figure 6.7**.

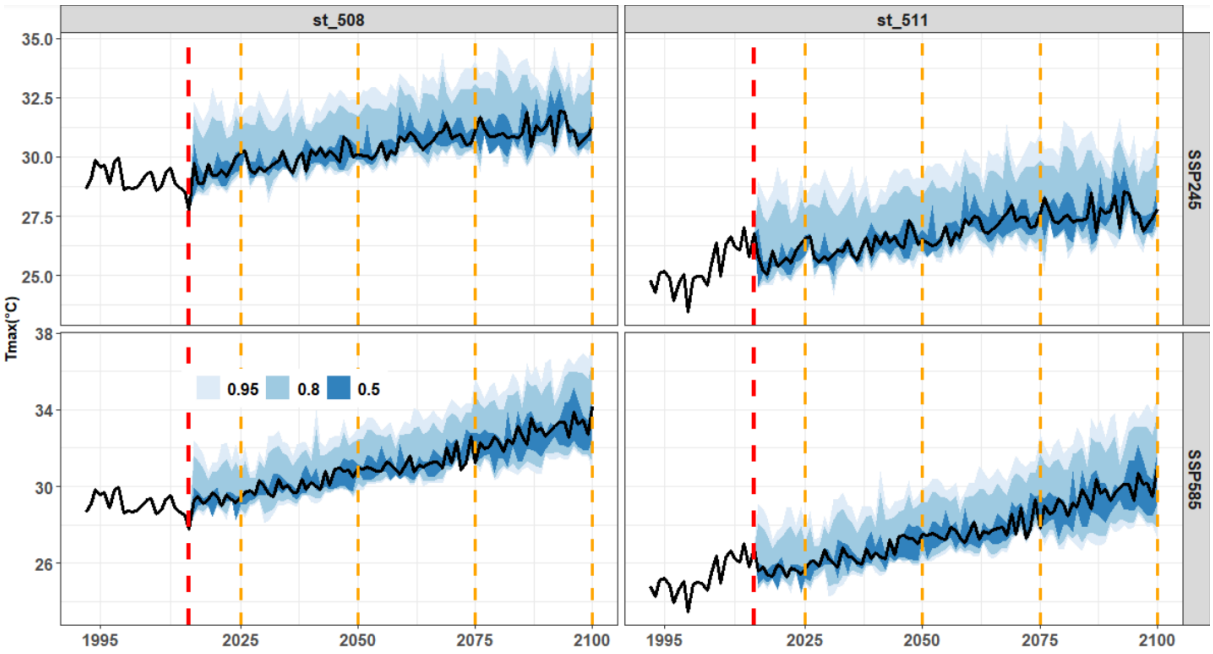

Figure 6.6: Trends in long-term annual average maximum temperature.

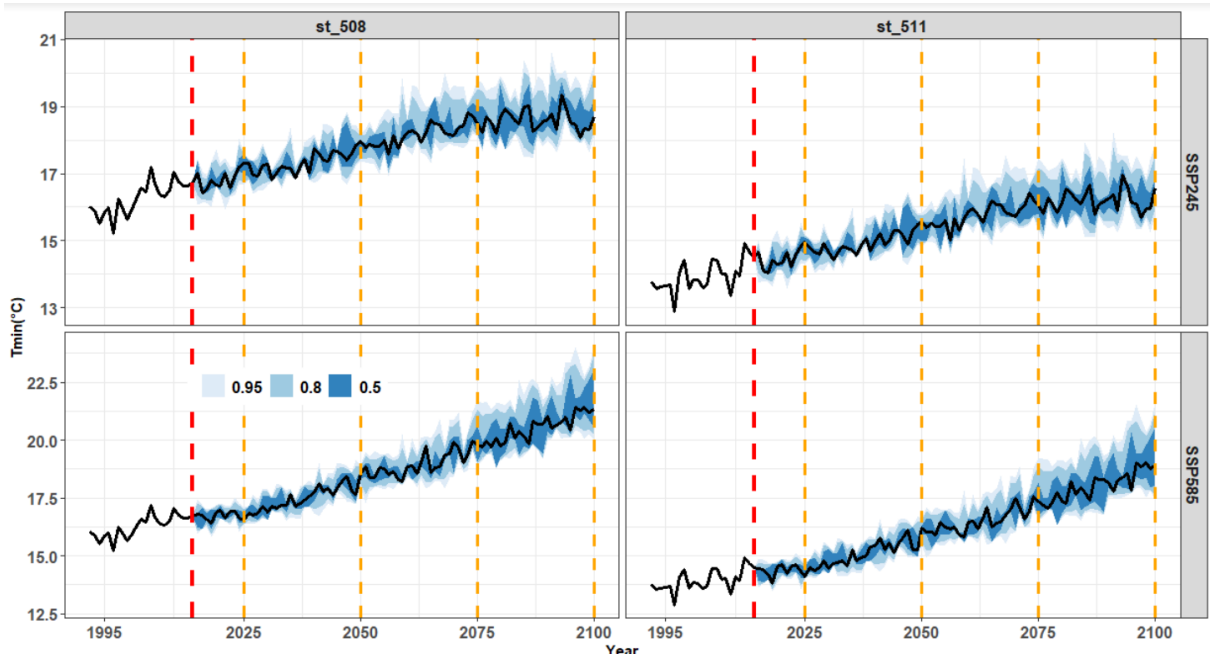

Figure 6.7: Trends in long-term annual average minimum temperature.

i. Maximum temperature

More acceptance and assurance are offered by the range of maximum temperature estimates made by various GCMs than by the range of precipitation forecasts. All changes for all GCMs, SSPs, and futures suggest an increase with both means and medians. As shown in **Table 6.8** for station

508, predicted average annual maximum temperatures for SSP245 scenarios, based on an ensemble of five GCMs, are slowly rising across three future periods relative to the baseline (29 °C) by 1.2 °C (for NF), 2 °C (for MF), and 2.4 °C (for FF). For SSP585, increases of 01.3°C (for NF), 2.5°C (for MF), and 4°C (for FF) are anticipated. Though the pace of rise changes from season to season, it is also rising. The DJF season is predicted to warm by 1.3°C in NF, 1.5°C in MF, and 2.6°C in FF under SSP245 (SSP585) scenarios, but the MAM season is predicted to warm by 1.4°C in NF, 2.3°C in MF, and 2.8°C (4.2°C) in FF. It demonstrates that warmer winters are anticipated in all of the investigated future periods in the Dang watershed. The projection's range of uncertainty is fairly significant throughout the winter (DJF) and pre-monsoon (MAM) seasons, as illustrated in **Figure 6.8**.

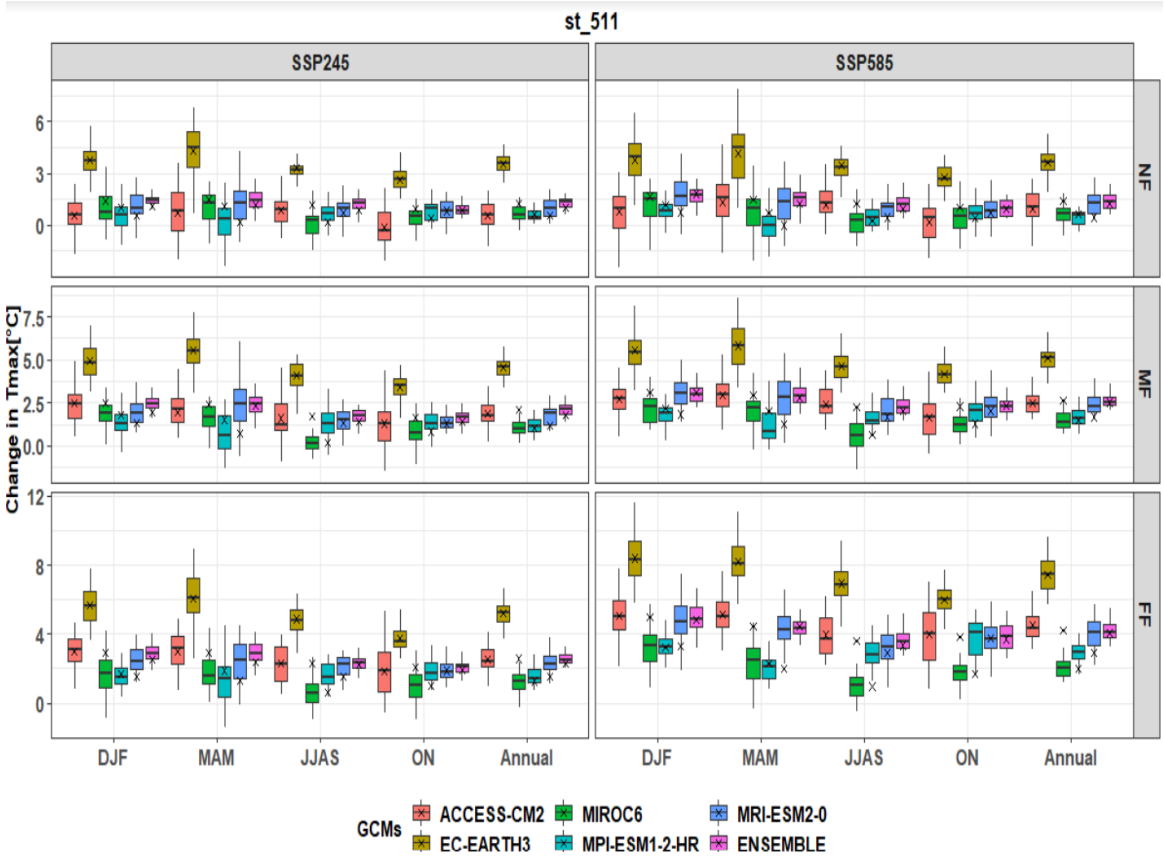

(a)

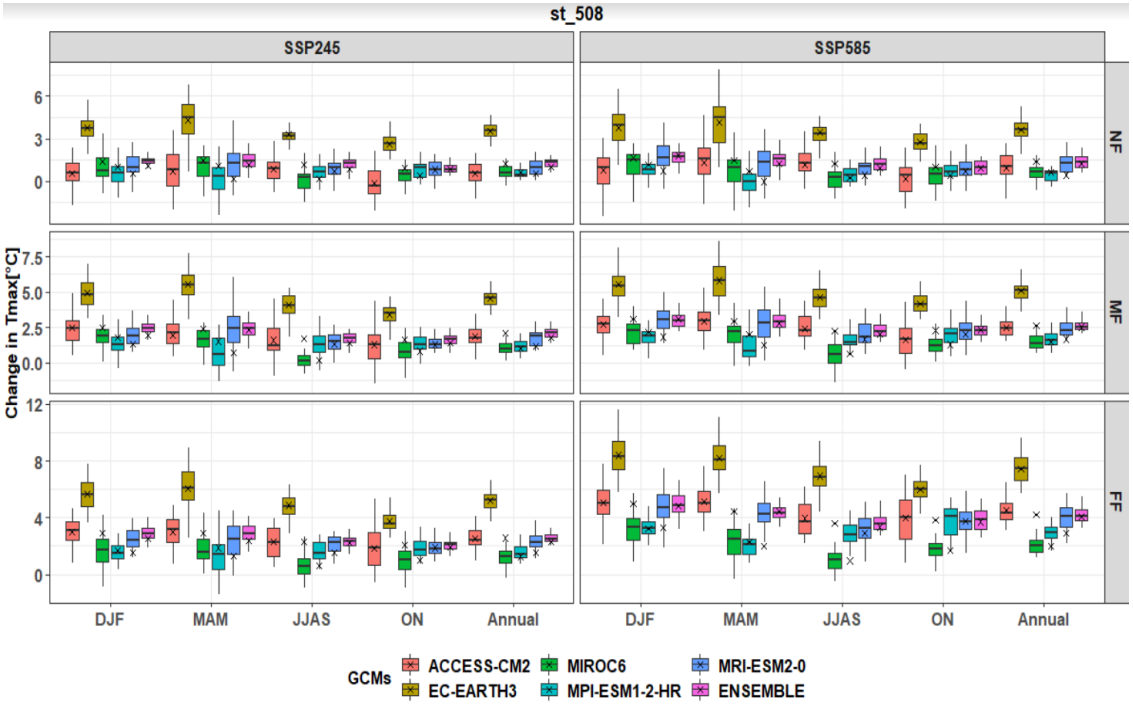

(b)

Figure 6.8: Range of projected change in future maximum temperature across future period for five GCMs under both scenarios (SSP245 and SSP585) at (a) Nayabasti station (index: 507), (b) Tulsipur stations (index: 508).

Table 6.8: Change in future maximum temperature [°C] projected at station Tulsipur (index: 508) based on ensemble of five GCMs under SSPs scenarios.

Season	Parameter	SSP245			SSP585			Baseline (°C)
		NF	MF	FF	NF	MF	FF	
Annual	mean	1.2	2.0	2.4	1.3	2.5	4.0	29.0
	range	0.6 - 1.6	1.4 - 2.6	2.0 - 3.0	0.6 - 2.1	2.0 - 3.6	3.3 - 4.9	
DJF	mean	1.3	2.3	2.6	1.5	2.8	4.5	22.8
	range	0.6 - 1.8	1.6 - 3.2	1.9 - 3.5	0.5 - 2.3	2.2 - 4.2	3.2 - 5.5	
JJAS	mean	1.2	1.7	2.3	1.2	2.2	3.5	31.7
	range	0.1 - 2.0	0.7 - 2.3	1.4 - 3.0	0.4 - 2.4	1.4 - 3.4	2.7 - 5.0	
MAM	mean	1.4	2.3	2.8	1.4	2.8	4.2	32.4
	range	0.2 - 2.4	0.8 - 3.2	1.6 - 3.7	-0.3 - 2.6	1.9 - 4.1	3.4 - 5.3	
ON	mean	0.9	1.6	2.0	1.0	2.2	3.7	28.0
	range	0.4 - 1.6	0.7 - 2.2	1.2 - 3.1	0.4 - 1.7	1.4 - 3.3	2.6 - 4.8	
Change is reported in °C								

Table 6.9: Change in future maximum temperature [°C] projected at Salyan Bazar station (index: 511) based on ensemble of five GCMs under SSPs scenarios.

Season	Parameter	SSP245			SSP585			Baseline (°C)
		NF	MF	FF	NF	MF	FF	
Annual	mean	0.6	1.2	1.6	0.5	1.8	3.1	25.3
	range	-0.5 - 1.7	0.4 - 2.1	0.8 - 2.8	-0.4 - 1.0	0.7 - 3.2	1.9 - 4.0	
DJF	mean	0.6	1.5	1.7	0.8	2.0	3.6	20.2
	range	-1.2 - 2.8	-0.6 - 3.0	0.4 - 2.8	-1.7 - 2.0	0.3 - 3.6	2.5 - 5.0	
JJAS	mean	0.8	1.4	1.6	0.5	1.7	3.0	27.4
	range	-0.6 - 2.8	-0.5 - 3.3	0.4 - 2.8	-0.3 - 1.5	0.6 - 3.4	1.4 - 4.5	
MAM	mean	0.2	0.8	1.4	0.0	1.3	2.1	27.6
	range	-2.4 - 2.5	-1.3 - 2.7	-1.4 - 4.5	-1.8 - 2.1	-0.2 - 3.8	1.0 - 3.5	
ON	mean	0.9	1.3	2.0	0.7	2.1	4.0	25.2
	range	-0.3 - 2.0	-0.1 - 2.5	0.8 - 3.4	-0.8 - 2.3	0.5 - 3.7	1.7 - 5.4	
Change is reported in °C								

ii. Minimum temperature

In comparison to the range of precipitation estimates, the range of lowest temperature projections across the several GCMs is more stable and predictable. All changes for all GCMs, SSPs, and futures suggest an increase with both means and medians. Based on an ensemble of five GCMs, for station 508 **Table 6.10** the SSP245 scenarios expected average annual minimum temperature slowly rises across three future periods relative to the baseline (16.3°C) by 1.1 °C (for NF), 2 °C (for MF), and 2.4 °C (for FF). For SSP585, increases of 1.2°C (for NF), 2.7°C (for MF), and 4.5°C (for FF) are anticipated. The rising propensity is the same in all seasons and for all circumstances, even if the rate of increase varies with the season. As shown in **Figure 6.9** and **Table 6.10**, the MAM season is predicted to warm by 1.3°C (1.4°C) in NF, 2.4°C (3.1°C) in MF, and 2.9°C (5.0°C) in FF under SSP245 (SSP585) scenarios, while the ON season is predicted to warm by 1.2°C (1.4°C) in NF, 2.4°C (3.3°C) in MF, and 2.9°C (5.8°C).

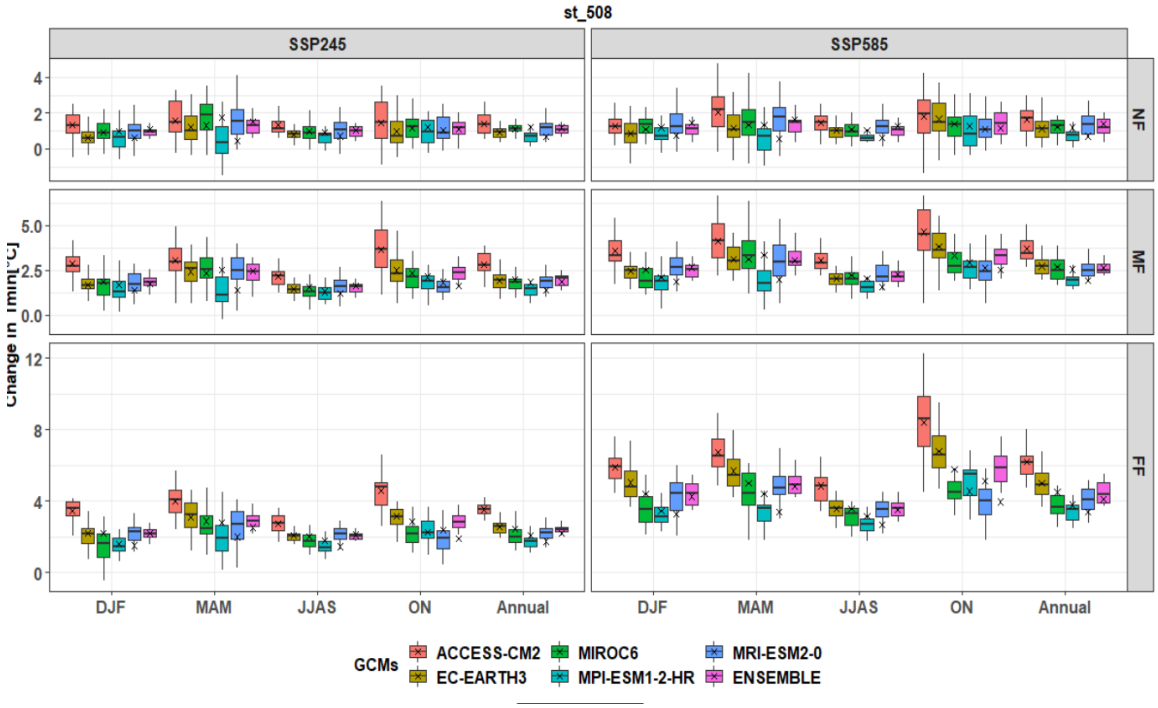

(a)

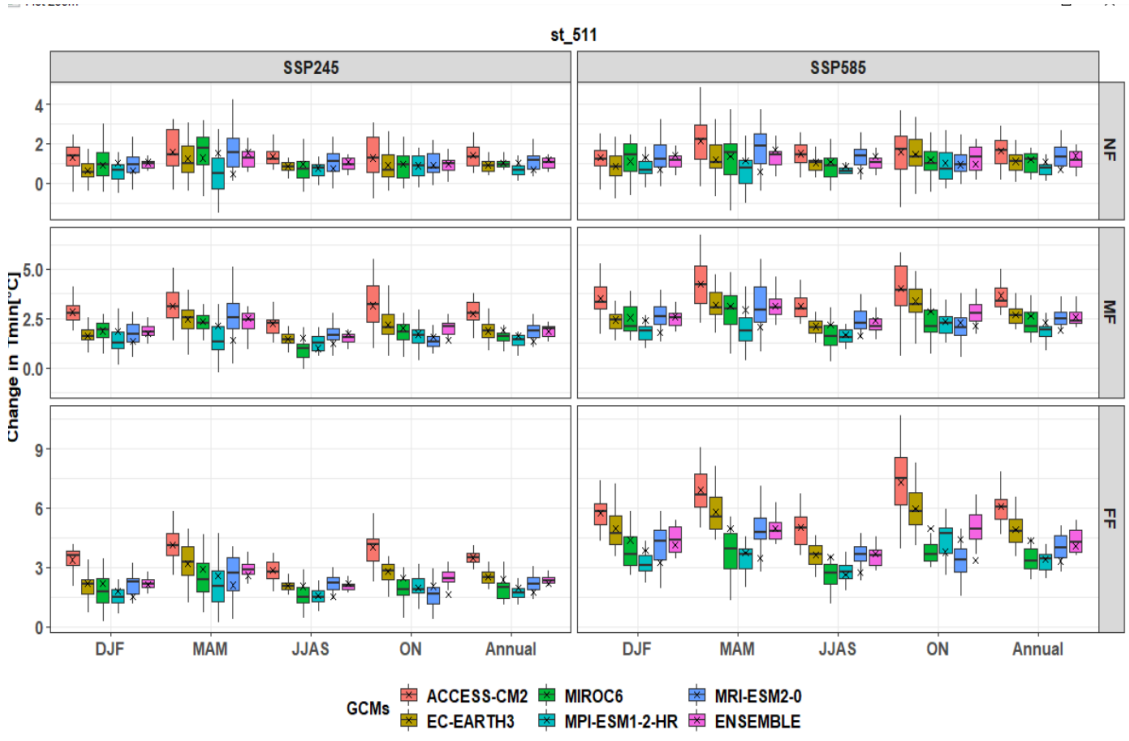

(b)

Figure 6.9: Range of projected change in future minimum temperature across future period for five GCMs under both scenarios (SSP245 and SSP585) at (a) Nayabasti station (index: 507), (b) Tulsipur stations (index: 508).

Table 6.10: Change in future minimum temperature at Tulsipur station (index: 508) for both SSP245 and SSP585 scenarios using 5 different GCMs under SSPs scenarios.

Season	Parameter	SSP245			SSP585			Baseline (°C)
		NF	MF	FF	NF	MF	FF	
Annual	mean	1.1	2.0	2.4	1.2	2.7	4.5	16.3
	range	0.6 - 1.5	1.4 - 2.5	2.1 - 2.9	0.4 - 2.0	2.2 - 3.9	3.7 - 5.5	
DJF	mean	0.9	1.9	2.2	1.1	2.5	4.4	7.4
	range	0.1 - 1.4	1.1 - 2.8	1.6 - 2.8	0.4 - 1.8	1.9 - 4.2	3.5 - 5.4	
JJAS	mean	1.0	1.6	2.0	1.1	2.2	3.6	22.9
	range	0.4 - 1.4	1.0 - 2.0	1.7 - 2.4	0.3 - 1.8	1.5 - 3.0	2.8 - 4.5	
MAM	mean	1.3	2.4	2.9	1.4	3.1	5.0	17.5
	range	0.6 - 2.3	1.0 - 3.2	1.7 - 3.8	-0.3 - 2.6	2.2 - 4.6	4.2 - 6.3	
ON	mean	1.2	2.4	2.9	1.4	3.3	5.8	14.3
	range	0.0 - 2.0	1.6 - 3.2	2.1 - 3.8	0.2 - 2.6	2.0 - 4.5	4.5 - 7.6	
Change is reported in °C								

Table 6.11: Change in future minimum temperature at Salyan Bazar station (index: 511) for both SSP245 and SSP585 scenarios using 5 different GCMs under SSPs scenarios.

Season	Parameter	SSP245			SSP585			Baseline (°C)
		NF	MF	FF	NF	MF	FF	
Annual	mean	0.7	1.4	1.7	0.7	1.9	3.3	13.9
	range	0.1 - 1.4	0.6 - 1.8	1.1 - 2.6	0.1 - 1.4	0.9 - 3.1	2.4 - 4.2	
DJF	mean	0.6	1.3	1.5	0.7	1.8	3.2	7.2
	range	-0.5 - 2.1	0.2 - 3.0	0.6 - 2.4	-0.6 - 1.8	0.3 - 3.2	2.2 - 4.3	
JJAS	mean	0.7	1.2	1.5	0.6	1.6	2.7	19.0
	range	-0.1 - 1.9	0.6 - 2.0	0.7 - 2.3	-0.1 - 1.2	0.9 - 2.2	1.8 - 3.8	
MAM	mean	0.5	1.4	2.1	0.6	2.1	3.5	14.8
	range	-1.5 - 2.7	-0.2 - 3.2	0.2 - 4.7	-1.0 - 2.4	0.3 - 4.1	2.0 - 4.5	
ON	mean	0.9	1.6	2.0	0.9	2.3	4.4	12.5
	range	-0.2 - 1.8	0.4 - 2.9	0.9 - 3.1	-0.3 - 2.6	1.3 - 3.5	2.6 - 5.9	
Change is reported in °C								

7 IMPACT OF CLIMATE CHANGE ON CROP YIELD

7.1 Model Calibration and Validation

We follow an indirect approach to calibrate soil fertility level due to lack of field observation data. Calibration is done based on farmer survey data; amount of fertilizer they applied to the field with reference to Nation Recommended Fertilizer Dose recommended by Department of Agriculture (DoA). Soil calibration is done by analyzing soil samples obtained from field as well as soil maps published by NARC (see section 7.1.2). Climate data input is obtained from projected precipitation and temperature under SSP245 and SSP585 scenarios (see section **6.2** and **6.3**). Other parameters such as irrigation and field management practices are obtained from results of farmer survey, described below in section 7.1.1.

7.1.1 Farmer survey

A total of 49 households were surveyed during our data collection phase. Some of the glimpses of our survey can be seen in **ANNEX B**. This survey became the basis for calibrating the AQUACROP model and validating soil texture obtained from soil map published by NARC. Our survey consisted of questionnaires related to crop pattern, crop yield, crop duration, use of fertilizers, and many more. For detailed information on questionnaires please see **ANNEX C**. The questionnaire was prepared and loaded into an android application called 'Form Box' and the same form was filled for each farmer. Later all the forms were exported as an excel file and valuable insights were drawn. The location of each household was recorded using GPS and later plotted as shown in **Figure 7.1**.

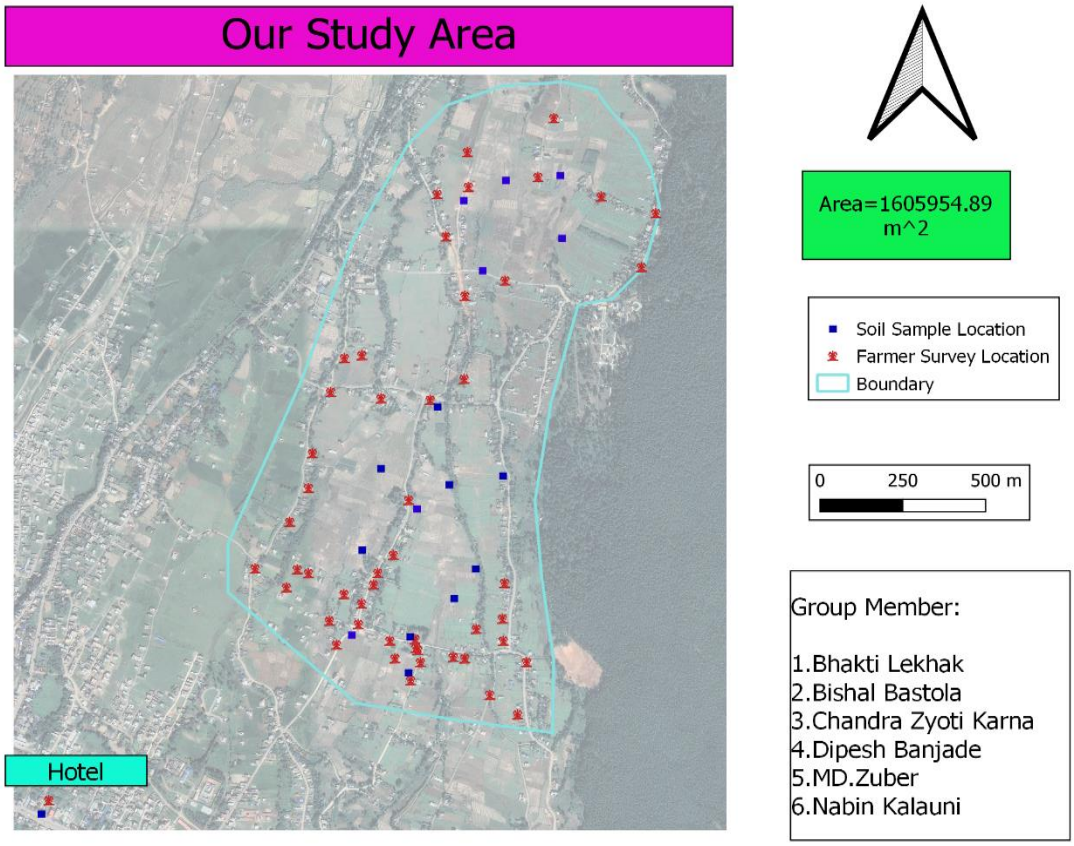

Figure 7.1: Soil sample collected and farmer survey location.

Regarding the history of farming and farmers in the study area, we found that all farmers are well experienced with 88% of farmers farming for as long as they can remember and 6% of farmers farming for the last 5-10 years and very few 6% farmers farming since 1-5 years and discussing the background of these 6% farmers who have been farming since 1-5 years are migrants who were practicing agriculture. The average land holding of each household was found to be 10 Katha with almost 69% having inherited land, 21 % having hired and only 10% having bought their land **Figure 7.2**. As we had planned to see the effect of climate change on rice production, we selected an area where 100% of farmers cultivated rice during monsoon season and after harvesting rice 29 % of farmers cultivated wheat and some cultivated mustard, gram, and maize in portions of their land.

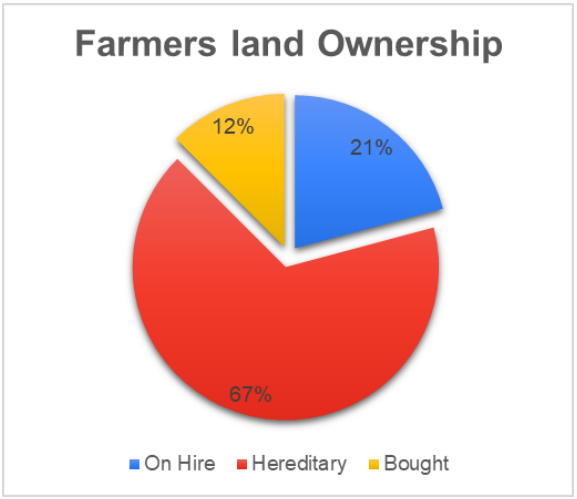

Figure 7.2: Distribution of Farmer land ownership

More than 95 % of farmers prefer to wait for monsoon rain for seed sowing, while the rest prefer fixed data at the end of Ashad. This trend is the result of the hustle they must do to get water to their plot. From our survey, we found that farmers are way more dependent on fertilizer for crop yield and in many cases, we found that about 60% of farmers were using 40% less fertilizer than National Recommended Fertilizer Dose (NRFD). And the remaining 40% of farmers were using fertilizer near to NRFD. Urea was found to be the most used fertilizer with 85% of farmers using it and 77% of farmers using DAP shown in **Figure 7.3**.

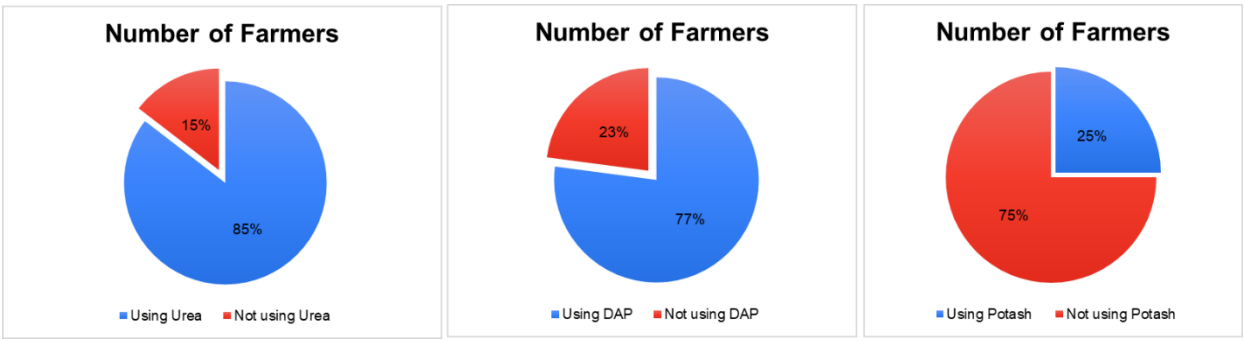

(a) (b) (c)

Figure 7.3: Distribution of fertilizer use percentiles (a) Urea, (b) DAP, (c) Potash

From our survey, we found out that the yield of both rice and wheat is more than the national survey. We concluded that the higher yield of crops is the result of the introduction of new seeds, fertilizers, and partiality of limited survey data. Besides the high use of fertilizers by 40% of farmers in Rice, farmers were not satisfied with the availability of fertilizers. They mentioned counterpart fertilizers or the unavailability of fertilizers in time is the main cause of low yield. Farmers are totally dependent on fertilizers for the yield that they invest a lot of money to buy fertilizers at high prices. Due to this reason, regardless of high yield farmers are not able to uplift their living standards. Most of the farmers even complained about the corruption during the distribution of government-supplied fertilizers.

For irrigation, 75% of farmers use water from the canal, 21% of farmers use water directly from Pato Khola, and only 4% depend on nearby water sources like Gotikhola and Sirkhola shown in **Figure 7.4**. All the farmers use flooding or furrow irrigation as a method of irrigation in the field.

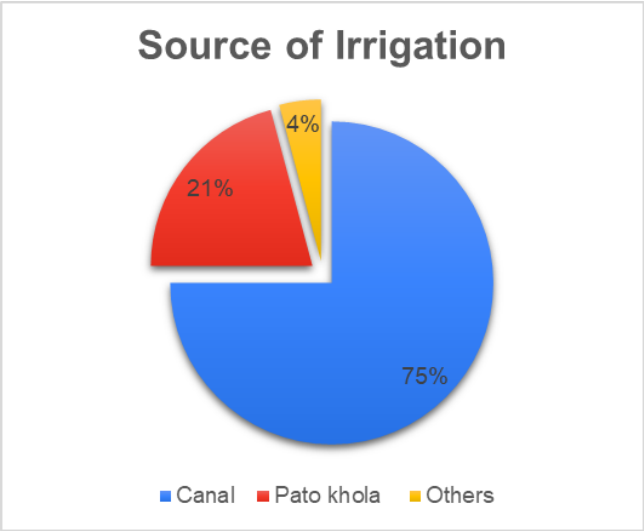

Figure 7.4: Sources of irrigation

From the survey, we found out that the availability of water for irrigation is good. But sometimes due to the arrival of late monsoon water level in rivers is low and cannel cannot draw enough water to be supplied to all farmers. During monsoon i.e., rice cultivation, 45% of farmers irrigate their land 30-40 times, 45% of farmers irrigate their land 20-30 times, 6% of farmers irrigate their land 20-30 times, and very few less than 2% of farmers irrigate their land less than 10 times during the life cycle of crop. This shows the adequacy of irrigation for rice crops. During wheat cultivation, 78% of farmers irrigate their crops more than one time. Among them 39% of farmers irrigated their crops twice and 22% of farmers did not irrigate their crop at all shown in **Figure 7.5**.

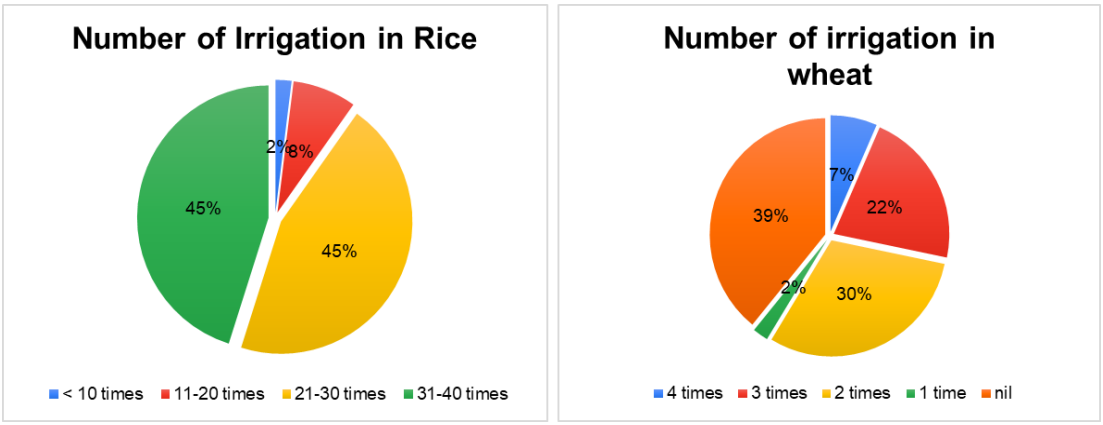

(a) (b)

Figure 7.5: Number of irrigations in (a) Rice and (b) Wheat

During the crop life of rice, 80% of farmers prefer to uproot weed. Among them most farmers prefer to uproot twice, and rest prefer only once. Regarding the use of pesticides almost all prefer to use pesticides only after the crop is attacked by pests, for these farmers take advice from nearby agrovet. The use of herbicide in crops is very limited, only 6% of farmers use herbicides.

7.1.2 Soil texture analysis

By measuring the relative proportions of the particle size classes, the soil textural class of the sample was determined by using the soil textural triangle of USDA (Soil Survey Manual, n.d.) as shown in **Figure 7.6** and **Figure 7.7**.

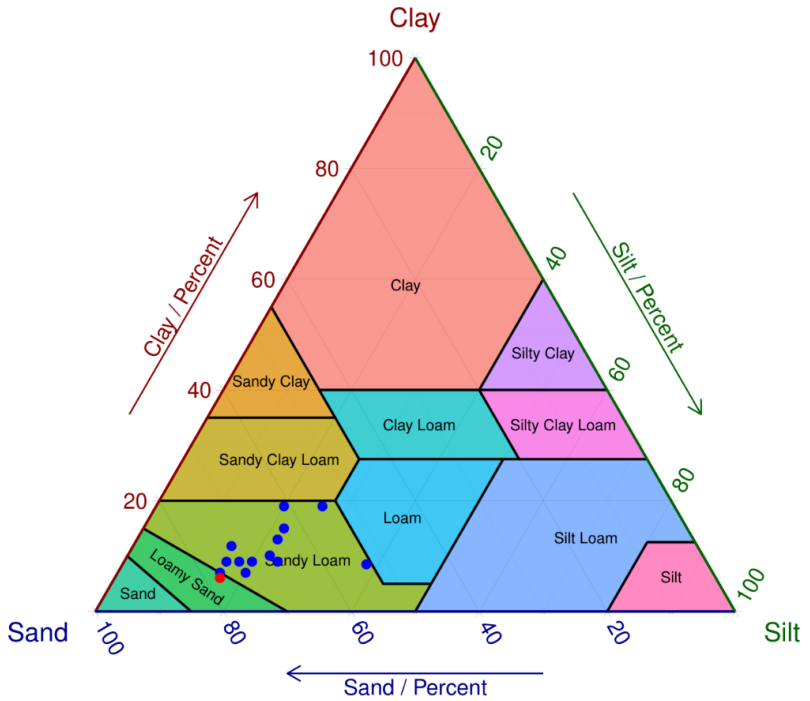

Figure 7.6: Textural classification of soil data collected from field.

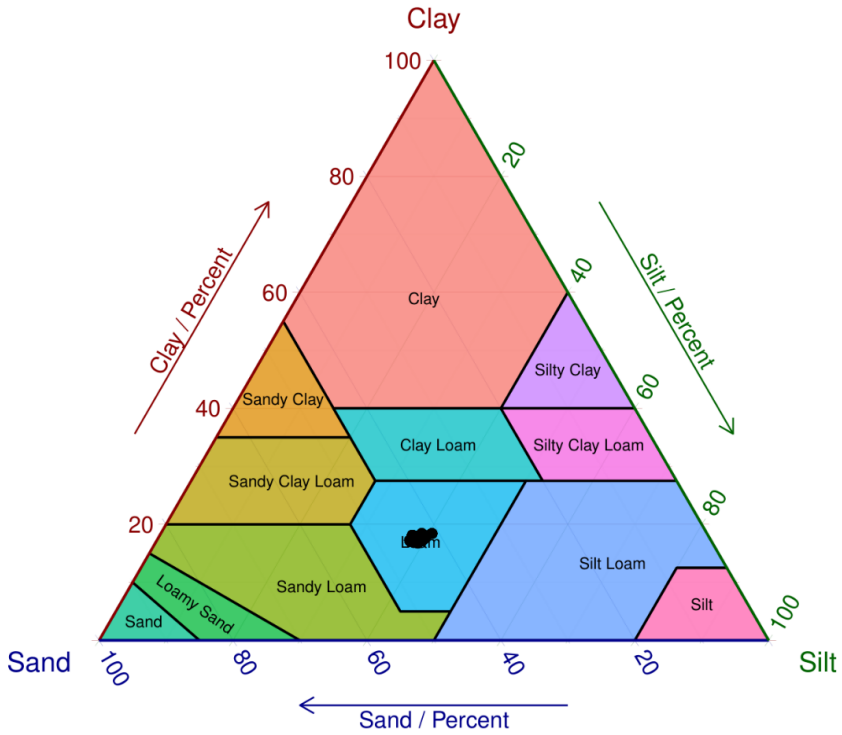

Figure 7.7: Textural classification of randomly sampled soil from NARC soil map

Soil hydraulic properties were determined based on pedotransfer function as explained in section 4.3.2. Results are presented in **Table 7.1** and **Table 7.2**

Table 7.1: Summary of Total Available Water (TAW) of soil samples collected from field.

Class	1	2	3
Range	**70-90**	**90-110**	**110-130**
Frequency	5	7	4
Mean	78.00	95.71	117.50
Median	80.00	100.00	115.00
Maximum	80.00	100.00	130.00
Minimum	70.00	90.00	110.00
Standard Deviation	4.47	5.35	9.57

Table 7.2: Summary of TAW of soil samples randomly sampled from NARC soil map.

Class	1	2	3	4	5
Range	**121-123**	**123-125**	**125-127**	**127-129**	**129-131**
Frequency	294	349	258	67	32
Mean	122.46	124.20	125.70	127.22	130.48
Median	122.69	124.35	125.64	127.11	130.48
Maximum	122.86	124.86	126.98	128.03	130.48
Minimum	121.90	123.11	125.08	127.07	130.48
Standard Deviation	0.36	0.46	0.61	0.30	0.00

The physical characteristics of the soil used in AquaCrop simulation studies, based on experimental analysis as well as sampling from the NARC soil map are presented in **Table 7.3.**

Table 7.3: Soil Physical characteristics of representative of major soil type used for crop yield simulation.

Soil Type	Permanent Wilting Point (%)	Field Capacity (vol%)	Saturation Point (%)	Total available Water (mm/m)	Saturated Hydraulic Conductivity (Ksat) mm/day
Sandy loam	10.8	23.1	45	123	464

7.1.3 Climate data

Reference evapotranspiration (ET_0) from 2000 to 2020 as calculated by AquaCrop was compared with New LocClim and from **Figure 7.8**, it is seen that the average computed daily ET_0 matches with mean monthly values estimated by New LocClim (Grieser et al., 2006).

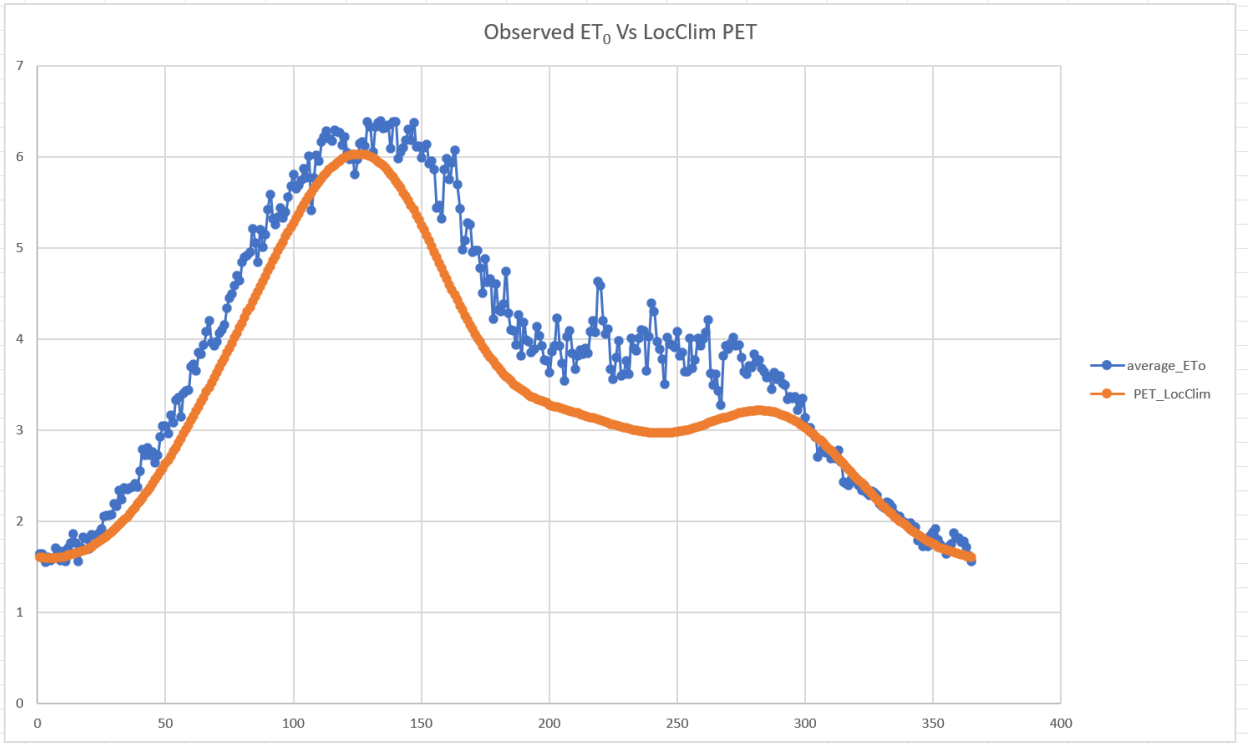

Figure 7.8: Mean monthly ET_0 (Orange line) for Tulsipur (New_LocClim) and average daily ET_0 (Blue line) calculated with the FAO Penman-Monteith method with daily data for 21 years (2000-2020) obtained from Tulsipur climatology station.

Precipitation and rainfall data for future projection is taken from the results of climate projection in section **6.2** and **6.3**. The ensemble means of five GCMs is taken as input to AquaCrop. Mean precipitation and its trend is shown in **Figure 7.9**. Reference evapotranspiration (ET_0) is calculated for future projections using the ensemble mean values of precipitation and temperature and the trend of ET_0 for both SSPs is shown in **Figure 7.10** (NF), **Figure 7.11** (MF), **Figure 7.12** (FF), **Figure 7.13** (overall).

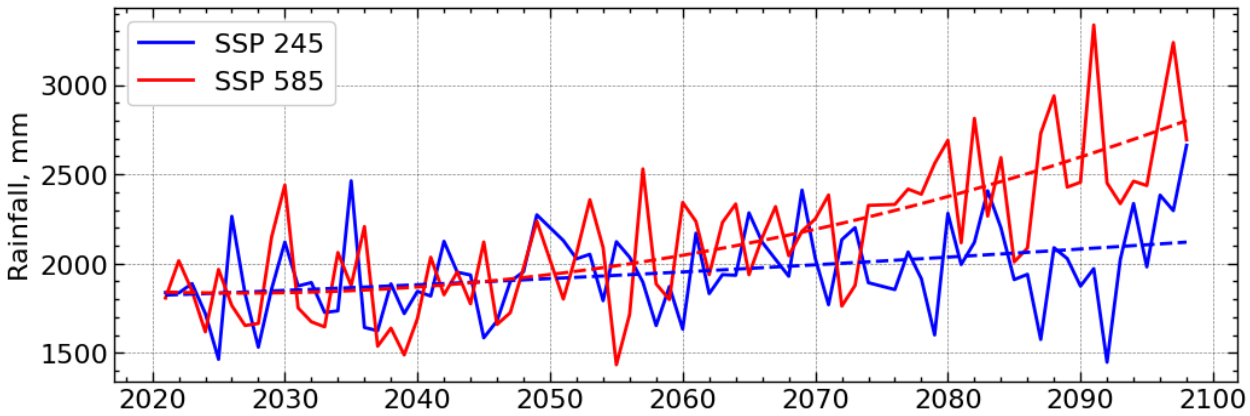

Figure 7.9: Overall Rainfall data for future scenario (2021-2099) with trend line showing increasing trend in which red dash line (SSP 585) leads blue dash line (SSP 245).

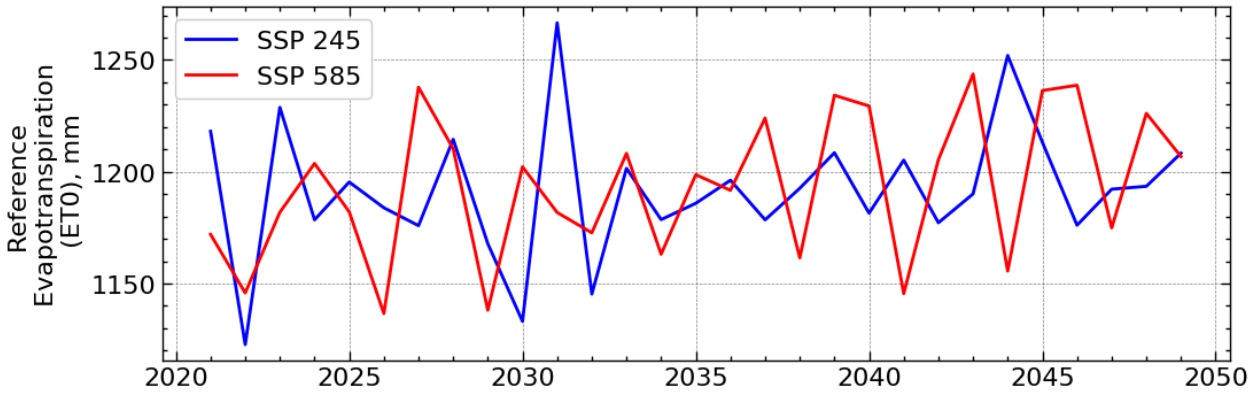

Figure 7.10: Reference evapotranspiration (ET_0) for Near future projection (2021-2050) with blue line for SSP 245 and red for SSP 585.

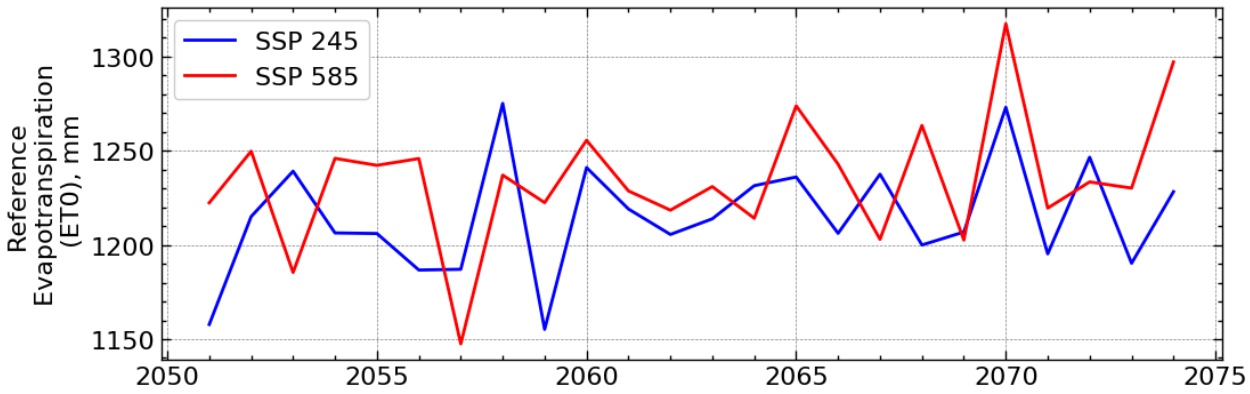

Figure 7.11: Reference evapotranspiration (ET_0) for Mid future projection (2051-2075) with blue line for SSP 245 and red for SSP 585.

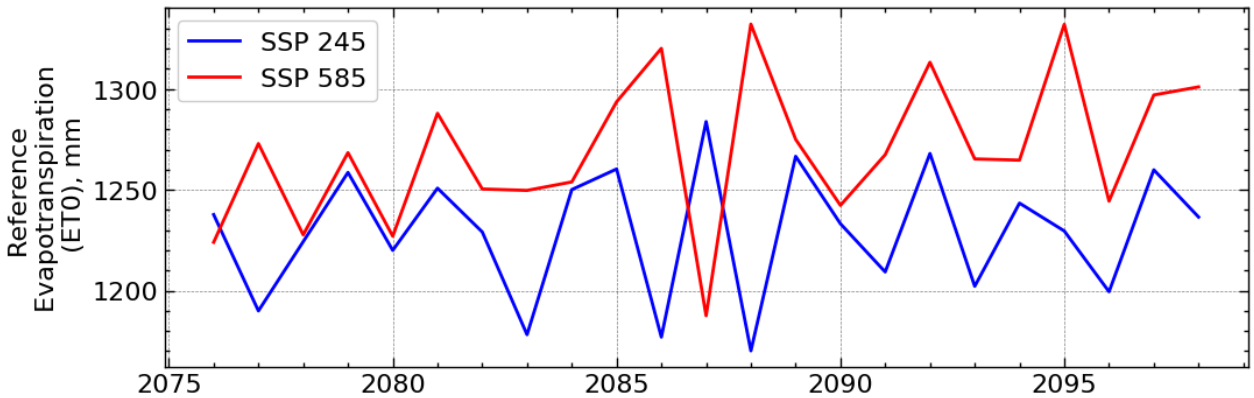

Figure 7.12: Reference evapotranspiration (ET_0) for Far future projection (2076-2099) with blue line for SSP 245 and red for SSP 585.

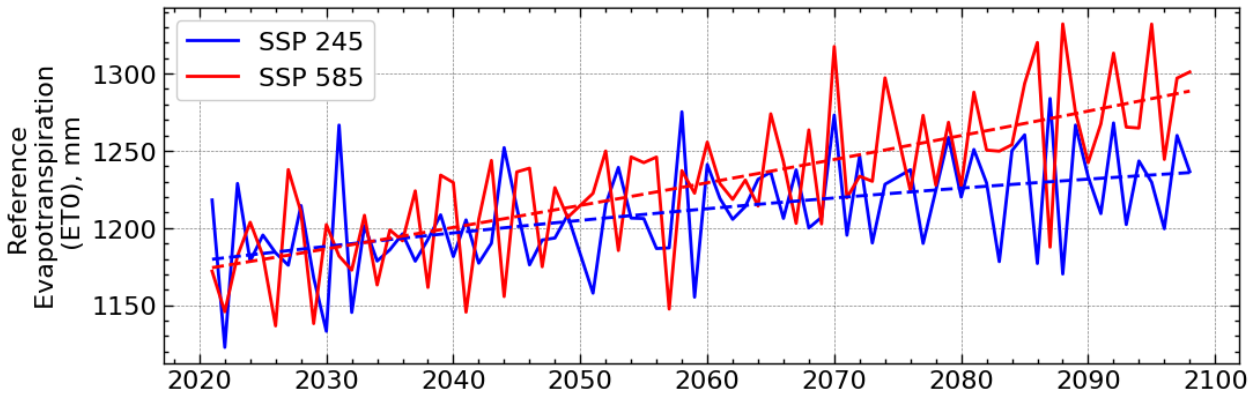

Figure 7.13: Reference evapotranspiration (ET_0) for future scenario (2021-2099) with trend line showing increasing trend in which red dash line (SSP 585) leads blue dash line (SSP 245).

Both SSP 245 and SSP 585 show climatic parameters rainfall (**Figure 7.9**), reference evapotranspiration (**Figure 7.13**) have an increasing trend.

7.1.4 Performance evaluation

A. Rice

Calibrated results for 10 years past yield data (2010-2020) published by MoALD and yield data according to farmer surveys with several fertility stress levels are presented in figure below in **Figure 7.14.**

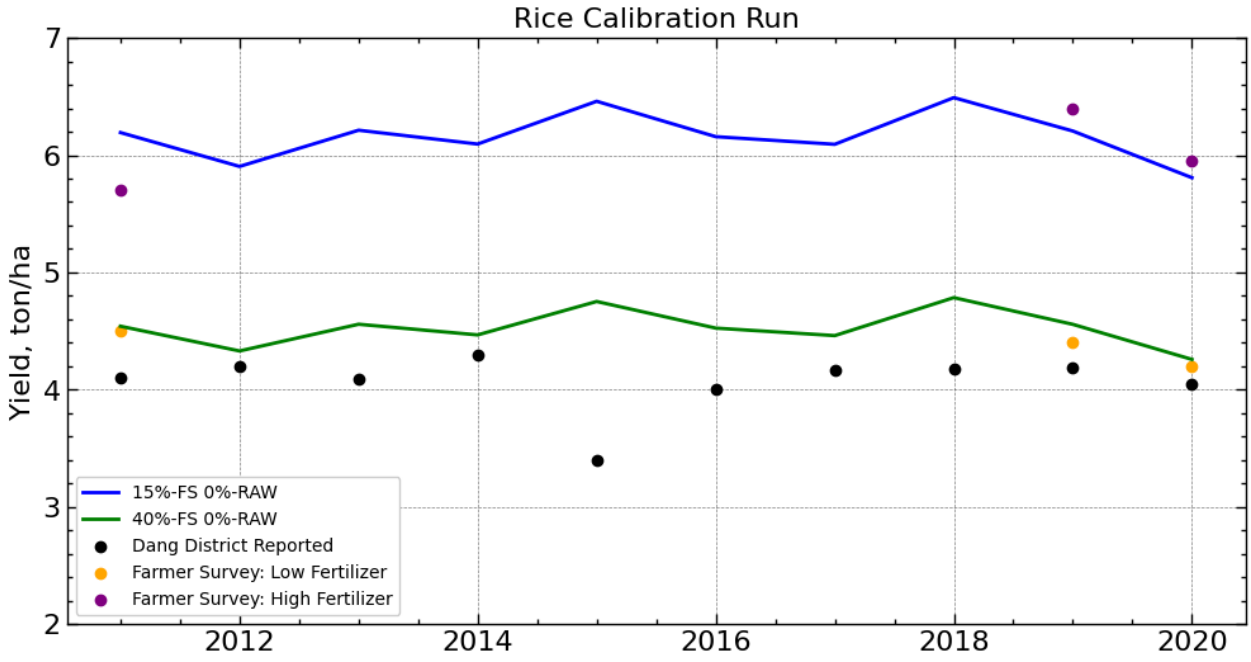

Figure 7.14: Rice: Ten years simulated yield data Vs Published data by MoALD and farmer survey.

In **Figure 7.14**, green line represents simulated yield with low fertilizer application (around 40% less than National Recommended Fertilizer Dose (NRFD) by DoA) and orange dots represent yield by those farmer who apply low fertilizer (<40%); Blue line indicates simulated yield with fertilizer application slightly lower than NRFD (i.e. 15%) and purple dots represent yield by those farmer who apply fertilizer nearly equal to NRFD (i.e. 15% less compared to NRFD). Black dots indicate

published yield by MoALD. After this calibration of the model, future yield projection has been performed for several stress levels under different irrigation strategies for both GCM Model SSP 245 and SSP 585 in Near Future (NF), Mid Future (MF) and in Far Future (FF).

Model performance is assessed by the correlation between simulated yield and yield obtained from farmer survey. As seen in **Figure 7.14**, simulated crop yield for both low and high fertilizer application match very well with the yields reported by farmers. The yield for Dang district reported by MoALD is on the lower side than our study area. In spite of that, the trend of simulated yield matches well with the MoALD reported yield for the whole of Dang, except for the outlier in 2015. The outlier can be explained by potential pest infection or hydrological extreme which is not simulated by AquaCrop. The Nash Sutcliffe Efficiency (NSE) of model simulated yield and MoALD yield is -2.79 and the Root Mean Squared Error (RMSE) is 0.567. The low value of NSE is well explained by the fact that our study area receives better irrigation than the whole of Dang district and consequently has a higher yield.

B. Wheat

Calibrated result for 20 years past yield data (2000-2020) published by MoALD and yield data according to farmer survey are presented in **Figure 7.15**.

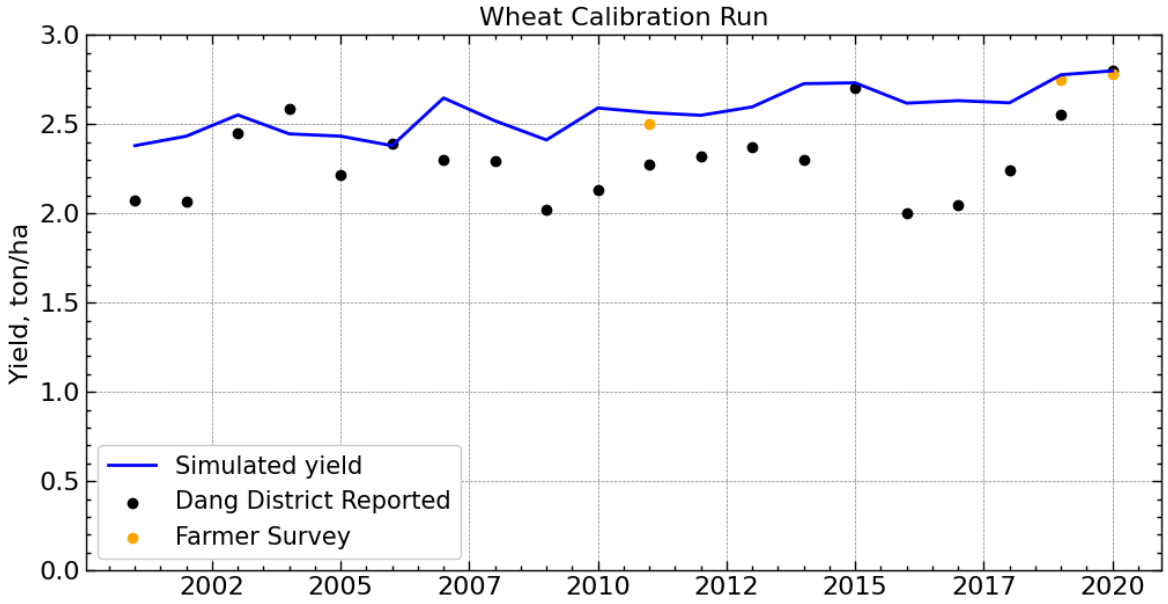

Figure 7.15: Wheat: Twenty years simulated yield data Vs Published data by MoALD and data given by the farmer.

After the calibration of the model, future yield projection has been performed for fertility stress levels 50% and for 0% (non-limiting condition) under different irrigation strategies for both GCM Model SSP 245 and SSP 585 in Near Future (NF), Mid Future (MF) and in Far Future (FF).

Model performance is assessed by the correlation between simulated yield and yield obtained from farmer survey. It is clearly observed, in **Figure 7.15**, that there is a good fit between simulated and farmer-reported yield. MoALD reported yield is again lower for the same reasons as that for rice. The NSE score of simulated and MoALD yield is -1.19 and RMSE is 0.326. The low NSE score is well explained by the water and fertilizer availability in our study area as compared to the whole of Dang district.

7.2 Climate Change Impact on Yield and Water Requirement of Rice

7.2.1 Baseline yield and water requirement

Baseline yield of rice is based on long-term historical average (2000-2020) of calibrated yield (**Figure 7.16**). 4.453 ton/ha was calculated as the baseline yield of rice. Similarly, net irrigation requirement and total water requirement, also calculated as long-term historical average, is found to be 731.6 mm and 2381.4 mm respectively.

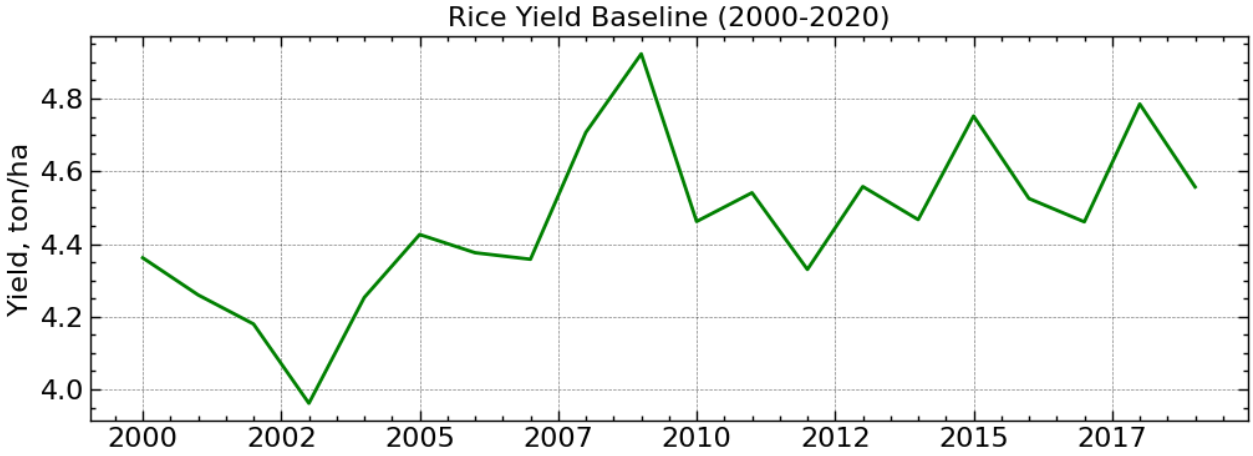

Figure 7.16: Baseline rice yield (2000-2020)

7.2.2 Change under low fertilizer input

A. Change in yield under different irrigation and climate change scenario

Simulated yield under moderate fertility stress in different future scenario (SSP245 and SSP585) with several irrigation application scenario (0%, 50%, 80% and 100%) RAW is shown in **Figure 7.17** and **Figure 7.18**.

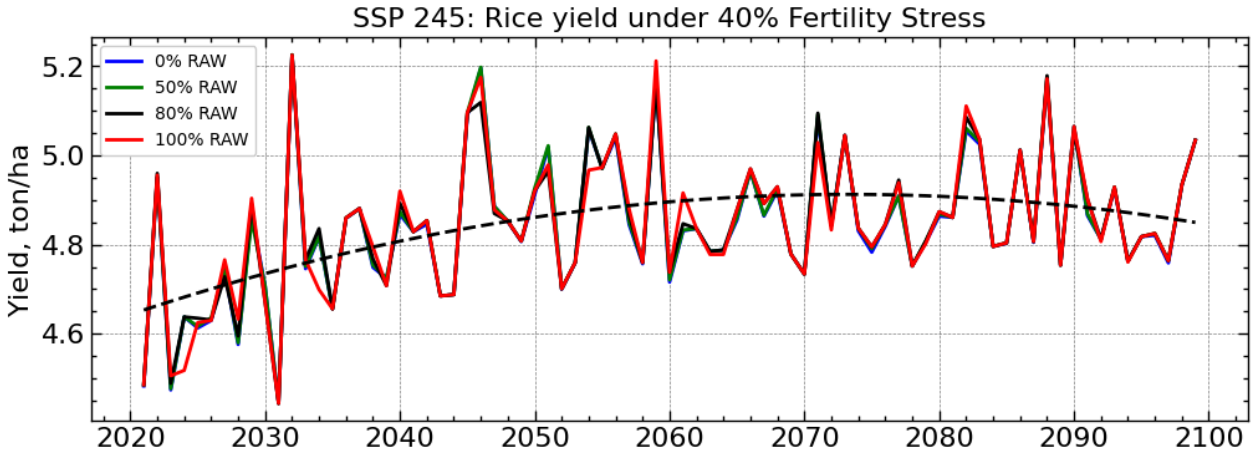

Figure 7.17: Rice yield in future (2021-2099) for SSP 245.

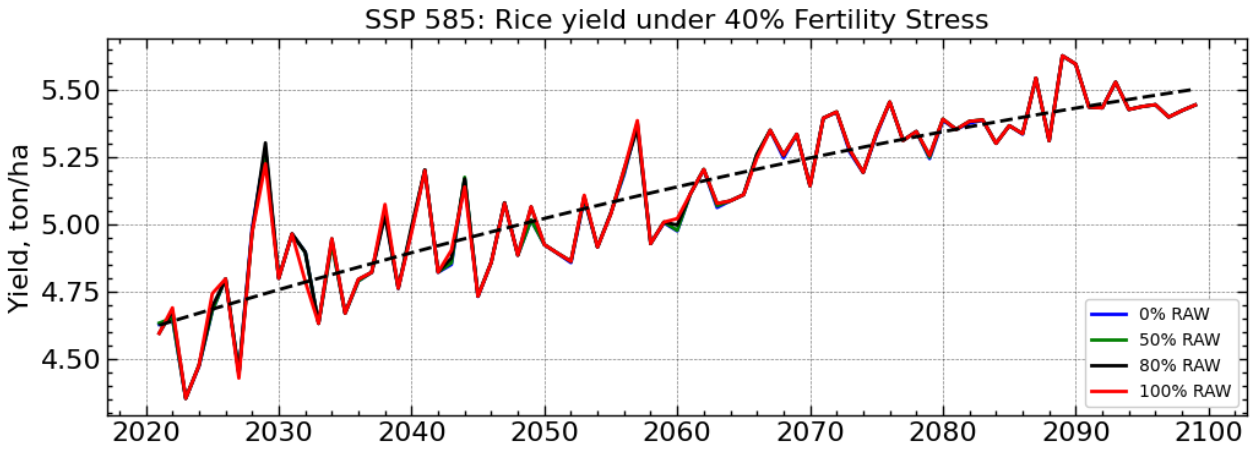

Figure 7.18: Rice yield in future (2021-2099) for SSP 585.

In the figure shown above from **Figure 7.17** to **Figure 7.18**, blue line represents yield under full irrigation strategies(i.e. irrigation is applied when water level drops below field capacity(RAW=0%), green shows yield under application of water when water level falls from field capacity(FC) to 50% Readily Available water (RAW), purple shows yield under irrigation applied when water level is reached to the canopy expansion threshold in field(i.e. RAW 80%) and Red line represents the yield under irrigation applied when water level drops to the stomata closure threshold in field (i.e. RAW=100%). Results from both SSP 245 (**Figure 7.17**) and SSP 585 (**Figure 7.18**) show an increasing trend of crop yield. For SSP 245 Yield could be increased by 0.459, 0.474, 0.468 and 0.468 ton/hectare or by 10.31%, 10.64%, 10.51%, 10.51% under different irrigation strategies 0%RAW, 50% RAW, 80%RAW, and 100%RAW respectively by year 2050 with reference to baseline yield. In AquaCrop 0% RAW means Water level is at Field Capacity and 200% RAW means Water level is at Permanent wilting point (PWP). Similarly, by the year 2075 yield could be increased by 0.33, 0.338, 0.342, 0.342 ton/hectare or 7.41%, 7.59%,7.68%,7.68% and by year 2099 it could rise by 0.581,0.581,0.581,0.581 or by 13.05%,13.05%,13.05%,13.05% under different irrigation strategies. For SSP 585 yield could be increased by 0.471 ton/hectare or by 10.58% by year 2050 and increased by 0.886 ton/hectare or by 19.9% by year 2075, and by 0.991 ton/hectare or 22.25% by year 2099 under different irrigation strategies. Here, we can observe no significant difference in yield under different irrigation scenarios in the case of SSP 585. Summary of percentage increase in rice yield under moderate fertility stress for different irrigation scenario are summarized in **Table 7.4**.

Table 7.4: % Increase in rice yield under moderate fertility stress for different irrigation scenario

Fertility Stress	Irrigation Scenario	SSP 245			SSP 585			Baseline (ton/ha)
		NF	MF	FF	NF	MF	FF	
40.00%	0% RAW	10.31	7.41	13.05	10.58	19.76	22.25	4.453
	50% RAW	10.64	7.59	13.05	10.58	19.90	22.25	
	80% RAW	10.51	7.68	13.05	10.58	19.90	22.25	
	100% RAW	10.51	7.68	13.05	10.58	19.90	22.25	

B. Change in Net Irrigation Requirement (NIR) and Total water requirement (TWR) under different irrigation and climate change scenario

Net Irrigation requirement (NIR) and Total water requirement (TWR) (Rainfall + NIR) under different irrigation strategies are shown in **Figure 7.19**, **Figure 7.20**, **Figure 7.21** and **Figure 7.22**,

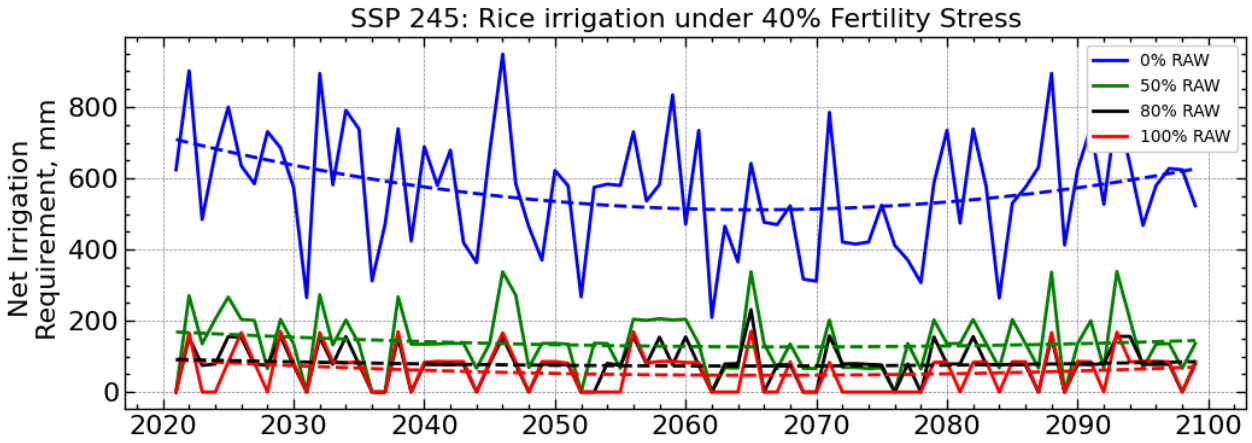

Figure 7.19: Rice net irrigation requirement in Future (2021-2099) for SSP 245.

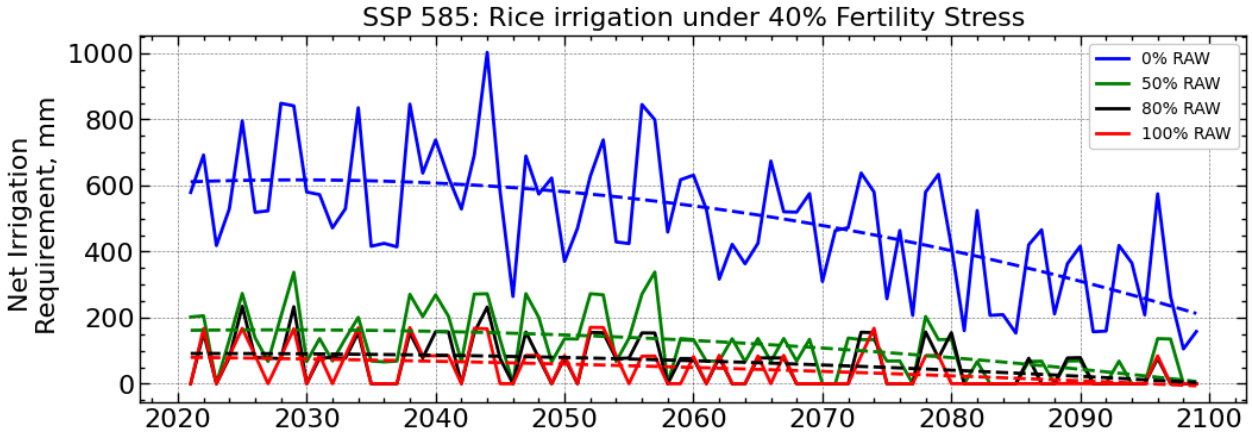

Figure 7.20: Rice net irrigation requirement in Future (2021-2099) for SSP 585.

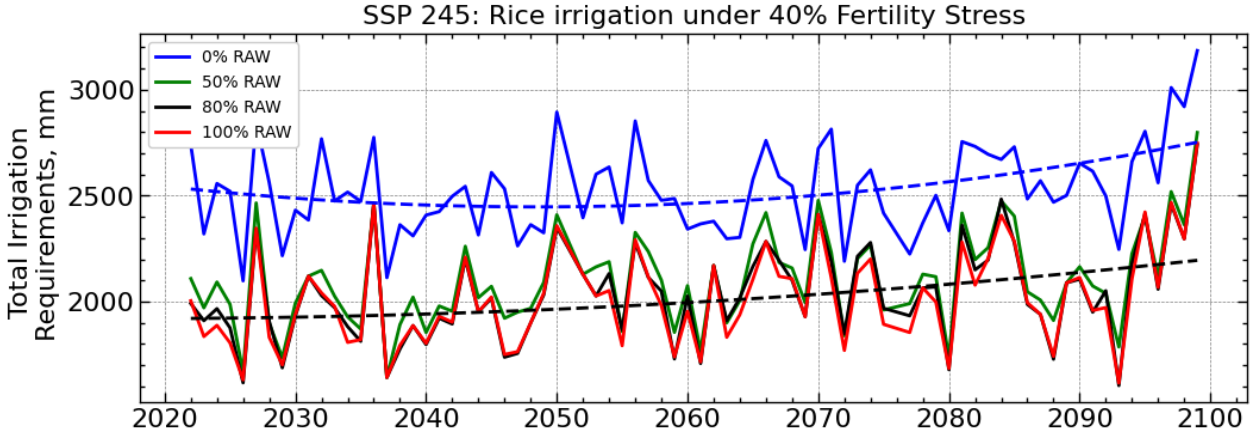

Figure 7.21: Rice total water requirement in future (2021-2099) for SSP 245.

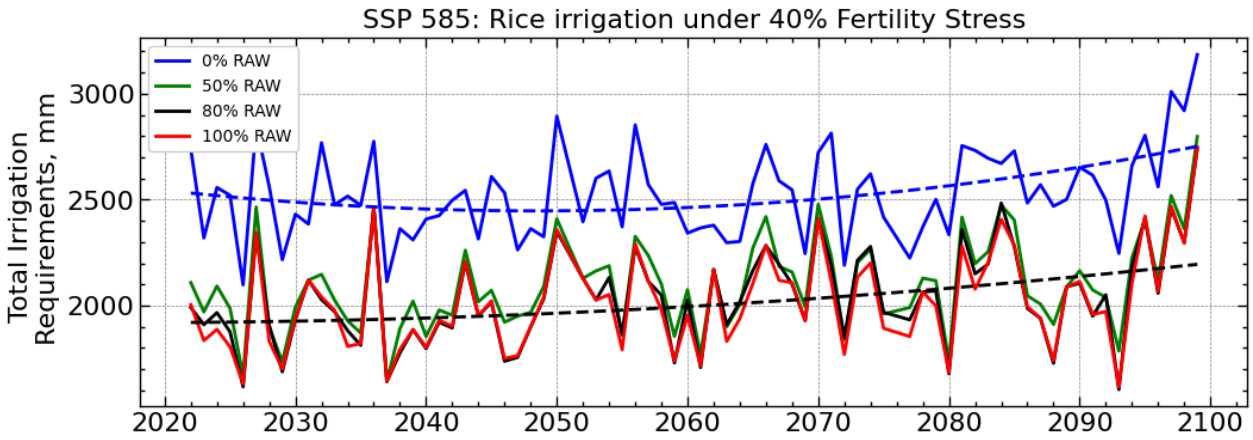

Figure 7.22: Rice total water requirement in future (2021-2099) for SSP 585.

The above plot shows Net irrigation Requirement (NIR) is slightly decreasing till mid future and again-trivial rise in the far future scenario for SSP 245. However, it is significantly decreasing till far future for SSP 585 shown in **Figure 7.20**. But overall water requirement (rainfall + NIR) for the growth of plants, an increasing trend has been observed for both SSPs. (Increasing trend of rainfall causes decreasing trend of irrigation water requirement). This can be explained by the rise of temperature leading to an increase in crop water requirements. Summary of percentage increase in NIR and TWR under moderate fertility stress for different irrigation scenario are summarized in **Table 7.5** and **Table 7.6** respectively.

Table 7.5: % Increase in rice NIR under moderate fertility stress for different irrigation scenario

Fertility Stress	Irrigation Scenario	SSP 245			SSP 585			Baseline (mm)
		NF	MF	FF	NF	MF	FF	
40.00%	0% RAW	-15.01	-28.29	-28.54	-49.41	-64.87	-78.40	731.6
	50% RAW	-88.31	-100.00	-88.33	-88.34	-100.00	-100.00	
	80% RAW	-81.31	-90.76	-81.41	-81.42	-90.64	-100.00	
	100% RAW	-89.48	-89.65	-89.17	-89.35	-100.00	-100.00	

Table 7.6: % Increase in rice TWR under moderate fertility stress for different irrigation scenario

Fertility Stress	Irrigation Scenario	SSP 245			SSP 585			Baseline (mm)
		NF	MF	FF	NF	MF	FF	
40.00%	0% RAW	2.93	3.86	7.97	2.38	8.58	18.75	2381.4
	50% RAW	-19.62	-15.98	-13.41	-20.09	-11.45	5.46	
	80% RAW	-16.34	-12.56	-10.13	-16.41	-8.20	7.16	
	100% RAW	-19.33	-14.41	-12.66	-19.34	-10.85	6.25	

7.2.3 Change under optimal fertilizer input.

A. Yield

Simulated yield under mild fertility stress in different future scenario with several irrigation application scenario is shown in **Figure 7.23** and **Figure 7.24**.

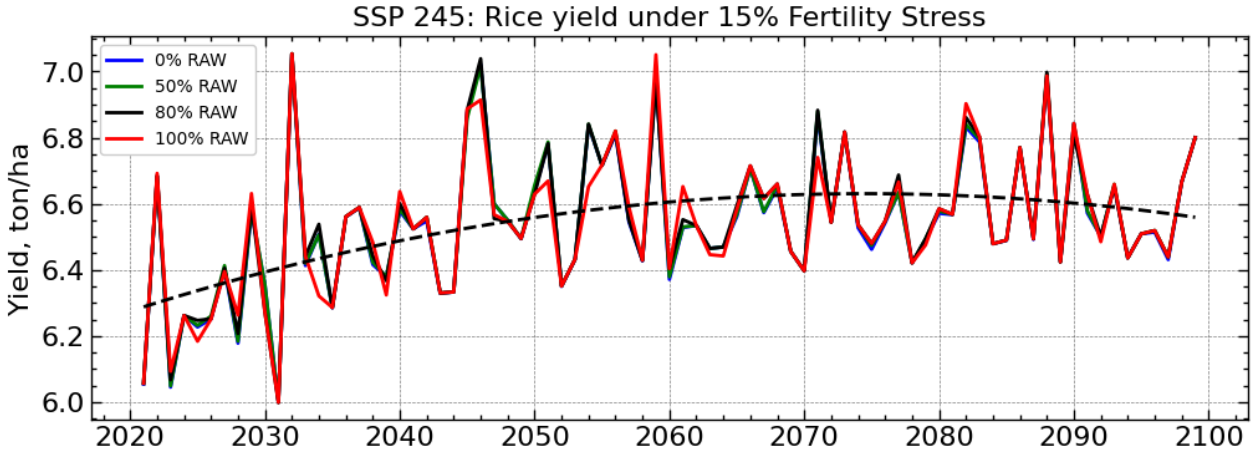

Figure 7.23: Rice yield in Future (2021-2099) for SSP 245.

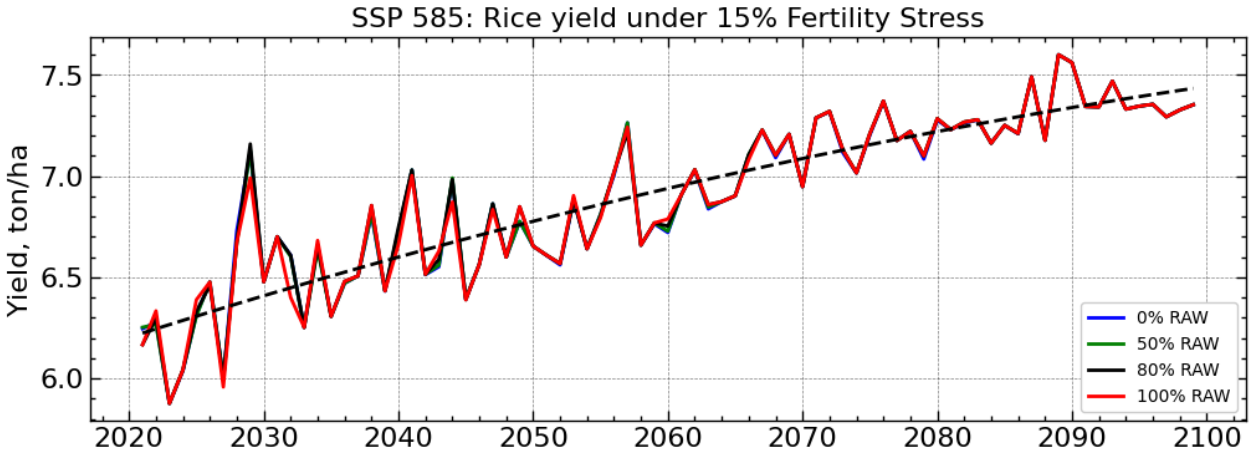

Figure 7.24: Rice yield in Future (2021-2099) for SSP 585 showing Increasing Trend.

In **Figure 7.23** and **Figure 7.24**, blue line represents yield under full irrigation strategies(i.e. irrigation is applied when water level falls below field capacity(RAW=0%), green shows yield under application of water when water level falls from field capacity(FC) to 50% Readily Available water (RAW), purple shows yield under irrigation applied when water level is reached to the canopy expansion threshold in field (i.e. RAW 80%) and Red line represents the yield under irrigation applied when water level drops to the stomata closure threshold in field(i.e. RAW=110%). Results from both SSP 245 and SSP 585 show an increasing trend of crop yield. For SSP 245 Yield could be increased by 2.184, 2.203, 2.176 and 2.176ton/hectare or by 49.05%, 49.47%, 48.87%, 48.87% under different irrigation strategies 0% RAW, 50% RAW, 80%RAW and 100%RAW respectively by the year 2050. Similarly, by the year 2075 yield could be increased by 2.009, 2.021, 2.027 and 2.027ton/hectare or 45.12%, 45.39%, 45.52%, 45.52%and by the year 2099, it could rise by 2.347or by 52.71% under different irrigation strategies. For SSP 585 yield could be increased by 2.201ton/hectare or by 49.43% by the year 2050 and increased by 2.758 ton/hectare or by 61.94% by the year 2075, and by 2.9ton/hectare or 65.12% by year 2099 under

different irrigation strategies. Here, we can observe no significant difference in yield under different irrigation scenarios in the case of SSP 585. Also, notable difference between two SSPs yields shows yield under SSP 585 has more magnitude than SSP 245. The lack of difference between irrigation scenarios is explained due to the abundance of rainfall in monsoon season for rice. Summary of percentage increase in rice yield under moderate fertility stress for different irrigation scenario are summarized in **Table 7.7**. Detailed plots are presented in **ANNEX D**.

Table 7.7: % Increase in rice yield under mild fertility stress for different irrigation scenario

Fertility Stress	Irrigation Scenario	SSP 245			SSP 585			Baseline (ton/ha)
		NF	MF	FF	NF	MF	FF	
15.00%	0% RAW	49.05	45.12	52.71	49.43	61.78	65.12	4.453
	50% RAW	49.47	45.39	52.71	49.43	61.94	65.12	
	80% RAW	48.87	45.52	52.71	49.43	61.94	65.12	
	100% RAW	48.87	45.52	52.71	49.43	61.94	65.12	

B. Change in Net Irrigation Requirement (NIR) and Total water requirement (TWR) under different irrigation scenario.

Net Irrigation requirement (NIR) and Total water requirement (TWR) (Rainfall + NIR) under different irrigation strategies are shown from **Figure 7.25** to **Figure 7.28**.

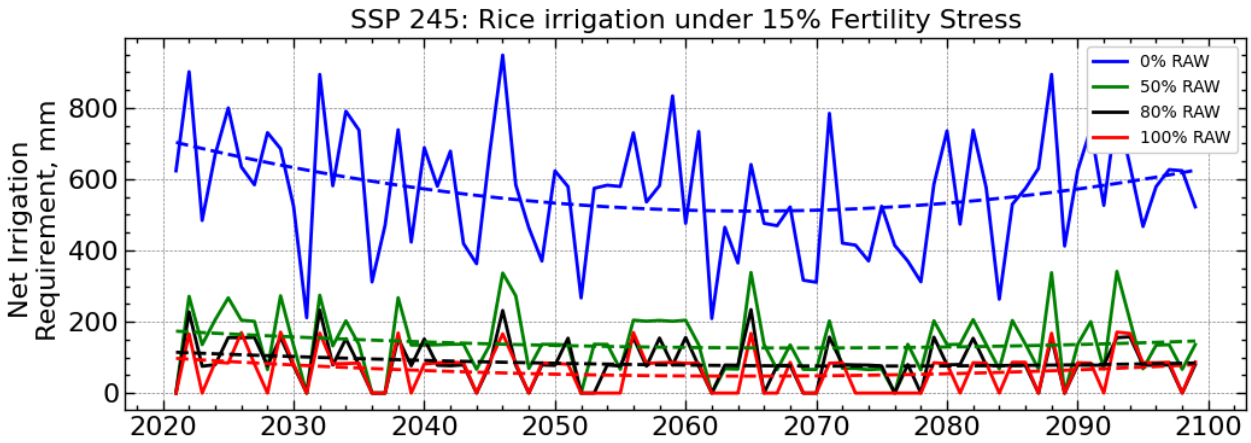

Figure 7.25: Rice net irrigation requirement in Future (2021-2099) for SSP 245.

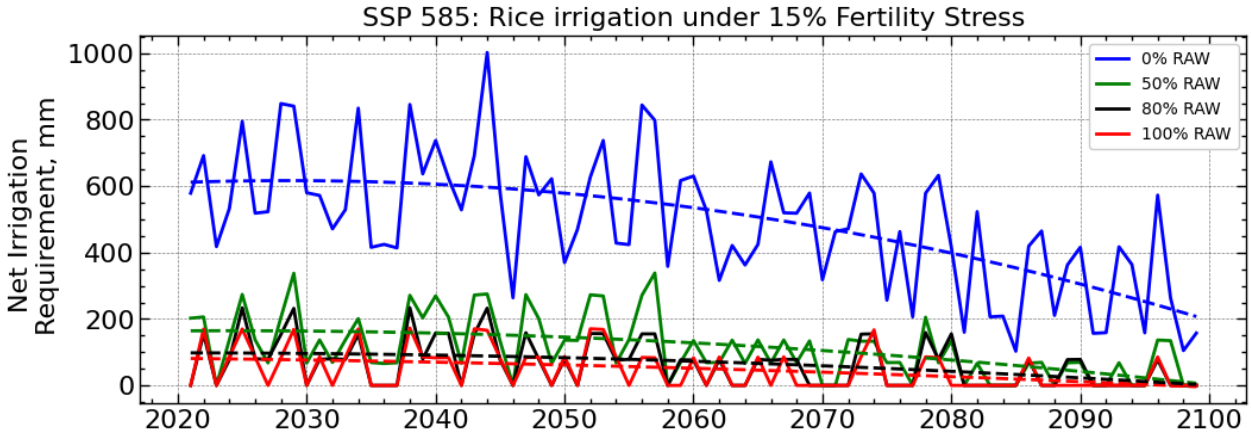

Figure 7.26: Rice net irrigation requirement in Future (2021-2099) for SSP 585.

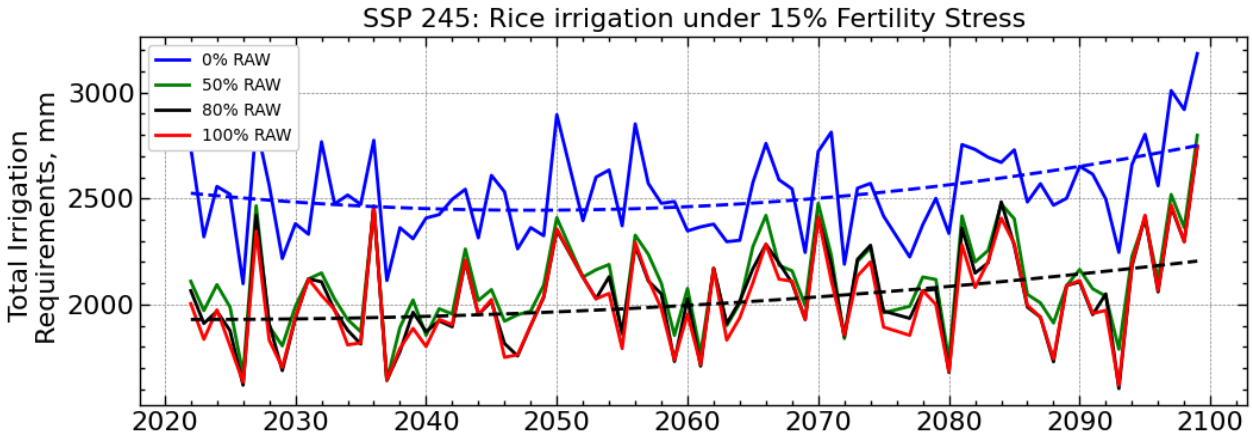

Figure 7.27: Rice total water requirement in future (2021-2099) for SSP 245.

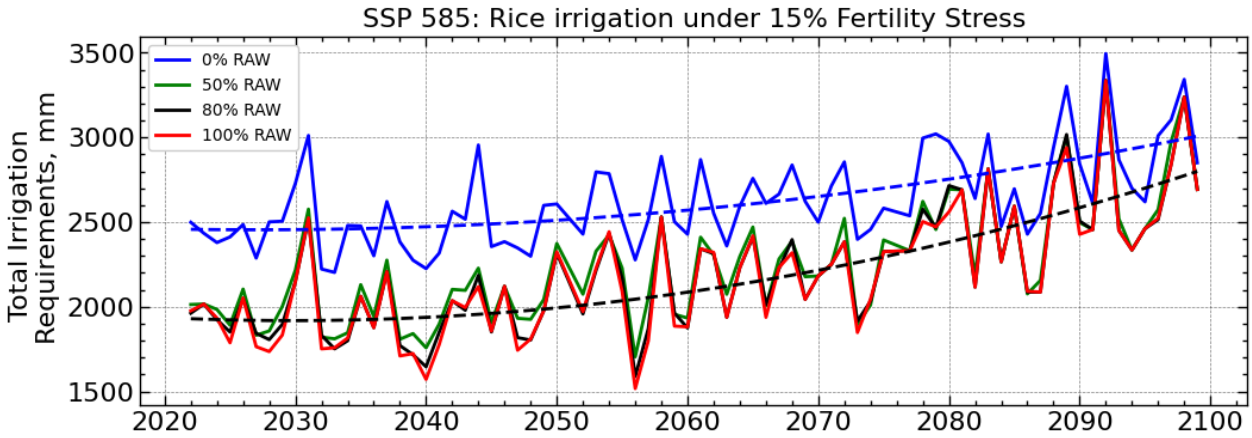

Figure 7.28: Rice total water requirement in future (2021-2099) for SSP 585.

The above plot shows Net irrigation Requirement (NIR) is slightly decreasing till mid future and again-trivial rise in the far future scenario for SSP 245 whereas it is significantly decreasing till far future for SSP 585. But overall water requirement (rainfall + NIR) for the growth of plants, an increasing trend has been observed for both SSPs. The increasing trend of rainfall causes decreasing trend of irrigation water requirement. The role of temperature in increasing crop water requirement is evident from **Figure 7.27** and **Figure 7.28**. Summary of percentage increase in NIR and TWR under moderate fertility stress for different irrigation scenario are summarized in **Table 7.8** and **Table 7.9** respectively.

Table 7.8: % Increase in rice NIR under mild fertility stress for different irrigation scenario

Fertility Stress	Irrigation Scenario	SSP 245			SSP 585			Baseline (mm)
		NF	MF	FF	NF	MF	FF	
15.00%	0% RAW	-14.83	-28.38	-28.62	-49.48	-64.94	-78.47	731.6
	50% RAW	-88.63	-100.00	-88.11	-88.14	-100.00	-100.00	
	80% RAW	-81.33	-90.77	-81.38	-81.38	-90.62	-100.00	
	100% RAW	-89.41	-89.61	-89.05	-89.26	-100.00	-100.00	

Table 7.9: % Increase in rice TWR under mild fertility stress for different irrigation scenario

Fertility Stress	Irrigation Scenario	SSP 245			SSP 585			Baseline (mm)
		NF	MF	FF	NF	MF	FF	
15.00%	0% RAW	2.77	3.76	7.96	2.37	8.40	18.54	2381.4
	50% RAW	-19.50	-15.84	-13.25	-19.96	-11.45	5.61	
	80% RAW	-16.24	-12.57	-10.11	-16.39	-8.31	7.04	
	100% RAW	-18.67	-14.28	-12.64	-19.11	-10.71	6.25	

7.2.4 Change under full dose fertilizer input.

A. Yield

Simulated Yield under non-limiting condition (no fertility stress) in different future scenario with several irrigation application scenario is shown in **Figure 7.29** and **Figure 7.30**.

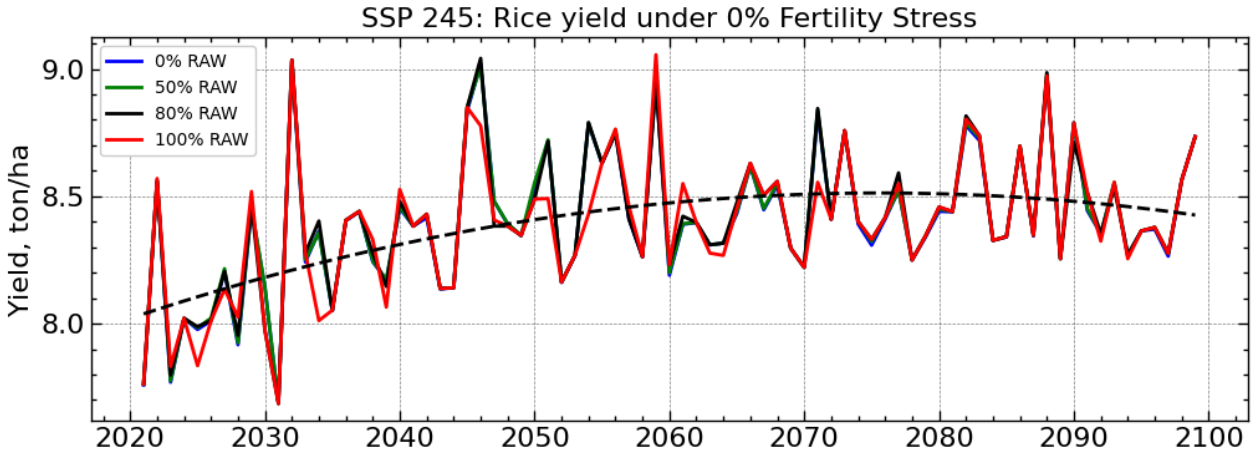

Figure 7.29: Rice yield in Future (2021-2099) for SSP 245.

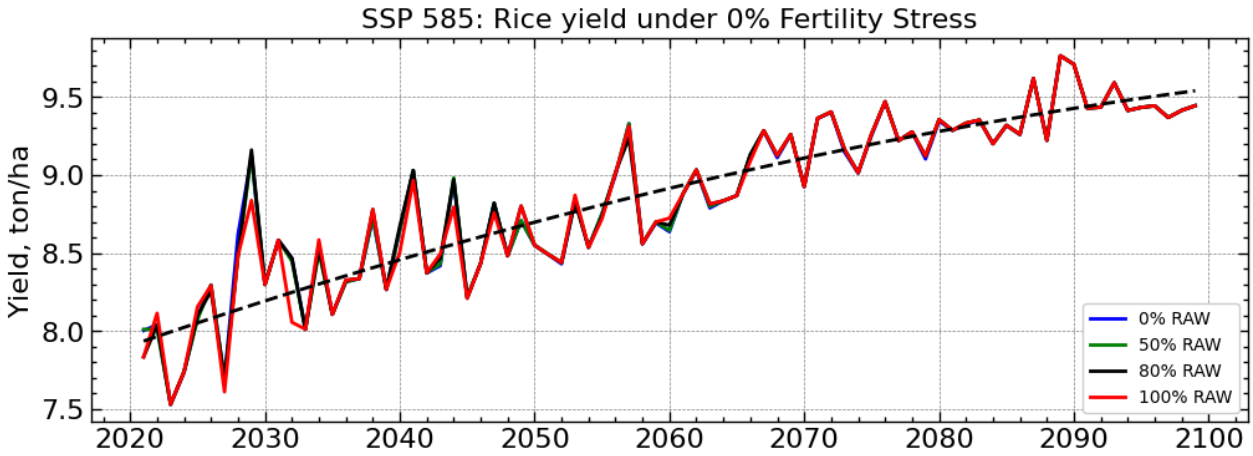

Figure 7.30: Rice yield in Future (2021-2099) for SSP 585 showing increasing trend.

In **Figure 7.29** and **Figure 7.30**, blue line represents yield under full irrigation strategies(i.e. irrigation is applied when water level falls below field capacity(RAW=0%), green shows yield

under application of water when water level falls from field capacity(FC) to 50% Readily Available water (RAW), purple shows yield under irrigation applied when water level is reached to the canopy expansion threshold in field(i.e. RAW 80%) and Red line represents the yield under irrigation applied when water level drops to the stomata closure threshold in field(i.e. RAW=110%).Results from both GCM SSP 245 and SSP 585 show an increasing trend of rice yield. For GCM SSP 245 Yield could be increased by 4.076,4.101,4.035 and 4.036 ton/hectare or by 91.53%, 92.10%, 90.61%, 90.64% under different irrigation strategies 0% RAW, 50% RAW, 80%RAW and 100%RAW respectively by year 2050.Similarly,by year 2075 yield could be increased by 3.855,3.87,3.878 and 3.878ton/hectare or 86.57%,86.91%,87.09%,87.09%and by the year 2099 it could rise by 4.281 or by 96.14%under different irrigation strategies. For GCM SSP 585 yield could be increased by 4.098 ton/hectare or by 92.03% by year 2050 and increased by 4.812 ton/hectare or by 108.06% by the year 2075, and by 4.992 ton/hectare or 112.10% by year 2099 under different irrigation strategies. Here, we can observe no significant difference in yield under different irrigation scenarios in the case of GCM SSP 585. Summary of percentage increase in rice yield under moderate fertility stress for different irrigation scenario are summarized in **Table 7.10**.

Table 7.10: % Increase in rice yield under no fertility stress for different irrigation scenario

Fertility Stress	Irrigation Scenario	SSP 245			SSP 585			Baseline (ton/ha)
		NF	MF	FF	NF	MF	FF	
0.00%	0% RAW	91.53	86.57	96.14	92.03	107.84	112.10	4.453
	50% RAW	92.10	86.91	96.14	92.03	108.06	112.10	
	80% RAW	90.61	87.09	96.14	92.03	108.06	112.10	
	100% RAW	90.64	87.09	96.14	92.03	108.06	112.10	

B. Change in Net Irrigation Requirement (NIR) and Total water requirement (TWR) under different irrigation scenarios.

Net Irrigation requirement (NIR) and Total water requirement (TWR) (Rainfall + NIR) under different irrigation strategies are shown in **Figure 7.31** to **Figure 7.34**.

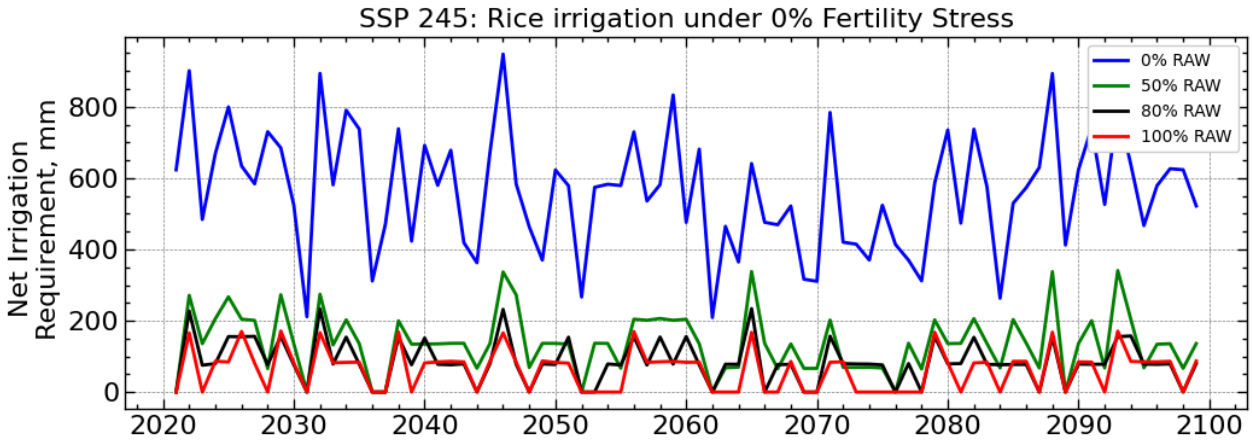

Figure 7.31: Rice net irrigation requirement in Future (2021-2099) for SSP 245.

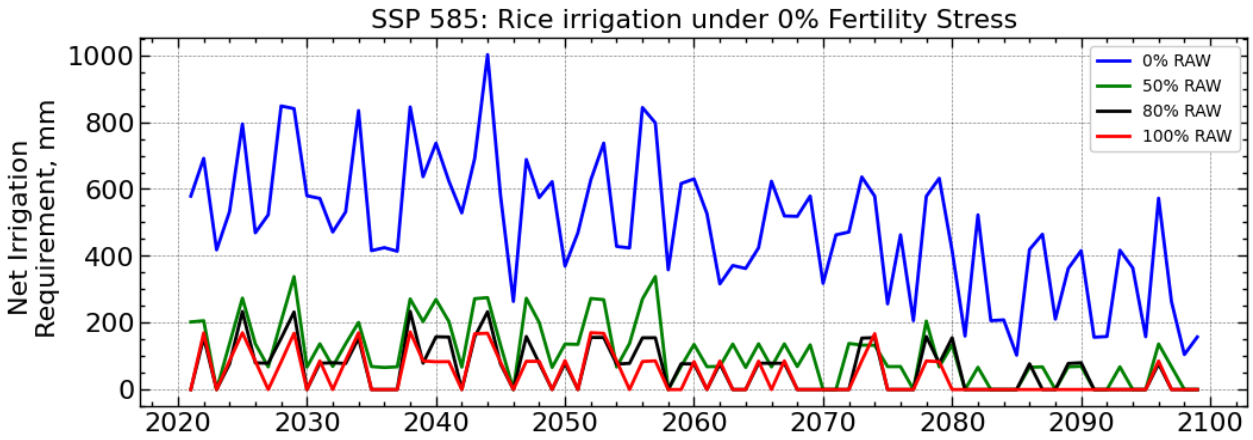

Figure 7.32: Rice net irrigation requirement in Future (2021-2099) for SSP 585.

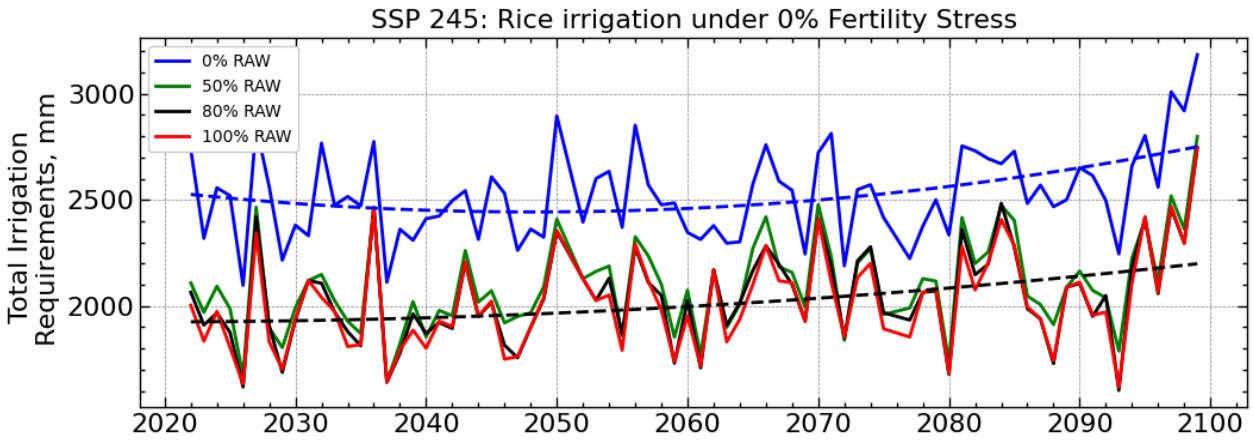

Figure 7.33: Rice total water requirement in Future (2021-2099) for SSP 245.

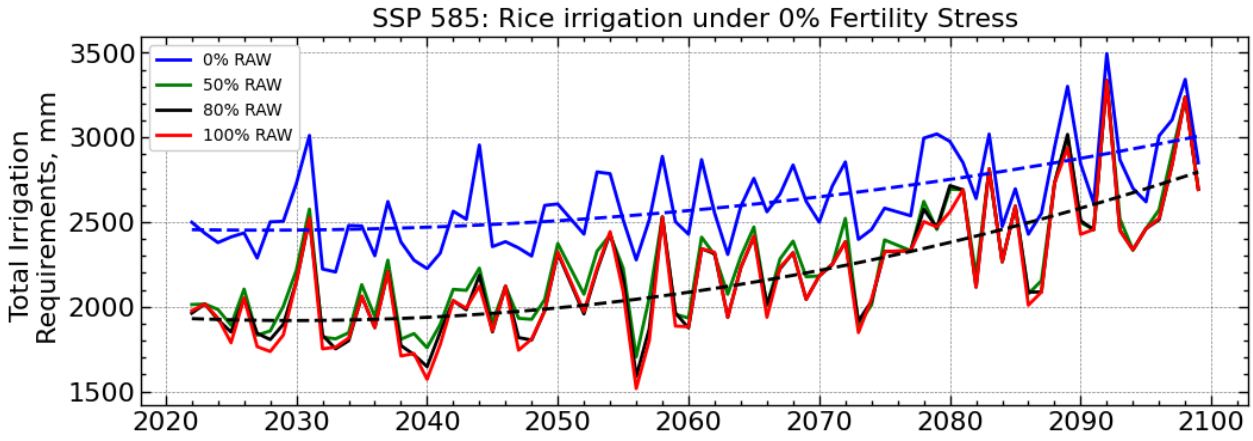

Figure 7.34: Rice total water requirement in Future (2021-2099) for SSP 585.

The above plot shows Net irrigation Requirement (NIR) is slightly decreasing till mid future and again-trivial rise in the far future scenario for SSP 245 whereas it is significantly decreasing till far future for SSP 585. But overall water requirement (rainfall + NIR) for the growth of plants, an increasing trend has been observed for both GCM. The increasing trend of rainfall causes decreasing trend of irrigation water requirement. In addition to rainfall, temperature also increases crop water requirement due to increased evapotranspiration. Summary of percentage increase in NIR and TWR under moderate fertility stress for different irrigation scenario are summarized in **Table 7.11** and **Table 7.12** respectively. Detailed plots are presented in **ANNEX E**.

Table 7.11: % Increase in rice NIR under no fertility stress for different irrigation scenario

Fertility Stress	Irrigation Scenario	SSP 245			SSP 585			Baseline (mm)
		NF	MF	FF	NF	MF	FF	
0.00%	0% RAW	-14.87	-28.40	-28.66	-49.51	-64.97	-78.50	731.6
	50% RAW	-88.66	-100.00	-88.12	-88.16	-100.00	-100.00	
	80% RAW	-81.36	-90.79	-81.41	-81.41	-90.62	-100.00	
	100% RAW	-89.43	-89.60	-89.08	-89.27	-100.00	-100.00	

Table 7.12: % Increase in rice TWR under no fertility stress for different irrigation scenario

Fertility Stress	Irrigation Scenario	SSP 245			SSP 585			Baseline (mm)
		NF	MF	FF	NF	MF	FF	
0.00%	0% RAW	2.77	3.66	7.95	2.29	8.22	18.52	2381.4
	50% RAW	-19.50	-15.84	-13.26	-19.96	-11.45	5.46	
	80% RAW	-16.33	-12.55	-10.12	-16.40	-8.32	6.92	
	100% RAW	-18.67	-14.29	-12.65	-19.11	-10.84	6.25	

7.3 Climate Change Impact on Water Requirements and Yield of Wheat

7.3.1 Baseline yield and water requirements

Baseline yield of wheat is based on long-term historical average (2000-2020) of calibrated yield (**Figure 7.35**). 2.569 ton/ha was calculated as the baseline yield of rice. Similarly, net irrigation requirement and total water requirement, also calculated as long-term historical average, is found to be 116.7 mm and 1831.4 mm respectively.

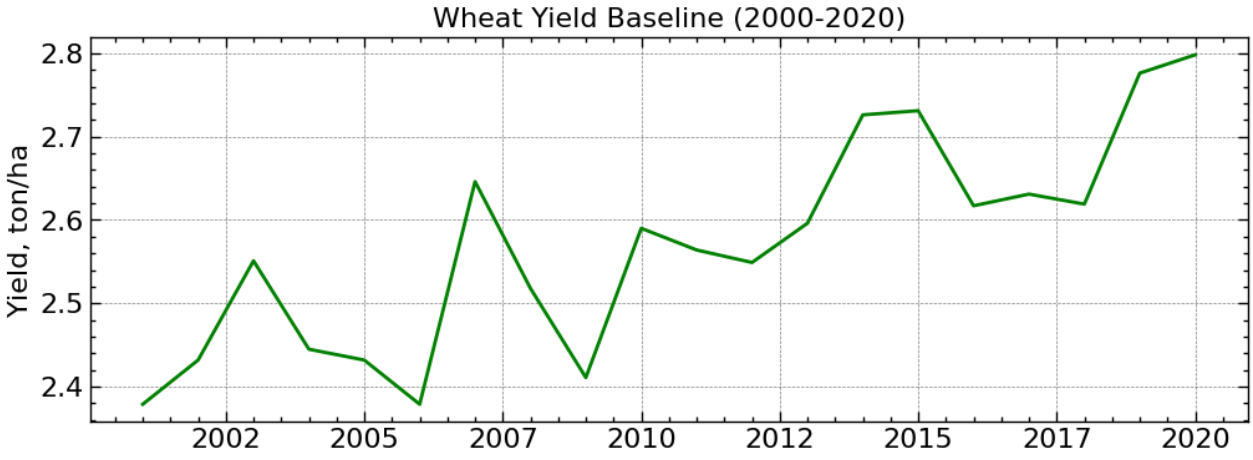

Figure 7.35: Baseline wheat yield (200-2020)

7.3.2 Change under low fertilizer input.

A. Change in yield under different irrigation scenario.

Simulated Yield under moderate fertility stress in different future scenario with several irrigation application scenario is shown in **Figure 7.36** and **Figure 7.37.**

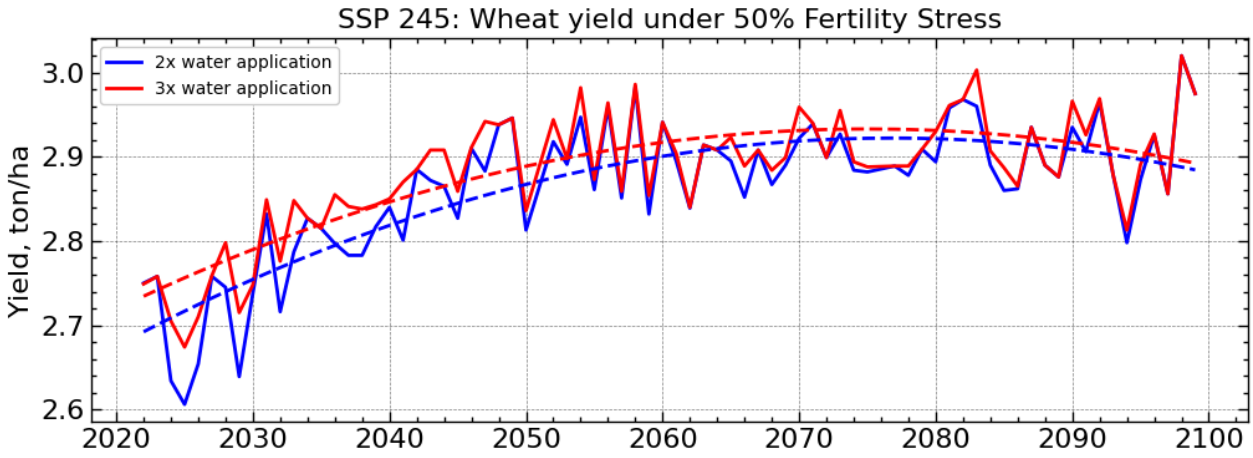

Figure 7.36: Wheat yield in Future (2021-2099) for SSP 245.

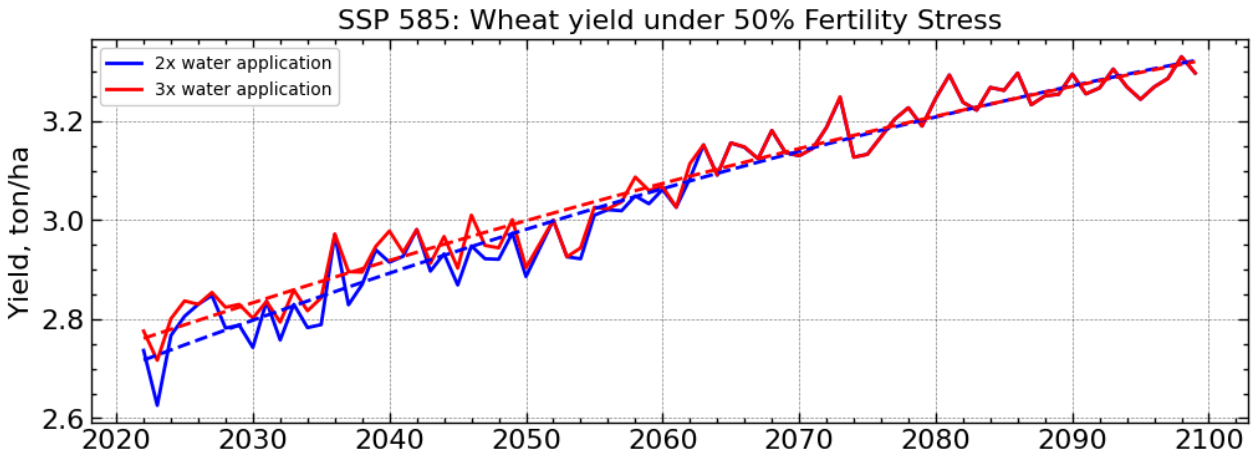

Figure 7.37: Wheat yield in Future (2021-2099) for SSP 585 showing Increasing Trend.

In **Figure 7.36** and **Figure 7.37**, the red line represents yield under three times application of water during its growing season (22 days, 70 days and 85 days) whereas blue represents yield corresponding to two times application of water (i.e., at 22 days and 70 days) during its growing season. Both SSPs show an increasing trend of yield, SSP 585 has sharper rise than SSP 245. In case of SSP 245, significant decrease in yield can be observed for two times application in a reference to three times application for all future scenarios; however, SSP 585 Shows decreasing trend till middle of mid future but thereafter no observable difference has been seen in yield. The reason behind no difference in yield for these two applications can be sharp increasing trend of rainfall in far future (SSP 585) and plant do not feel water stress even in two times application during its growing season but in case of SSP 245 (Gradual increasing trend of rainfall), two times applications might not fulfill the thirst of plant sufficiently during its growing cycle. The resulted value of the yield under different irrigation scenario for both SSP 245 and SSP 585 are presented in the **Table 7.13**.

Table 7.13: % Increase in wheat yield under moderate fertility stress for different irrigation scenario

Fertility Stress	Irrigation Scenario	SSP 245			SSP 585			Baseline (ton/ha)
		NF	MF	FF	NF	MF	FF	
50.00%	2 times	9.50	12.18	15.80	12.34	21.95	28.34	2.569
	3 times	10.39	12.42	15.80	13.04	21.95	28.34	

B. Change in Net Irrigation Requirement (NIR) and Total water requirement (TWR) under different irrigation scenarios.

Net Irrigation requirement (NIR) and Total water requirement (TWR) (Rainfall + NIR) under two application of irrigation strategies are shown in **Figure 7.38** to **Figure 7.41**.

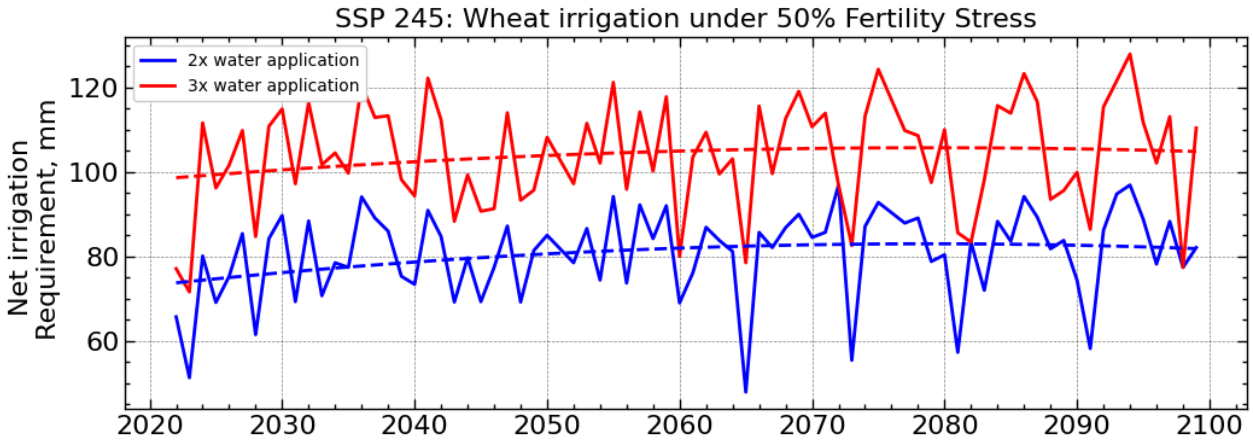

Figure 7.38: Wheat net irrigation requirement in Future (2021-2099) for SSP 245.

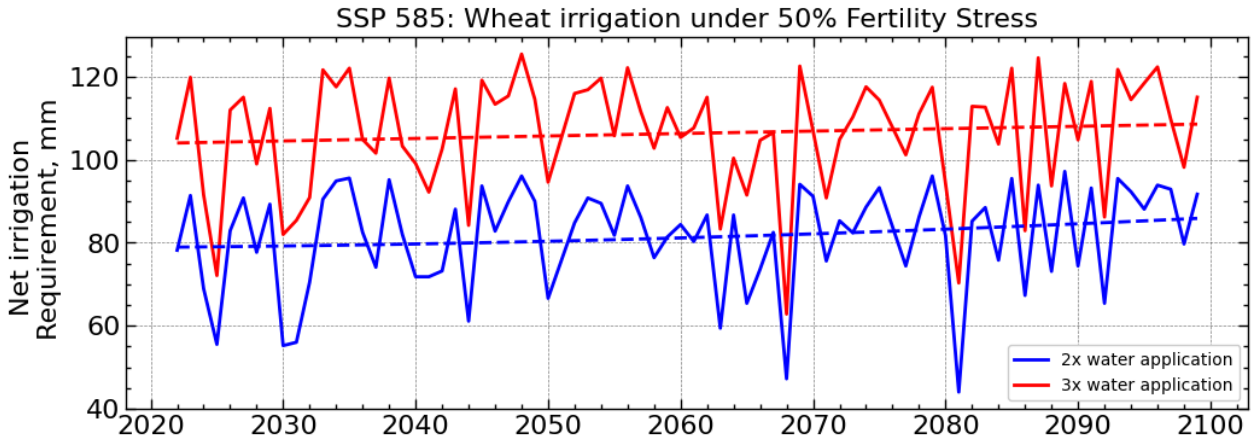

Figure 7.39: Wheat net irrigation requirement in Future (2021-2099) for SSP 585.

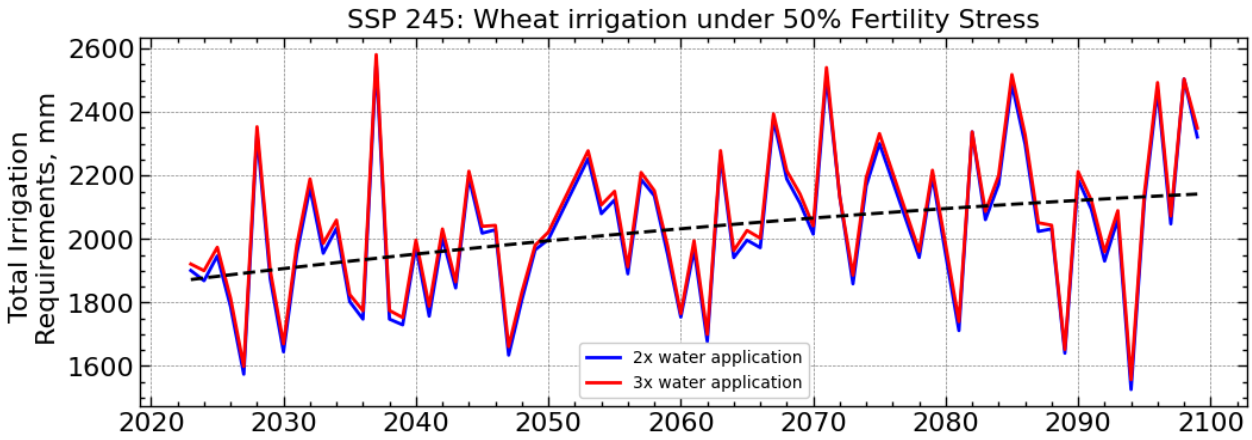

Figure 7.40: Wheat total water requirement in Future (2021-2099) for SSP 245.

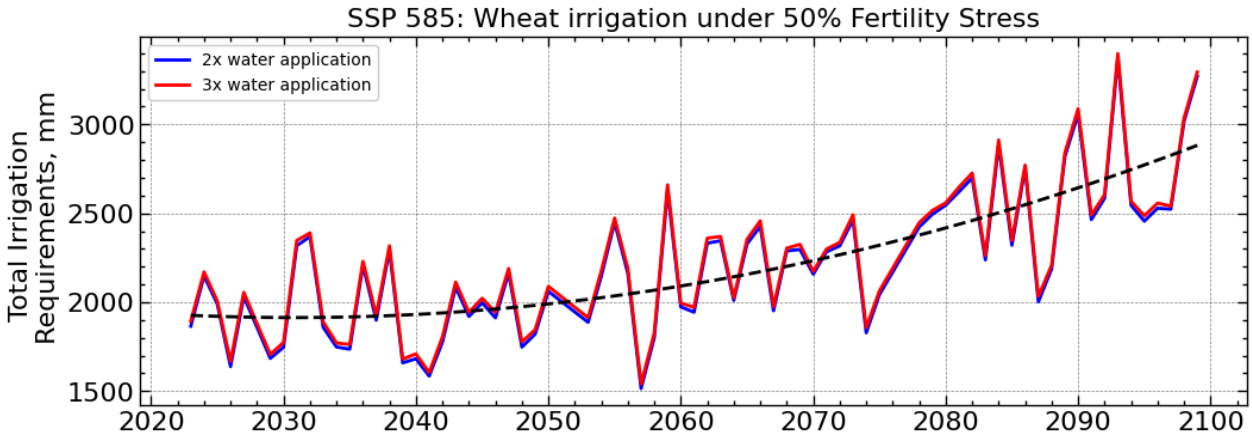

Figure 7.41: Wheat total water requirement in future (2021-2099) for SSP 585.

From the above figure, a rising trend of irrigation requirement has been observed for both SSPs. Summary of percentage increase in NIR and TWR under moderate fertility stress for different irrigation scenario are summarized in **Table 7.14** and **Table 7.15** respectively. Detailed plots are presented in **ANNEX F**.

Table 7.14: % Increase in wheat NIR under moderate fertility stress for different irrigation scenario

Fertility Stress	Irrigation Scenario	SSP 245			SSP 585			Baseline (mm)
		NF	MF	FF	NF	MF	FF	
50.00%	2 times	-27.16	-20.48	-29.65	-42.93	-20.05	-21.42	116.7
	3 times	-7.28	6.51	-5.40	-18.94	-1.97	-1.37	

Table 7.15: % Increase in wheat TWR under moderate fertility stress for different irrigation scenario

Fertility Stress	Irrigation Scenario	SSP 245			SSP 585			Baseline (mm)
		NF	MF	FF	NF	MF	FF	
50.00%	2 times	1.69	9.20	9.78	1.55	13.12	37.54	1831.4
	3 times	3.00	10.47	11.02	2.94	14.46	38.84	

7.3.3 Change under full dose fertilizer input.

A. Change in yield under different irrigation scenario.
Simulated yield under non-limiting condition (no fertility stress) in different future scenario with two irrigation application scenarios are shown in **Figure 7.42** and **Figure 7.43**.

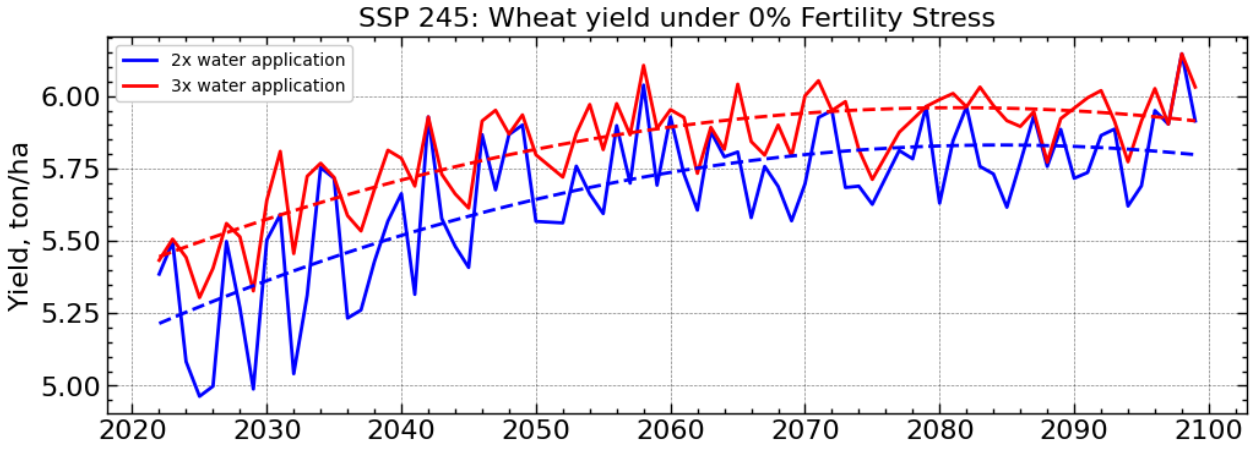

Figure 7.42: Wheat yield in Future (2021-2099) for SSP 245 Showing.

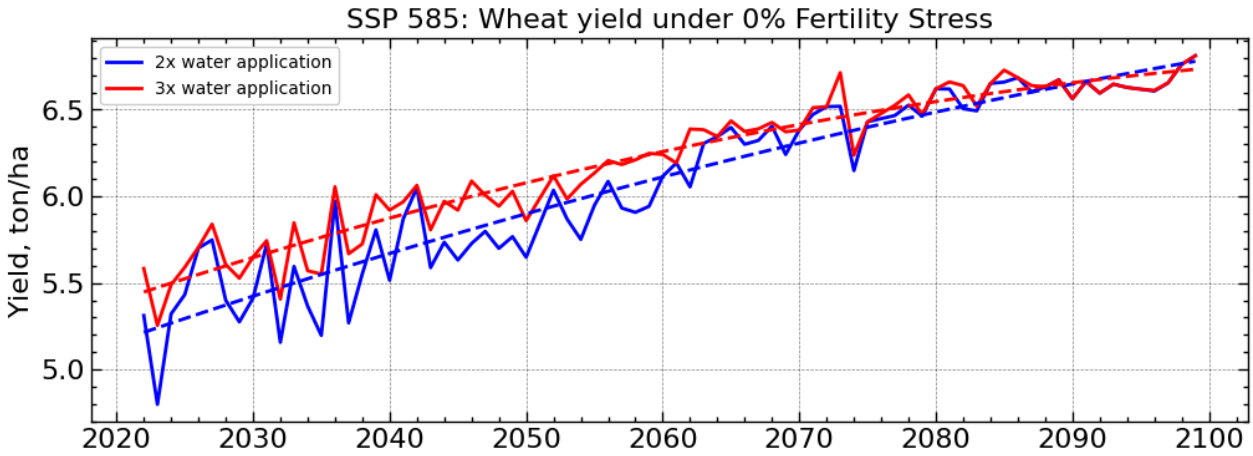

Figure 7.43: Wheat yield in Future (2021-2099) for SSP 585 Showing.

The above figure depicts a significant increasing trend of yield for all future scenarios in SSP 585 whereas in SSP 245 Significant increasing trend has been observed for the near future but after that trivial increasing trend has been obtained. Also, in SSP 245, Significant yield gap has been observed for two different irrigation strategies for all future scenarios whereas in SSP 585

significant yield gap has been observed till middle of the mid future, thereafter no change in yield for one time less application of water during growing season of wheat. The resulting value of the yield under different irrigation scenarios for both SSP 245 and SSP 585 are presented in the **Table 7.16**.

Table 7.16: % Increase in wheat yield under no fertility stress for different irrigation scenario

Fertility Stress	Irrigation Scenario	SSP 245			SSP 585			Baseline (ton/ha)
		NF	MF	FF	NF	MF	FF	
0.00%	2 times	116.70	119.00	130.21	119.85	150.29	165.12	2.569
	3 times	125.65	122.34	134.76	128.07	150.29	165.12	

B. Change in Net Irrigation requirement (NIR) and Total water requirement under different irrigation scenarios.

(TWR) (Rainfall+ NIR) under two application of irrigation strategies are shown in **Figure 7.44**, **Figure 7.45**, **Figure 7.46** and **Figure 7.47**,

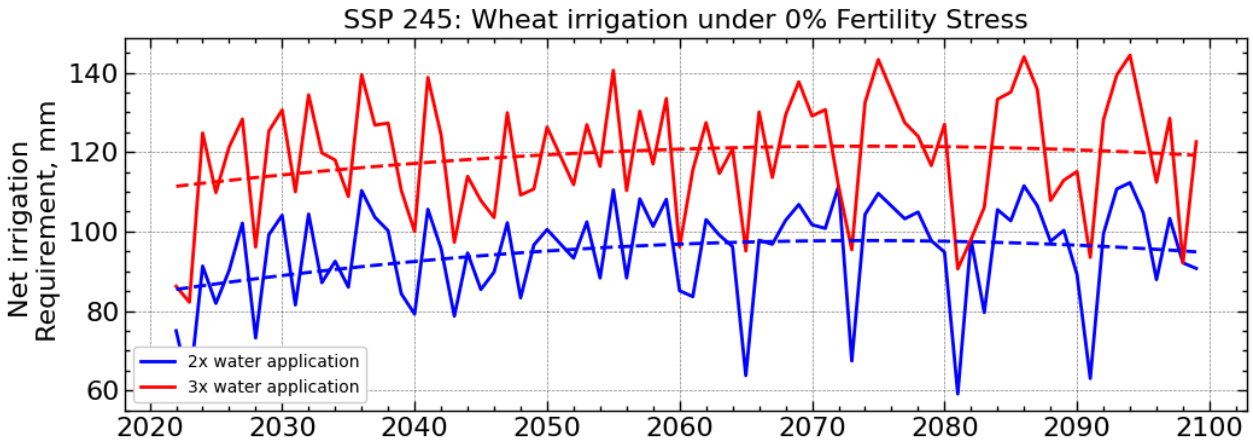

Figure 7.44: Wheat net irrigation requirement in Future (2021-2099) for SSP 245.

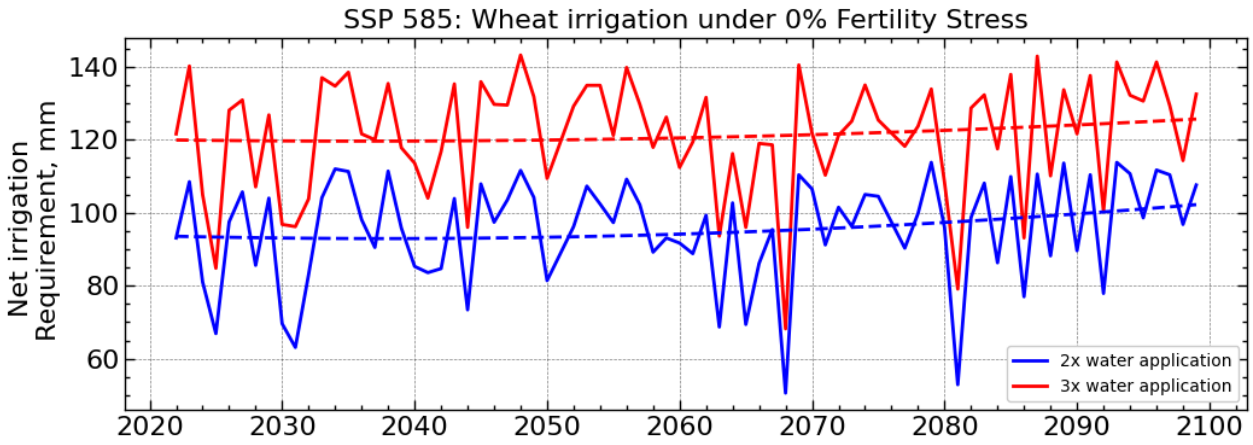

Figure 7.45: Wheat net irrigation requirement in future (2021-2099) for SSP 585.

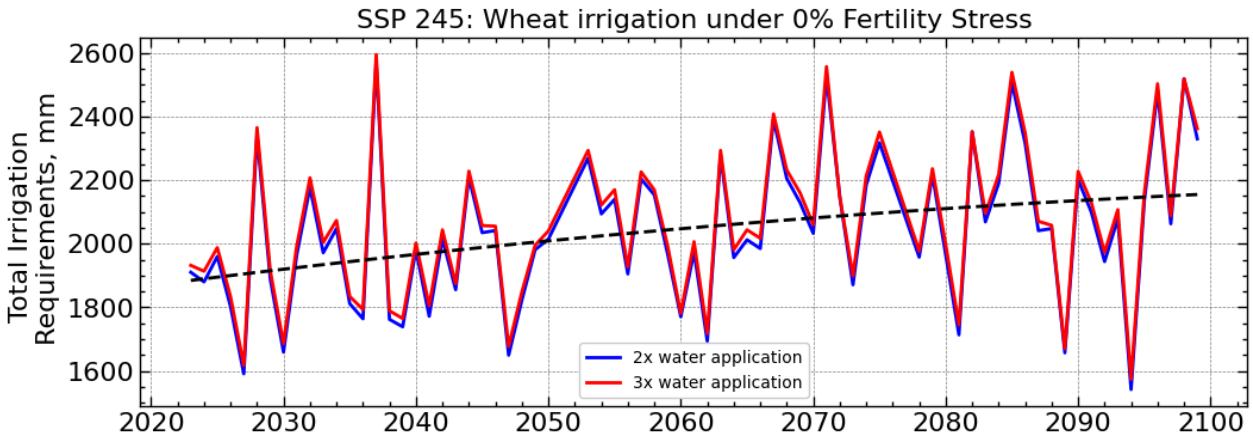

Figure 7.46: Wheat total water requirement in future (2021-2099) for SSP 245.

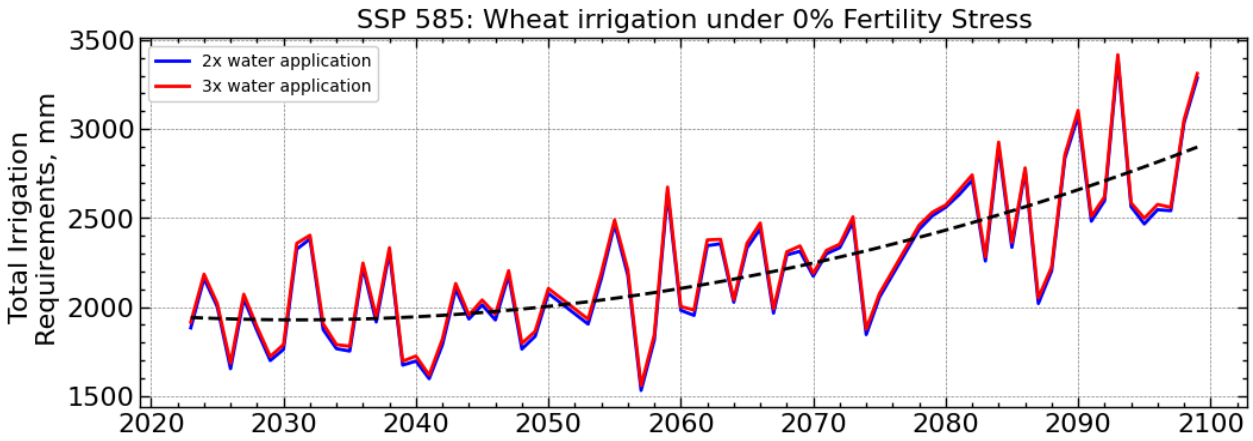

Figure 7.47: Wheat total water requirement in future (2021-2099) for SSP 585.

From the above figure, a rising trend of irrigation requirement has been observed for both SSPs. Summary of percentage increase in NIR and TWR under moderate fertility stress for different irrigation scenario are summarized in **Table 7.17** and **Table 7.18** respectively. Detailed plots are presented in **ANNEX G**.

Table 7.17: % Increase in wheat NIR under no fertility stress for different irrigation scenario

Fertility Stress	Irrigation Scenario	SSP 245			SSP 585			Baseline (mm)
		NF	MF	FF	NF	MF	FF	
50.00%	2 times	-27.16	-20.48	-29.65	-42.93	-20.05	-21.42	116.7
	3 times	-7.28	6.51	-5.40	-18.94	-1.97	-1.37	

Table 7.18: % Increase in wheat TWR under no fertility stress for different irrigation scenario

Fertility Stress	Irrigation Scenario	SSP 245			SSP 585			Baseline (mm)
		NF	MF	FF	NF	MF	FF	
50.00%	2 times	1.69	9.20	9.78	1.55	13.12	37.54	1831.4
	3 times	3.00	10.47	11.02	2.94	14.46	38.84	

8 PRACTICAL IMPLICATIONS OF RESULTS

The GCMs based on CMIP6 have indicated that Dang district will experience a rise in temperature and changes in rainfall patterns. This rise in temperature has various adverse effects on water resource management and agriculture productivity in the region. It will lead to an increase in evaporation and water requirements, thereby putting stress on groundwater sources, which is a common source of drinking water in the Terai and Mid-hills regions of Nepal. This will also result in a surge in domestic water demand, a decline in water quality, and an increase in water demand in the agricultural sector. Even though there may be an increase in rainfall in the future, it may not be enough to meet the region's water demand, leading to periodic water shortages.

Moreover, increased rainfall may result in extreme natural events like floods, landslides, and storms. Flash floods may be more prevalent in urban areas due to low infiltration of precipitation to replenish groundwater sources because of artificial impermeable structures and development activities. The current water infrastructure may not be sufficient to handle this increase in rainfall, as it is designed for low-intensity and less frequent design floods. However, if harvested appropriately, increased rainfall may contribute to the sustainability of current water supplies.

While increased temperatures and CO_2 emissions may aid in the growth of important crops by improving photosynthetic processes, water usage efficiency, shortening physiological periods, and soil microbial activity, there are negative effects too. For instance, a decrease in grain filling period due to increased respiration, fertilizer use efficiencies, shift in agricultural zone, increased insect pest population, desertification, increased soil erosion, evapotranspiration, and reduced mineral nutrient content in different crops can adversely affect the region's agriculture and food system. Therefore, it is essential to adopt suitable policies, mitigation, and adaptation strategies to combat the negative effects, while practicing appropriate measures to harness the positive effects of precipitation, especially in agriculture areas.

9 CONCLUSIONS AND RECOMMENDATIONS

9.1 Conclusions

The overall conclusions of our study are summarized below:

i. The climate information system that was developed as part of the project has a high degree of utility in climate research. It can save researchers the hassle of having to assess data quality and fill gaps in station data provided by DHM. The high R^2 score of 0.913 between the station data and interpolated data reflects the accuracy of gridded interpolation product and its applicability as a substitute for station data.

ii. Progressive and excessive warming is expected in Dang for both scenarios, with SSP585 predicting extreme heating in the future. Also, more heating will occur in the winter season rather than summer. This is particularly worrying for the winter crop cycle as it increases temperature stress on winter crops. Both night and day temperatures are found to increase in the future, which could adversely affect the biota of this region. Annual and monsoon rainfall are expected to increase progressively in Dang in the future with the more extreme SSP585 scenario predicting up to 59% increase in in the far future. Rise in monsoon rainfall is concerning since it maximizes the likelihood of extremes such as floods, landslides and storms which could have devastating consequences on agriculture and infrastructure. On the other hand, winter rainfall is projected to decrease in all stations in Dang. This could lead to energy and water scarcity in the dry seasons, which would be disastrous for the winter crop cycle.

iii. Rice yield is projected to greatly increase, especially under the SSP585 scenario, with yield doubled in the far future when full dosage of fertilizer is provided. This can be explained due to the high increase in rainfall and CO_2 emissions in this scenario. However, in the more conservative SSP245 scenario, the yield while still increasing, starts to trend downwards in the far future because the CO_2 emissions is not high enough to counteract the increasing temperature stress on the crop. Irrigation scenarios have virtually no impact on rice yield since it is a monsoon crop and increasing rainfall is sufficient to irrigate the crop. Extreme events such as flooding are expected to increase in monsoon in the future which would greatly hamper rice yield. Total water requirement of rice is projected to increase in both SSP scenarios due to increased temperature stress.

iv. Wheat yield also shows a similarly sharp rise under SSP585 and high fertilization scenarios. Irrigation scenarios, on the other hand, make a distinct impact on wheat yield. Due to the lower amounts of rainfall in winter, irrigation plays a vital role in meeting its crop water demands. With winters projected to be drier and hotter, wheat yield could be severely impacted in spite of the CO_2 fertilization effect. Total water requirement of wheat is also found to increase in both SSP scenarios due to increased temperature stress.

v. Survey of farmers in our study area shows that they receive adequate irrigation from the canal. However, late advent of monsoon can cause scarcity of water for irrigation. Shifting of seasonal cycles due to climate change could further exacerbate this problem. An excessive

dependence on inorganic fertilizers was observed among farmers in our study area. While they reported rapid increase in crop yield, continued excessive application of inorganic fertilizers over the organic alternatives is likely to lead to overall deterioration of soil, groundwater, and human health in the long term. Multiple farmers complained about the high cost and bureaucratic difficulties of obtaining fertilizers which is a big detriment to sustainable agriculture.

9.2 Recommendations

The recommendations in this study advise following policies and using technology to address the consequences of climate change:

i. Policy/Practice: Irrigation scenario is observed to impact wheat yield. Crop water requirement of wheat is also projected to increase, which coupled with decreased rainfall in winter seasons, could cause major loss of productivity for winter crops like wheat. So it is essential to promote irrigation that goes beyond the conventional surface water irrigation and promote groundwater irrigation in conjunction with streamflow irrigation. In light of the excessive use of chemical fertilizers, organic fertilizers should be promoted to achieve soil carbon sequestration. This involves increasing soil carbon content by capturing atmospheric CO_2 through changes in land management techniques. Several land management practices are suggested in the literature to promote soil carbon sequestration, such as cropping system intensity and rotation practices, zero-tillage and conservation tillage methods, nutrient management, mulching and use of crop residues and manure, incorporation of biochar, use of organic fertilizers, and water management (Fawzy et al., 2020).
ii. Further research: Studies have to be conducted taking into account the loss in crop yield due to extreme weather events such as floods, landslides, heatwaves and droughts. Since there is some skepticism in literature regarding the extent of fertilizing effect of CO_2, crop yield studies should be carried out by considering two scenarios: one that takes the fertilizing effect into account and one that does not. The effect of year-round cropping pattern on individual crop also have to be assessed since the types of crop sown in a field in different seasons determine the soil nutrients and stress on groundwater resources. The potential of different irrigation schemes to meet the rising water requirements have to be researched thoroughly.

REFERENCES

Abedinpour, M., Sarangi, A., Rajput, T. B. S., Singh, M., Pathak, H., & Ahmad, T. (2012). Performance evaluation of AquaCrop model for maize crop in a semi-arid environment. *Agricultural Water Management*, *110*, 55–66. https://doi.org/10.1016/j.agwat.2012.04.001

Adger, W. N. (2006). Vulnerability. *Global Environmental Change*, *16*(3), 268–281. https://doi.org/10.1016/j.gloenvcha.2006.02.006

Adhikari, S., Shrestha, D., Nepal, B., Chhetri, T., & Bhattarai, S. (2022). Identification of Summer Monsoon Onset over Nepal by using Satellite-Derived OLR Data. *Jalawaayu*, *2*, 19–32. https://doi.org/10.3126/jalawaayu.v2i1.45391

Ainsworth, E. A., & Long, S. P. (2005). What have we learned from 15 years of free-air CO2 enrichment (FACE)? A meta-analytic review of the responses of photosynthesis, canopy properties and plant production to rising CO2. *New Phytologist*, *165*(2), 351–372. https://doi.org/10.1111/j.1469-8137.2004.01224.x

Allan, R., Pereira, L., & Smith, M. (1998). Crop evapotranspiration-Guidelines for computing crop water requirements-FAO Irrigation and drainage paper 56 (Vol. 56).

Anderegg, W. R. L., Prall, J. W., Harold, J., & Schneider, S. H. (2010). Expert credibility in climate change. *Proceedings of the National Academy of Sciences of the United States of America*, *107*(27), 12107–12109. https://doi.org/10.1073/pnas.1003187107

Bai, H., Xiao, D., Wang, B., Liu, D. L., Feng, P., & Tang, J. (2021). Multi-model ensemble of CMIP6 projections for future extreme climate stress on wheat in the North China plain. *International Journal of Climatology*, *41*(S1), E171–E186. https://doi.org/10.1002/joc.6674

Bates, B., Kundzewicz, Z. W., Wu, S., Burkett, V., Doell, P., Gwary, D., Hanson, C., Heij, B., Jiménez, B., Kaser, G., Kitoh, A., Kovats, S., Kumar, P., Magadza, C. H. D., Martino, D., Mata, L., Medany, M., Miller, K., & Arnell, N. (2008). *Climate Change and Water. Technical Paper of the Intergovernmental Panel on Climate Change*.

Beck, H., Pan, M., Roy, T., Weedon, G., Pappenberger, F., van Dijk, A., Huffman, G., Adler, R., & Wood, E. (2019). Daily evaluation of 26 precipitation datasets using Stage-IV gauge-radar data for the CONUS. *Hydrology and Earth System Sciences*, *23*, 207–224. https://doi.org/10.5194/hess-23-207-2019

Beguería, S., Vicente-Serrano, S. M., Tomás-Burguera, M., & Maneta, M. (2016). Bias in the variance of gridded data sets leads to misleading conclusions about changes in climate variability. *International Journal of Climatology*, *36*(9), 3413–3422. https://doi.org/10.1002/joc.4561

Berg, P., Feldmann, H., & Panitz, H.-J. (2012). Bias correction of high resolution regional climate model data. *Journal of Hydrology*, *448–449*, 80–92. https://doi.org/10.1016/j.jhydrol.2012.04.026

Bindoff, N. L., Willebrand, J., Artale, V., Cazenave, A., Gregory, J. M., Gulev, S., Hanawa, K., Le Quere, C., Levitus, S., Nojiri, Y., Shum, C. K., Talley, L. D., Unnikrishnan, A. S., Josey, S. A., Tamisiea, M., Tsimplis, M., & Woodworth, P. (2007). *Observations: Oceanic climate change and sea level* (S. Solomon, D. Qin, M. Manning, Z. Chen, M. Marquis, K. B. Averyt, M. Tignor, & H. L. Miller, Eds.; pp. 385–428). Cambridge University Press. https://archive.ipcc.ch/publications_and_data/ar4/wg1/en/ch5.html

Bishop, C., & Abramowitz, G. (2012). Climate Model Dependence and the Replicate Earth Paradigm. *Climate Dynamics*, *41*. https://doi.org/10.1007/s00382-012-1610-y

BODC. (2012, October 1). *Climate and Forecast (CF) netCDF format—The format used by BODC to distribute model data*. British Oceanographic Data Centre. https://www.bodc.ac.uk/resources/delivery_formats/cfnetcdf_format/

Book, I. I. (2016). AquaCrop training handbooks.

Bouras, E., Jarlan, L., Khabba, S., Er-Raki, S., Dezetter, A., Sghir, F., & Tramblay, Y. (2019). Assessing the impact of global climate changes on irrigated wheat yields and water requirements in a semi-arid environment of Morocco. *Scientific Reports*, *9*, 19142. https://doi.org/10.1038/s41598-019-55251-2

Boxall, A. B. A., Hardy, A., Beulke, S., Boucard, T., Burgin, L., Falloon, P. D., Haygarth, P. M., Hutchinson, T., Kovats, R. S., Leonardi, G., Levy, L. S., Nichols, G., Parsons, S. A., Potts, L., Stone, D., Topp, E., Turley, D. B., Walsh, K., Wellington, E. M. H., & Williams, R. J. (2009). Impacts of Climate Change on Indirect Human Exposure to Pathogens and Chemicals from Agriculture. *Environmental Health Perspectives*, *117*(4), 508–514. https://doi.org/10.1289/ehp.0800084

Calzadilla, A., Rehdanz, K., Betts, R., Falloon, P., Wiltshire, A., & Tol, R. S. J. (2013). Climate change impacts on global agriculture. *Climatic Change*, *120*(1), 357–374. https://doi.org/10.1007/s10584-013-0822-4

Carneiro, B., Resce, G., Läderach, P., Schapendonk, F., & Pacillo, G. (2022). What is the importance of climate research? An innovative web-based approach to assess the influence and reach of climate research programs. *Environmental Science & Policy*, *133*, 115–126. https://doi.org/10.1016/j.envsci.2022.03.018

Chand, M. B., Bhattarai, B. C., Pradhananga, N. S., & Baral, P. (2021). Trend Analysis of Temperature Data for the Narayani River Basin, Nepal. *Sci*, *3*(1), Article 1. https://doi.org/10.3390/sci3010001

Dangol, S., Talchabhadel, R., & Pandey, V. P. (2022). Performance evaluation and bias correction of gridded precipitation products over Arun River Basin in Nepal for hydrological applications. *Theoretical and Applied Climatology*, *148*(3), 1353–1372. https://doi.org/10.1007/s00704-022-04001-y

Deutsch, L. P., & Gailly, J. (1996). *ZLIB Compressed Data Format Specification version 3.3* (Request for Comments RFC 1950). Internet Engineering Task Force. https://doi.org/10.17487/RFC1950

Dinku, T., Thomson, M. C., Cousin, R., del Corral, J., Ceccato, P., Hansen, J., & Connor, S. J. (2018). Enhancing National Climate Services (ENACTS) for development in Africa. *Climate and Development*, *10*(7), 664–672. https://doi.org/10.1080/17565529.2017.1405784

Doney, S., Ruckelshaus, M., Duffy, J., Barry, J., Chan, F., English, C., Galindo, H., Grebmeier, J., Hollowed, A., Knowlton, N., Polovina, J., Rabalais, N., Sydeman, W., & Talley, L. (2012). Climate Change Impacts on Marine Ecosystems. *Annual Review of Marine Science*, *4*, 11–37. https://doi.org/10.1146/annurev-marine-041911-111611

Doran, P. T., & Zimmerman, M. K. (2009). Examining the scientific consensus on climate change. *Eos, Transactions American Geophysical Union*, *90*(3), 22–23.

Drake, B. G., Gonzàlez-Meler, M. A., & Long, S. P. (1997). More efficient plants: A consequence of rising atmospheric CO2? *Annual Review of Plant Biology*, *48*(1), 609–639.

Dulal, H., Brodnig, G., Thakur, H., & Green-Onoriose, C. (2010). Do the poor have what they need to adapt to climate change? A case study of Nepal. *Local Environment*, *15*, 621–635. https://doi.org/10.1080/13549839.2010.498814

Eaton, B., Gregory, J., Drach, B., Taylor, K., Hankin, S., Caron, J., Signell, R., Bentley, P., Rappa, G., Höck, H., Pamment, A., Juckes, M., Raspaud, M., Horne, R., Whiteaker, T., Blodgett, D.,

Zender, C., & Lee, D. (2021). *NetCDF Climate and Forecast (CF) Metadata Conventions v1.9*. CF Conventions Committee.

Edwards, P. N. (2011). History of climate modeling. *WIREs Climate Change*, *2*(1), 128–139. https://doi.org/10.1002/wcc.95

Enayati, M., Bozorg-Haddad, O., Bazrafshan, J., Hejabi, S., & Chu, X. (2021). Bias correction capabilities of quantile mapping methods for rainfall and temperature variables. *Journal of Water and Climate Change*, *12*(2), 401–419. https://doi.org/10.2166/wcc.2020.261

Eyring, V., Bony, S., Meehl, G. A., Senior, C. A., Stevens, B., Stouffer, R. J., & Taylor, K. E. (2016). Overview of the Coupled Model Intercomparison Project Phase 6 (CMIP6) experimental design and organization. *Geoscientific Model Development*, *9*(5), 1937–1958. https://doi.org/10.5194/gmd-9-1937-2016

Falloon, P., & Betts, R. (2010). Climate impacts on European agriculture and water management in the context of adaptation and mitigation—The importance of an integrated approach. *Science of The Total Environment*, *408*, 5667–5687. https://doi.org/10.1016/j.scitotenv.2009.05.002

FAO. (2017). *AquaCrop training handbooks. Book I: Understanding AquaCrop. April 2017*. FAO. https://www.fao.org/documents/card/fr/c/ec22b063-15ed-4ad1-b57f-74b047e4e0cb/

FAO. (2022). Nepal at a glance | FAO in Nepal | Food and Agriculture Organization of the United Nations. https://www.fao.org/nepal/fao-in-nepal/nepal-at-a-glance/en/

Fawzy, S., Osman, A. I., Doran, J., & Rooney, D. W. (2020). Strategies for mitigation of climate change: A review. *Environmental Chemistry Letters*, *18*, 2069–2094.

Fenech, A., Comer, N., & Gough, B. (2002). SELECTING A GLOBAL CLIMATE MODEL FOR UNDERSTANDING FUTURE PROJECTIONS OF CLIMATE CHANGE. 13.

Field, C., Lobell, D., Peters, H., & Chiariello, N. (2007). Feedbacks of Terrestrial Ecosystems to Climate Change *. *A. Rev. Environ. Resour.*, *32*. https://doi.org/10.1146/annurev.energy.32.053006.141119

Fischer, G., Tubiello, F. N., van Velthuizen, H., & Wiberg, D. A. (2007). Climate change impacts on irrigation water requirements: Effects of mitigation, 1990–2080. *Technological Forecasting and Social Change*, *74*(7), 1083–1107. https://doi.org/10.1016/j.techfore.2006.05.021

Food and Agriculture Organization of the United Nations (Director). (2016a, November 28). *Crop development AquaCrop—Training module Nr. 4.3, April 2016*. https://www.youtube.com/watch?v=qK0OGps1bW0

Food and Agriculture Organization of the United Nations (Director). (2016b, November 28). *Irrigation management AquaCrop—Training module Nr. 5.1 (Unit 5. Management), April 2016*. https://www.youtube.com/watch?v=o5P35ogKDvw

Food and Agriculture Organization of the United Nations (Director). (2016c, November 28). *Reference evapotranspiration AquaCrop—Training module Nr. 2.2, April 2016*. https://www.youtube.com/watch?v=gtV_RpXsMJI

Foster, T., Brozović, N., Butler, A. P., Neale, C. M. U., Raes, D., Steduto, P., Fereres, E., & Hsiao, T. C. (2017). AquaCrop-OS: An open source version of FAO's crop water productivity model. *Agricultural Water Management*, *181*, 18–22. https://doi.org/10.1016/j.agwat.2016.11.015

Gauchan, D., Thapa Magar, D. B., Gautam, S., Singh, S., & Singh, U. S. (2014). Strengthening seed system for rice seed production and supply in Nepal. *IRRI-NARC Collaborative EC-IFAD Funded Project on Seed Net Development. Socioeconomics and Agricultural Research Policy Division, Nepal Agricultural Research Council, Nepal. 40p.*

Goddard, L. (2016). From science to service. *Science*, *353*(6306), 1366–1367. https://doi.org/10.1126/science.aag3087

Grieser, J., Gommes, R., & Bernardi, M. (2006). New LocClim–the local climate estimator of FAO. *Geophysical Research Abstracts, 8*(08305), 2.

Hamed, M. M., Nashwan, M. S., & Shahid, S. (2022). A novel selection method of CMIP6 GCMs for robust climate projection. *International Journal of Climatology*, *42*(8), 4258–4272. https://doi.org/10.1002/joc.7461

Hankin, S. C., Blower, J. D., Carval, T., Casey, K. S., Donlon, C., Lauret, O., Loubrieu, T., Srinivasan, A., Trinanes, J., Godøy, Ø., Mendelssohn, R., Signell, R. P., Beaujardiere, J. de L., Cornillon, P., Blanc, F., Rew, R., & Harlan, J. (2010). *NetCDF-CF-OPeNDAP: Standards for ocean data interoperability and object lessons for community data standards processes*. *2*. https://doi.org/10.5270/OceanObs09.cwp.41

Hassell, D., Gregory, J., Blower, J., Lawrence, B. N., & Taylor, K. E. (2017). A data model of the Climate and Forecast metadata conventions (CF-1.6) with a software implementation (cf-python v2.1). *Geoscientific Model Development*, *10*(12), 4619–4646. https://doi.org/10.5194/gmd-10-4619-2017

Haylock, M. R., Hofstra, N., Tank, A. M. G., Klok, E. J., Jones, P., & New, M. (2008). A European daily high-resolution gridded dataset of surface temperature and precipitation. *J. Geophys. Res.*, *113*, D20119. https://doi.org/10.1029/2008JD10201

Herrera, S., Gutiérrez, J. M., Ancell, R., Pons, M. R., Frías, M. D., & Fernández, J. (2012). Development and analysis of a 50-year high-resolution daily gridded precipitation dataset over Spain (Spain02). *International Journal of Climatology*, *32*(1), 74–85. https://doi.org/10.1002/joc.2256

Hsiao, T. C., Heng, L., Steduto, P., Rojas-Lara, B., Raes, D., & Fereres, E. (2009). AquaCrop—The FAO Crop Model to Simulate Yield Response to Water: III. Parameterization and Testing for Maize. *Agronomy Journal*, *101*(3), Article 3. https://doi.org/10.2134/agronj2008.0218s

Hulme, M., RM, D., Ngara, T. N. M., New, M., & Lister, D. (2001). African Climate Change: 1900-2100. *CLIMATE RESEARCH, 17*, 145–168. https://doi.org/10.3354/cr017145

ICIMOD. (2011). Glacial Lakes and Glacial Lake Outburst Floods in Nepal | HimalDoc. https://lib.icimod.org/record/27755

IOOS. (2016, May 9). *Data Publishing: Data Access Services, Formats, and Metadata*. The U.S. Integrated Ocean Observing System (IOOS). https://ioos.noaa.gov/data/data-standards/data-publishing/

IPCC. (2018). Glossary—Global Warming of 1.5 ºC. An IPCC Special Report on the impacts of global warming of 1.5°C above pre-industrial levels and related global greenhouse gas emission pathways, in the context of strengthening the global response to the threat of climate change, sustainable development, and efforts to eradicate poverty. *Cambridge University Press*, 541–562. https://doi.org/10.1017/9781009157940.008

IPCC. (2021a). Summary for Policymakers. In: Climate Change 2021: The Physical Science Basis. Contribution of Working Group I to the Sixth Assessment Report of the Intergovernmental Panel on Climate Change. *Cambridge University Press*, 3–32.

IPCC. (2021b). Technical Summary. In: Climate Change 2021: The Physical Science Basis. Contribution of Working Group I to the Sixth Assessment Report of the Intergovernmental Panel on Climate Change. *Cambridge University Press*, 3–32.

Isaaks, E. H., & Srivastava, R. M. (1989). An introduction to applied geostatistics: Oxford University Press, 561. *Search In*.

Isotta, F. A., Frei, C., Weilguni, V., Perčec Tadić, M., Lassègues, P., Rudolf, B., Pavan, V., Cacciamani, C., Antolini, G., Ratto, S. M., Munari, M., Micheletti, S., Bonati, V., Lussana, C., Ronchi, C., Panettieri, E., Marigo, G., & Vertačnik, G. (2014). The climate of daily precipitation

in the Alps: Development and analysis of a high-resolution grid dataset from pan-Alpine rain-gauge data. *International Journal of Climatology*, *34*(5), 1657–1675. https://doi.org/10.1002/joc.3794

Jakob Themeßl, M., Gobiet, A., & Leuprecht, A. (2011). Empirical-statistical downscaling and error correction of daily precipitation from regional climate models. *International Journal of Climatology*, *31*(10), 1530–1544. https://doi.org/10.1002/joc.2168

Jolliff, J. K., Kindle, J. C., Shulman, I., Penta, B., Friedrichs, M. A. M., Helber, R., & Arnone, R. A. (2009). Summary diagrams for coupled hydrodynamic-ecosystem model skill assessment. *Journal of Marine Systems*, *76*(1), 64–82. https://doi.org/10.1016/j.jmarsys.2008.05.014

Khayatnezhad, M., Gholamin, R., Jamaati-e-Somarin, S., & Zabihi-e-Mahmoodabad, R. (2011). The leaf chlorophyll content and stress resistance relationship considering in corn cultivars (Zea mays). *Adv. Environ. Biol*, *5*(1), 118–122.

Knox, J., Hess, T., Daccache, A., & Wheeler, T. (2012). Climate change impacts on crop productivity in Africa and South Asia. *Environmental Research Letters*, *7*, 034032. https://doi.org/10.1088/1748-9326/7/3/034032

Liang, Z., Tang, T., Li, B., Liu, T., Wang, J., & Hu, Y. (2017). Long-term streamflow forecasting using SWAT through the integration of the random forests precipitation generator: Case study of Danjiangkou Reservoir. *Hydrology Research*, *49*(5), 1513–1527. https://doi.org/10.2166/nh.2017.085

Liu, X., Li, Z., & Attarod, P. (2021). Editorial: Understanding Hydrological Extremes and Their Impact in a Changing Climate: Observations, Modeling and Attribution. *Frontiers in Earth Science*, *8*. https://doi.org/10.3389/feart.2020.632186

Mendelsohn, R. (2008). The Impact of Climate Change on Agriculture in Developing Countries. *Journal of Natural Resources Policy Research*, *1*(1), 5–19. https://doi.org/10.1080/19390450802495882

Moriondo, M., Giannakopoulos, C., & Bindi, M. (2011). Climate change impact assessment: The role of climate extremes in crop yield simulation. *Climatic Change*, *104*(3), 679–701. https://doi.org/10.1007/s10584-010-9871-0

Morison, J. I. (1987). Intercellular CO2 concentration and stomatal response to CO2. *Stomatal Function*, *229*, 252.

NASA. (2021, May 20). *Climate and Forecast (CF) Metadata Conventions*. Earthdata; Earth Science Data Systems, NASA. http://www.earthdata.nasa.gov/esdis/esco/standards-and-references/climate-and-forecast-cf-metadata-conventions

Nyunt, C. T., Koike, T., & Yamamoto, A. (2016). Statistical bias correction for climate change impact on the basin scale precipitation in Sri Lanka, Philippines, Japan and Tunisia [Preprint]. Engineering Hydrology/Modelling approaches. https://doi.org/10.5194/hess-2016-14

OGC. (2022). OGC network Common Data Form (netCDF) standards suite | OGC. https://www.ogc.org/standards/netcdf

O'Neill, B. C., Kriegler, E., Riahi, K., Ebi, K. L., Hallegatte, S., Carter, T. R., Mathur, R., & van Vuuren, D. P. (2014). A new scenario framework for climate change research: The concept of shared socioeconomic pathways. *Climatic Change*, *122*(3), 387–400. https://doi.org/10.1007/s10584-013-0905-2

Oreskes, N. (2004). The scientific consensus on climate change. *Science*, *306*(5702), 1686–1686.

Parry, M. L., Rosenzweig, C., Iglesias, A., Livermore, M., & Fischer, G. (2004). Effects of climate change on global food production under SRES emissions and socio-economic scenarios. *Global Environmental Change*, *14*(1), 53–67. https://doi.org/10.1016/j.gloenvcha.2003.10.008

Passioura, J. B. (1996). Simulation Models: Science, Snake Oil, Education, or Engineering? *Agronomy Journal*, *88*(5), 690–694. https://doi.org/10.2134/agronj1996.00021962008800050002x

Peng, S., Huang, J., Sheehy, J. E., Laza, R. C., Visperas, R. M., Zhong, X., Centeno, G. S., Khush, G. S., & Cassman, K. G. (2004). Rice yields decline with higher night temperature from global warming. *Proceedings of the National Academy of Sciences*, *101*(27), 9971–9975.

Python Docs. (2023). *tkinter—Python interface to Tcl/Tk*. Python Documentation. https://docs.python.org/3/library/tkinter.html

Raäisaänen, J. (2007). How reliable are climate models? *Tellus A: Dynamic Meteorology and Oceanography*, *59*(1), 2–29. https://doi.org/10.1111/j.1600-0870.2006.00211.x

Raes, D., Geerts, S., Kipkorir, E., Wellens, J., & Sahli, A. (2006). Simulation of yield decline as a result of water stress with a robust soil water balance model. *Agricultural Water Management*, *81*(3), 335–357. https://doi.org/10.1016/j.agwat.2005.04.006

Raes, D., Steduto, P., Hsiao, T. C., & Fereres, E. (2009). AquaCrop—The FAO Crop Model to Simulate Yield Response to Water: II. Main Algorithms and Software Description. *Agronomy Journal*, *101*(3), Article 3. https://doi.org/10.2134/agronj2008.0140s

Ralph F. Keeling & Charles D. Keeling. (2017). Atmospheric Monthly In Situ CO2 Data—Mauna Loa Observatory, Hawaii (Archive 2022-02-04). In Scripps CO2 Program Data. UC San Diego Library Digital Collections. https://doi.org/10.6075/J08W3BHW

Rew, R., & Davis, G. (1990). NetCDF: an interface for scientific data access. *IEEE Computer Graphics and Applications*, *10*(4), 76–82. https://doi.org/10.1109/38.56302

Salman, M., García-Vila, M., Fereres, E., Raes, D., & Steduto, P. (2021). The AquaCrop model–Enhancing crop water productivity: Ten years of development, dissemination and implementation 2009–2019 (Vol. 47). Food & Agriculture Org.

Semenov, M., & Stratonovitch, P. (2010). Use of multi-model ensembles from global climate models for assessment of climate change impacts. *Climate Research*, *41*, 1–14. https://doi.org/10.3354/cr00836

Shrestha, N. (2014). Improving cereal production in the Terai Region of Nepal: Assessment of field management strategies through a model based approach.

Shrestha, N., Raes, D., Batelaan, O., & Kumar Sah, S. (2014). Improving Cereal Production in the Terai Region of Nepal: Assessment of Field Management Strategies through a Model Based Approach. https://lirias.kuleuven.be/1740959

Shrestha, N., Raes, D., & Sah, S. K. (2013). Strategies to improve cereal production in the Terai region (Nepal) during dry season: Simulations with aquacrop. *Procedia Environmental Sciences*, *19*, 767–775.

Smit, B., & Wandel, J. (2006). Adaptation, adaptive capacity and vulnerability. *Global Environmental Change*, *16*(3), 282–292. https://doi.org/10.1016/j.gloenvcha.2006.03.008

Smith, M. (1992). *CROPWAT: A Computer Program for Irrigation Planning and Management*. Food & Agriculture Org. https://books.google.com/books?id=p9tB2ht47NAC

Soil Survey Manual. (n.d.). Natural Resources Conservation Service. Retrieved April 23, 2023, from https://www.nrcs.usda.gov/resources/guides-and-instructions/soil-survey-manual

Solomon S, et. al.,. (2007). *Climate Change 2007: The Physical Science Basis*. Intergovernmental Panel on Climate Change (IPCC).

Steduto, P., Hsiao, T. C., Raes, D., & Fereres, E. (2009). AquaCrop—The FAO Crop Model to Simulate Yield Response to Water: I. Concepts and Underlying Principles. *Agronomy Journal*, *101*(3), Article 3. https://doi.org/10.2134/agronj2008.0139s

Taylor, K. E. (2001). Summarizing multiple aspects of model performance in a single diagram. *Journal of Geophysical Research: Atmospheres*, *106*(D7), 7183–7192. https://doi.org/10.1029/2000JD900719

Taylor, R. (1990). Interpretation of the Correlation Coefficient: A Basic Review. *Journal of Diagnostic Medical Sonography*, *6*(1), 35–39. https://doi.org/10.1177/875647939000600106

Tebaldi, C., & Knutti, R. (2007). The use of the multi-model ensemble in probabilistic climate projections. *Philosophical Transactions of the Royal Society A: Mathematical, Physical and Engineering Sciences*, *365*(1857), 2053–2075. https://doi.org/10.1098/rsta.2007.2076

Timsina, J., & Connor, D. J. (2001). Productivity and management of rice–wheat cropping systems: Issues and challenges. *Field Crops Research*, *69*(2), 93–132.

Trenberth, K. E., Marquis, M., & Zebiak, S. (2016). The vital need for a climate information system. *Nature Climate Change*, *6*(12), Article 12. https://doi.org/10.1038/nclimate3170

Tsukaguchi, T., Kawamitsu, Y., Takeda, H., Suzuki, K., & Egawa, Y. (2003). Water Status of Flower Buds and Leaves as Affected by High Temperature in Heat-Tolerant and Heat-Sensitive Cultivars of Snap Bean (*Phaseolus vulgaris* L.). *Plant Production Science*, *6*(1), Article 1. https://doi.org/10.1626/pps.6.24

Turner, J., & Marshall, G. J. (2011). *Climate Change in the Polar Regions*. Cambridge University Press.

Unidata. (2022). *NetCDF* (4.9). https://doi.org/10.5065/D6H70CW6

Vanuytrecht, E., Raes, D., Steduto, P., Hsiao, T. C., Fereres, E., Heng, L. K., Garcia Vila, M., & Mejias Moreno, P. (2014). AquaCrop: FAO's crop water productivity and yield response model. *Environmental Modelling & Software*, *62*, 351–360. https://doi.org/10.1016/j.envsoft.2014.08.005

Vincent, K., Dougill, A. J., Dixon, J. L., Stringer, L. C., & Cull, T. (2017). Identifying climate services needs for national planning: Insights from Malawi. *Climate Policy*, *17*(2), 189–202. https://doi.org/10.1080/14693062.2015.1075374

Wayne, G. (2013). The Beginner's Guide to Representative Concentration Pathways. 25.

Wheeler, T., & von Braun, J. (2013). Climate Change Impacts on Global Food Security. *Science*, *341*(6145), 508–513. https://doi.org/10.1126/science.1239402

Willmott, C. J., & Matsuura, K. (2005). Advantages of the mean absolute error (MAE) over the root mean square error (RMSE) in assessing average model performance. *Climate Research*, *30*(1), 79–82. https://doi.org/10.3354/cr030079

Wing, I. S., Cian, E. D., & Mistry, M. N. (2021). Global vulnerability of crop yields to climate change. *Journal of Environmental Economics and Management*, *109*, 102462. https://doi.org/10.1016/j.jeem.2021.102462

Woodward, G., Perkins, D. M., & Brown, L. E. (2010). Climate change and freshwater ecosystems: Impacts across multiple levels of organization. *Philosophical Transactions of the Royal Society B: Biological Sciences*, *365*(1549), 2093–2106. https://doi.org/10.1098/rstb.2010.0055

WorldBank. (2010). *World Development Report 2010: Development and Climate Change* (world). World Bank. https://elibrary.worldbank.org/doi/epdf/10.1596/978-0-8213-7987-5

Xavier, A. C., King, C. W., & Scanlon, B. R. (2016). Daily gridded meteorological variables in Brazil (1980–2013). *International Journal of Climatology*, *36*(6), 2644–2659. https://doi.org/10.1002/joc.4518

Yohe, G., & Tol, R. S. J. (2002). Indicators for social and economic coping capacity—Moving toward a working definition of adaptive capacity. *Global Environmental Change*, *12*(1), 25–40. https://doi.org/10.1016/S0959-3780(01)00026-7

ANNEX A: TIMELINE OF PROJECT

ID	Task Name	Duration	Start
1	**Final Year Project**	**277 days**	**Sat 4/9/22**
2	Idntification of Topic	7 days	Sat 4/9/22
3	**Literature Review**	**35 days**	**Wed 4/20/22**
4	Interpolation Techniques & Climate Information System	30 days	Wed 4/20/22
5	Climate Projection	30 days	Wed 4/20/22
6	Crop Modelling	35 days	Wed 4/20/22
7	**Perliminary Results**	**35 days**	**Wed 6/8/22**
8	Acquisition of Grided Data	10 days	Wed 6/8/22
9	Selection of Study Area	3 days	Wed 6/8/22
10	**Climate Projection**	**35 days**	**Wed 6/8/22**
11	Selection of GCM	3 days	Wed 6/8/22
12	Downscaling	7 days	Mon 6/13/22
13	Bias Correction	10 days	Wed 6/22/22
14	Senario Analysis	15 days	Wed 7/6/22
15	Finalization of Input Parameter for AquaCrop Modelling	25 days	Wed 7/27/22
16	Presentation (End of 7th semster)	1 day	Wed 8/31/22
17	Board Exam (7th Semester)	32 days	Thu 9/1/22
18	Start of 8th semester	1 day	Mon 10/17/22
19	**Farmer and Soil Survey**	**22 days**	**Tue 10/18/22**
20	Preparation of questionnaire	8 days	Tue 10/18/22
21	Tools and Material Arrangement	7 days	Fri 10/28/22
22	Field Survey	7 days	Tue 11/8/22
23	**Application Development**	**35 days**	**Thu 11/17/22**
24	Terminal Application	20 days	Thu 11/17/22
25	GUI Development	15 days	Thu 12/15/22
26	**Finalization of Input Variables**	**15 days**	**Thu 1/5/23**
27	Farmer Survey Interperation	4 days	Thu 1/5/23
28	Soil Sample Analysis	15 days	Thu 1/5/23
29	Climate Data	7 days	Thu 1/5/23
30	**Aquacrop Modelling**	**22 days**	**Thu 1/26/23**
31	Give Input	5 days	Thu 1/26/23
32	Calibration and Validation	10 days	Thu 2/2/23
33	Finalize Model	7 days	Thu 2/16/23
34	Run Model for Climate Data	10 days	Mon 2/27/23
35	Interperation of Data	5 days	Mon 3/13/23
36	Draft Report Preparation	7 days	Mon 3/20/23
37	Board Exam (8th Semester)	19 days	Fri 3/24/23
38	Final Report Preparation	5 days	Wed 4/26/23
39	Presentation Preparation	3 days	Thu 4/27/23

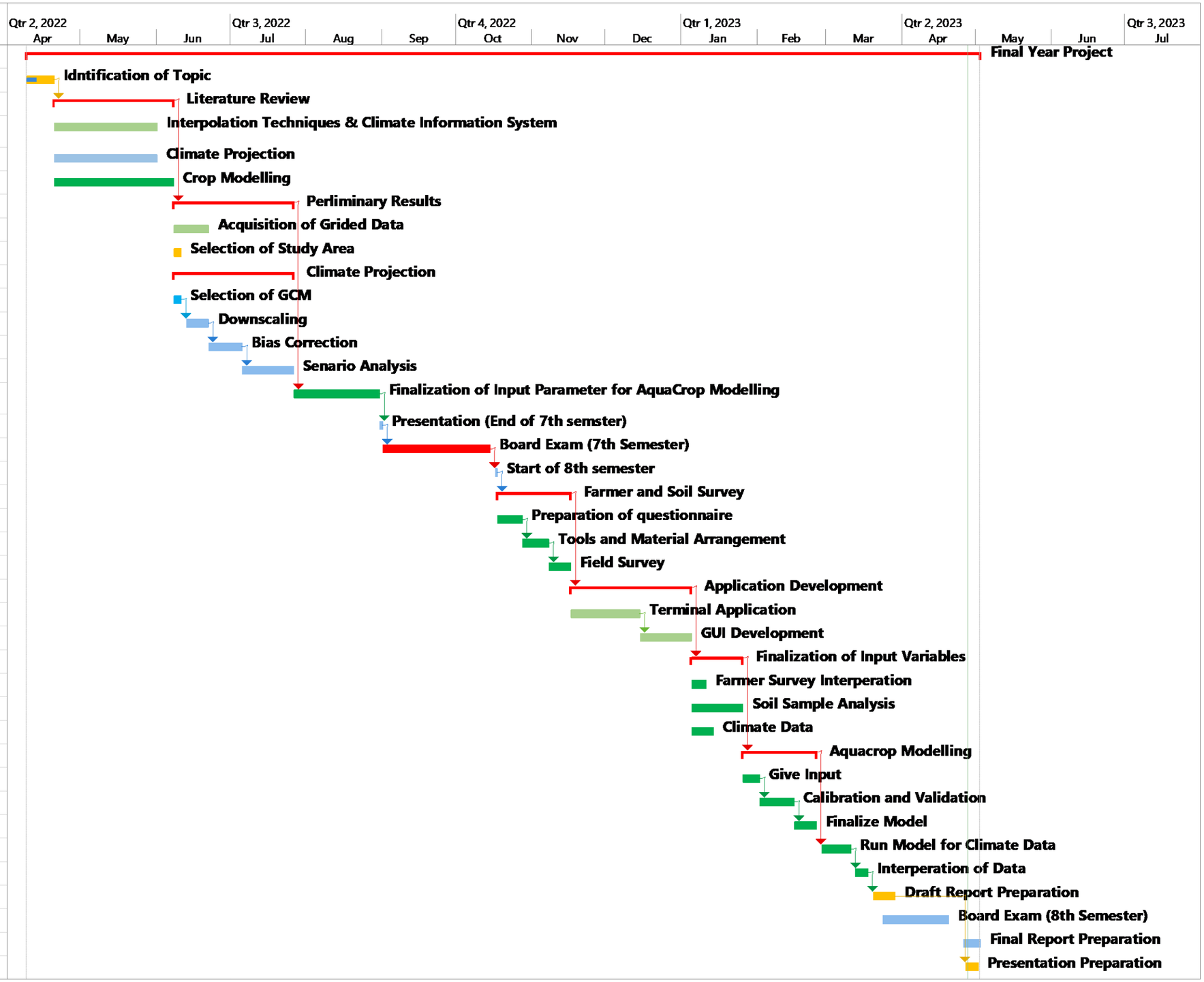

ANNEX B: GLIMPSES OF FARMER SURVEY

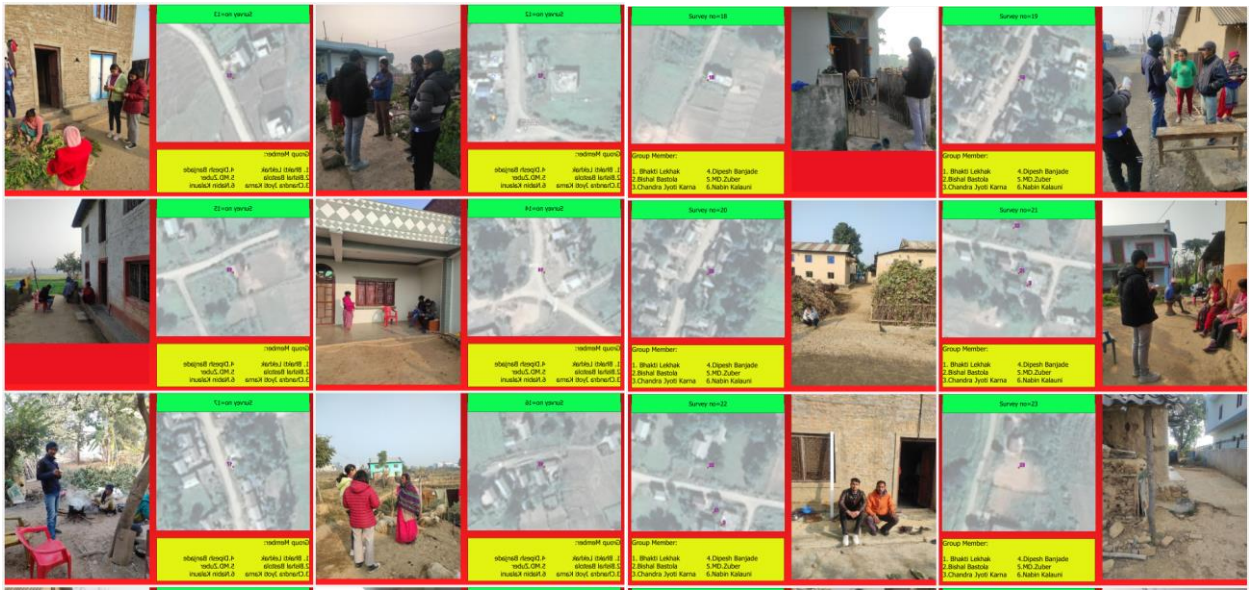


Survey no=44
Group Member:
1. Bhakti Lekhak
2.Bishal Bastola
3.Chandra Jyoti Karna
4.Dipesh Banjade
5.MD.Zuber
6.Nabin Kalauni
Survey no=45
Group Member:
1. Bhakti Lekhak
2.Bishal Bastola
3.Chandra Jyoti Karna
4.Dipesh Banjade
5.MD.Zuber
6.Nabin Kalauni
Survey no=46
Group Member:
1. Bhakti Lekhak
2.Bishal Bastola
3.Chandra Jyoti Karna
4.Dipesh Banjade
5.MD.Zuber
6.Nabin Kalauni
Survey no=47
Group Member:
1. Bhakti Lekhak
2.Bishal Bastola
3.Chandra Jyoti Karna
4.Dipesh Banjade
5.MD.Zuber
6.Nabin Kalauni
Survey no=48
Group Member:
1. Bhakti Lekhak
2.Bishal Bastola
3.Chandra Jyoti Karna
4.Dipesh Banjade
5.MD.Zuber
6.Nabin Kalauni
Survey no=49
Group Member:
1. Bhakti Lekhak
2.Bishal Bastola
3.Chandra Jyoti Karna
4.Dipesh Banjade
5.MD.Zuber
6.Nabin Kalauni

ANNEX C: QUESTIONNAIRE FOR FARMER SURVEY

Farmer Household Survey		
Demography		
Survey no:		
Phone no		
GPS Co-ordinates:		
How long have you been farming:	[1] 1 year [2] 1-5 years [3] 5-10 years [4] more than 10 years [5] As long as I can remember	
Farm Size:		
Type of farm (Upland [1] 'Khet' [2] Lowland [3])		
Type of ownership:	[1] Bought [2] Hereditary [3] On hire [4] looking after for someone [99] Others (Specify)	
माटो कस्तो छ	[1] sandy (बलौटे) [2] loamy (चिम्ट्याइलो) [3] Clayey (चिल्लो मसिनो)	
Main factor affecting planting of crop.		
Factors	**Rice**	**Wheat**
[1] After first rainfall		
[2] Depending on SWC		
[3] Fixed time (when?)		
[4] Others (specify)		
Yield Comparison		
Yield	**Rice**	**Wheat**
10 Years earlier		
Last year		
This year		
Market Price of Yield (Rs/kg)		

Crop Phenology	
Sowing Date बिउ कहिले राखिन्छ?	
Transplanting Date कहिले रोपिन्छ?	
No of plants transplanted/m^2 कति कति टाढा रोपिन्छ ?	
Date of recovery कहिले सर्छ?	
Maximum canopy cover धपक्क खेत ढाक्ने कहिले हुन्छ?	
Date of flowering फुल कहिले लाग्छ?	
Duration of flowering फुल कति समय सम्म रहन्छ?	
Grain filling दाना कहिले पसाउछ?	
Date of senescence पात पहेंलो हुन कहिले देखि हुन्छ?	
Harvesting बालि कहिले उठाइन्छ?	
Length of growing cycle	
Fertilizer Usage	
Urea सेतो गेडा मल	
DAP खैरो गेडा मल	
Potash रातो मल	

Zinc		
Micronutrients(vitamin)		
Farmyard manure गोबर मल		
Others		
Irrigations Information		
Duration		
Source of irrigation सिचाई को श्रोत		
Type of irrigation सिचाई को तरिका		
First irrigation		
No of irrigation		
Last irrigation		
Weeds Control		
Pesticides किटनासक		
No of times uprooted weeds ? गोडमेल कति पटक गरिन्छ?		
Herbicide झाडीनासक		

ANNEX D: PROJECTED RICE YIELD

0 % Fertility Stress:

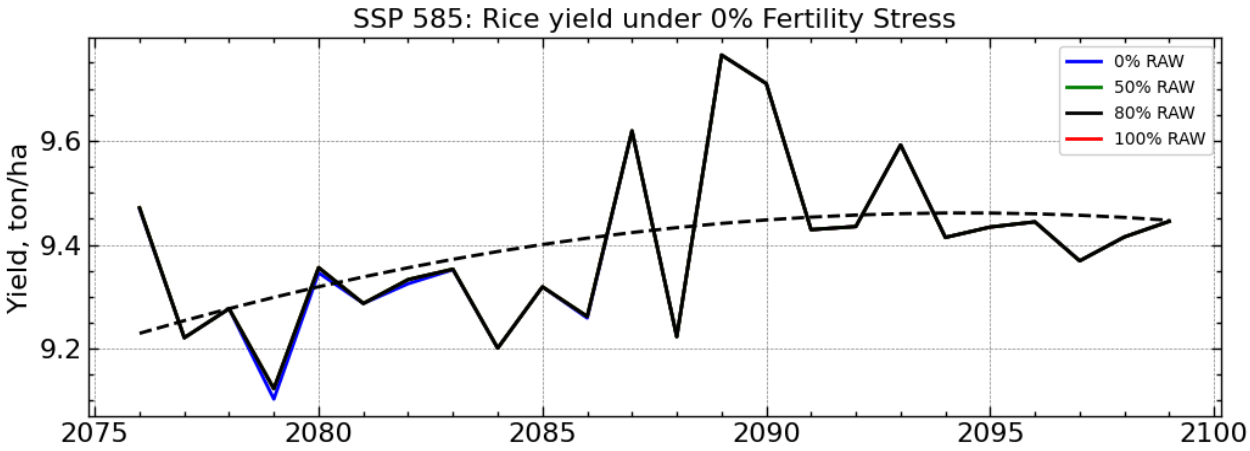

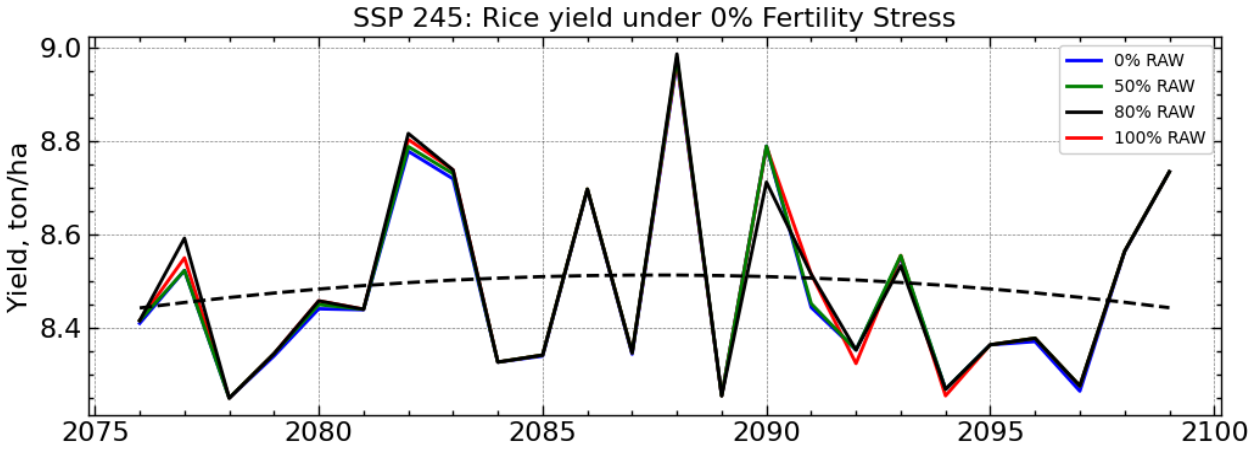

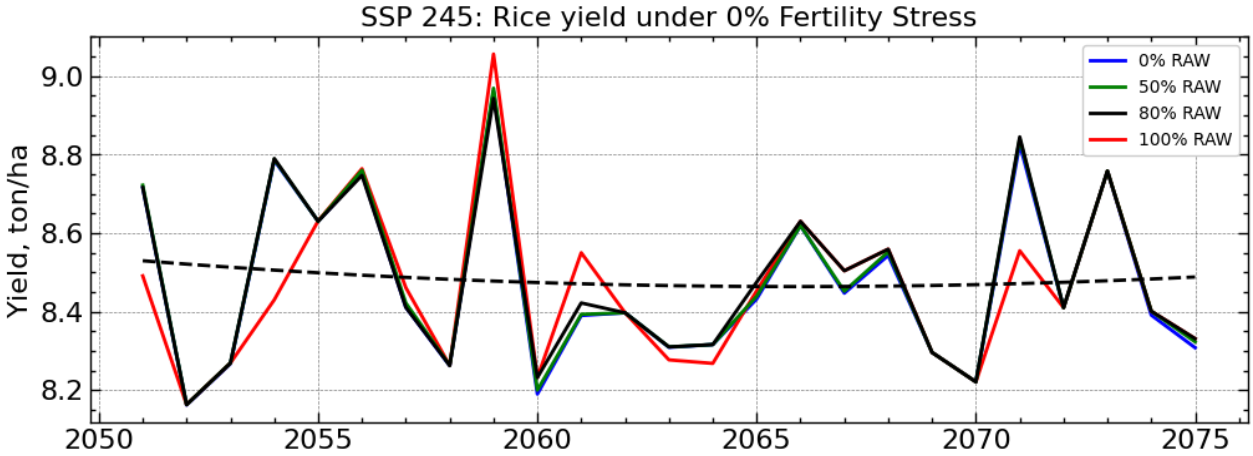

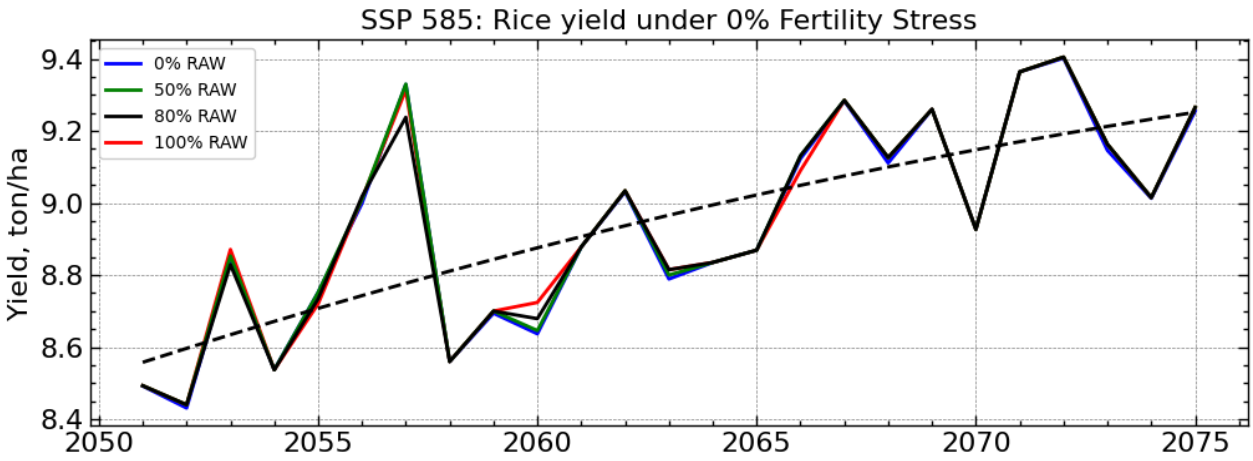
SSP 585: Rice yield under 0% Fertility Stress
0% RAW
50% RAW
80% RAW
100% RAW
Yield, ton/ha
9.4
9.2
9.0
8.8
8.6
8.4
2050
2055
2060
2065
2070
2075

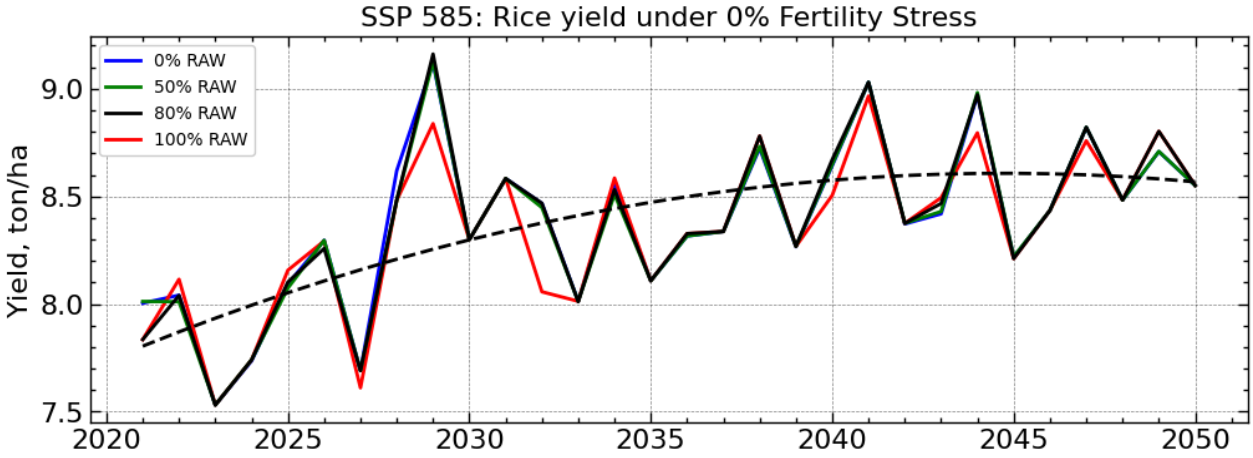
SSP 585: Rice yield under 0% Fertility Stress
0% RAW
50% RAW
80% RAW
100% RAW
Yield, ton/ha
9.0
8.5
8.0
7.5
2020
2025
2030
2035
2040
2045
2050

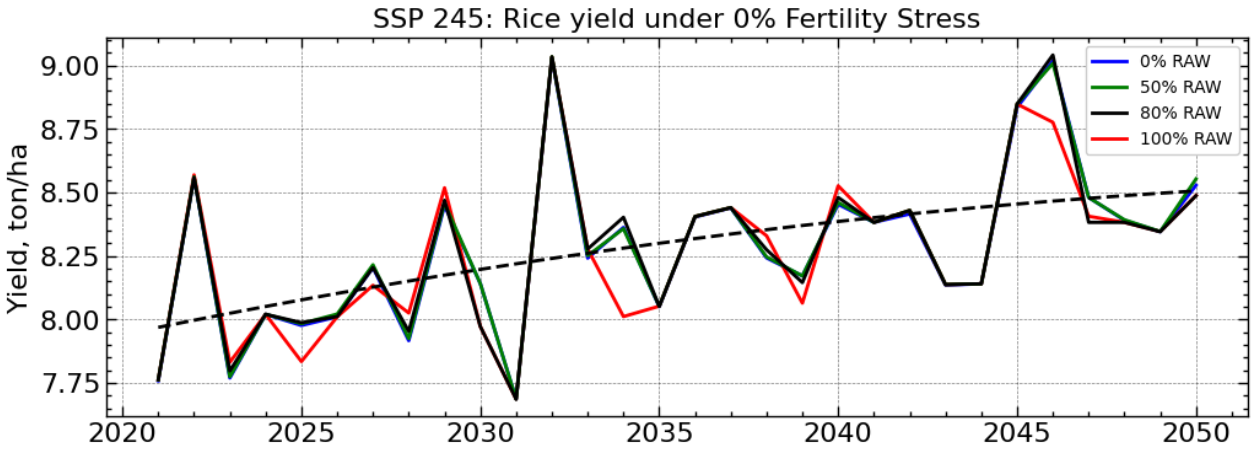
SSP 245: Rice yield under 0% Fertility Stress
0% RAW
50% RAW
80% RAW
100% RAW
Yield, ton/ha
9.00
8.75
8.50
8.25
8.00
7.75
2020
2025
2030
2035
2040
2045
2050

15% Fertility Stress:

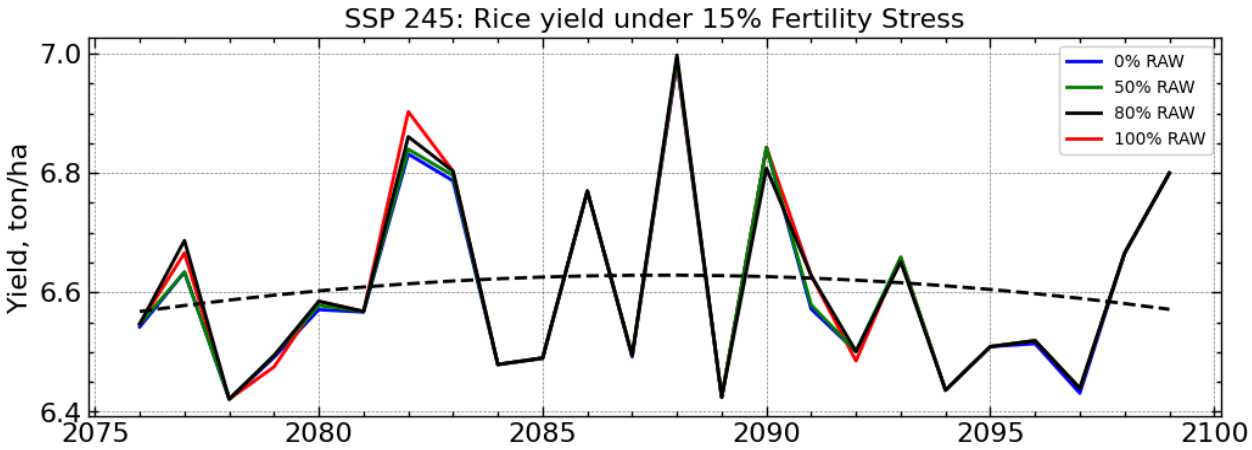

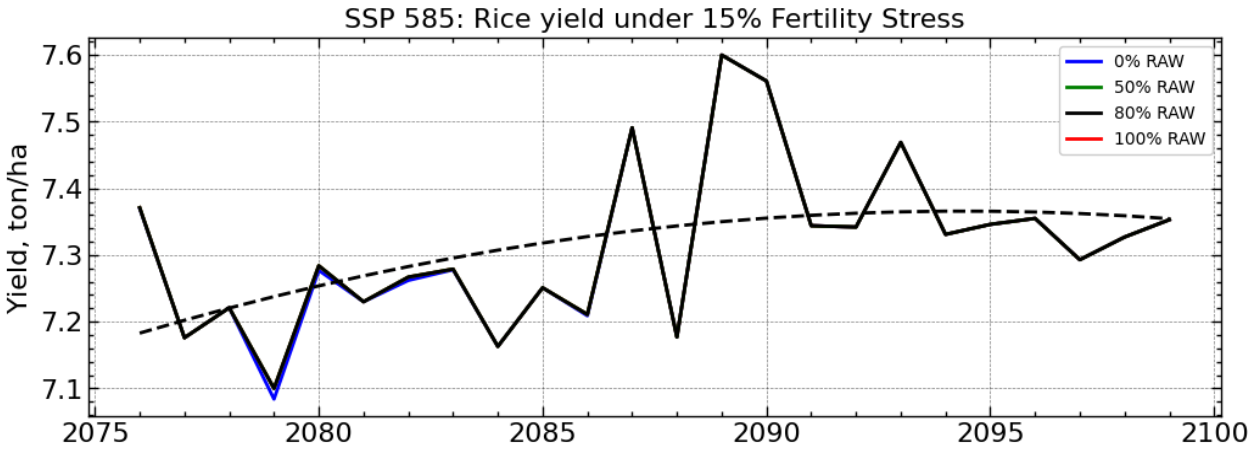

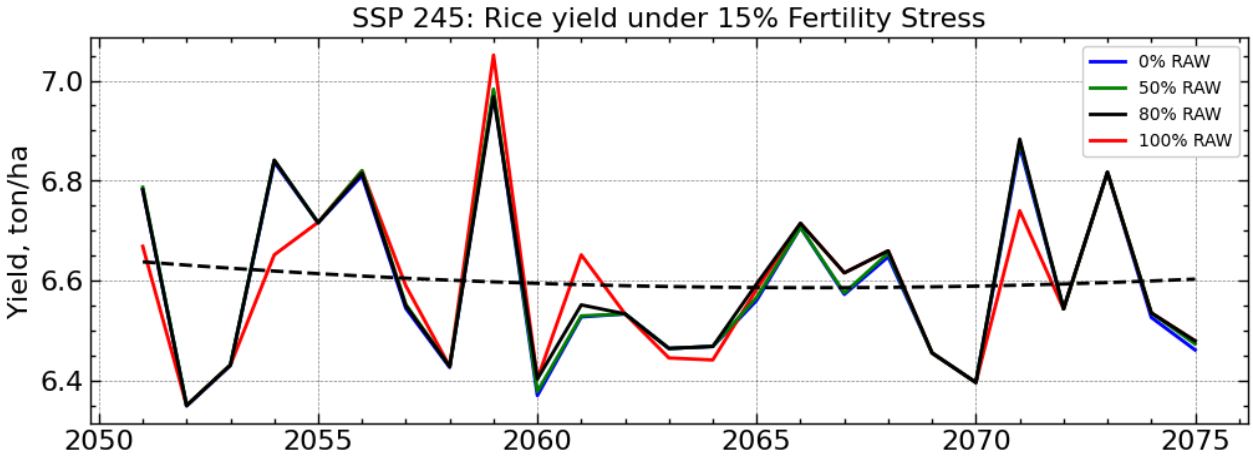

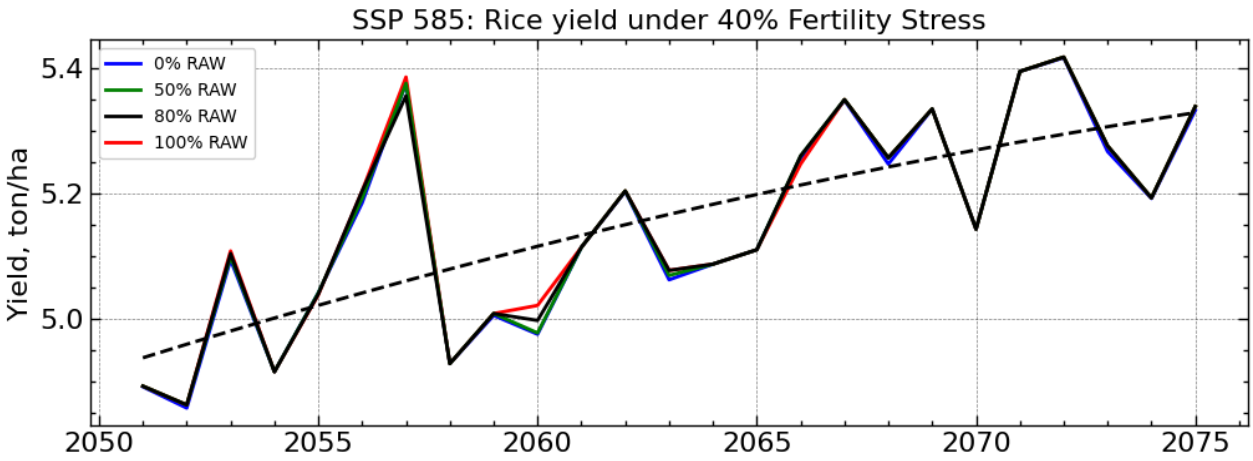
SSP 585: Rice yield under 40% Fertility Stress
0% RAW
50% RAW
80% RAW
100% RAW
Yield, ton/ha
5.4
5.2
5.0
2050
2055
2060
2065
2070
2075

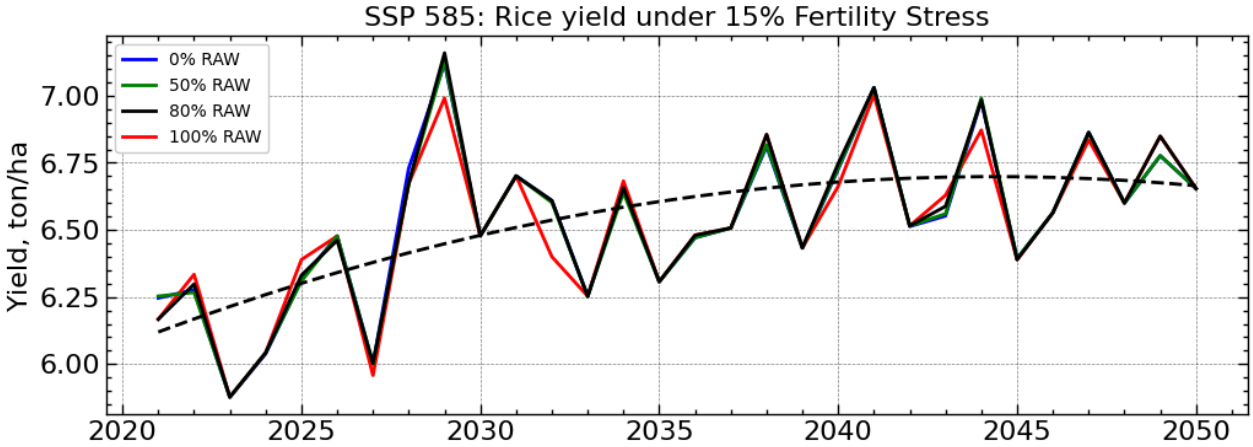
SSP 585: Rice yield under 15% Fertility Stress
0% RAW
50% RAW
80% RAW
100% RAW
Yield, ton/ha
7.00
6.75
6.50
6.25
6.00
2020
2025
2030
2035
2040
2045
2050

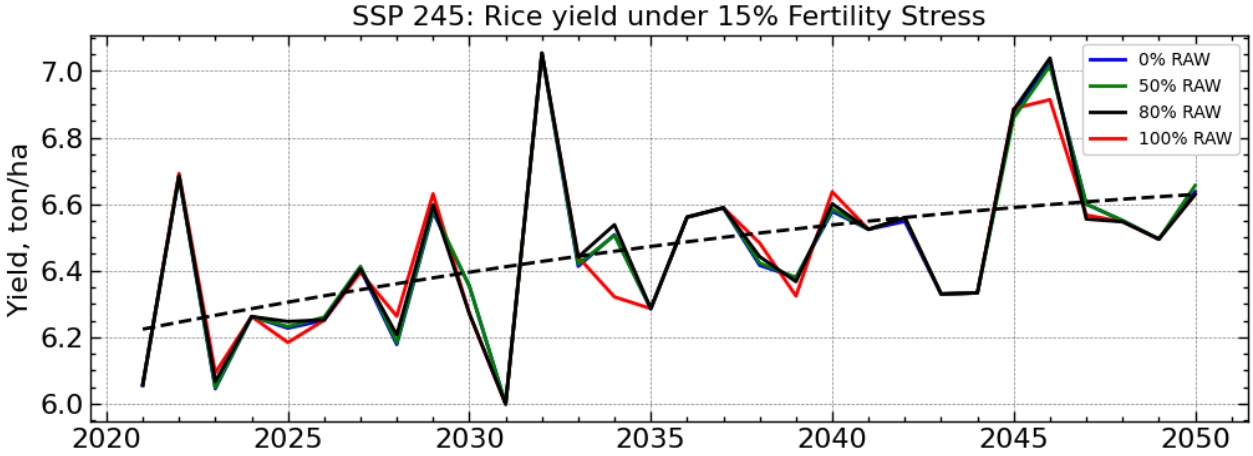
SSP 245: Rice yield under 15% Fertility Stress
0% RAW
50% RAW
80% RAW
100% RAW
Yield, ton/ha
7.0
6.8
6.6
6.4
6.2
6.0
2020
2025
2030
2035
2040
2045
2050

40% Fertility Stress:

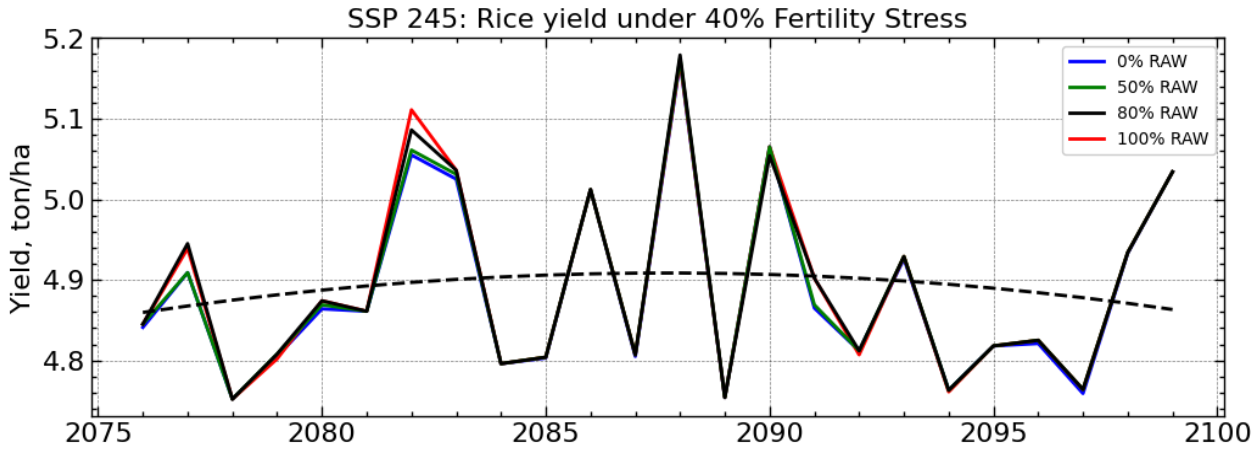

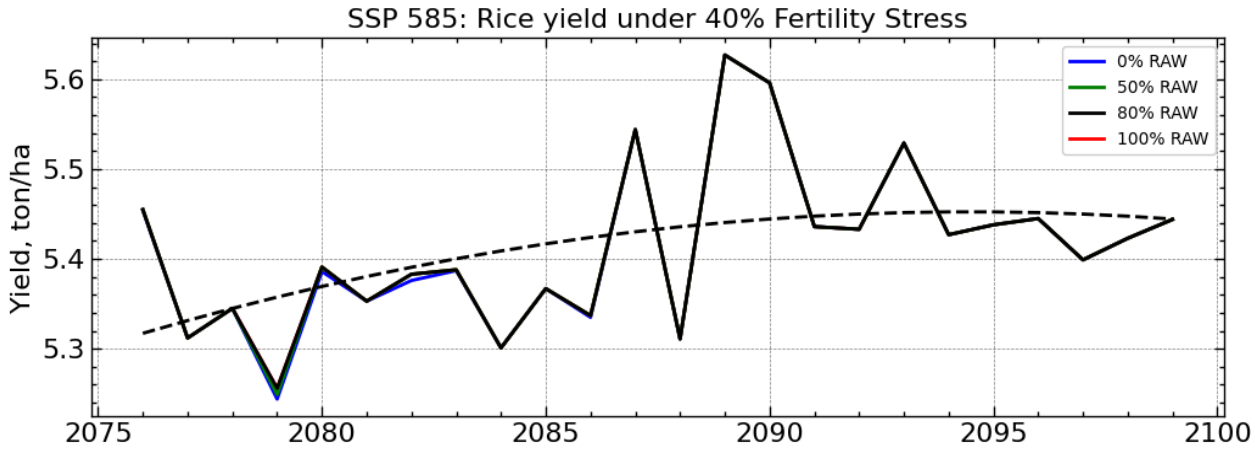

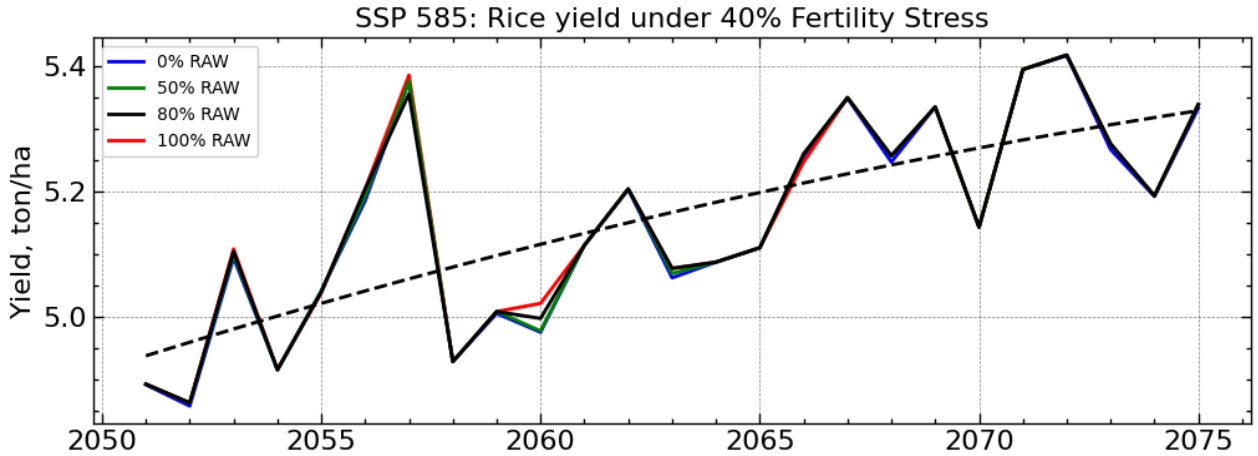

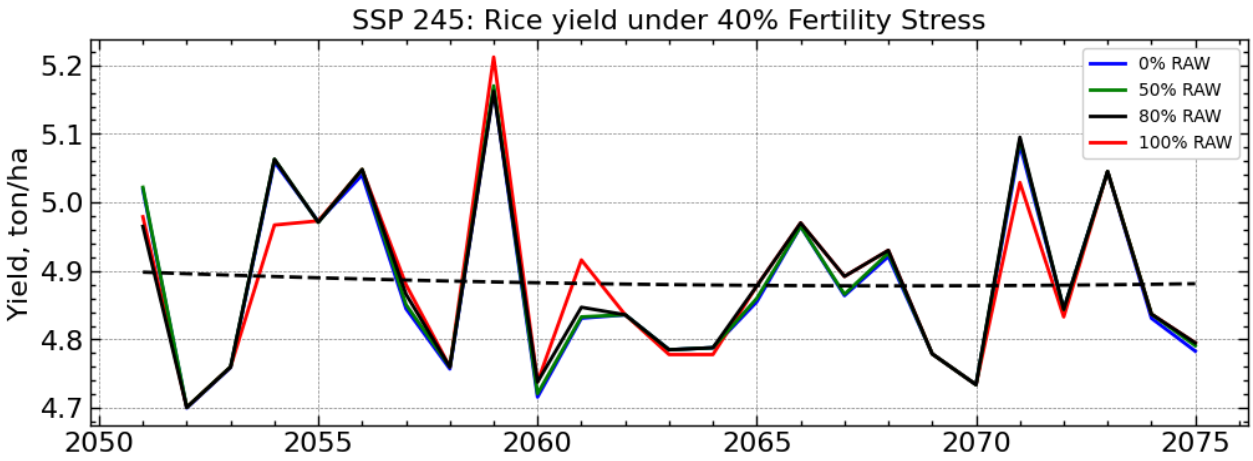
SSP 245: Rice yield under 40% Fertility Stress
Yield, ton/ha
0% RAW
50% RAW
80% RAW
100% RAW
5.2
5.1
5.0
4.9
4.8
4.7
2050
2055
2060
2065
2070
2075

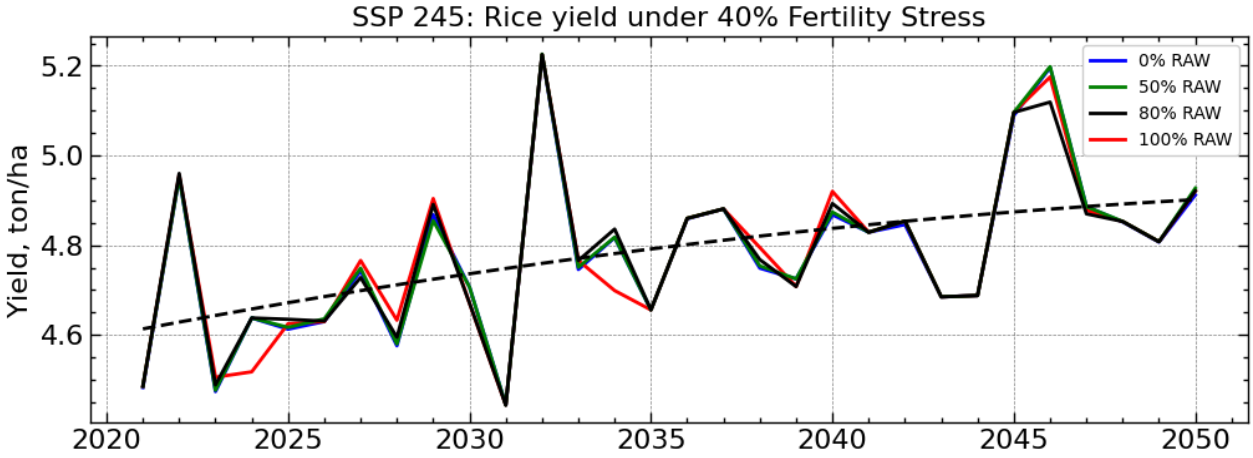
SSP 245: Rice yield under 40% Fertility Stress
Yield, ton/ha
0% RAW
50% RAW
80% RAW
100% RAW
5.2
5.0
4.8
4.6
2020
2025
2030
2035
2040
2045
2050

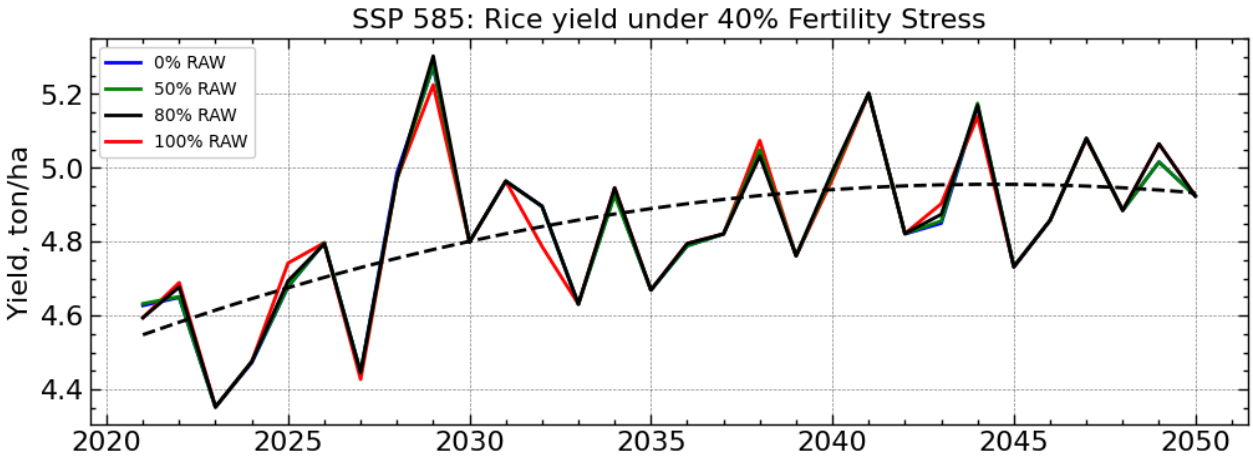
SSP 585: Rice yield under 40% Fertility Stress
Yield, ton/ha
0% RAW
50% RAW
80% RAW
100% RAW
5.2
5.0
4.8
4.6
4.4
2020
2025
2030
2035
2040
2045
2050

ANNEX E: PROJECTED RICE WATER REQUIREMENT

0% Fertility:

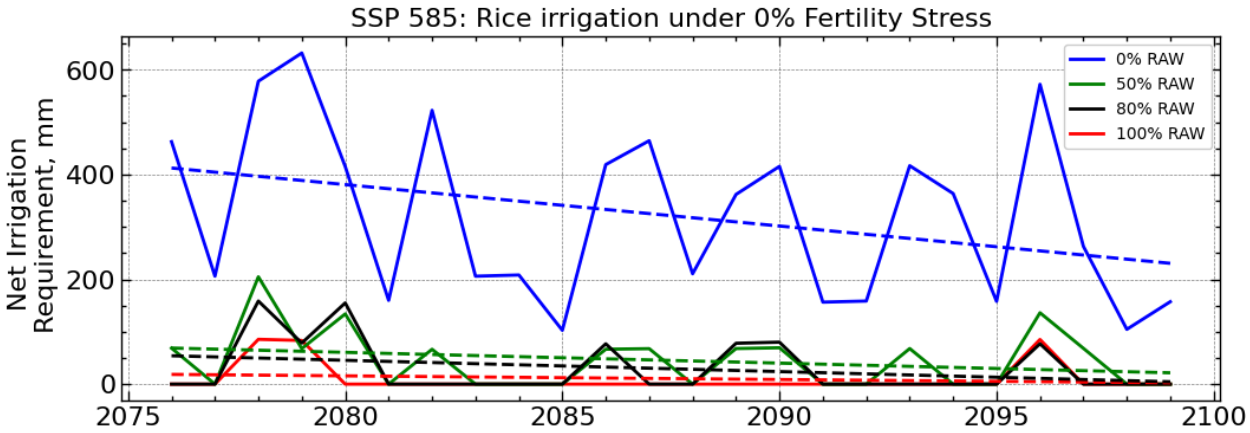

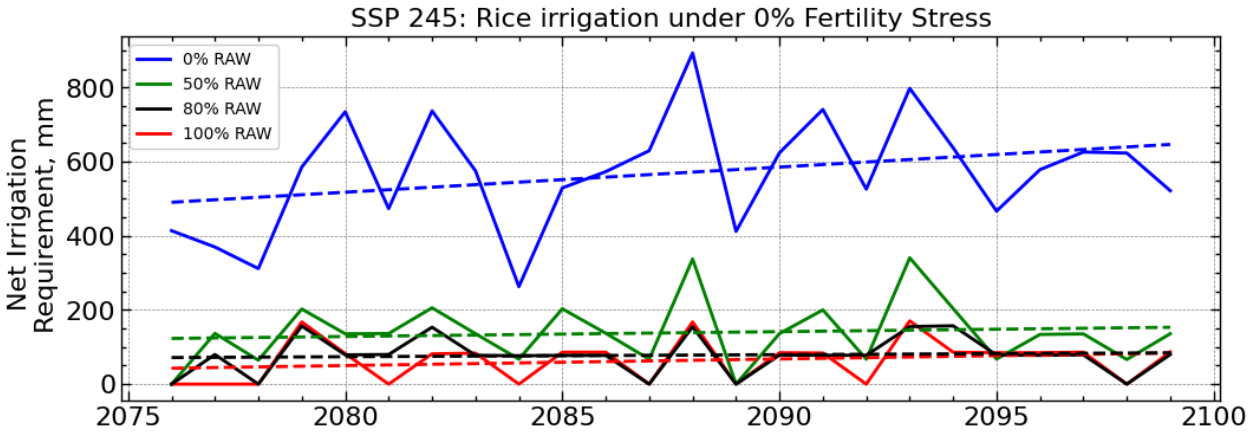

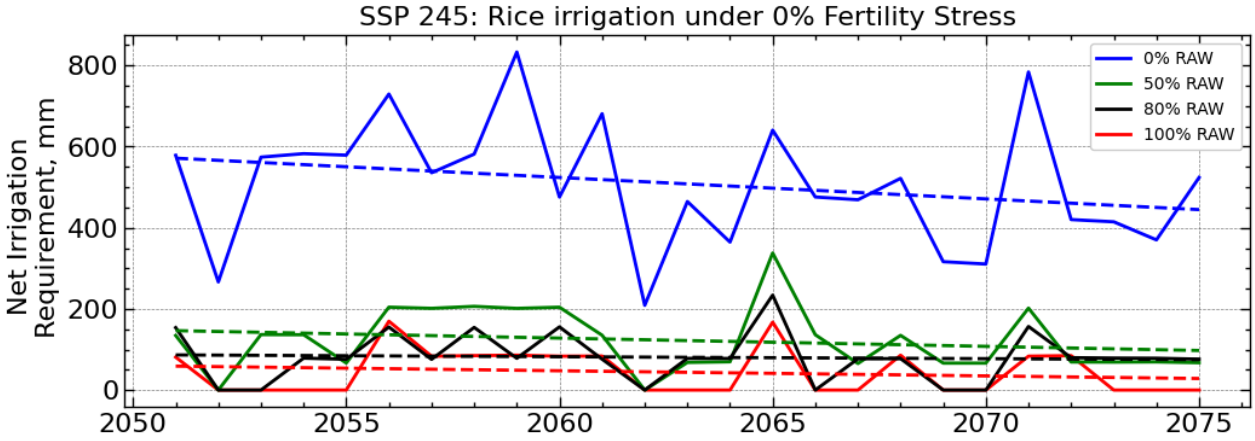

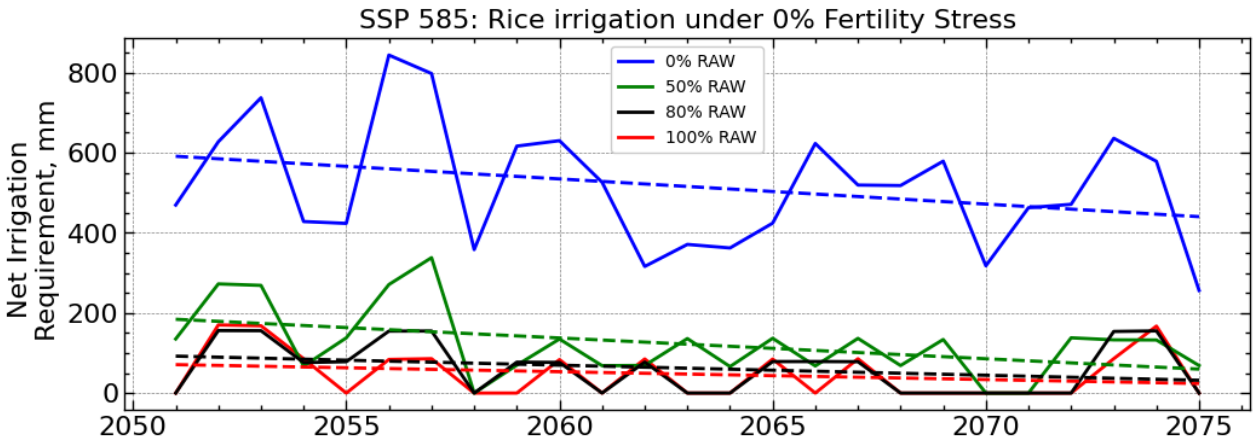
SSP 585: Rice irrigation under 0% Fertility Stress
Net Irrigation Requirement, mm
0% RAW
50% RAW
80% RAW
100% RAW
0
200
400
600
800
2050
2055
2060
2065
2070
2075

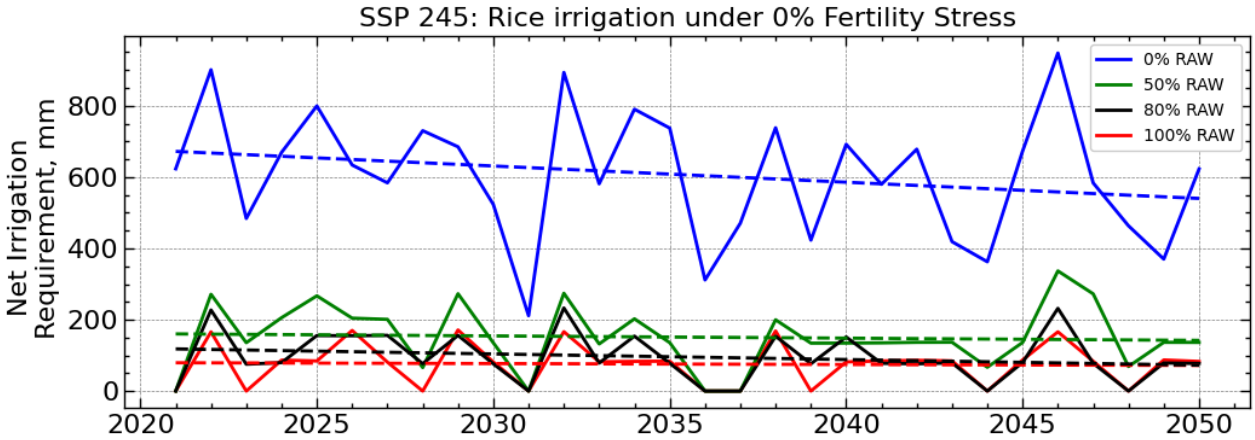
SSP 245: Rice irrigation under 0% Fertility Stress
Net Irrigation Requirement, mm
0% RAW
50% RAW
80% RAW
100% RAW
0
200
400
600
800
2020
2025
2030
2035
2040
2045
2050

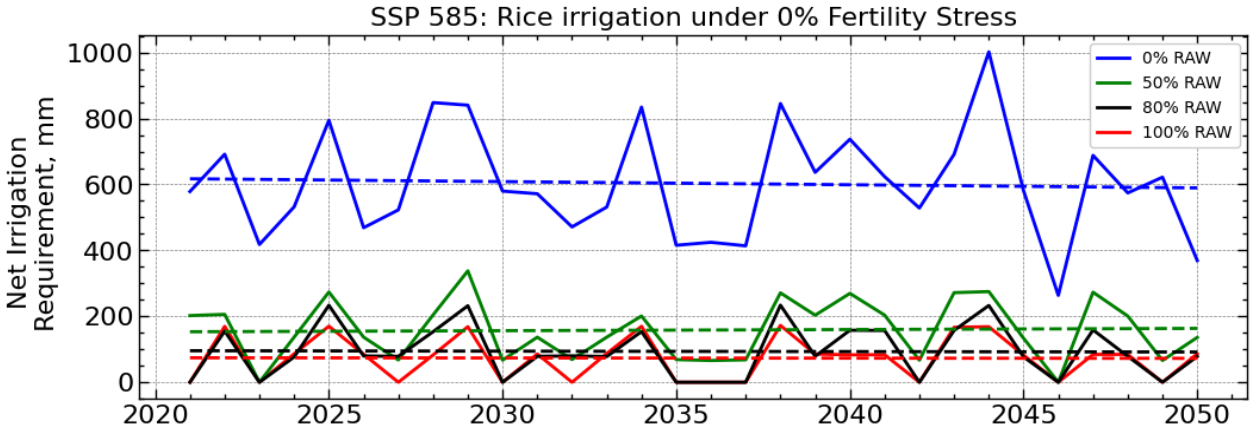
SSP 585: Rice irrigation under 0% Fertility Stress
Net Irrigation Requirement, mm
0% RAW
50% RAW
80% RAW
100% RAW
0
200
400
600
800
1000
2020
2025
2030
2035
2040
2045
2050

15% Fertility Stress:

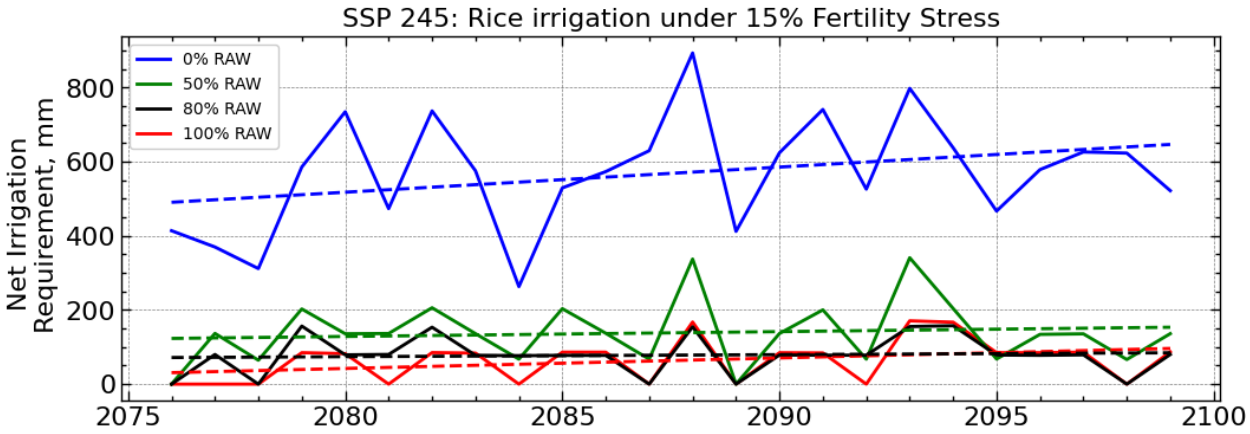

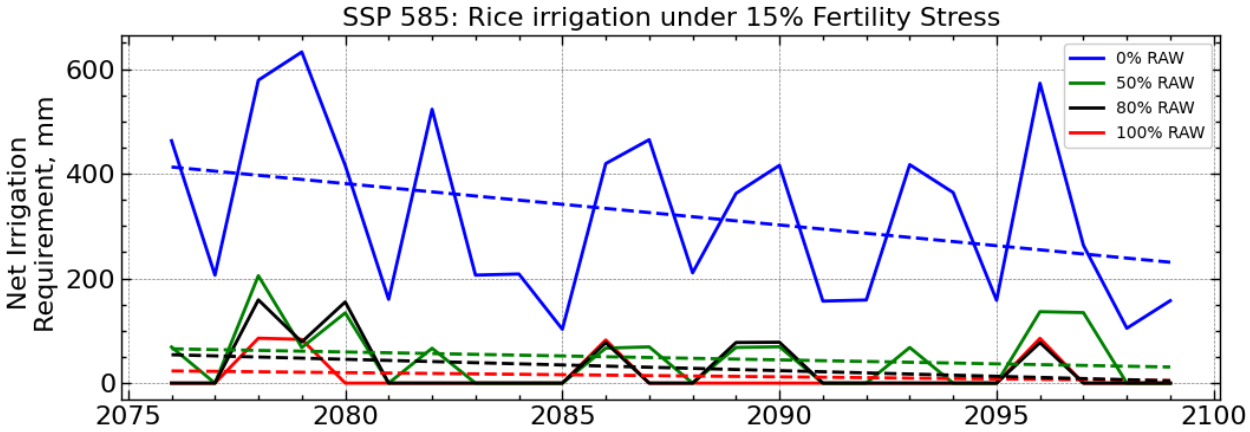

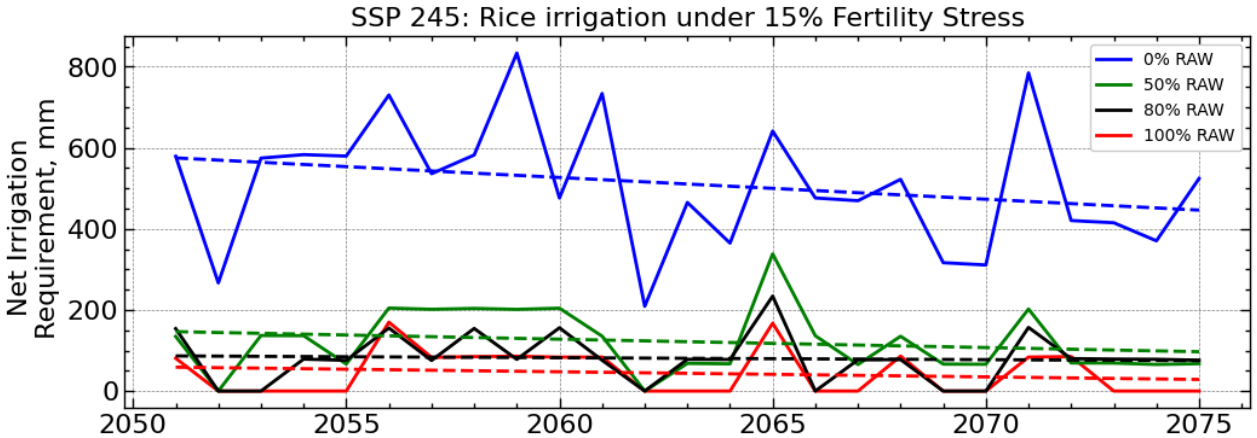

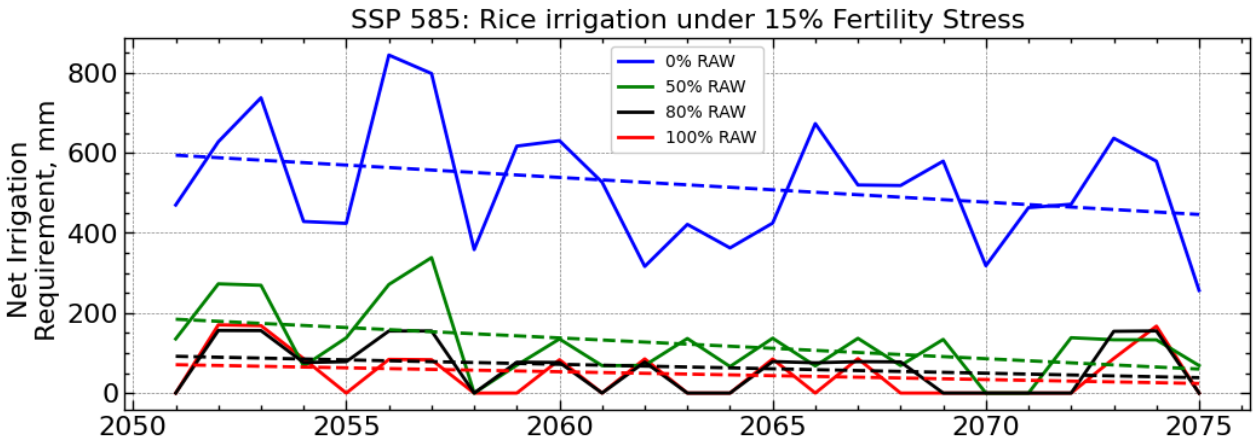
SSP 585: Rice irrigation under 15% Fertility Stress
Net Irrigation Requirement, mm
0% RAW
50% RAW
80% RAW
100% RAW
0
200
400
600
800
2050
2055
2060
2065
2070
2075

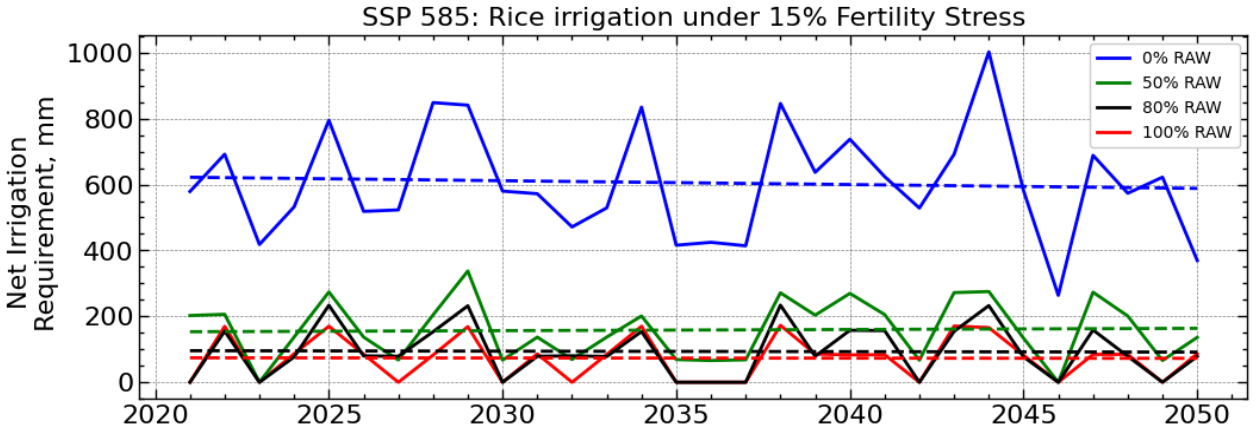
SSP 585: Rice irrigation under 15% Fertility Stress
Net Irrigation Requirement, mm
0% RAW
50% RAW
80% RAW
100% RAW
0
200
400
600
800
1000
2020
2025
2030
2035
2040
2045
2050

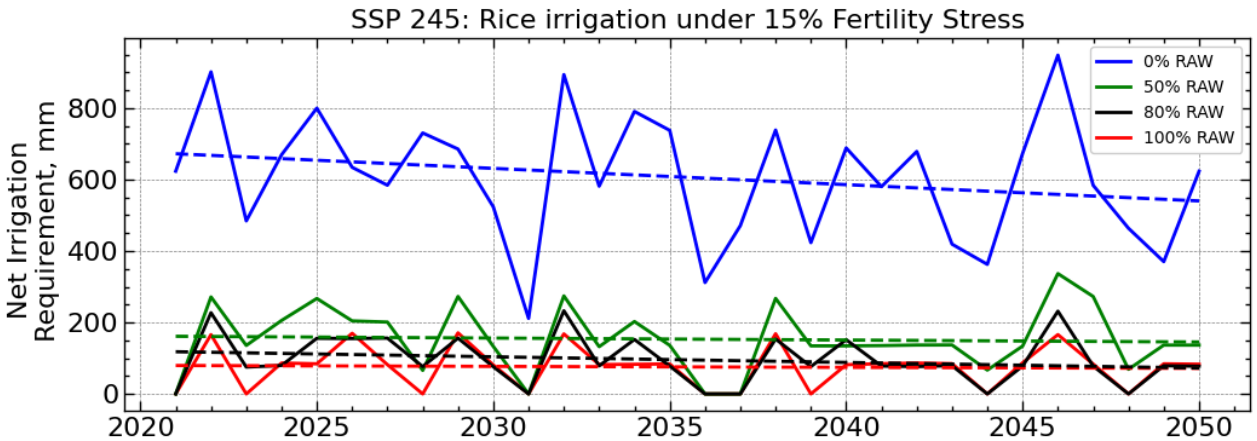
SSP 245: Rice irrigation under 15% Fertility Stress
Net Irrigation Requirement, mm
0% RAW
50% RAW
80% RAW
100% RAW
0
200
400
600
800
2020
2025
2030
2035
2040
2045
2050

40% Fertility Stress:

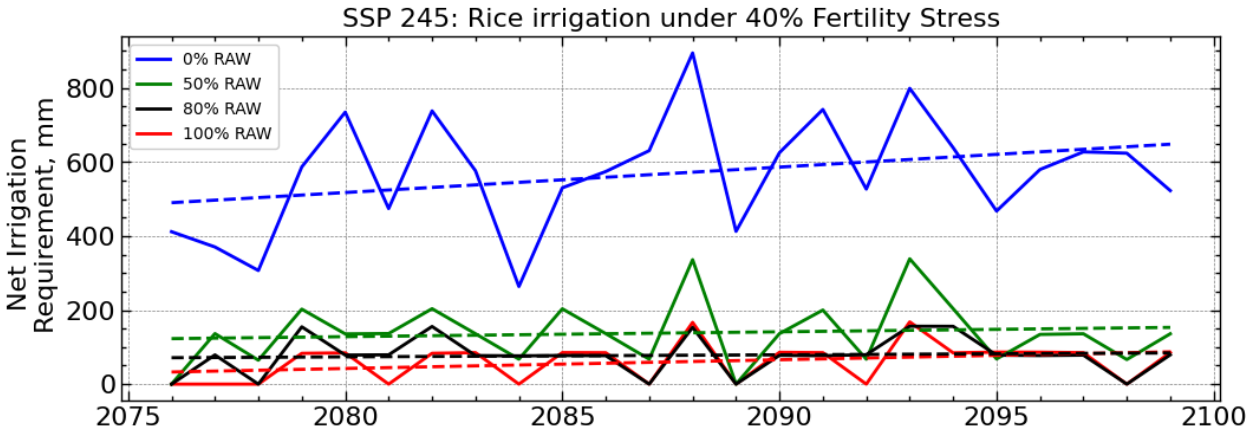

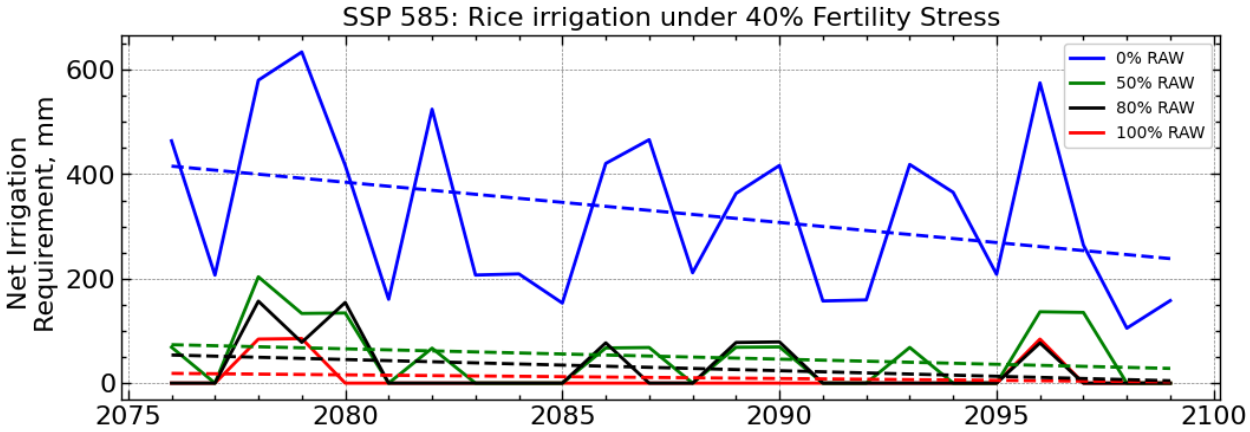

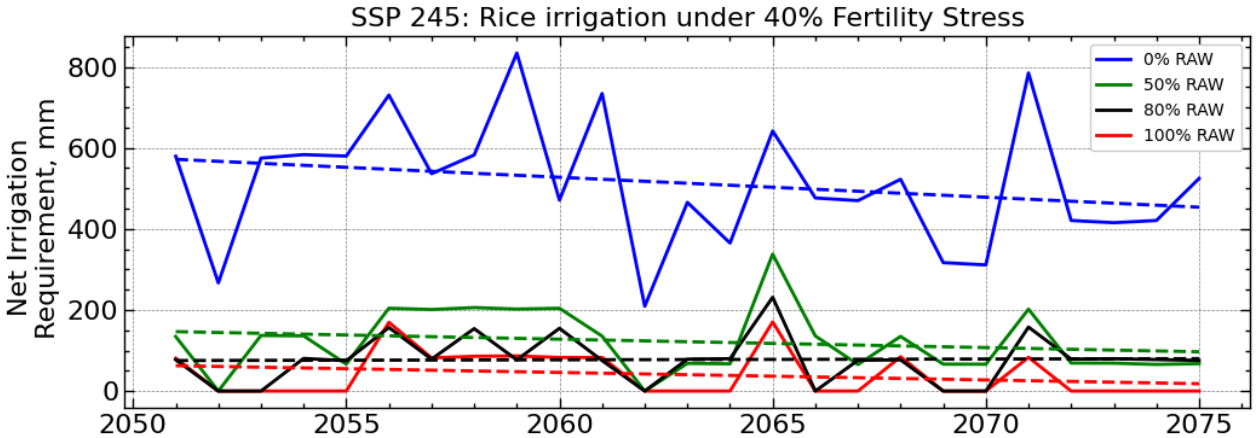

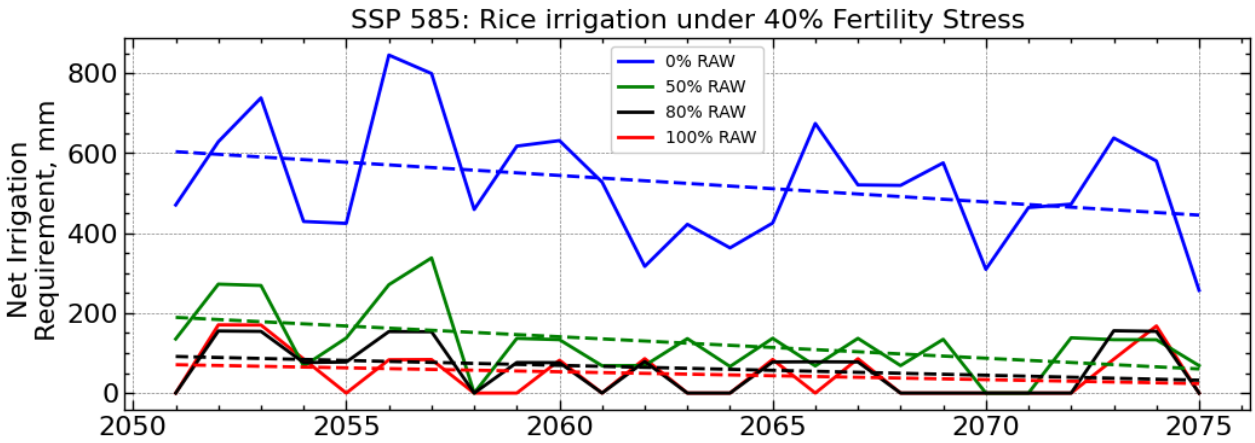
SSP 585: Rice irrigation under 40% Fertility Stress
Net Irrigation Requirement, mm
0% RAW
50% RAW
80% RAW
100% RAW
0
200
400
600
800
2050
2055
2060
2065
2070
2075

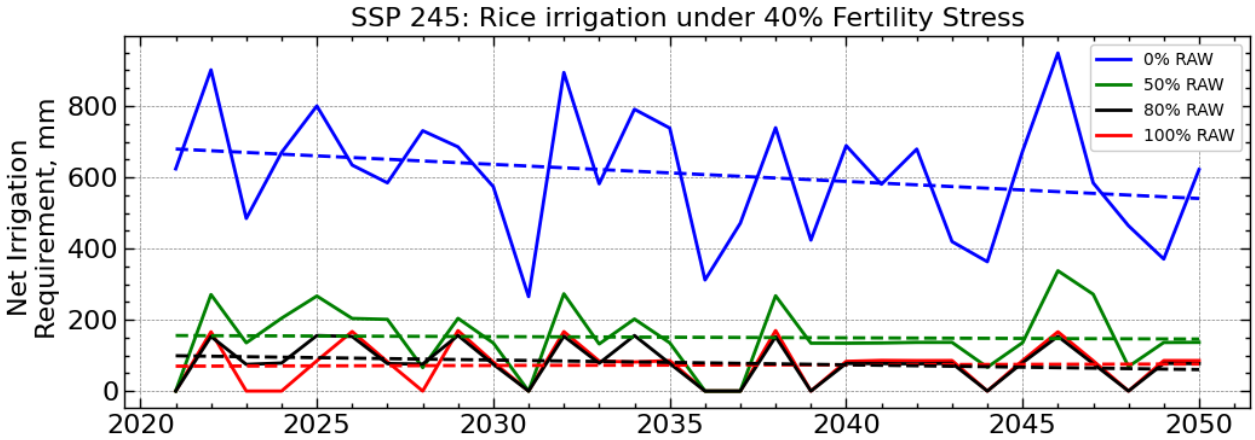
SSP 245: Rice irrigation under 40% Fertility Stress
Net Irrigation Requirement, mm
0% RAW
50% RAW
80% RAW
100% RAW
0
200
400
600
800
2020
2025
2030
2035
2040
2045
2050

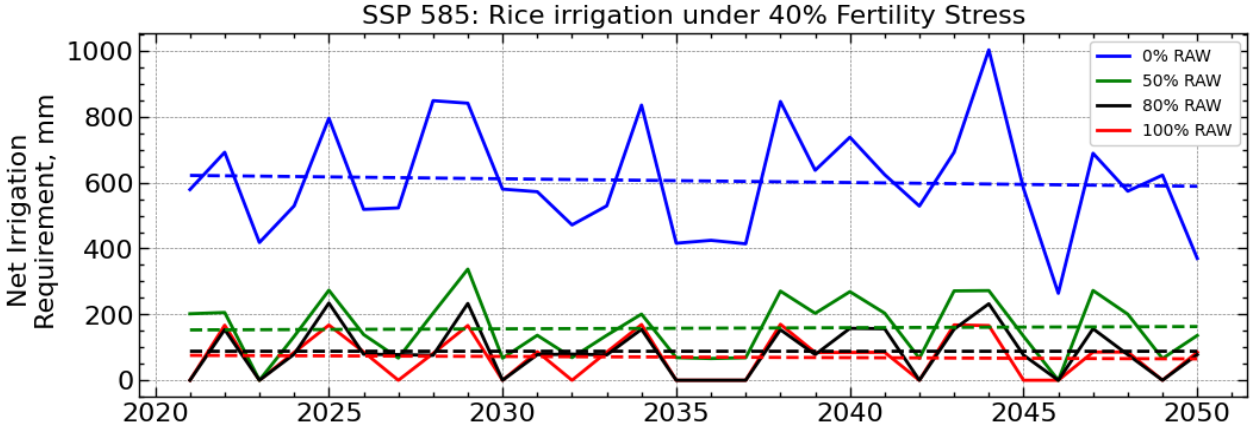
SSP 585: Rice irrigation under 40% Fertility Stress
Net Irrigation Requirement, mm
0% RAW
50% RAW
80% RAW
100% RAW
0
200
400
600
800
1000
2020
2025
2030
2035
2040
2045
2050

ANNEX F: PROJECTED WHEAT YIELD

0% Fertility Stress:

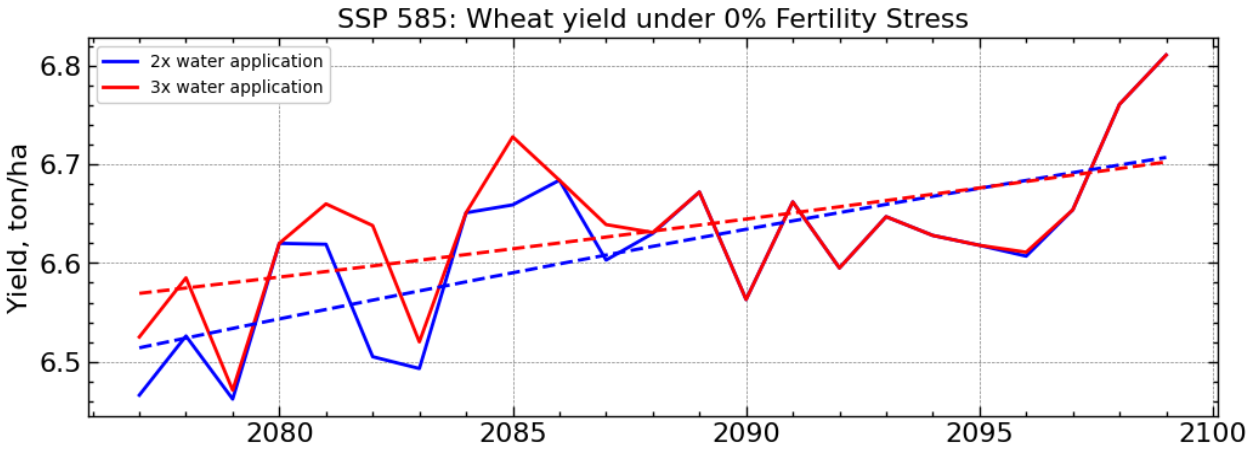

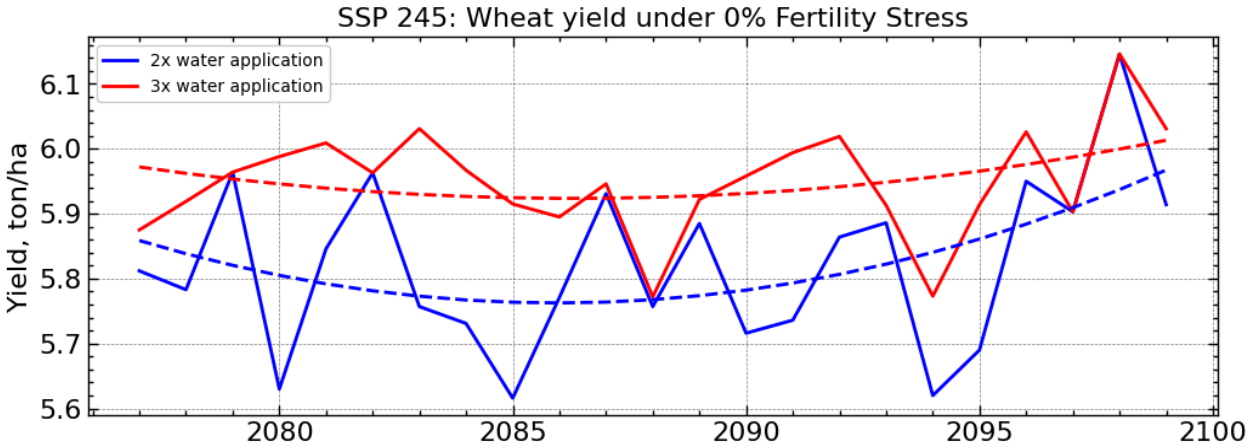

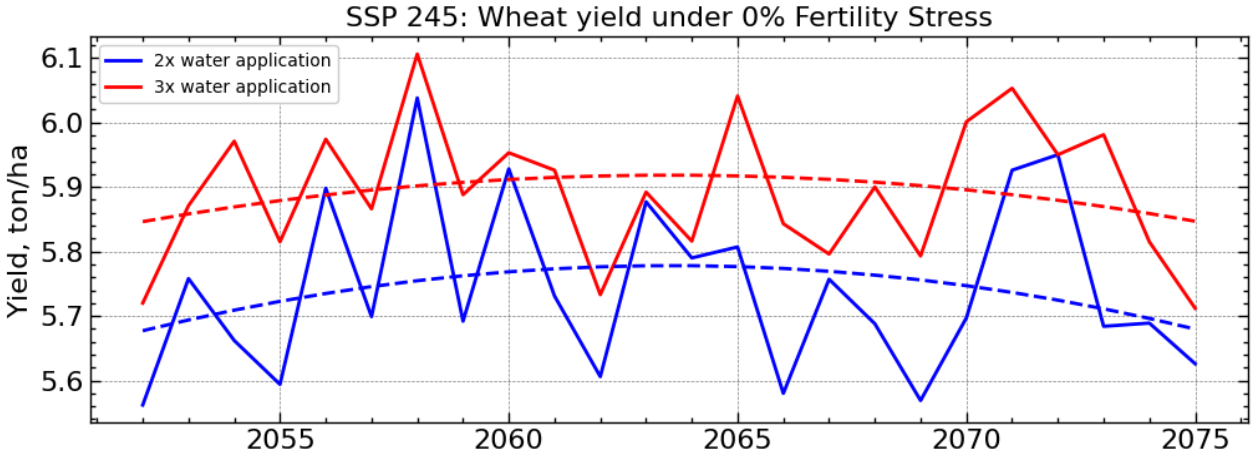

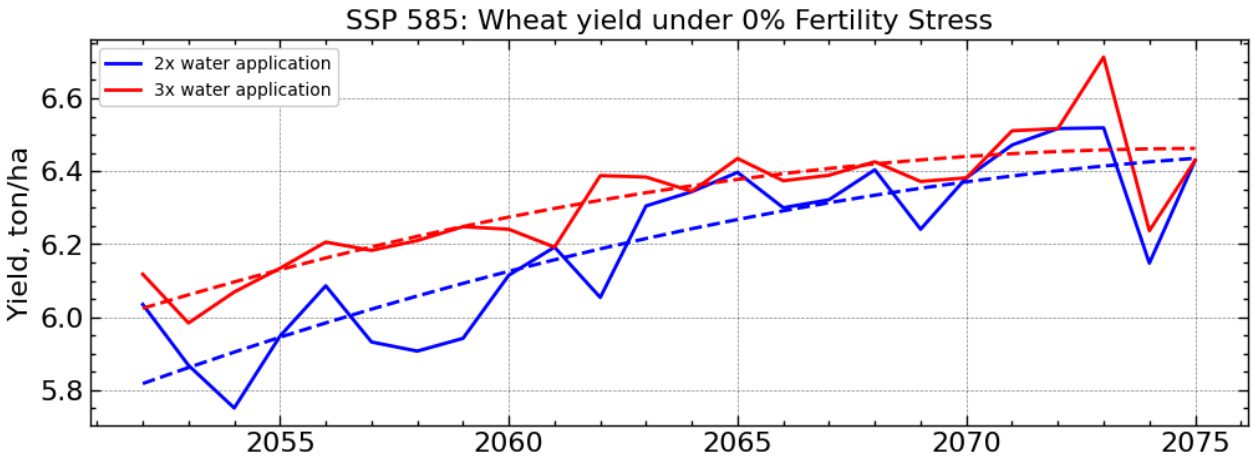
SSP 585: Wheat yield under 0% Fertility Stress
2x water application
3x water application
Yield, ton/ha
6.6
6.4
6.2
6.0
5.8
2055
2060
2065
2070
2075

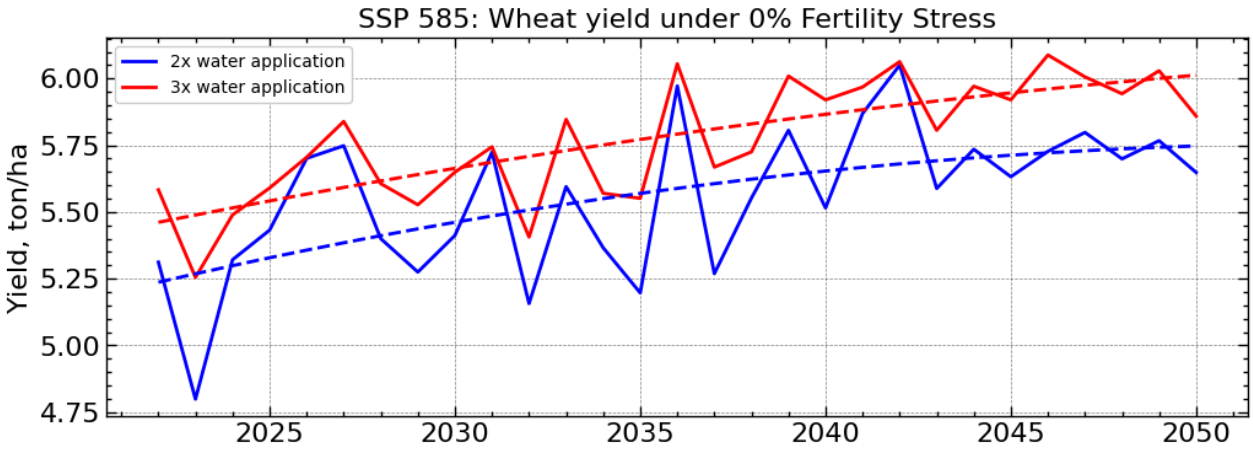
SSP 585: Wheat yield under 0% Fertility Stress
2x water application
3x water application
Yield, ton/ha
6.00
5.75
5.50
5.25
5.00
4.75
2025
2030
2035
2040
2045
2050

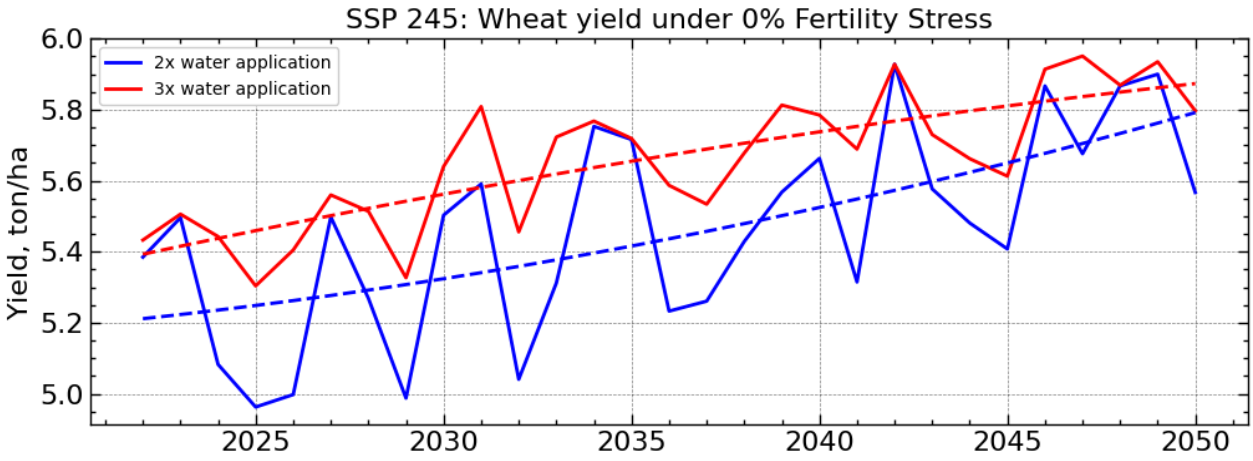
SSP 245: Wheat yield under 0% Fertility Stress
2x water application
3x water application
Yield, ton/ha
6.0
5.8
5.6
5.4
5.2
5.0
2025
2030
2035
2040
2045
2050

50% Fertility Stress:

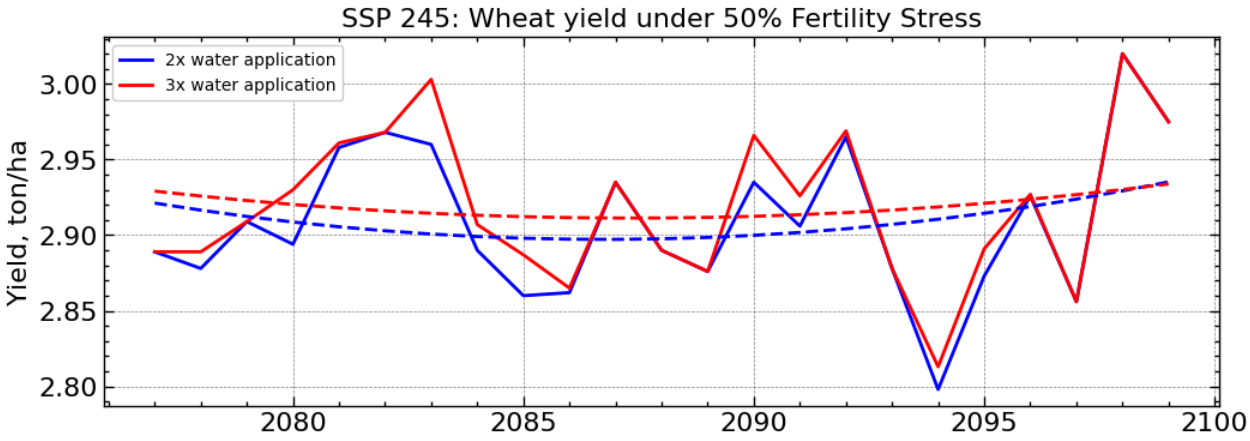

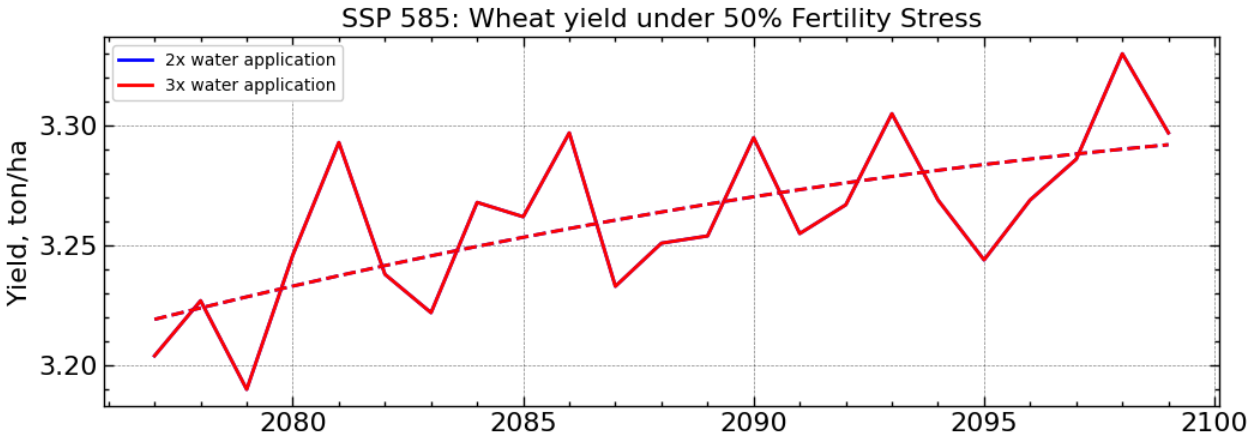

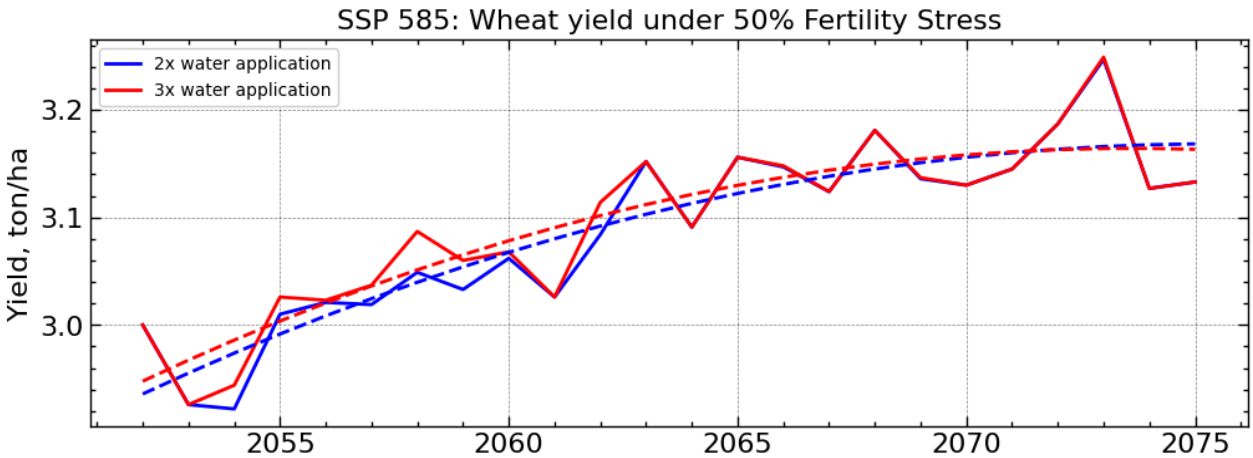

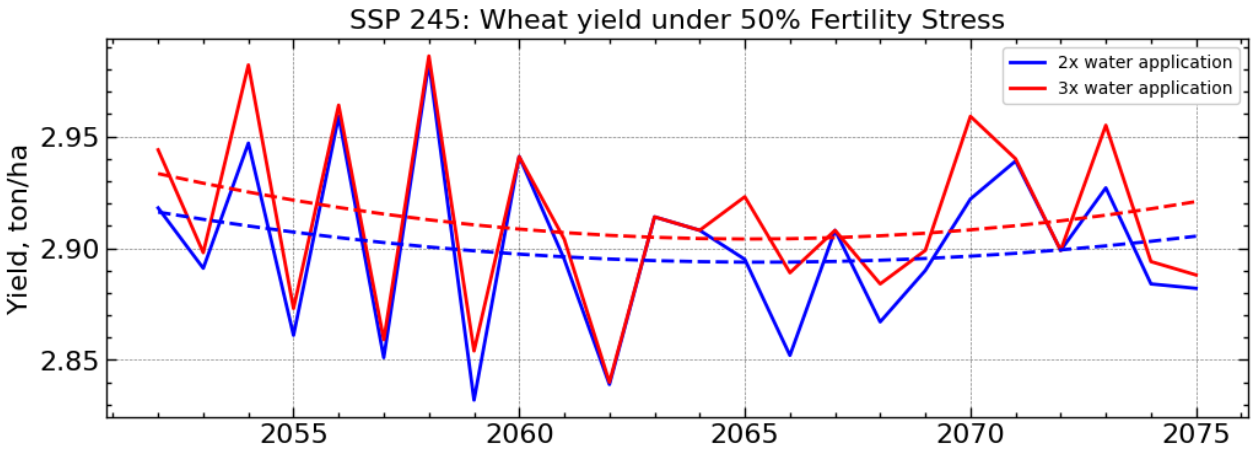
SSP 245: Wheat yield under 50% Fertility Stress
2x water application
3x water application
Yield, ton/ha
2.95
2.90
2.85
2055
2060
2065
2070
2075

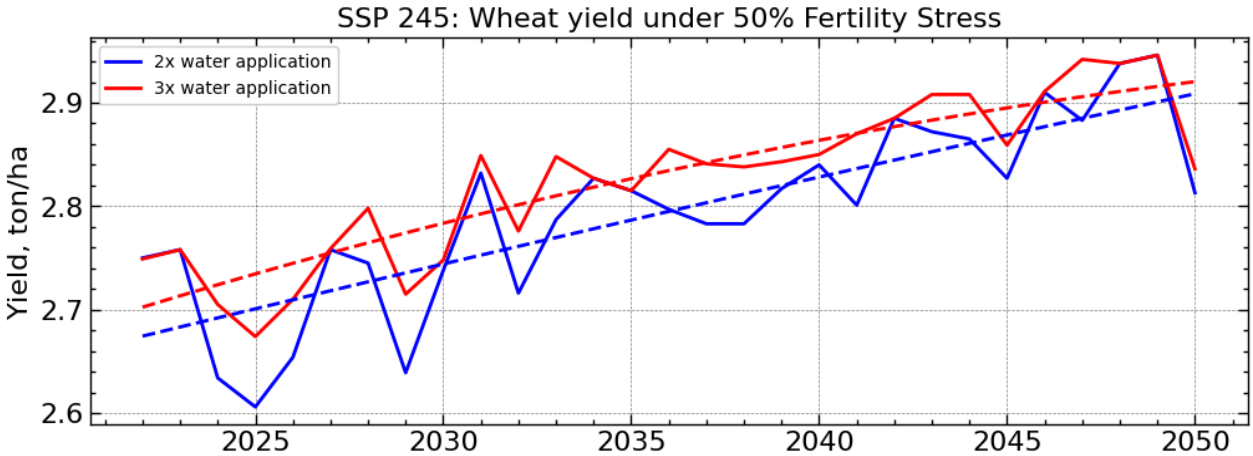
SSP 245: Wheat yield under 50% Fertility Stress
2x water application
3x water application
Yield, ton/ha
2.9
2.8
2.7
2.6
2025
2030
2035
2040
2045
2050

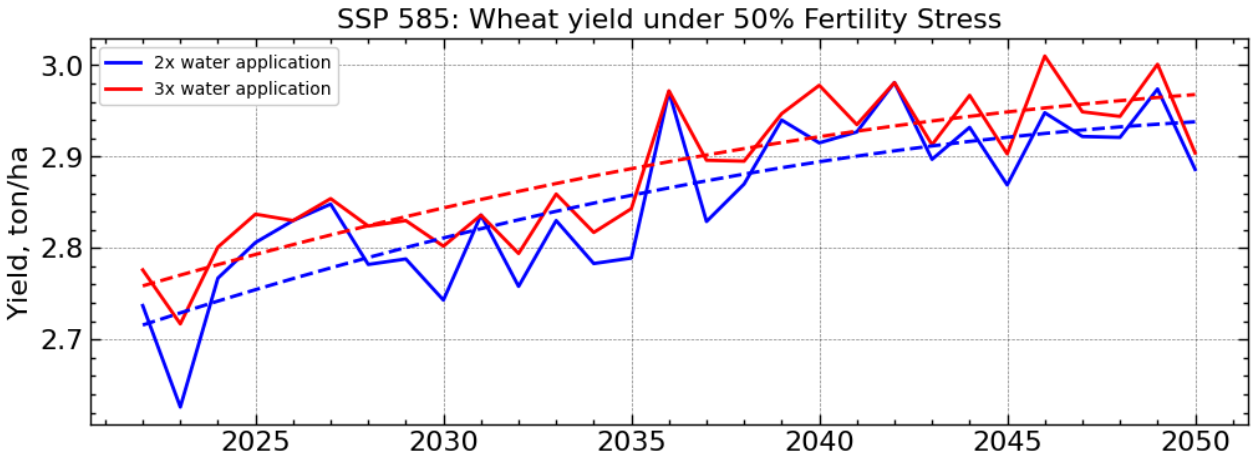
SSP 585: Wheat yield under 50% Fertility Stress
2x water application
3x water application
Yield, ton/ha
3.0
2.9
2.8
2.7
2025
2030
2035
2040
2045
2050

ANNEX G: PROJECTED WHEAT WATER REQUIREMENT

0% Fertility Stress:

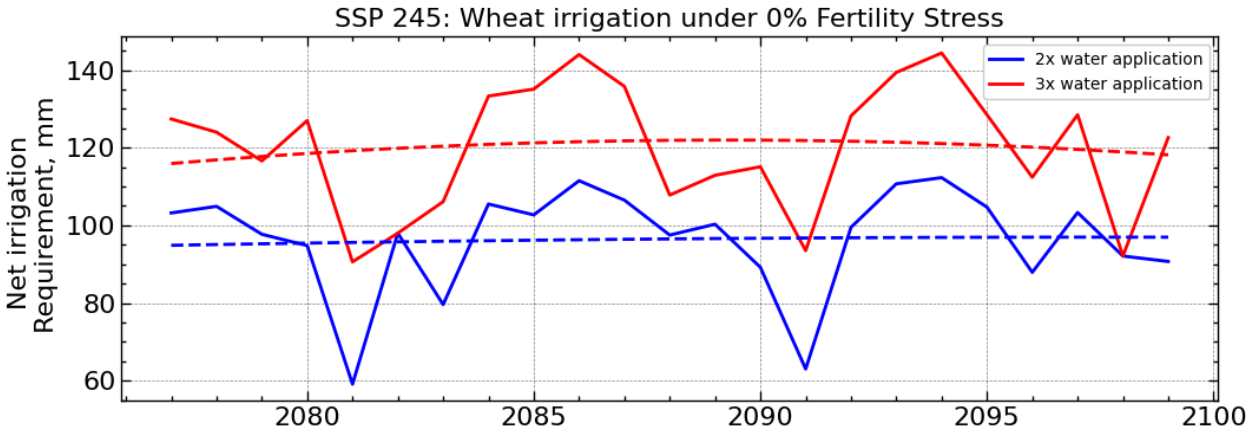

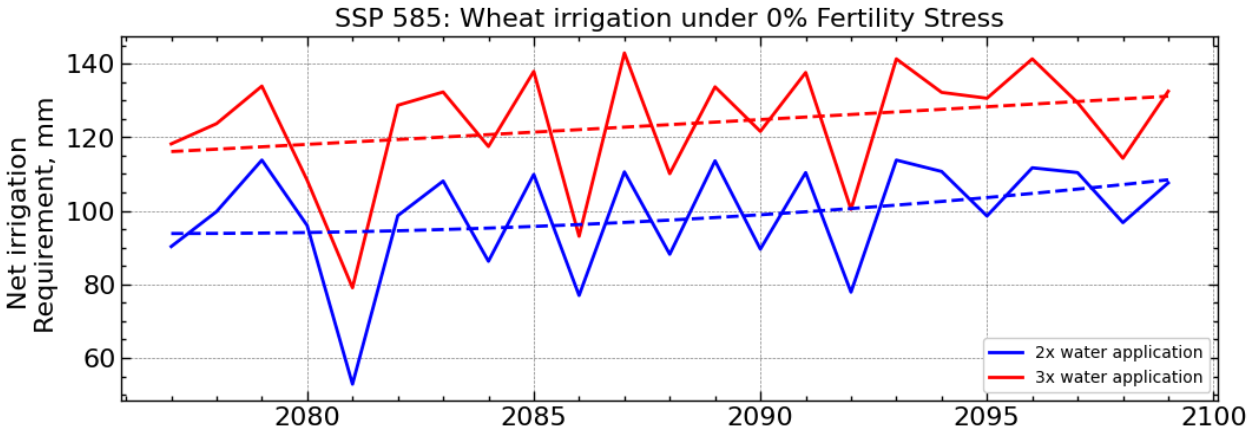

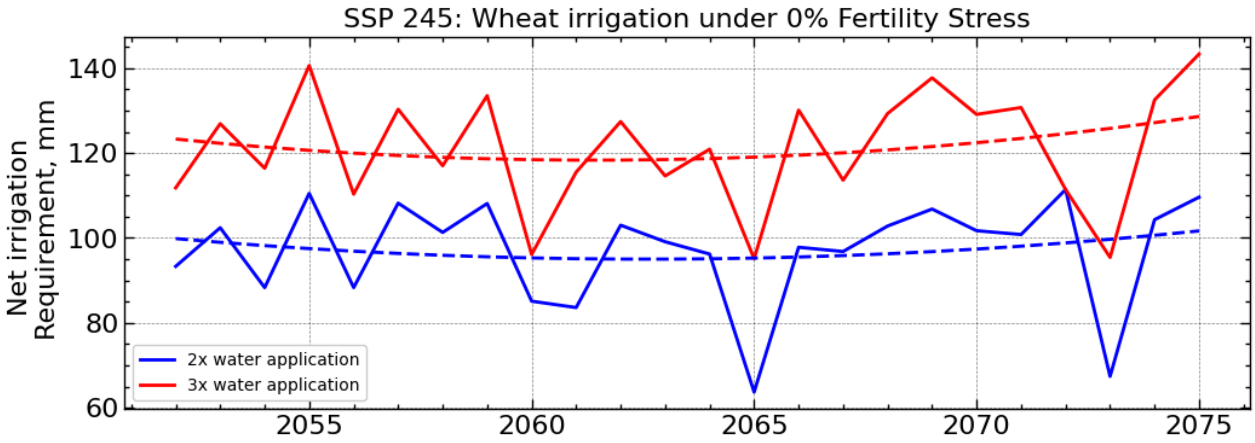

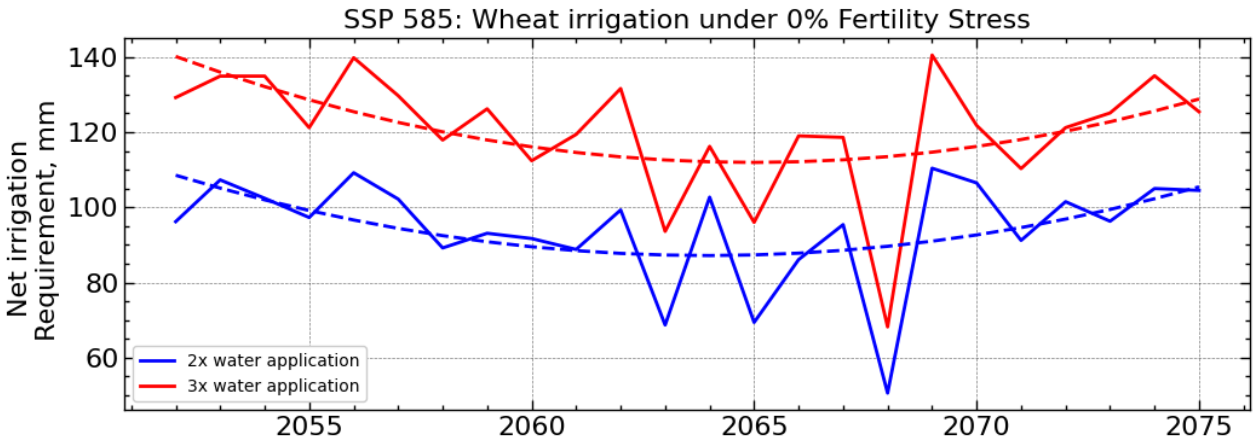
SSP 585: Wheat irrigation under 0% Fertility Stress
Net irrigation Requirement, mm
140
120
100
80
60
2055
2060
2065
2070
2075
2x water application
3x water application

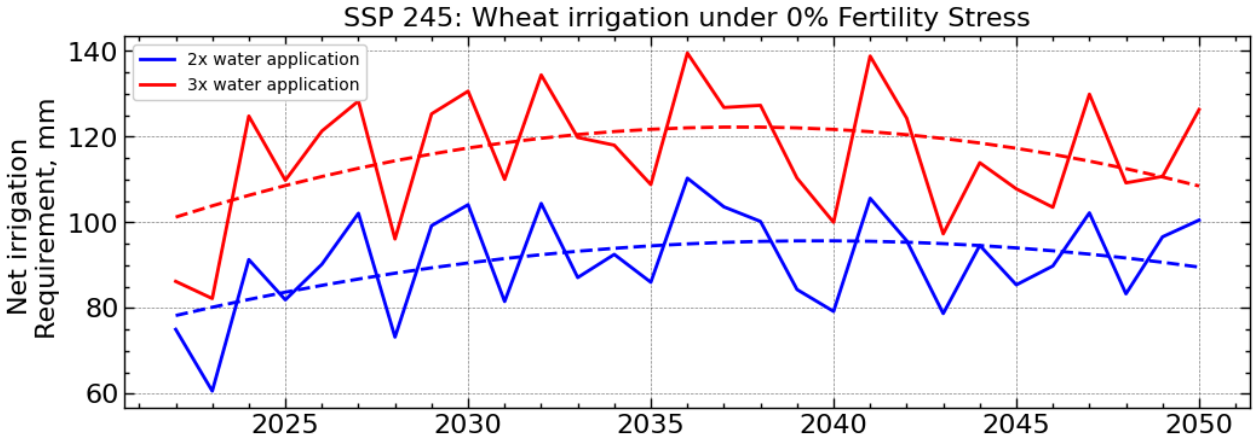
SSP 245: Wheat irrigation under 0% Fertility Stress
Net irrigation Requirement, mm
140
120
100
80
60
2025
2030
2035
2040
2045
2050
2x water application
3x water application

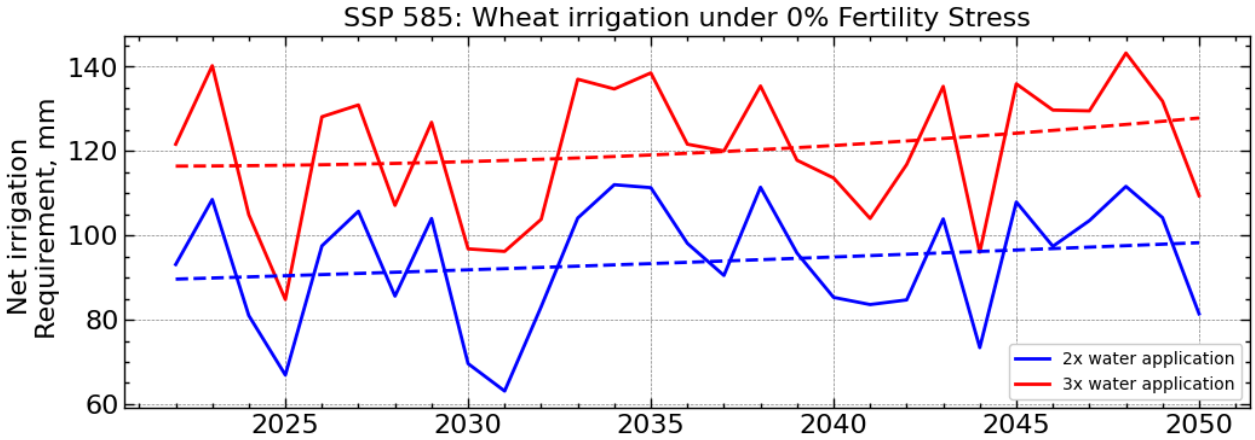
SSP 585: Wheat irrigation under 0% Fertility Stress
Net irrigation Requirement, mm
140
120
100
80
60
2025
2030
2035
2040
2045
2050
2x water application
3x water application

50% Fertility Stress:

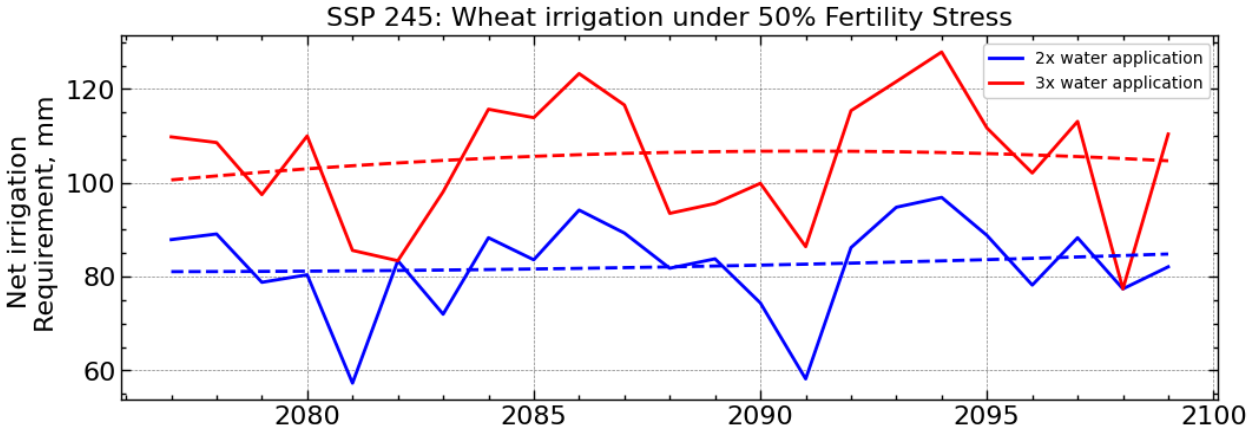

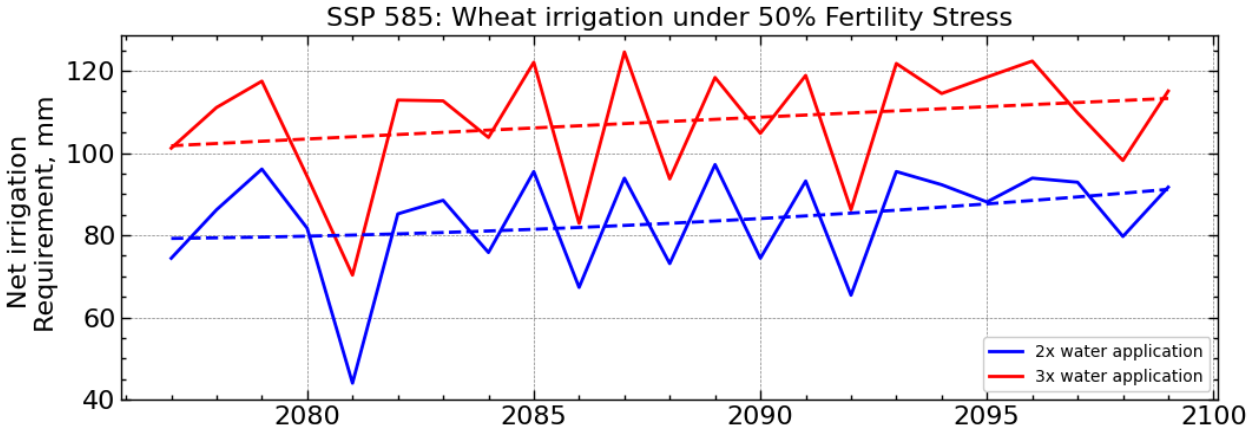

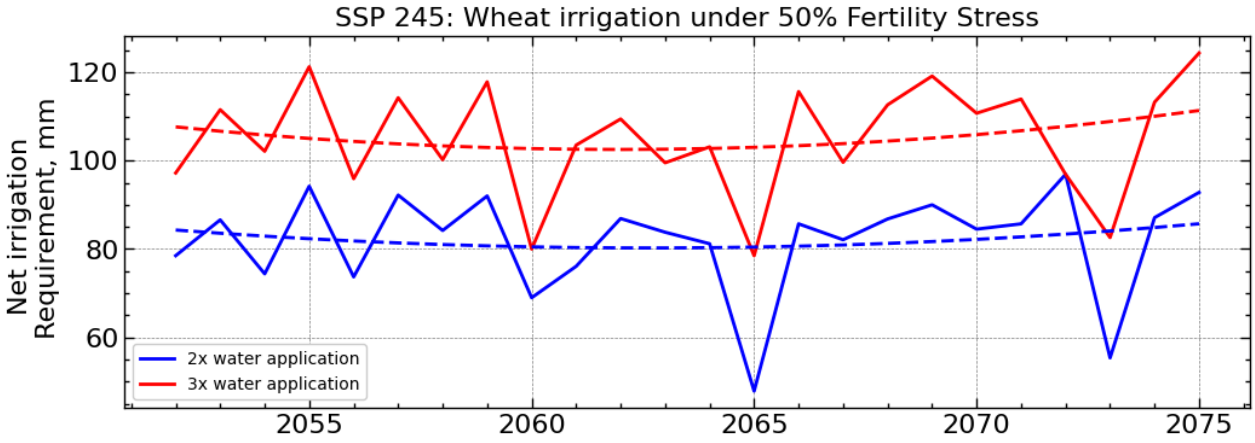

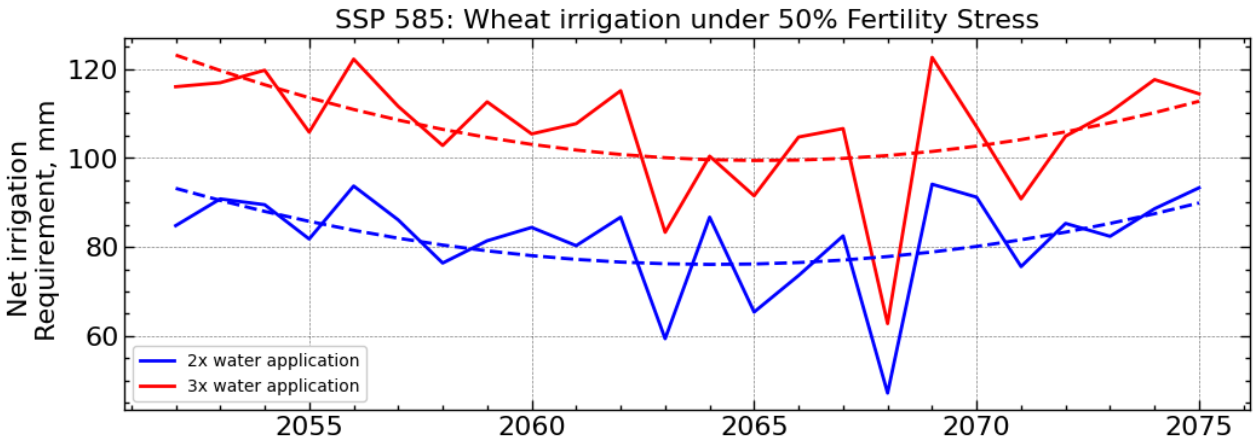
SSP 585: Wheat irrigation under 50% Fertility Stress
Net irrigation Requirement, mm
120
100
80
60
2x water application
3x water application
2055
2060
2065
2070
2075

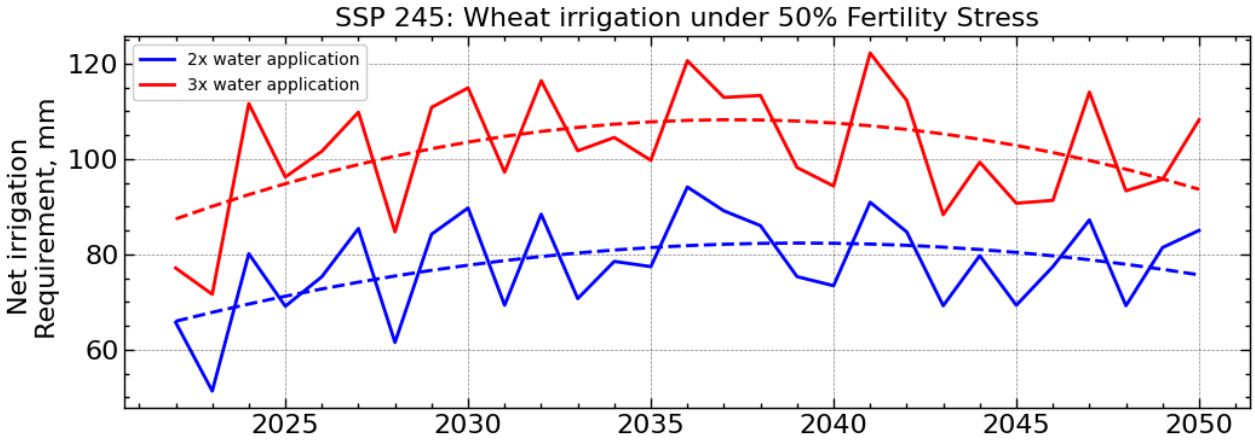
SSP 245: Wheat irrigation under 50% Fertility Stress
Net irrigation Requirement, mm
120
100
80
60
2x water application
3x water application
2025
2030
2035
2040
2045
2050

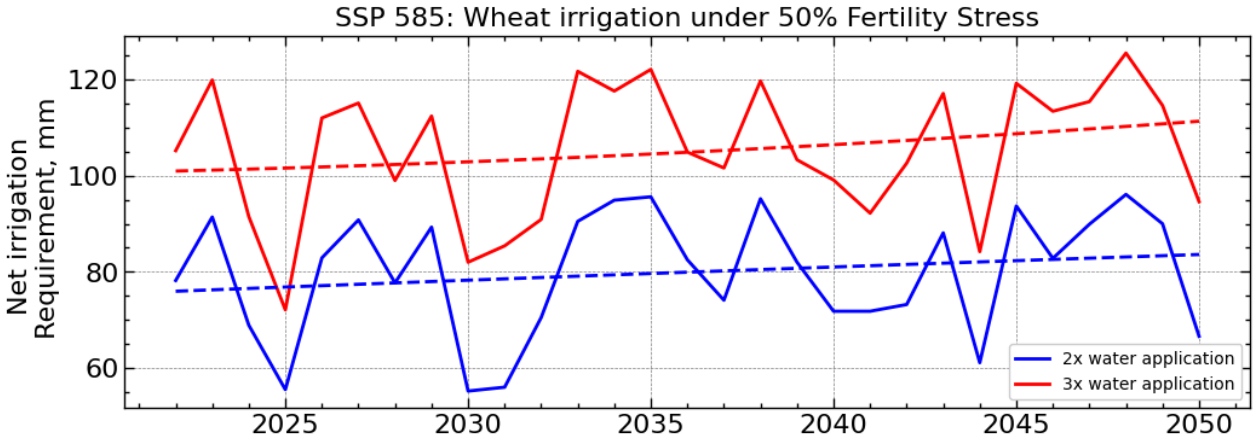
SSP 585: Wheat irrigation under 50% Fertility Stress
Net irrigation Requirement, mm
120
100
80
60
2x water application
3x water application
2025
2030
2035
2040
2045
2050